RESEARCH AND DEVELOPMENT OF NICKEL BASED CATALYSTS FOR CARBON DIOXIDE REFORMING OF METHANE

A Thesis

Submitted to the College of Graduate Studies and Research

in Partial Fulfillment of the Requirements

for the Degree of Doctor Philosophy

in the Department of Chemical Engineering

University of Saskatchewan

Saskatoon, Saskatcheean

By

Jianguo Zhang

PERMISSION TO USE

In presenting this thesis in partial fulfillment of the requirements for a Doctor of Philosophy Degree from the University of Saskatchewan, I agree that the libraries of the University of Saskatchewan may make this thesis freely available for inspection. I further agree that permission for copying of this thesis in any manner, in whole or in part, for scholarly purpose may be granted by the professors who supervised my thesis work or, in their absence, by the Head of the Department or the Dean of the College of Graduate Research and Studies in which the thesis work was complete. It is understood that any copying or publication or use of this thesis or parts thereof for financial gain shall not be allowed without my written permission. It is also understood that due recognition shall be given to me and to the University of Saskatchewan in any scholarly use which may be made of any material in my thesis.

Requests for permission to copy or to make other use of material in this thesis in whole or parts shall be addressed to:

Head of the Department of Chemical Engineering

Univerisity of Saskatchewan

Saskatoon, Saskatchewan

Canada S7N 5A9

ABSTRACT

Consuming two major greenhouse gases, carbon dioxide (CO_2) and methane (CH_4), to produce synthesis gas, which is a mixture of carbon monoxide (CO) and hydrogen (H_2), CO_2 reforming of CH_4 shows significant environmental and economic benefits. However, the process has not found wide industrial application due to severe catalyst deactivation, basically caused by carbon formation. Therefore, it is of great interest to develop stable catalysts without severe deactivation. This work is primarily focused on the development of novel nickel-based catalysts to achieve stable operation for CO_2 reforming of CH_4.

Following Dowden's strategy of catalyst design, a series of nickel-based catalysts are designed with a general formula: Ni-Me/$AlMgO_x$ (Me = Co, Cu, Fe, or Mn). The designed catalysts are prepared using co-precipitation method and tested for CO_2 reforming of CH_4. Catalyst screening showed that the Ni-Co/$AlMgO_x$ catalyst has superior performance in terms of activity and stability to other Ni-Me/AlMgOx (Me = Cu, Fe, or Mn) catalysts. A 2000 h long-term deactivation test has shown that the Ni-Co/$AlMgO_x$ has high activity and excellent stability for CO_2 reforming of CH_4.

Further investigation on the Ni-Co/$AlMgO_x$ catalysts shows that adjusting Ni/Co ratio and Ni-Co loading can significantly affect the catalyst performance. Carbon free operation for CO_2 reforming of CH_4 can be achieved on the catalysts with a Ni/Co close to 1 and Ni-Co overall loading between 4-10 %. In addition, calcination temperature

shows important impacts on the performance of Ni-Co/$AlMgO_x$ catalysts. A calcination temperature range of 700-900 ^oC is recommended.

The Ni-Co/$AlMgO_x$ catalysts are characterized using various techniques such as ICP-MS, BET, CO-chemiosorption, XRD, TPR, TG/DTA, TEM, and XPS. It has been found that the high activity and excellent stability of Ni-Co/$AlMgO_x$ catalysts can be ascribed to its high surface area, high metal disperation, small particle size, strong metal-support interaction, and synergy between Ni and Co.

Kinetic studies have shown that the CH_4 decomposition and CO_2 activation could be the rate-determining steps. Both Power-Law and Langmuir-Hinshelwood kinetic models can fit the experiment data with satisfactory results.

ACKNOWLEDGEMENT

I would like to sincerely express my great gratitude to Dr. Hui Wang and Dr. Ajay K. Dalai for being my supervisors and supporting this work financially. I appreciate their patience, guidance and encouragement during the research and writing of the thesis.

I would like to extend my special appreciation to my advisory committee: Dr. R. Evitts, Dr. M. Nemati, Dr. D.-Y. Peng, and Dr. S. Urquhart at the University of Saskatchewan for their guidance and valuable advice throughout the research and thesis preparation.

Furthermore, I would like to thank all the supporting staff in the Department of Chemical Engineering: Ms. Jean Horosko, Ms. Kelly Bader, Mr. Ted Wallentiny, Mr. Richard Blondin, and Mr. Dragan Cekic for their support during the research.

My sincere thanks also go to my friends. I would like to acknowledge Haijun Sun, Dongmei Fang, Deming Wang, Ramin Azargohar, and Christian Botchwey for their help and friendship during my research and studies at the University of Saskatchewan.

My gratitude goes to my parents and sister, who never stop wishing me the best of luck. Lastly, I would like to thank my wife Ruihong Yu for her love and support, without which the studies and research over the last five years in Saskatoon would not have been possible.

TABLE OF CONTENTS

LIST OF TABLES

LIST OF FIGURES

1 INTRODUCTION

This chapter introduces the background and the development of carbon dioxide (CO_2) reforming of methane (CH_4) technology. The significance of CO_2 reforming of CH_4 is discussed. The research objectives and the structure of the thesis are outlined.

1.1 GREENHOUSE GAS AND SYNTHESIS GAS

1.1.1 Greenhouse gas emission

Greenhouse gases are the components in the atmosphere proposed to cause an increase in surface temperature of the globe, which is known as the greenhouse effect. Greenhouse gases include carbon dioxide (CO_2), methane (CH_4), oxides of nitrogen (NO_x), ozone (O_3), and others. Fig. 1.1 shows the distribution of major greenhouse gases in atmosphere. Clearly, CO_2 and CH_4 are the two most abundant greenhouse gases.

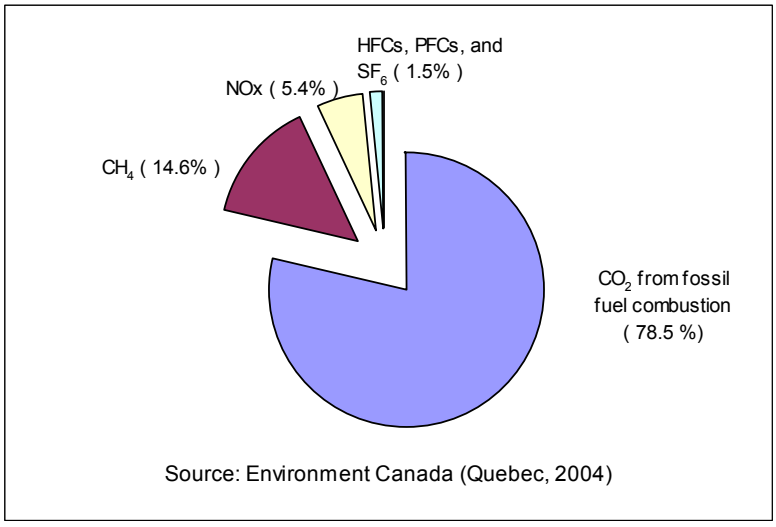

Fig. 1.1 Greenhouse gas distribution in Canada

Most of the CO_2 emission is a result of fossil fuel combustion. In the United States, for example, the combustion of fossil fuel for generating electricity contributed to 2.215×10^9 tonnes of CO_2 accounting for 40.5 % CO_2 emissions in 1998 (DOE, 2000). It was estimated that 60 % global CH_4 emissions are related to human-related activities (IPCC, 2001). In the United States, landfills are the largest human-related source of CH_4 accounting for 34 % of all CH_4 emissions, around 1.58×10^8 tonnes of CO_2 equivalents (EPA, 2006). In Canada, 2.2×10^7 tonnes of CO_2 equivalent greenhouse gases from landfills accounts for 3 % total greenhouse emissions (Environment Canada, 2004). With increasing concerns about abrupt climate changes caused by global warming, the reduction of greenhouse gas emission attracts great attention. As a result of increasing interest in greenhouse gas mitigation, chemical processes to utilize greenhouse gas are becoming important with great of interest.

Landfill is a big contributor of greenhouse emission. However, landfill gas is composed of approximately 50 % of CH_4 and 50 % of CO_2, which makes it a perfect feedstock for CO_2 reforming of CH_4. As indicated by Eq. 1.1, CO_2 reforming of CH_4 process is potentially the most effective way to utilize these two greenhouse gases together to reduce greenhouse gas emission while to produce valuable synthesis gas. In the following section, the technologies for synthesis gas production will be discussed.

$$CH_4 + CO_2 \leftrightarrow 2CO + 2H_2 \qquad \Delta H^0_{298\,K} = 247\ \text{kJ} \tag{1.1}$$

1.1.2 Production of synthesis gas

Synthesis gas is a mixture of hydrogen (H_2) and carbon monoxide (CO). It is one

of the most important industrial feedstocks from which a variety of chemicals can be produced by varying the H_2/CO ratio. The major processes of synthesis gas production are presented in Table 1.1. Synthesis gas can be produced through four processes: 1) steam reforming; 2) partial oxidation; 3) CO_2 reforming, also called dry reforming; and 4) autothermal reforming.

Table 1.1 Processes producing synthesis gas

Process	Reaction Equation	ΔH^{o}_{298K} (kJ)
Steam reforming	$CH_4 + H_2O \leftrightarrow CO + 3H_2$	206
Partial oxidation	$CH_4 + 0.5O_2 \leftrightarrow CO + 2H_2$	-36
Dry reforming	$CH_4 + CO_2 \leftrightarrow 2CO + 2H_2$	247
Autothermal reforming	$CH_4 + 2O_2 \leftrightarrow CO_2 + 2H_2O$	-802
	(Methane in excess)	
	$CH_4 + CO_2 \leftrightarrow 2CO + 2H_2$	247
	$CH_4 + H_2O \leftrightarrow CO + 3H_2$	206

Steam reforming is the well-developed and dominant technology for the production of synthesis gas or hydrogen. It can be coupled with CO_2 reforming of CH_4 to adjust the H_2/CO ratio to meet feedstock requirement for downstream processes. As steam reforming requires huge enegy supply, the exothermal partial oxidation appears to be a good alternative as an exothermic process. However, the economics of partial oxidation is restricted by the cost of pure oxygen supply. Currently, the steam reforming process is still the least expensive process for synthesis gas and/or hydrogen production. Autothermal reforming is a combination of non-catalytic partial oxidation and catalytic reforming. It was developed to perform oxidation and reforming in a single reactor. However, undesired

reactions in the combustion zone lead to carbon deposition on the down stream tubes causing serious problems of equipment damage, pressure drop, and poor heat transfer (Pena et al., 1996). CO_2 reforming of CH_4 has attracted extensive attention since 1980s. With a H_2/CO ratio of 1, the synthesis gas produced by CO_2 reforming of CH_4 is a desirable feedstock for Fischer-Tropsh synthesis (Gadalla and Bower, 1988) and the synthesis of oxygenates (Burch and Petch, 1992; Alyea et al., 1993).

In addition, CO_2 reforming of CH_4 is considered to store solar energy or nuclear energy (Chubb, 1980; Fraenkel et al., 1986; Levy et al., 1992) through a chemical energy transmission system (CETS). The concept of CETS is shown in Fig. 1.2. The endothermic reforming is carried out when energy such as solar energy or nuclear energy is available. Then the products can be stored or transported to another location where energy is required. Finally, exothermic reaction is carried out to release energy.

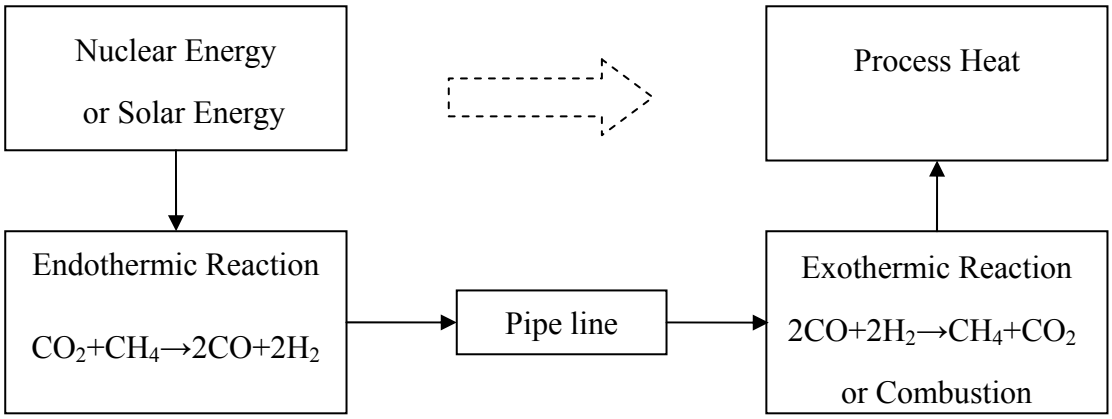

Fig. 1.2 The chemical energy transmission system (CETS)

From the above discussion, it can be seen that CO_2 reforming of CH_4 can be used for reducing greenhouse gas emission through landfill gas conversion, providing feedstock for F-T synthesis, or transferring energy through a CETS. It indicates that CO_2 reforming of CH_4 has great potential economic and environmental benefits. Following sections will discuss the development of CO_2 reforming of CH_4 technology.

1.2 DEVELOPMENT OF CO_2 REFORMING OF CH_4

1.2.1 Overview

Fischer and Tropsch have reported on CO_2 reforming of CH_4 on various base metals in 1928 (Fischer and Tropsch, 1928). Before the 1980s, research on CO_2 reforming of CH_4 was focused on producing synthesis gas with suitable H_2/CO ratios to synthesize hydrocarbons and related products from materials other than petroleum (Reitmeier et al., 1948). From the 1980s to 1990s, a significant amount of attention was paid to the CO_2 reforming of CH_4 - methanation cycle for the application of solar energy (Chubb 1980; McCrary et al., 1982). However, the extensive investigation started from 1990s came up with the increasing concerns about greenhouse effects and energy shortages. In the following section, development of catalysts for CO_2 reforming of CH_4 is discussed and the current commercial processes involving CO_2 reforming of CH_4 are introduced.

1.2.2 Development of reforming catalysts

It is well known that CO_2 reforming of CH_4 can be catalyzed by most of the transition metals. Table 1.2 shows most of the catalyst systems that have been developed

since 1928. It has been shown that many metals such as Ni, Pt, Pd, Ru, Rh and Ir are investigated extensively over different supports. However, there is a serious problem of catalyst deactivation associated with CO_2 reforming of CH_4. Catalyst deactivation has been well known since 1928 (Fischer and Tropsch, 1928) over different metals catalysts. Carbon deposition, sintering, and/or metal oxidation could be the major causes of catalyst deactivation (Slagtern et al., 1997). Different deactivation mechanism is associated with different catalyst system. For example, Hu and Ruckenstein (2004) reported in a review for CO_2 reforming of CH_4 that carbon formation rather than sintering is the main cause of platinum-containing catalyst deactivation.

Table 1.2 Development of reforming catalysts

Time	Catalyst	Reference
1928	Cu/Stuttgarter Masse, Fe/Al_2O_3, Co/Al_2O_3, Ni/Al_2O_3, $Ni/MgCO_3$	Fischer and Tropsch, 1928
1928 to 1979	Ni catalysts	Clark et al., 1949; Bodrov et al., 1967
	Cu/SiO_2	Lewis et al., 1949
	Ni/SiO_2	Sodesawa et al., 1984
	Ni/Al_2O_3	Chubb, 1980; McCrary et al., 1982; Rudnitskii et al., 1984; Tokunaga et al., 1989
	Pd/Al_2O_3	Sakai et al., 1984
	Pd/SiO_2,Pd/TiO_2, Pd/Zeolites	Masai et al., 1988
1980 to 1989	Fe/Al_2O_3,Co/Al_2O_3, Ni/SiO_2	Tokunaga et al., 1989
	Ni/Al_2O_3-CaO-TiO_2	Gadalla et al., 1989
	Ni/Al_2O_3-MgO	Gadalla et al., 1989
	$Ni/MgAl_2O_3$	Gadalla and Bower, 1988**;** Gadalla et al., 1989

Table 1.2 Contined

Time	Catalyst	Reference
1990 to 2007	Ni/Al_2O_3	Osaki et al., 1994; 1995; Takayasu, 1993; Vernon et al., 1992; Swaan et al., 1994, Zhang et al., 1994; 1995; 1996; Kim et al., 1994; Tang et al., 1995; Chen et al., 1994; Bhattacharyya et al., 1994; Ruckenstein et al., 1996; 1997; Hu et al., 1996; 1997; Ashcroft et al., 1991; Blom et al., 1994; Seshan et al., 1994; Takano et al., 1994; Chang et al., 1996; Horiuchi et al., 1996; Tang et al., 2000; Osaki et al., 2001; Seok et al., 2002; Tomishige et al., 2002; Hou et al., 2003; Huang et al., 2005
	Ni/SiO_2	Osaki et al., 1994; Takayasu, 1993; Bradford et al., 1996; 1997; 1998; Kim et al., 1994; Tang et al., 1995; Ruckenstein et al., 1996; 1997; Hu et al., 1996; 1997; Takano et al., 1996; Gronchi et al., 1996; Fei et al., 2004
	Ni/Al_2O_3-CaO, Ni/Al_2O_3-CaO-MgO	Zhang et al., 1994; 1996; Horiuchi et al., 1996; Tang et al., 1995
	Ni/Al_2O_3-CeO_2	Chang et al., 1996
	Ni/Al_2O_3-La_2O_3	Blom et al., 1994; Chang et al., 1996; Slagtern et al., 1997
	Ni/Al_2O_3-MgO	Takayasu, 1993; Tang et al., 1995; Chang et al., 1996; Tsyganok et al., 2001; Tsyganok et al., 2003; Roh et al., 2007
	$Ni/MgAl_2O_4$	Rostrup-Nielsen and Hansen, 1993
	Ni/Al_2O_3-SiO_2	Swaan et al., 1994; Choudhary et al., 1995
	Ni/α-Al_2O_3/Ce-SiO_2	Roh et al., 2002
	Ni/BaO	Ruckenstein and Hu, 1995
	Ni/CeO_2-ZrO_2, Ni-CeO	Potdar et al., 2002; Kim et al., 2007
	Ni/C	Bradford and Vannice, 1996
	Ni/CaO	Choudhary et al., 1995; 1996; Zhang et al., 1994; 1995; 1996, Ruckenstein and Hu, 1995
	Ni/MgO	Osaki et al., 1994; 1996; Takayasu 1991; 1993; Rostrup-Nielsen, 1993; Swaan et al., 1994; Bradford and Vannice,1996; Ruckenstein et al., 1995; 1996; 1997; Hu et al., 1996; 1997; Kroll et al., 1996; Chen et al., 1999
	Ni/MgO-CaO	Yamazaki et al., 1992
	Ni/MgO-SiO_2	Takayasu et al., 1993, Takano et al., 1994
	Ni/MgO-SiO_2-Al_2O_3	Choudhary et al., 1995
	Ni/MgO-Re_2O_3-Al_2O_3	Wang et al., 1995
	Ni/La_2O_3	Zhang et al., 1995; 1996; 1996; Gronchi et al., 1996; Blom et al., 1994
	Ni/TiO_2	Osaki et al., 1994; 1996; 1997; Bradford and Vannice, 1996; Takanabe et al., 2005

Table 1.2 Contined

Time	Catalyst	Reference
	Ru/Al_2O_3	Vernon et al., 1992; Richardson et al., 1990, Ashcroft et al., 1991; Solymosi et al., 1991; Claridge et al., 1994
	Ru/CeO_2, Ru/La_2O_3, Ru/TiO_2, Ru/ZrO_2	Basini et al., 1995; Menad et al., 2003
	Ru/MgO	Rostrup-Nielsen et al., 1993; Qin et al., 1994; Takayasu et al., 1991; Basini et al., 1995; Qin et al., 1996; Schuurman et al., 2000
	Rh/Al_2O_3	Erdohelyi et al., 1993; Vernon et al., 1992; Richardson et al., 1990; Tsipopuriari et al., 1994; Kroll et al., 1996; Bhat et al., 1997; Ashcroft et al., 1991; Solymosi et al., 1991; Basini et al., 1995; Claridge et al., 1994, Nakamura et al., 1994, Walter et al., 1994; Zhang et al., 1996; Efstathiou et al., 1996; Mark et al., 1994; Ferreira-Aparicio et al., 2000
	Rh/Al_2O_3-SiO_2	Walter et al., 1994
	Rh/MgO	Basini et al., 1995; Zhang et al., 1996
	Rh/TiO_2	Bhat et al., 1997; Erdohelyi et al., 1993; Rasko and Solymosi, 1997; Tsipopuriari et al., 1994; Nakamura et al., 1994; Zhang et al., 1996
	Rh/TiO_2-SiO_2	Erdohelyi et al., 1993; Basini et al., 1995; Tsipopuriari et al., 1994; Mark et al., 1996; Nakamura et al., 1994; Zhang et al., 1996
	Pd/A_2O_3	Erdohelyi et al., 1994; Vernon et al., 1992; Swaan et al., 1994; Ashcroft et al., 1991; Solymosi et al., 1991; Mark et al., 1996; Gustafson et al., 1991
	Pd/MgO	Rostrup-Nielsen et al., 1993; Erdohelyi et al., 1994; Qin et al., 1994;1996; Takayasu et al., 1991
	Pd/TiO_2, Pd/SiO_2	Erdohelyi et al., 1994
	Ir/Al_2O_3	Takayasu et al., 1993; Takano et al., 1994
	Ir/MgO	Choudhary et al., 1995; Qin et al., 1994; 1996; Basini et al., 1995
	Ir/SiO_2	Erdohelyi et al., 1997
	Ir/TiO_2	Erdohelyi et al., 1997; Basini et al., 1995
	Pt/Al_2O_3	Ross et al., 1996; Vernon et al., 1992; Seshan et al., 1994; Chang et al., 1996; Solymosi et al., 1991; Mark et al., 1996; Efstathiou et al., 1996; Gustafson et al., 1991; Bitter etal.,1996; 1997; Nagaoka et al., 2000; Zhang et al., 2003
	Pt/MgO	Rostrup-Nielsen et al., 1993; Qin et al., 1994;1996
	Pt/SiO_2	Bradford et al., 1998
	Pt/TiO_2	Ross et al., 1996; Bradford et al., 1998
	Pt/ZrO_2	Nagaoka et al., 2000; Noronha et al., 2003
	Pt/ZrO_2-Al_2O_3	Souza et al., 2001

From Table 1.2, one also can see that a variety of supports or support combinations have been investigated since the nature of supports has significant effects on the performances and properties of catalysts. Supports have many functions but the most important is to maintain a stable physical surface, especially at high reaction temperatures. Therefore, the support itself must resist to thermal transformation at high temperatures, which means catalyst support must have high melting points. The melting points of catalyst supports that are most often studied in CO_2 reforming of CH_4 are tabulated in Table 1.3 (Richardson, 1989).

Table 1.3 Melting point of catalyst support materials

Support	Melting point (^oC)
Al_2O_3	2318
SiO_2	1973
MgO	3073
CaO	2853
TiO_2	2113
ZrO_2	2988
CeO_2	2873
La_2O_3	2588

Al_2O_3 and SiO_2 are two of the most often investigated catalyst supports with high specific surface area. MgO and CaO are studied due to their high melting points which favor stable catalyst surfaces at high reaction temperatures. Also, their basicity is believed to suppress carbon formation by promoting the activation of CO_2 (Zhang et al., 1994; Horiuchi et al., 1996; Yamazaki et al., 1992). TiO_2 and ZrO_2 are reducible metal oxides on

which metals are electron-rich and always show strong metal-support interaction (SMSI). SMSI is believed to be critical to resisting carbon formation. The oxides of rare-earth elements such as CeO_2 and La_2O_3 are investigated due to their ability to release and uptake oxygen (Eq. 1.2 and Eq. 1.3). When used as supports, these kinds of oxygen-ion conducting oxides are known to enhance catalytic performance resulting from the metal-support interactions (Metclfe and Sundaresan, 1988; Cho, 1991).

$$CeO_2 \leftrightarrow CeO_{2-x} + \frac{x}{2}O_2 \qquad 0 < x < 2 \tag{1.2}$$

$$La_2O_3 \leftrightarrow La_2O_{3-x} + \frac{x}{2}O_2 \tag{1.3}$$

Even though same active metals and supports are selected to make a catalyst, the performances of catalysts may be very different since catalyst performances are easily affected by a variety of other factors other than composition, such as preparation methods, thermal treatments, activation procedures, content of active components, precursors of active components, etc. This maybe the reason why some catalyst systems such as Ni/Al_2O_3 and Ni/MgO have been studied frequently by different research groups resulting in very different results and conclusions.

As discussed above, a lot of investigations have been conducted to develop catalysts for CO_2 reforming of CH_4. However, severe deactivation is still the major barrier preventing CO_2 reforming of CH_4 technology from large-scale industrial application. Currently, CALCOR and SPARG processes are the two commercial processes involving CO_2 reforming of CH_4. In the following sections, CALCOR and SPARG processes are briefly introduced.

1.2.3 CALCOR process

The CALCOR process (Teuner et al., 2001) was designed to produce high purity CO on-site to overcome problems involved in toxic CO transportation. A simplified flow sheet for CALCOR standard process, generalized from the work of Teunner et al. (2001) is shown in Fig. 1.3.

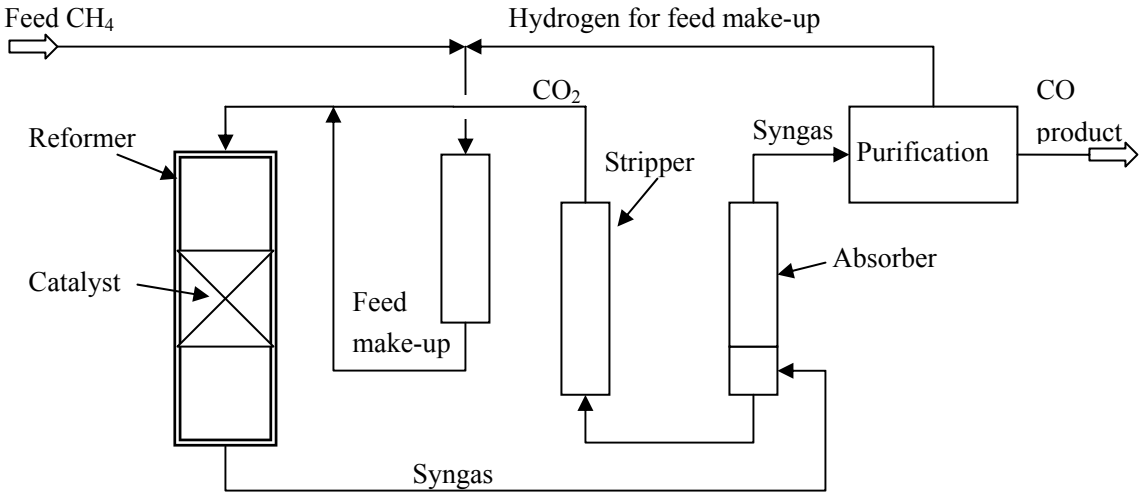

Fig. 1.3 Schematic of the CALCOR standard process (Teuner et al., 2001)

The CALCOR standard process is a catalytic reforming process of CH_4 or liquefied petroleum gas (LPG) at high temperature and low pressure. The feed has to be hydrodesulphurized before it is mixed with CO_2. When passing the reformer tubes, which are charged with reforming catalysts, the feed mixture is converted into synthesis gas consisting of CO, H_2, CO_2, H_2O and trace CH_4. Then the CO_2 is removed and recovered after the synthesis gas is cooled to ambient temperature. Finally, CO purification is conducted to remove H_2, CH_4, and traces of CO_2. The recovered CO_2 is recycled to the reforming process and the tail gas from the purification unit is burned as fuel.

1.2.4 SPARG process

The SPARG process, sulphur-passivated reforming (Udengaard et al., 1992), was designed to provide a synthesis makeup gas with a relatively low H_2/CO ratio for the synthesis of acetic acid, dimethyl ether and oxo-alcohols. It was commercialized in Sterling's Texas City Plant in 1987. A simplified flow sheet of SPARG process generalized from the work of Udengaard et al. (1992) is shown in Fig. 1.4.

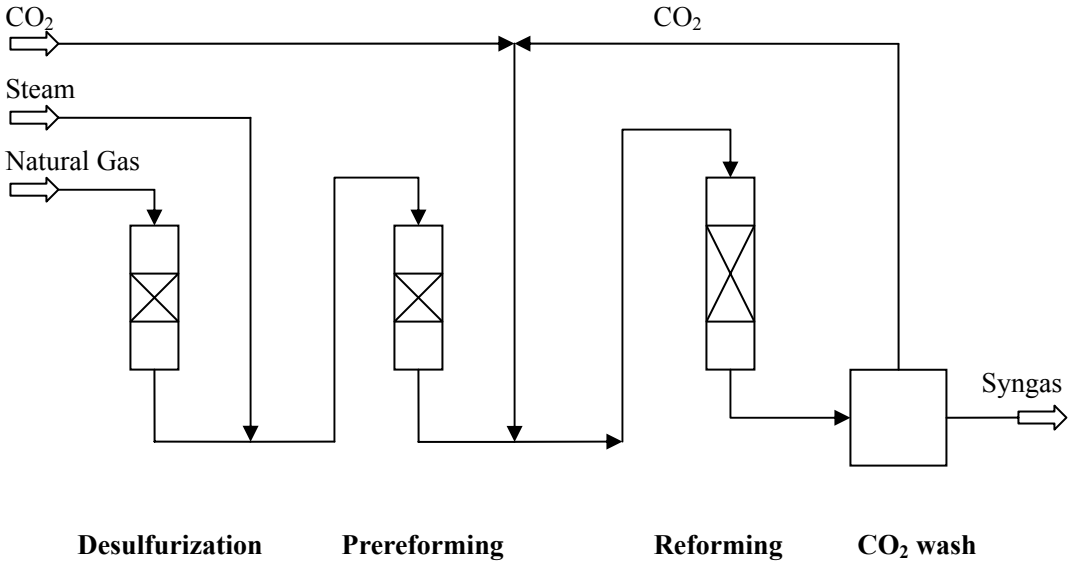

Fig. 1.4 Schematic of the SPARG process (Udengaard et al., 1992)

In the SPARG process, the natural gas is desulphurized and then mixed with steam to undergo pre-reforming. Until the prereformer was installed, Sterling had to interrupt operation every 2-3 months to remove carbon. In the tubular reformer, reforming catalyst is passivated by adding sulphur to the feed to block carbon formation sites. That is, bigger nickel sites favouring carbon formation are poisoned by sulphur while a fraction of smaller nickel sites sufficient for the reforming reaction remains intact. A molar ratio of

H_2/CO =1.8 was achieved at Sterling by controlling the molar H_2/hydrocarbon C ratio = 0.9 and the molar CO_2/hydrocarbon C ratio = 0.54.

1.3 SUMMARY OF CO_2 REFORMING OF CH_4 TECHNOLOGY

CO_2 reforming of CH_4 has attracted great attention due to both environment and energy concerns. The major problem of CO_2 reforming of CH_4 has been long known as the catalyst deactivation, which could be caused by carbon formation, sintering, and/or metal oxidation. The carbon formation problem can be reduced by adding steam as described in the SPARG process. The commercial application of CO_2 reforming of CH_4 is achieved in the CALCOR process and the SPARG process. However, a more interesting and challenging way is to develop a catalyst to overcome deactivation. The catalysts suffer severe deactivation as described above (section 1.2.1), primarily, as a result of carbon formation. The sintering problem shall be able to overcome through providing stable support surface for active components at high temperatures. Significant research work has been focused on finding an ideal catalyst support, which is stable at high temperature while maintaining a high surface area for catalysis. As for metal oxidation it has been reported that the formation of alloy can retard the process of oxidation during reaction. All of the efforts in overcoming carbon formation, sintering, and/or metal oxidation can be deemed to solve the catalyst deactivation problem associated with CO_2 reforming of CH_4.

1.4 RESEARCH OBJECTIVES AND SCOPE

Considering the major problems associated with CO_2 reforming of CH_4, the primary objective of this research is to develop a catalyst with long-term stability without severe deactivation and with the promise of industrialization.

The nickel-based non-precious metal catalysts are determined as the research objects with the consideration of catalyst cost and metal availability. Research and development of the catalysts for CO_2 reforming of CH_4 in this research includes: 1) catalyst design following Dowden's procedure (Dowden et al., 1968); 2) catalyst screening to find best catalyst composition for CO_2 reforming of CH_4; 3) catalyst characterization using different techniques to understand the surface properties, bulk properties, and electronic properties of the developed catalysts; 4) investigation on catalyst composition and pre-treatment procedures to find the best catalyst formulation that can meet the primary objective of the research; 5) kinetics study and mechanisms discussion.

1.5 ORGANIZATION OF THE THESIS

1 Introduction introduces some background and the development of CO_2 reforming of CH_4 technology. The necessity and significance of CO_2 reforming of CH_4 is discussed. The research and development status of this technology is presented.

2 Catalyst design and preparation method focuses on the catalyst design and preparation method. The reaction network of reactions involved in CO_2 reforming of CH_4

system and the stoichiometrically independent reactions that are required to depict the whole reaction network are analysed. Equilibrium compositions as a function of temperature, pressure, CO_2/CH_4 ratio, and inert gases are discussed. Also, carbon formation is analysed from a thermodynamic point of view. The catalyst formula is proposed based on desirable catalytic properties for the reaction. The catalyst preparation method is determined. Catalyst testing and products analysis are also introduced.

3 Development of long-term stable nickel catalysts for CO_2 reforming of CH_4 presents the catalyst development and screening which includes catalytic material determination and catalyst preliminary screening resulting in the research object of Ni-Co/$AlMgO_x$ system. Long-term stability testing and carbon formation behaviour are investigated over the Ni-Co/$AlMgO_x$. Also, catalyst characterization is conducted, which includes elemental composition determination, carbon formation analysis, reducibility test, and characterization of elemental oxidation states.

4 Effects of Ni and Co content on the Ni-Co/$AlMgO_x$ bimetallic catalysts for CO_2 reforming of CH_4 focuses on the Ni-Co content of Ni-Co/$AlMgO_x$ catalysts. The investigation on the effects of Ni-Co content on catalyst properties and performance are conducted with an attempt to avoid carbon formation. Catalysts with various Ni-Co contents are comparatively investigated. The relationship between catalyst performance and catalyst properties is discussed. The major cause of carbon formation on Ni-Co bimetallic catalyst is identified. Finally, carbon free operation for CO_2 reforming of CH_4 over a Ni-Co/$AlMgO_x$ is achieved.

5 Effects of calcination temperatures on the Ni-Co/AlMgO_x bimetallic catalysts for CO_2 reforming of CH_4 is based on the effects of calcination temperature on the catalyst properties and performance. The evolution behavior of catalyst structure during calcinations is presented.

6 Kinetic studies of CO_2 reforming of CH_4 over Ni-Co/AlMgO_x Catalyst is the systematic experimental and kinetic study of CO_2 reforming of CH_4 using a 0.04Ni0.05Co/AlMgO_x catalyst. The kinetic behaviour of the 0.04Ni0.05Co /AlMgO_x catalyst in the reforming reaction is investigated as a function of temperature and partial pressures of CO_2 and CH_4 in a temperature range 923-1023 K. The mechanism of the CO_2 reforming reaction has been discussed based on experimental observation considering literature. Rate limiting steps are identified. Both Power-Low model and Langmuir-Hinshelwood (L-H) model are developed and discussed.

7 Conclusions and recommendations is a summary for major conclusions of the research work. Future works are recommended.

2 CATALYST DESIGN AND PREPARATION

This chapter presents the catalyst design and preparation. The catalyst design described in this chapter follows the Dowden's strategy of catalyst design (Dowden et al. 1968), which starts from the stoichiometric analysis of the network of reaction, through thermodynamic analysis, reaction mechanism hypothesis, desirable catalytic property defining, and ends with catalyst composition requirement. Catalyst preparation methodology is also discussed. Preliminary experimental results are used to validate the calculation of equilibrium compositions.

2.1 CATALYST DESIGN

2.1.1 Defining objectives for catalyst design

In this research, new catalysts are proposed following the procedures of Dowden's strategy of catalyst design (Dowden et al., 1968) whose major procedures, as shown in Fig. 2.1, include stoichiometric analysis, thermodynamic analysis, proposed mechanism, necessary catalyst properties, catalytic material screening, and proposed catalysts and their compositions. The major objectives of the catalyst design are 1) the identification of desired properties of catalysts for CO_2 reforming of CH_4; 2) the desired catalyst compositions; and 3) the selection of catalytic materials. The following sections start with the stoichiometric analysis of the network of reaction involved in CO_2 reforming of CH_4.

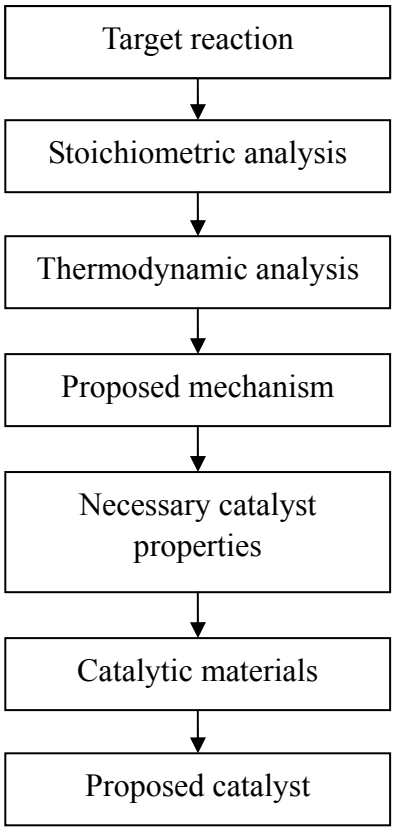

Fig.2.1 Steps in the catalyst design (Dowden et al., 1968)

2.1.2 Target reaction

The target reaction in this research is shown by Eq. 2.1. In this reaction CH_4 is reformed with CO_2 to produce CO and H_2, which is called synthesis gas.

$$CO_2 + CH_4 \leftrightarrow 2CO + 2H_2 \tag{2.1}$$

The reaction is highly endothermic. At a temperature lower than 916 K, the reaction Gibbs free energy change is positive, i.e. $\Delta G^{o}_{r,T<916K} > 0\,\text{kJ}$. From the thermodynamic perspective, CO_2 reforming of CH_4 is not likely to occur spontaneously at a temperature lower than 916 K. Therefore, temperatures higher than 916 K should be employed. However, the chance of side reactions increases at higher temperatures. Therefore, first of all, a system of reactions was developed stoichiometrically at 1023 K.

1023 K is the reaction temperature commonly found for CO_2 reforming of CH_4 in literature (Bradford and Vannice, 1999). Then, the reactions that are not likely to occur spontaneously are eliminated using simple thermodynamic principle, i.e. reactions with positive Gibbs free energy change are ruled out.

2.1.3 Stoichiometric analysis

Stoichiometrically possible reactions are listed as: 1) primary reactant reactions, 2) reactant self-interactions, 3) reactant cross-interactions, 4) reactant-product reactions, and 5) product-product reactions (Richardson 1989). However, only the reactions involving chemically stable compounds at 1023 K are considered to be physically realistic. The Gibbs free energy change $\Delta G^0_{r,1023K}$ of reaction can be calculated using the third law method (Kyle, 1999). Detailed procedures are introduced in Appendix D.

2.1.3.1 Primary reactant reaction

CO_2 and CH_4 are the primary reactants involved in CO_2 reforming of CH_4. The primary reactant reactions as shown in Table 2.1 are hereby defined as the ones involving only one primary reactant molecule. One can see that the CH_4 decomposition is the only primary reactant reaction in CO_2 reforming of CH_4. CH_4 decomposition is thermodynamically favourable while a single CO_2 molecule does not react at 1023 K.

Table 2.1 Primary reactant reaction

Reaction	$\Delta G^0_{r,1023K}$ (kJ)
Single CO_2 does not react at 1023 K	Not appliable
$CH_4 \leftrightarrow C + 2H_2$	-22

2.1.3.2 Reactant self-interaction reactions

The reactant self-interaction reactions are those involving two molecules of the same reactant. As presented in Table 2.2, C_2 hydrocarbons can be produced through the interaction of CH_4 molecules, while there is no reaction between two CO_2 molecules. At 1023 K the Gibbs free energy changes of the CH_4 self-interaction reactions are all greater than zero. From the thermodynamic perspective, these reactions are not favourable at 1023 K. Therefore, at this temperature their existence in CO_2 reforming of CH_4 reaction system can be neglected.

Table 2.2 Reactant self-interaction reactions

Reaction	$\Delta G^0_{\mathrm{r,1023K}}$ (kJ)
No reaction between two CO_2 at 1023K	Not applicable
$2CH_4 \leftrightarrow C_2H_6 + H_2$	71
$2CH_4 \leftrightarrow C_2H_4 + 2H_2$	77
$2CH_4 \leftrightarrow C_2H_2 + 3H_2$	126

2.1.3.3 Reactant cross-interaction reactions

The reactions between different reactant molecules are defined as reactant cross-interaction reactions which include the target reaction (Eq. 2.1) and other parallel cross-interaction reactions as listed in Table 2.3. They are thermodynamically favourable.

Table 2.3 Reactant self interaction reactions

Reaction	$\Delta G^o_{r,\,1023K}$ (kJ)
$CH_4 + CO_2 \leftrightarrow 2CO + 2H_2$	-31
$CH_4 + 2CO_2 \leftrightarrow 3CO + H_2O + H_2$	-31
$CH_4 + 3CO_2 \leftrightarrow 4CO + 2H_2O$	-27

2.1.3.4 Reactant-product reactions

One type of side reactions are those taking place between the reactant and the product molecules as reported in Table 2.4. Reverse water-gas shift reaction (RWSR) is the major side reaction in CO_2 reforming of CH_4 (Bradford et al., 1999). This side reaction consumes H_2 and produces side product H_2O. Therefore, the RWSR is kept for further investigation even though its Gibbs free energy of reaction is positive as shown in Table 2.4. The side product of H_2O can also react with CH_4 leading to steam reforming. The side reaction between CO_2 and C deposit may serve as the carbon removal reaction.

Table 2.4 Reactant-product reactions

Reaction	$\Delta G^0_{r,\,1023K}$ (kJ)
$CH_4 + 2H_2O \leftrightarrow CO_2 + 4H_2$	-35
$CH_4 + H_2O \leftrightarrow CO + 3H_2$	-33
$CO_2 + C \leftrightarrow 2CO$	-9
$CO_2 + H_2 \leftrightarrow CO + H_2O$	2
$CO_2 + 2H_2 \leftrightarrow C + 2H_2O$	13
$CO_2 + 4H_2 \leftrightarrow CH_4 + 2H_2O$	35

2.1.3.5 Product-product reactions

Side reactions can also occur between product molecules as presented in Table 2.5. From the thermodynamic point of view, the reaction between H_2O and C deposit is likely to occur while other reactions between CO and H_2 are not favourable at 1023 K.

Table 2.5 Product-product reactions

Reactions	$\Delta G^0_{r,\,1023K}$ (kJ)
$H_2O + C \leftrightarrow H_2 + CO$	-11
$CO + H_2 \leftrightarrow HCHO$	122
$CO + 2H_2 \leftrightarrow CH_3OH$	150
$nCO + mH_2 \leftrightarrow C_nH_{2(m-n)} + nH_2O$	>0

2.1.3.6 Network of reaction

From above discussion, in addition to the target reaction (Eq. 2.1), the possible side reactions that are thermodynamically favourable at 1023 K are steam reforming of CH_4 and RWSR (Table 2.4), CH_4 decomposition (Table 2.1), reactant cross reactions (Table 2.3), and carbon removal reactions (Table 2.4 and 2.5). They are listed as follows:

$$CO_2 + CH_4 \overset{K_1}{\longleftrightarrow} 2CO + 2H_2 \quad (2.1)$$

$$CO_2 + H_2 \overset{K_2}{\longleftrightarrow} CO + H_2O \quad (2.2)$$

$$H_2O + CH_4 \overset{K_3}{\longleftrightarrow} CO + 3H_2 \quad (2.3)$$

$$CH_4 \overset{K_4}{\longleftrightarrow} C + 2H_2 \quad (2.4)$$

$$C + CO_2 \overset{K_5}{\longleftrightarrow} 2CO \quad (2.5)$$

$$C + H_2O \overset{K_6}{\longleftrightarrow} CO + H_2 \quad (2.6)$$

$$CH_4 + 2CO_2 \overset{K_7}{\longleftrightarrow} 3CO + H_2O + H_2 \quad (2.7)$$

$$CH_4 + 3CO_2 \overset{K_8}{\longleftrightarrow} 4CO + 2H_2O \quad (2.8)$$

To simplify discussion, independent reactions which are sufficient to describe the reaction system have been determined. The number of independent reactions was determined by obtaining the rank of the stoichiometric coefficient matrix (Fogler, 1986). The stoichiometric coefficient matrix is expressed by Eq. 2.9 where the coefficients of reactants are taken with a negative sign and those of products are taken with a positive sign. Reducing the matrix, Eq. 2.10 can be derived from Eq. 2.9.

The rank of the matrix indicated by Eq. 2.10 is 3, and correspondingly any three independent equations can be selected to describe the reaction system sufficiently. For

example, Eq. 2.1, Eq. 2.2, and Eq. 2.4 as one set of independent reactions can be chosen. It is also noted that there is one reaction out of any three independent reactions involves carbon formation or removal.

	CH_4	CO_2	CO	H_2	H_2O	C
Eq.2.1	−1	−1	2	2	0	0
Eq.2.2	0	−1	1	−1	1	0
Eq.2.3	−1	0	1	3	−1	0
Eq.2.4	−1	0	0	2	0	1
Eq.2.5	0	−1	2	0	0	−1
Eq.2.6	0	0	1	1	−1	−1
Eq.2.7	−1	−2	3	1	1	0
Eq.2.8	−1	−3	4	0	2	0

(2.9)

	CH_4	CO_2	CO	H_2	H_2O	C
Eq.2.1	−1	−1	2	2	0	0
Eq.2.2	0	−1	1	−1	1	0
Eq.2.3	0	0	0	0	0	0
Eq.2.4	−1	0	0	2	0	1
Eq.2.5	0	0	0	0	0	0
Eq.2.6	0	0	0	0	0	0
Eq.2.7	0	0	0	0	0	0
Eq.2.8	0	0	0	0	0	0

(2.10)

2.1.4 Thermodynamic analysis

2.1.4.1 Equilibrium constant

For homogeneous gas-phase reactions at low to moderate pressures, the equilibrium constant can be written as (Kyle, 1999):

$$K = \prod \left[\frac{y_j P}{\hat{f}_j^o} \right]^{v_j} \tag{2.11}$$

where P is overall pressure and y_j is vapour molar fraction of species j. $\hat{f}_j^o$ is the standard fugacity of species j, which is 1 atm at standard state (Kyle, 1999). The condition of equilibrium for a chemical reaction at temperature T is:

$$\Delta G^o = -RT \ln K \tag{2.12}$$

where R is the gas law constant and ΔG^o is the standard Gibbs free energy change representing the conversion of reactants in their standard states to products in their standard states. The ΔG^o is a function only of temperature and can be calculated by the third law method (Kyle, 1999) at different temperatures (see Appendix-D for detailed procedures). Then, reaction equilibrium constant can be calculated from Eq. 2.13:

$$K = e^{-\Delta G^o / RT} \tag{2.13}$$

The variation of the reaction equilibrium constant for the reactions of Eq. 2.1-2.6 with various temperatures is shown in Fig. 2.2. Eq. 2.7 and 2.8 are basically combinations of Eq.2.1 and 2.2 so that thery not considered.

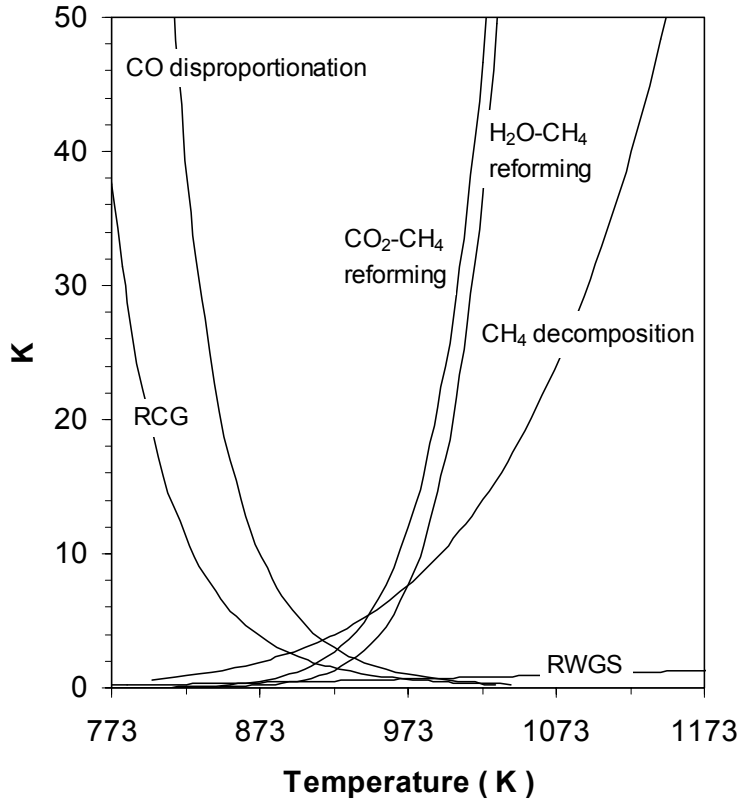

Fig.2.2 Variation of reaction equilibrium constants *K* with temperatures

CO_2-CH_4 reforming: CO_2 reforming of CH_4 (Eq. 2.1); H_2O-CH_4 reforming: steam reforming of CH_4 (Eq. 2.2); RWSR: reverse water-gas shift reaction (Eq. 2.3); CH_4 decomposition (Eq. 2.4); CO disproportionation (the reverse reaction of Eq. 2.5); RCG: reverse carbon gasification (the reverse reaction of Eq. 2.6).

Firstly, for the strong endothermic reforming reactions, Eq. 2.1 (ΔH^{o}_{298K} = 247 kJ), Eq. 2.2 (ΔH^{o}_{298K} = 206 kJ), and CH_4 decomposition (Eq. 2.4, ΔH^{o}_{298K} =75 kJ), the equilibrium constant increases dramatically with the increase in temperatures and hence higher temperatures favor higher equilibrium conversions. Secondly, RWSR reaction (Eq. 2.3, ΔH^{o}_{298K} = 41 kJ) is a moderately endothermic reaction. Its equilibrium constant increases slowly with the temperature increase. Lastly, CO disproportionation (the reverse reaction of Eq. 2.5, ΔH^{o}_{298K} = -172 kJ) and the reverse carbon gasfication reaction (RCG,

the reverse reaction of Eq. 2.6, ΔH^{o}_{298K} = -131kJ) are highly exothermic reactions. Their equilibrium constants decrease dramatically with the increase in temperatures and conversions are suppressed at higher temperatures. Hence carbon formation from these two reactions is unfavorable at higher reaction temperatures.

2.1.4.2 Equilibrium composition as a function of temperature

The variation of equilibrium composition with temperatures can be determined by solving a group of nonlinear equations relating the moles of each component to the equilibrium constant of independent reactions according to Eq. 2.11. In this thesis, the equilibrium composition as a function of reaction temperature is calculated based on two independent reactions without considering the third one involving carbon formation. The reaction involving carbon formation is not considered due to the very small magnitude (6.3×10^{-4} %) of carbon formation in comparison with the total carbon element involving CO_2 reforming of CH_4 (Zhang et al., 2007). Fig. 2.3 shows the effects of reaction temperature on the equilibrium composition at 1 atm and initial $CH_4/CO_2/N_2$ ratio of 1/1/0.

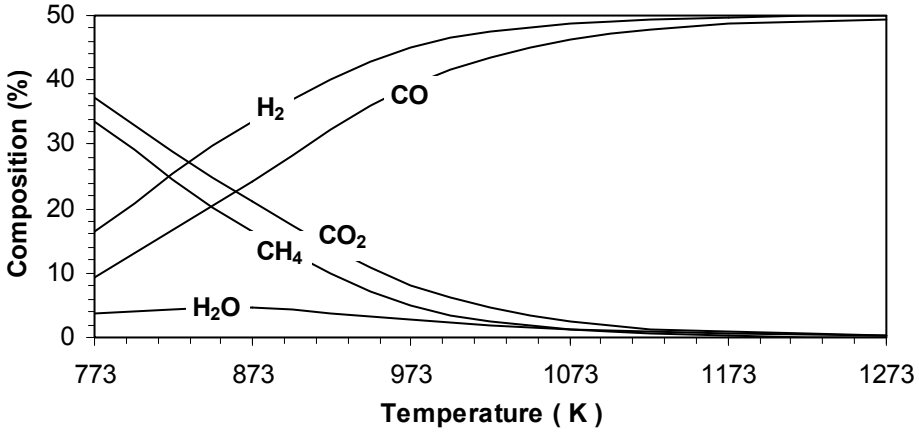

Fig. 2.3 Variation of equilibrium composition with temperatures

From Fig. 2.3, it can be seen that the proportions of H_2 and CO increase while the fractions of H_2O, CH_4, and CO_2 decrease with the increase in temperatures. The effects of temperatures on the equilibrium composition can be ascribed to that at higher temperatures the contribution of RWSR becomes less due to its moderately endothermic property in comparison with the strong endothermic property of CO_2 reforming of CH_4 (Eq. 2.1) and CH_4 decomposition (Eq. 2.4). As a result of the temperature influence on RWSR, the molar ratio of H_2 to CO becomes closer to unity at higher temperatures (Fig. 2.3) since less fraction of H_2 is converted to H_2O through the RWSR. Therefore, it is preferable to apply a higher temperature, such as 1023 K, to reduce the reactant concentration and, as a result, to increase the CO and H_2 concentrations in the product stream. As discussed above, the effect of side reaction, RWSR, is relatively insignificant at higher reaction temperatures.

2.1.4.3 Equilibrium composition as a function of total pressure

Fig. 2.4 shows the effects of total pressure on the equilibrium composition.

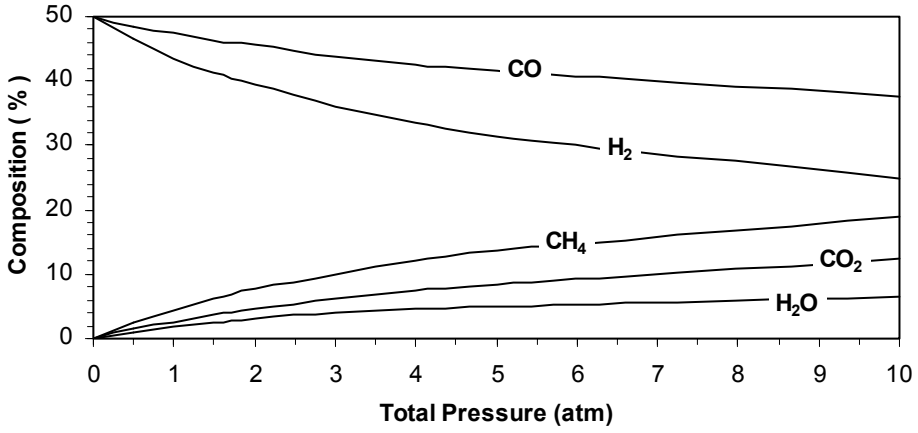

Fig.2.4 Effects of total pressure on equilibrium composition at 1023 K and initial $CO_2/CH_4/N_2$ ratio of 1/1/0

One can see that the reactant concentrations increase with the increase in total pressure while the product concentrations drop. As a reaction with increase in volume, the equilibrium of CO_2 reforming of CH_4 (Eq. 2.1) shifts to the left-hand side at higher total pressures while the equilibrium of RWSR (Eq. 2.2) as a volume constant reaction is not affected by the total pressure changes.

Using the equilibrium composition data, the CH_4 conversion and H_2 selectivity can be calculated and the detailed calculation procedures are described in Appendix E. Fig. 2.5 shows the CH_4 conversion as a function of reaction temperatures and pressures at initial $CH_4/CO_2/N_2$ ratio of 1/1/0. Fig. 2.6 shows the variation of H_2 selectivity with reaction temperatures and pressures at initial $CH_4/CO_2/N_2$ ratio of 1/1/0. The observations from the two figures are the same: conversion and selectivity increase with temperature increases while droping with the increase in pressures.

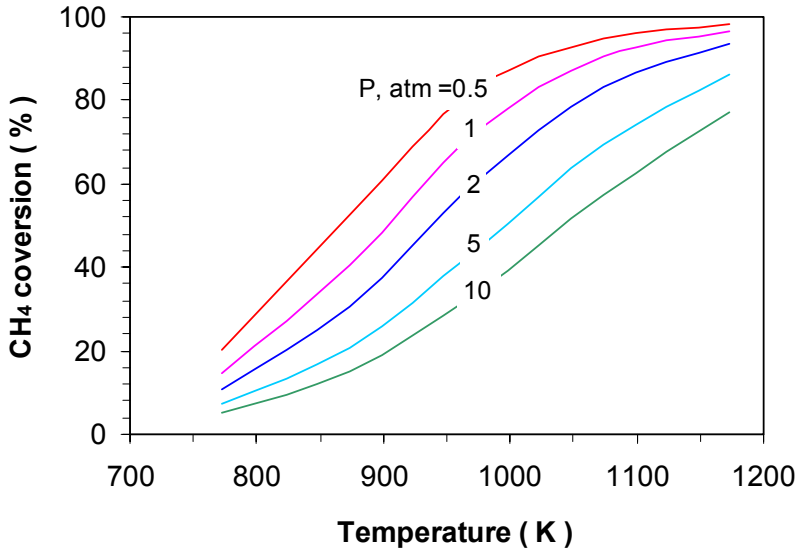

Fig. 2.5 Effects of temperatures and pressures on CH_4 conversion

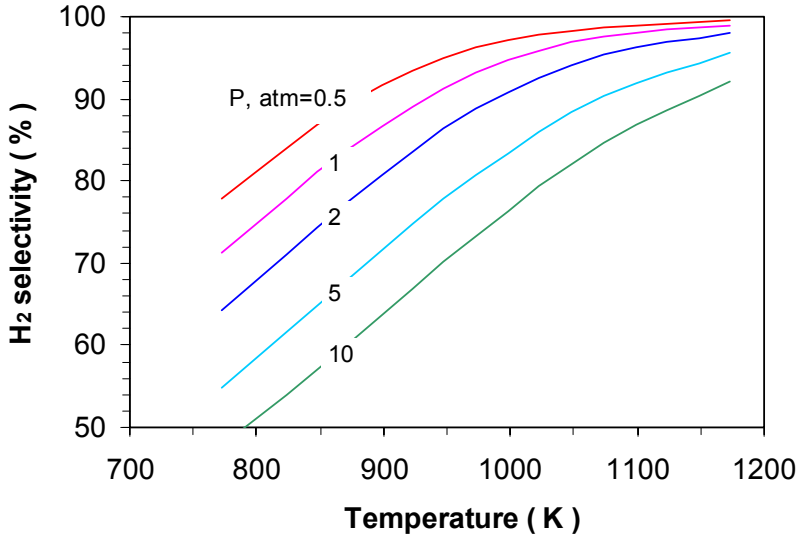

Fig.2.6 Effects of temperatures and pressures on H_2 selectivity

2.1.4.4 Equilibrium composition as a function of initial CO_2/CH_4 molar ratio

The equilibrium composition as a function of initial CO_2/CH_4 molar ratio is shown in Fig. 2.7. It is seen that the composition of CH_4 decreases quickly due to the increase in CH_4 reaction with CO_2. At the initial CO_2 to CH_4 ratio of 3, most of CH_4 is reacted. At around CO_2 to CH_4 ratio of 1, H_2 reaches its maximum. When CO_2 to CH_4 ratio is higher than 1, more product H_2 reacts with CO_2 through RWSR, resulting in the decrease in H_2 and the increase in both CO and H_2O. After H_2O reaches its maximum level, reactions tend to stop due to the depletion of CH_4. The product concentrations drop gradually due to the dilution effect of CO_2.

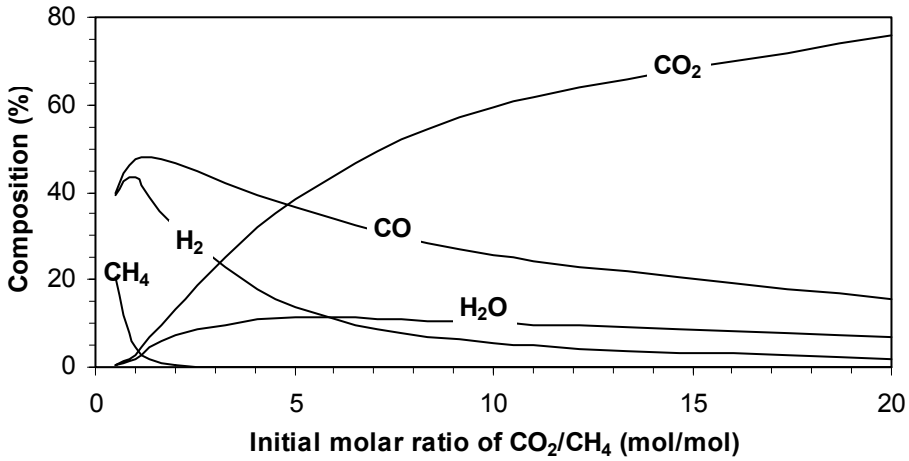

Fig.2.7 Effects of initial CO_2/CH_4 on equilibrium composition at 1023 K and 1 atm

2.1.4.5 Effects of inert N_2

In most of the experiments of this research, inert N_2 was employed as the internal standard for GC analysis. The effects of N_2 on conversion and selectivity at 1 atm, various temeratures, and initial CH_4/CO_2 ratio of 1/1 were calculated and the results are shown in Fig. 2.8. It can be seen that the existence of N_2 can enhance both CH_4 conversion and H_2 selectivity at various temperatures, the higher the N_2 concentration, the higher the degree of enhancement on CH_4 conversion and H_2 selectivity.

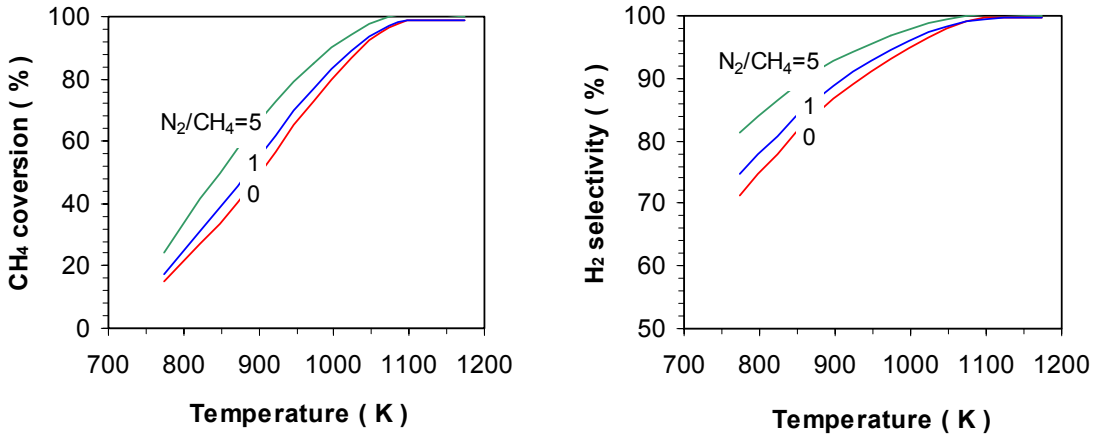

Fig.2.8 Effects of inert N_2 gas on CH_4 conversion and H_2 selectivity

2.1.4.6 Carbon formation

In this section, carbon formation is discussed using a thermodynamic analysis method that Ginsberg et al. (2005) used. The reactions involving carbon formation are those represented by Eq. 2.4, 2.5, and 2.6. According to Eq. 2.11, the equilibrium constants of these three reactions can be expressed by Eq. 2.14-2.16:

$$\mathrm{CH_4} \xleftrightarrow{\mathrm{K_4}} \mathrm{C} + 2\mathrm{H_2} \qquad K_4 = \left(\frac{p^{\mathrm{e}}_{\mathrm{H_2}}}{\hat{f}^{\mathrm{o}}_{\mathrm{H_2}}} \right)^2 \Bigg/ \left(\frac{p^{\mathrm{e}}_{\mathrm{CH_4}}}{\hat{f}^{\mathrm{o}}_{\mathrm{CH_4}}} \right) \tag{2.14}$$

$$\mathrm{C} + \mathrm{CO_2} \xleftrightarrow{\mathrm{K_5}} 2\mathrm{CO} \qquad K_5 = \left(\frac{p^{\mathrm{e}}_{\mathrm{CO}}}{\hat{f}^{\mathrm{o}}_{\mathrm{CO}}} \right)^2 \Bigg/ \left(\frac{p^{\mathrm{e}}_{\mathrm{CO_2}}}{\hat{f}^{\mathrm{o}}_{\mathrm{CO_2}}} \right) \tag{2.15}$$

$$\mathrm{C} + \mathrm{H_2O} \xleftrightarrow{\mathrm{K_6}} \mathrm{CO} + \mathrm{H_2} \qquad K_6 = \left(\frac{p^{\mathrm{e}}_{\mathrm{CO}}}{\hat{f}^{\mathrm{o}}_{\mathrm{CO}}} \right) \left(\frac{p^{\mathrm{e}}_{\mathrm{H_2}}}{\hat{f}^{\mathrm{o}}_{\mathrm{H_2}}} \right) \Bigg/ \left(\frac{p^{\mathrm{e}}_{\mathrm{H_2O}}}{\hat{f}^{\mathrm{o}}_{\mathrm{H_2O}}} \right) \tag{2.16}$$

where, superscript e is used to indicate the partial pressure at equilibrium state. $\hat{f}^{\mathrm{o}}_{\mathrm{j}}$ is the standard fugacity of species j. At any state including equilibrium state, three parameters α, β, and γ are also defined accordingly as shown by Eq. 2.17-2.19:

$$\alpha = \left(\frac{p_{\mathrm{H_2}}}{\hat{f}^{\mathrm{o}}_{\mathrm{H_2}}} \right)^2 \Bigg/ \left(\frac{p_{\mathrm{CH_4}}}{\hat{f}^{\mathrm{o}}_{\mathrm{CH_4}}} \right) \tag{2.17}$$

$$\beta = \left(\frac{p_{\mathrm{CO}}}{\hat{f}^{\mathrm{o}}_{\mathrm{CO}}} \right)^2 \Bigg/ \left(\frac{p_{\mathrm{CO_2}}}{\hat{f}^{\mathrm{o}}_{\mathrm{CO_2}}} \right) \tag{2.18}$$

$$\gamma = \left(\frac{p_{CO}}{\hat{f}^{o}_{CO}} \right) \left(\frac{p_{H_2}}{\hat{f}^{o}_{H_2}} \right) \Bigg/ \left(\frac{p_{H_2O}}{\hat{f}^{o}_{H_2O}} \right) \tag{2.19}$$

When the system is at equilibrium conditions, we have:

$$\alpha = K_4,\ \beta = K_5,\ \text{and}\ \gamma = K_6 \tag{2.20}$$

If $\alpha < K_4$, $\beta > K_5$, and $\gamma > K_6$, all the reactions move toward the direction of carbon formation. Carbon formation is favourable. However, if $\alpha > K_4$, $\beta < K_5$, and $\gamma < K_6$, carbon formation is not thermodynamically favourable. At a certain initial $CO_2/CH_4/N_2$ ratio and 1 atm, trial and error method can be used to solve a group of non-linear equations to find a certain border temperature above which carbon formation is not thermodynamically favourable, i.e. $\alpha > K_4$, $\beta < K_5$, and $\gamma < K_6$. As shown in Fig. 2.9, carbon formation zone and carbon free zone are obtained. The presence of inert gas, N_2, can slightly affect the border between carbon formation zone and carbon free zone. However, at the ideal feed ratio of CO_2/CH_4=1/1, carbon formation is seen inevitable from Fig. 2.9. The increase of CO_2 in feed may inhibit carbon formation. However, it is not practical to use excess CO_2 to inhibit carbon formation from an industrial point of view due to the high cost of product separation. Therefore, at the industrially practical conditions, i.e. CO_2/CH_4 = 1/1 and 923 K < T < 1323 K, the only way to suppress carbon formation is to seek carbon resistant catalysts on which the extent of carbon formation does not cause catalyst deactivation.

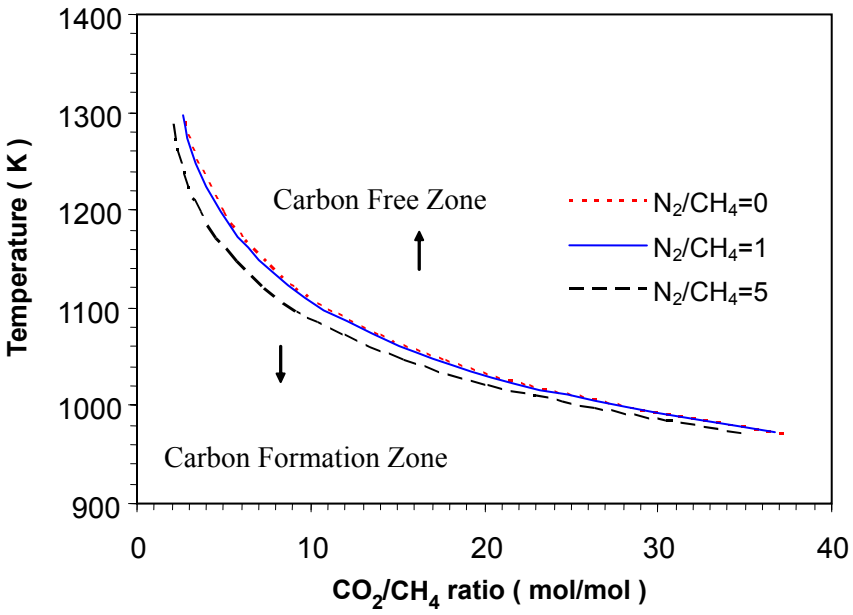

Fig. 2.9 Effects of CO_2/CH_4 ratio and inert gas N_2 on limiting temperatures below which carbon formation occurs at 1 atm

2.1.5 Proposed mechanism

The dissociation of CH_4 is believed as one of the initial steps for the methane reforming reaction (Hickman and Schmidt, 1993). Two H_2 molecules and one CO molecule are formed via H and CH_x (x = 0-3) species originated from the dissociation of CH_4. The presence of CH_x species on the surface of catalysts have been confirmed through pulsing experiments (Osaki et al., 2001; Yan et al., 2003) and transient isotopic studies (Bradford and Vannice, 1996; Aparicio et al., 1997). It is reported that reversible adsorption of CH_4 on the surface of catalyst leads to cracking of CH_4 and the cracking is a rate determining step (RDS) while CH_4 adsorption is at equilibrium (Schuurman et al., 1998; Tsipouriari and Verykios, 1999; 2001):

$$CH_4 + M \leftrightarrow CH_4 - M \qquad \text{Equilibrium} \qquad (2.21)$$

$$CH_4 - M \rightarrow C - M + 2H_2 \qquad \text{RDS} \qquad (2.22)$$

where M is the active sites on metals.

The participation of CO_2 molecules can be through its dissociative chemisorption. Infrared spectroscopy has indicated that CO_2 can dissociate to carbon monoxide and adsorbed O (Bitter et al., 1997; 1998). The carbon monoxide formed is released to the gas phase immediately (Solymosi, 1991).

$$CO_2 + 2S \leftrightarrow CO\text{-}S + O - S \qquad (2.23)$$

where S is the active sites on support.

Rostrup-Nielsen and Hansen (1993) and Kim et al. (1994) assumed the dissociative chemisorption of CO_2 as limiting step. However, Hei et al. (1998) reported that both dissociation of CH_4 and CO_2 may be rate-limiting steps based on the same magnitude of the activation barrier of them. Kroll et al. (1996) suggested that the oxidation step, as represented by Eq. 2.24, should be rate-limiting step due to the lack of kinetic isotopic effect for the formation of CO during the CO_2 reforming of CH_4:

$$C - M + O - S \rightarrow CO + M + S \qquad (2.24)$$

where, C-M originated from the dissociation of CH_4 and O-S from the dissociation of CO_2. The participation of CO_2 may also be through directly reacting with the C-M species in the form of intact activated molecule (Eq. 2.25) (Erdohelyi et al., 1991; Mark et al., 1994; 1996; Schuurman et al., 1998).

$$CO_2 + C - M \rightarrow 2CO + M \qquad (2.25)$$

Based on above discussion, a surface reaction mechanism is proposed for defining the necessary properties of catalysts for CO_2 reforming of CH_4. As shown in Fig. 2.10, the dissociative chemisorption of CH_4 occurs on the metallic centers as the metallic state of catalysts is believed to be responsible for the CH_4 activation (Yan et al., 2003). The absorption of CO_2 is supposed to take place on the surface of support since the carbon in CO_2 molecule as a Lewis acid centre tends to react with Lewis base centre of an oxide. The reaction between M-C species and activated S-CO_2 is assumed as the rate determining step based on the following logic and fact: 1) if the dissociation of CH_4 is RDS, carbon accumulation is unlikely to occur; and 2) carbon accumulation has been a well-known challenge for CO_2 reforming of CH_4, which means carbon species formation rate is higher than carbon species removal rate.

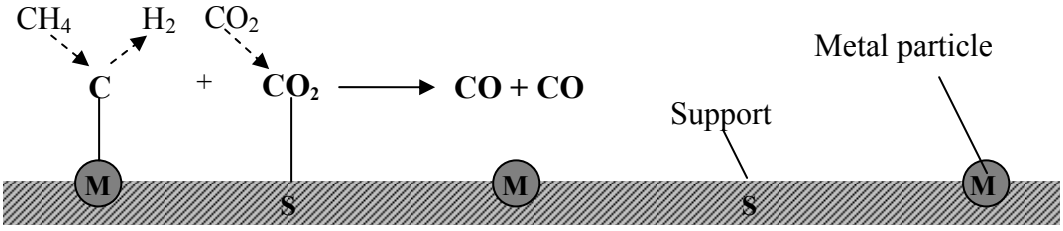

Fig. 2.10 Proposed surface mechanism for CO_2 reforming of CH_4

2.1.6 Desired catalyst properties

An ideal catalyst has high activity, good selectivity, and excellent stability. Activity is the term used to describe qualitatively how effective a given catalyst is in carrying out a specified reaction (Cornils et al., 2003). For CO_2 reforming of CH_4, based

on the proposed mechanism, catalysts should facilitate the rate determining step (Eq. 2.24) to improve the reaction rate. Good selectivity can be obtained if catalysts can inhibit side reactions such as RWSR and carbon formation reactions. As forementioned, the major causes of catalyst deactivation for CO_2 reforming of CH_4 are carbon formation, sintering, and metal oxidation. Therefore, the desired properties of proposed catalysts can be defined based on the proposed surface mechanism and previous stoichiometric and thermodynamic analysis along with the general principles of catalyst development and the common challenges of catalysts in CO_2 reforming of CH_4. The desired properties are described as P 1-5 as given below:

P-1 Surface dehydrogenation sites that can enhance the dissociation of methane to CH_x species and remove H species from the intermediate to form hydrogen;

P-2 Surface carbon dioxide adsorption sites that promote the activation or participation of CO_2 to remove C species derived from the decomposition of CH_4;

P-3 Adjacent surface sites of P-1 and P-2 that will facilitate the reaction between C species and activated CO_2 molecules so that the overall reaction rate can be improved;

P-4 Thermal stability that can retain catalyst physical and mechanic properties thus phase transitions and crystal transformation could be avoided at high reaction temperatures, such as 1023 K;

P-5 Uniform and stable dispersion of active components with small particle sizes which can promote CO_2 reforming of CH_4 while suppress carbon formation or

other undesired reactions because carbon formation active sites are believed larger than reforming active sites (Rostrup-Nielsen, 1984).

2.1.7 Scope of catalytic materials for CO_2 reforming of CH_4

A catalyst is basically composed of active component, secondary active component or promoter, catalyst support. The common metals used in catalysts are shown in Table 2.6.

Table 2.6 Physical data of common metals used in catalysts (Anderson, 1975)

Metal	Atomic weight	Crystal structure	Lattice parameter (nm)	Neighbour atomic distance (nm)	Melting point (K)
Al	26.98	f.c.c.	0.404	0.286	1033
Ba	137.34	b.c.c.	0.501	0.434	998
Cr	52	b.c.c.	0.289	0.249	2163
Co	48.93	f.c.c.	0.355	0.251	1768
Cu	63.54	f.c.c.	0.361	0.255	1356
Ir	192.2	f.c.c.	0.383	0.271	2683
Fe	55.85	b.c.c.	0.286	0.248	1808
La	138.91	h.c.p.	0.372; 0.606	0.371	1193
Mg	24.31	h.c.p.	0.321; 0.521	0.32	924
Mn	54.94	Complex	-	-	1517
Mo	95.94	b.c.c.	0.314	0.272	2883
Ni	58.71	f.c.c.	0.352	0.249	1726
Pd	106.4	f.c.c.	0.388	0.275	1825
Pt	195.09	f.c.c.	0.392	0.277	2042
K	39.10	b.c.c.	0.531	0.462	337
Re	186.2	h.c.p.	0.276; 0.445	0.274	3453
Rh	102.91	f.c.c.	0.380	0.268	2239
Ru	101.07	h.c.p.	0.270; 0.427	0.267	2523
Ag	197.87	f.c.c.	0.408	0.288	1234
Na	22.99	b.c.c.	0.428	0.371	371
Ti	47.96	h.c.p.	0.295; 0.468	0.293	1948
W	183.85	b.c.c.	0.316	0.274	3683
V	50.94	b.c.c.	0.302	0.263	2163
Zn	65.37	h.c.p.	0.266; 0.494	0.266	692
Zr	91.22	h.c.p.	0.322; 0.512	0.319	2125

2.1.7.1 Determination of primary active component

It is well known that CO_2 reforming reaction with CH_4 can be catalyzed by most transition metals. The activity of common catalytic metals for dehydrogenation or hydrogenation follows the order given below (Trimm, 1980).

Ru, Rh, Pd, Ir, Pt > Fe, Co, Ni > W, Cr-Cu

Among them, the precious metals, such as ruthenium (Ru) and rhodium (Rh), and the non-precious metal nickel (Ni) have been studied extensively (Ostrupnielsen et al., 1993, Erdohelyi et al., 1993; Portugal et al., 2002; Richardson, 2003). It has been found that supported precious metal such as Rh, Ru, Pd, Pt, and Ir catalysts can provide stable operations for carbon dioxide reforming of methane and less carbon can be formed during the reaction (Bradford and Vannice, 1999) in comparison with non-precious metal catalysts. However, from an industrial standpoint, it is more practical to develop non-precious metal-based catalysts to avoid high cost and restricted availability of precious metals. Ni has drawn remarkable attention in this area due to its high activity and wide availability (Rostrup-Nielsen, 1997). In this research, Ni is chosen as the primary active component to meet the desired catalyst property described in P-1. However, Ni catalysts suffer severe catalyst deactivation. To overcome the problems of catalyst deactivation, the investigation of secondary active components (or catalyst promoters) and catalyst supports has attracted significant attention (Osaka and Mori, 2001; Seok et al., 2002; Dias and Assaf, 2003; Quincoces et al., 2001; 2002; Frusteri et al., 2001). Therefore, a secondary active component and catalyst support are also determined in the catalyst

design in this thesis.

2.1.7.2 Determination of targeted secondary active component

It is well known that a secondary active component or promoter can increase the performance and stability of the catalysts for CO_2 reforming of CH_4 in comparison with the corresponding monometallic catalysts (Sinfelt, 1983; Ponec et al., 1995). Tomisshge et al., (2000) investigated the additive of Sn, Ge, and Ga to a NiO-MgO solid solution and found that the addition of Sn can effectively decrease the carbon formation which was mainly resulted from the methane decomposition. The addition of Cr (Zhang et al., 1998; Wang et al., 2003) and Mn (Choi et al., 1998; Seok et al., 2002) was reported to have significant effect on the inhibition of carbide formation which was believed to be the intermediate for carbon formation (Trimm, 1997). Catalyst performance can also be improved when partial NiO was replaced with CoO in the NiO-MgO solid solution (Choudhary and Mamman, 1998). It was believed that a homogeneous alloy of Co and Ni and a small Ni substitution of Co dramatically enhance the catalyst activity and stability by improved resistance to metal oxidation (Takanabe et al., 2005).

In this research, the investigation for a secondary active component focuses on Co and Mn. Fe and Cu have also been investigated due to their high activity to dehydrogenation or hydrogenation (Trimm, 1980) and their close electronic configuration to that of Ni (Table 2.9). However, Cr was not considered due to its highly hazardous property which can impose great risk for workplace safety when Cr-containg dust problem arises.

2.1.7.3 Determination of catalyst support

From the thermodynamic point of view, as discussed, a high reaction temperature must be chosen to achieve high reactant conversion. However, at high temperatures, the active metal crystallites in the catalysts would contact each other through thermal motion. Even at the Hutting temperature, which is 0.3 times of the melting point of the substance, the surface atoms would have enough energy to overcome the weak surface crystal forces, then diffuse and form necks to decrease the surface energy (Richardson, 1989) resulting in sintering deactivation. Therefore, a high-melting point material should be used to increase resistance to sintering by providing a stable surface so that the desired catalyst property of P-4 can be met. MgO was selected because of its high melting point of 3346 K. Also the basic MgO can function as basic centers on the support for the activation of CO_2 because basicity was believed to promot the activation of acidic CO_2 and suppress carbon formation (Yamazaki et al., 1992; Horiuchi et al., 1996). In addition, the desired property of P-2 is also met by the existence of basic MgO as support. However, MgO has low specific surface area. Therefore, the high surface material Al_2O_3 is proposed to compensate the low surface area of MgO. Thus, a mixed framework of $AlMgO_x$ is proposed with the consideration of making use of the high thermal stability of MgO and the high specific surface area of Al_2O_3. At this stage of catalyst design, a catalyst formula, Ni-Me/$AlMgO_x$ (Me=Co, Fe, Cu, or Mn) is proposed correspondingly. With the proposed catalyst composition, the desired catalyst property of P-3 can be realized through the close contact of active component with support using proper catalyst preparation method, which

is also supposed to facilitate another desired property of P-5, the uniform dispersion of active component in the catalyst.

2.2 CATALYST PREPARATION

Most industrial catalysts are manufactured using either precipitation method or impregnation method (Delmon et al., 1976; 1979). Precipitated catalysts are generally prepared by rapid mixing of concentrated solutions of metal salts with a precipitating reagent while impregnated catalysts are made through the impregnation of active components onto a support material (Cornils et al., 2003). Details of a catalyst preparation process for a given catalyst are not always patented but rather kept as a business secret. Therefore, only some broad principles are available in the published literature. In the following sections, the two most often used industrial catalyst preparation methods are briefly discussed.

2.2.1 Precipitation method

2.2.1.1 Precipitating process and unit operation

Precipitation is usually defined as a process obtaining a solid from a liquid solution (Wijngaarden et al., 1998). To produce a precipitated catalyst, an amorphous or crystalline precipitate or gel needs to be generated first by mixing two or more solutions or suspensions of materials. The wet precipitate is then gone through filtration, washing, drying, calcination, and forming to become a fresh catalyst. A schematic of the typical precipitation process and major unit operations are shown in Fig. 2.11.

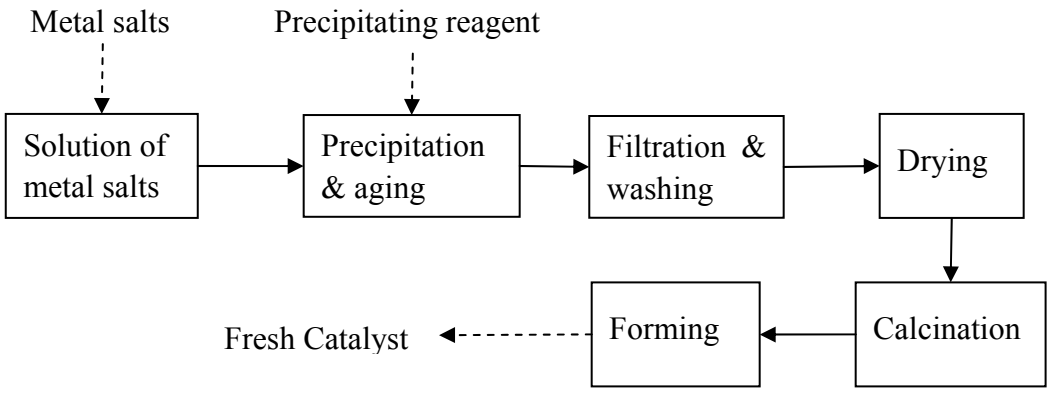

Fig. 2.11 Schematic of typical preparation process of precipitated catalysts

As presented in Fig. 2.11, a certain type and amount of metal salts are chosen and dissolved based on catalyst design, and then are precipitated by adding a precipitating reagent. A precipitate is obtained and unwanted ions are removed after filtration and washing. The precipitate is usually in the form of hydroxide, carbonate, oxalate, formate, or citrate. Water is removed by drying the precipitate. Designed catalyst is made after calcinating and forming by following certain procedures. The final precipitated catalyst is in the form of oxide or intimate mixed oxides. The size of crystallites present in the precipitated catalysts is typically in the range of 3-15 nm (Twigg, 1989).

2.2.1.2 Chemistry of precipitation

When a metal salt is dissolved in water, the metal ions are solvated by water molecules. The coordinated water molecules can be deprotonated to produce hydroxide or even oxide species. The deprotonation processes can be expressed by the following equilibria which depend on the charge of the metal and the pH of the solution (Jolivet et al., 1994).

$$[M-OH_2]^{n+} \xleftrightarrow{H^+} [M-OH]^{(n-1)+} \xleftrightarrow{H^+} [M=O]^{(n-2)+} \quad (2.26)$$

The formation of the oxides is favored for highly charged metal ions and/or high pH of the solution. There are several possibilities to shift the equilibria from the left-hand side to the right-hand side of Eq. 2.26, i.e., to obtain oxides from hydrated metal salts. For instance, a compound such as potassium hydroxide (KOH) can be used to raise the pH gradually, i.e., to remove the protons from the equilibrium. This corresponds to moving from left-hand side to right-hand side in Eq. 2.26 at a given charge. Alternatively, the solution can be simply aged at elevated temperatures. A higher temperature promotes dissociation of protons from the hydrated metal ions. The mechanism of the polycondensation of the hydroxide compounds eventually leads to precipitates (Jolivet et al., 1994). This process may be affected by the factors such as salt concentration, pH, nature of the counter ions, and temperatures.

2.2.1.3 Set-up for precipitation

The industrial process for the synthesis of large quantities of precipitated catalysts is the controlled double jet precipitation (CDJP) process (Jolivet et al., 1994). Compared with the CDJP process, most of the lab scale set-ups are very simple. A simple schematic of precipitation set-up is shown in Fig. 2.12. To make a precipitated catalyst in lab, simply introduce both solutions simultaneously into a beaker while stirring. The flow rates of both solutions are adjustable and can be fixed by control valves. The pH of the precipitation solution is monitored through pH indicators and maintained between 7 and 10. A precipitate can be generated in the process of precipitation. Then the following

filtration, washing, drying, calcination, and forming can be performed to make a fresh precipitated catalyst.

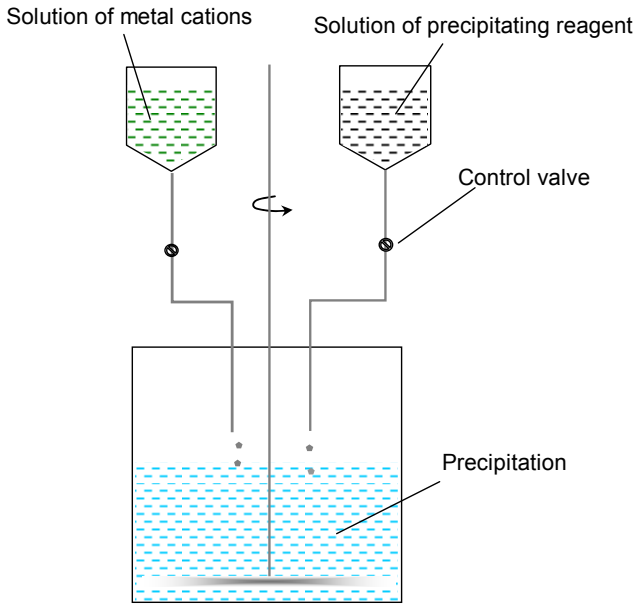

Fig. 2.12 Schematic of lab scale precipitation set-up

2.2.1.4 Advantages and disadvantages of precipitation method

Major advantages of precipitated catalysts can be generalized as: 1) uniform mixing on a molecular scale of different catalyst components; and 2) uniform distribution of active species throughout the catalyst. However, the precipitated catalysts may be more costly because significant portion of active components are inside the catalyst bulk in comparison with impregnated catalysts. Also, it is a challenge to form a catalyst with very small particle size and a surface area higher than 200 m^2/g (Wijngaarden et al., 1998).

2.2.2 Impregnation method

Impregnation of support material with a solution containing metal salts is one of

widely used catalyst preparation methods. In comparison with other catalyst preparation methods (Gaigneaux, 2002), impregnation method is simpler. A scheme for the production of an impregnated catalyst is shown in Fig. 2.13.

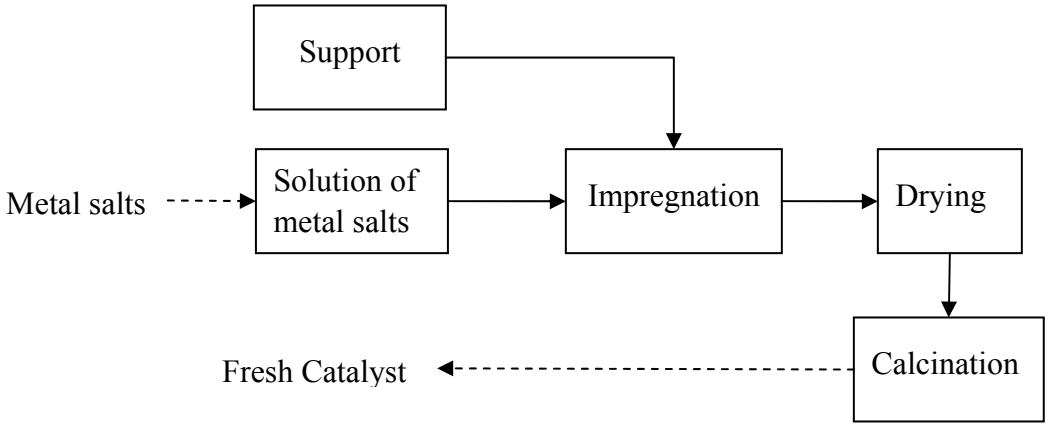

Fig. 2.13 Schematic of preparation process of impregnated catalysts

It can be seen from Fig. 2.13 that initially a solution containing active components is made. In the next step either the support material is dipped into the solution or the solution is sprayed onto the support. Drying is then performed to remove water or other solvent after the active component adsorbed into the pore system of the support. A fresh catalyst can be produced after calcination which converts the soluble salts into the insoluble oxides on the surface of supports.

The advantages of a impregnated catalyst are 1) well defined pore structure and surface area which are determined by commercially available supports; 2) more economic than precipitated catalysts, especially, in the cases of precious metal catalysts; 3) clear separation of active phases and support phases. A disadvantage of an impregnated catalyst is that only limited amount of active components can be incorporated in the catalyst. Also,

it is a challenge to produce uniform distribution of multi active components on a support through impregnation process. The support may adsorb certain components preferentially on the surface due to chromatographic effects (Wijngaarden et al., 1998).

2.2.3 Catalyst preparation

2.2.3.1 Determination of preparation method

As discussed in Section 1.2.2 of Chapter 1, the development of catalysts for CO_2 reforming of CH_4, most of transition metals that can be used to catalyze the reaction as well as most of readily available commercial supports have been investigated intensively and extensively. Unfortunately, catalyst deactivation basically due to carbon formation is still the major challenge in CO_2 reforming of CH_4. Therefore, repeated research on the metals and supports that have already been extensively investigated is most unlikely to provide satisfied solutions to the existing challenge. The development of novel catalyst system is of great interest.

In principle, catalysts are composed of active phases and support phases. According to the catalyst design (see Section 2.1.7), the designed catalyst includes primary and secondary active components supported on a combined or composite support. In order to determine the most suitable catalyst preparation method, a decision chart, Table 2.7, is made based on the desired catalytic property of P-5 (see Section 2.1.6).

Table 2.6 The decision chart for the selection of catalyst preparation method

Merit	Description	Precipitation method	Impregnation method
1	Uniform distribution of multi-active components	Easy	Difficult
2	Molecular scale mixing of catalyst components	Easy	Difficult
3	Surface area up to 200 m^2/g	Easy	Easy
4	Surface area higher than 200 m^2/g	Difficult	Easy
5	High metal dispersion	Easy	Easy
6	High metal loading	Easy	Difficult
7	Relative low cost	Difficult	Easy
8	Instrument availability	Easy	Easy

From Table 2.6, it is clear that the precipitation method has some advantages over the impregnation method in achieving uniform distribution of multi-active components. High surface area is a desired property for catalysts because of the surface nature of catalysis. However, the surface area of an impregnated catalyst actually depends on whether a support with such high surface area is commercially available. With such kinds of material commercially unavailable for support, the uniform composite support ($AlMgO_x$) can only be made through precipitation method. Also, considering that a surface area higher than 200 m^2/g may not be necessary for high temperature reforming reactions, the advantage of producing high surface area catalyst through impregnation method may not be necessary either. A precipitated catalyst is likely more expensive than an impregnated catalyst. But it is not an issue in this case as the objective of the study is to

develop nickel-based non-precious metal catalysts. With the low cost of non-precious metals in comparison with precious metals, precipitation method will not result in a significant rise in catalyst cost. In this research, precipitation method is determined as the catalyst preparation method based on above discussion. The following section is a detailed description of catalyst preparation procedures.

2.2.3.2 Catalyst preparation procedure

Six basic catalyst preparation steps used in the synthesis of precipitated catalysts in our laboratory are described as follows.

1) **Solution preparation:** The solution containing various metal salts is prepared through dissolving metal precursors using de-ionized water. The selection of specific metals and their precursors is dependent on proposed catalyst composition.

2) **Precipitation:** The precipitation of metals will be made through adjusting the pH value of the solution to 7-10 by adding precipitating reagent solution using the set-up shown in Fig. 2.13. Many bases and basic compounds could be the precipitating reagents. In this research, mild basic compounds are preferred such as potassium carbonate (K_2CO_3), sodium carbonate (Na_2CO_3), and ammonia hydroxide (NH_4OH).

3) **Filtration and washing**: Filtration operation is used to remove most of water and unwanted ions. Washing is performed to remove unwanted ions from the filtration cake. The filtration cake is washed using de-ionized water at room temperature until the pH value of washing flow is closing to 7.

4) **Drying:** After removing most of unwanted ions by washing, the precipitate cake contains a significant portion of water. The precipitate is then dried in an oven at 120 ^{o}C for 12 h to remove the water.

5) **Calcination:** The catalyst calcination is one of the most important pre-treatment procedures. Catalyst calcination at a temperature slightly higher than catalytic reaction temperature is a common practice in catalyst preparation. High temperature process can generate strong interaction between metals and oxide support, resulting in the formation of stable catalysts (Somorjai, 1994). In this research the ramp rate of furnace is set 2 ^{o}C/min and calcination temperatures are from 500 ^{o}C to 1100 ^{o}C. Thermally unstable compounds in the catalyst are decomposed to oxides. Also, solid-state reactions may take place between the decomposed products to form new phases.

6) **Sieving:** After calcination at a specific temperature, the catalyst is ground and sieved to four groups with different particle sizes, i.e., 0.075-0.150 mm, 0.150-0.180 mm, 0.180-0.250 mm, and 0.250-0.355 mm. In most of catalyst testing experiments, the catalysts with the particle sizes between 0.150-0.180 mm are used unless otherwise specified.

2.3 PRELIMINARY EXPERIMENTS

As mentioned in section 2.1.4.2 of this Chapter, the equilibrium composition is calculated based on two independent reactions instead of three without considering the

carbon formation reaction. In this section, preliminary experiments were performed to evaluate the validity of the calculations for equilibrium compositions in this Chapter.

Following the catalyst preparation procedure described in section 2.2.3.3 of this Chapter, a 6wt%Ni9wt%Co/$AlMgO_x$ bimetallic catalyst was prepared by coprecipitation from an aqueous solution of nickel nitrate (98 wt% purity, Lancaster Synthesis Inc., USA), cobalt nitrate (99 wt% purity, Aldrich Chemical Company, USA), magnesium nitrate (97 wt% purity, EMD Chemicals Inc., Mexico), and aluminium nitrate (98 wt% purity, EMD Chemical Inc., Germany). The catalyst was calcined at 900 ^{o}C for 6 h.

CO_2 reforming of CH_4 over the Ni-Co/$AlMgO_x$ catalyst was carried out in a bench-top, micro fixed-bed quartz reactor (Autoclave, USA) with an inner diameter of 6 mm. Reactant gas consisting of an equimolar mixture of N_2 (99.9 % purity, Praxair Canada Inc.), CH_4 (99.2 % purity, Praxair Canada Inc.) and CO_2 (99.9 % purity, Praxair Canada Inc.) was introduced at the atmospheric pressure. Before testing, the catalyst was reduced by a H_2 (99.9 % purity, Praxair Canada Inc.) and N_2 mixture with a molar ratio of 1:4 at 800 ^{o}C for 4 h. The product gas was analysed using an on-line Agilent 6890N GC, equipped with TCD and a GS-GASPRO capillary column (J&W Scientific) of 60 m in length and 0.32 mm in inner diameter. Helium (Ultra high purity 5.0, PRAXAIR Canada Inc.) was used as the carrier gas. The GC oven temperature was first set -60 ^{o}C for 3 mins and then increased to 200 ^{o}C with a ramp rate of 25 ^{o}C/min.

The results of the preliminary experiment of CO_2 reforming of CH_4 are shown by the solid lines in Fig. 2.14 and Fig. 2.15. The first comparison between the measured

composition (solid lines) and the calculated composition (dotted lines) based on three independent reactions (Eq. 2.1, 2.2, and Eq. 2.4) at the existence of inert N_2 is presented in Fig. 2.14. It can be seen that the ratio of H_2/CO is higher than 1 for the calculated data while less than 1 for the measured data, i.e. $(H_2/CO)_{measured}<1$ while $(H_2/CO)_{calculated}>1$. Correspondingly, the ratio of CH_4 to CO_2 is higher than 1 for the measured composition while it is lower than 1 for the calculated composition, i.e. $(CH_4/CO_2)_{measured}>1$ while $(CH_4/CO_2)_{calculated}<1$. The observation indicates that the actual composition is different with the equilibrium composition calculated using three independent reactions. Most likely, some reactions may be far from their equilibrium state due to kinetic restriction.

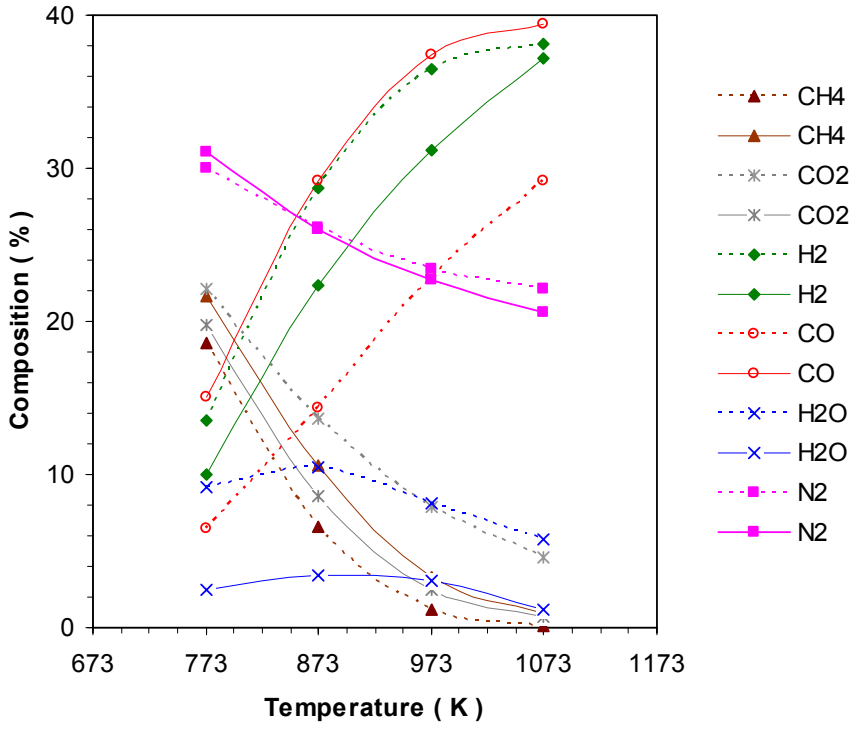

Fig. 2.14 Comparison between measured (solid lines) and calculated composition (dotted lines) based on three independent reactions of Eq. 2.1, 2.2, and 2.4 at 1 atm and initial $CO_2/CH_4/N_2$=1/1/1

Fig.2.15 presents the comparison between the measured composition (solid lines) and the calculated composition (dotted lines) based on two independent reactions without considering carbon formation reaction is presented in Fig. 2.15. It is clear that there is a better fit between the calculated composition and the measured composition in Fig. 2.15.

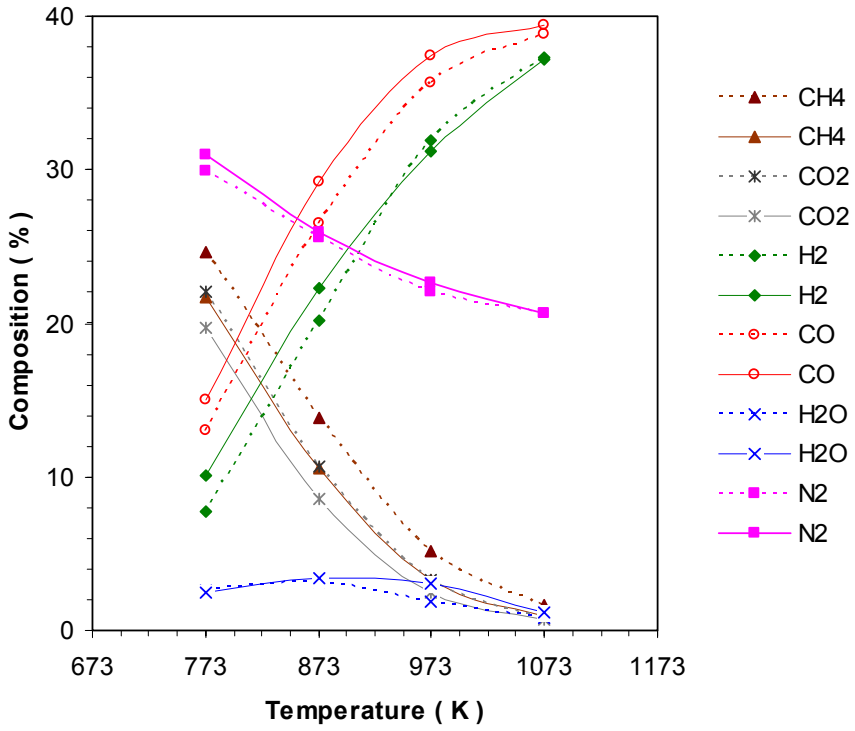

Fig. 2.15 Comparison between measured (solid lines) and calculated composition (dotted lines) based on two independent reactions: Eq. 2.5 and 2.6 at 1 atm and initial $CO_2/CH_4/N_2$=1/1/1

The experiments indicate that the magnitude of the carbon formation reaction is insignificant in comparison with the total reactions in CO_2 reforming of CH_4 on the new developed catalyst. The comparisons also show that it is reasonable to calculate the equilibrium compositions using two independent reactions without considering carobn formation reaction.

3 DEVELOPMENT OF LONG-TERM STABLE Ni CATALYSTS FOR CO_2 REFORMING OF CH_4

A similar version of this chapter was copyrighted and published in **Journal of Catalysis:** Zhang, J., Wang, H., Dalai, A.K., "Development of stable bimetallic catalysts for carbon dioxide reforming of methane", *J. Catal.* 249 (2) 300-310 (**2007**).

CONTRIBUTION OF Ph.D. CANADIDATE

Experiments were planned and performed by Jianguo Zhang. Hui Wang and Ajay K. Dalai provided guidance in planning the experiment. The submitted manuscript was written by Jianguo Zhang, while Hui Wang and Ajay K. Dalai provided comments and suggestions for revison.

CONTRIBUTION OF THIS CHAPTER TO THE OVERALL STUDY

Based on the designed catalyst compositions in Chapter 2, this chapter presents experiments on the catalyst screening among various Ni-Me bimetallic combinations for CO_2 reforming of CH_4. The work involves the catalyst preparation and catalyst testing. This work resulted in the long-term stable Ni-Co/$AlMgO_x$ bimetallic catalysts for CO_2 reforming of CH_4, which is determined as the primary research object in the following research. This work also provides preliminary characterization for the catalysts.

ABSTRACT

The designed Ni-Me/AlMgO_x (Me = Co, Fe, Cu, or Mn) bimetallic catalysts were prepared using co-precipitation method. Catalyst screening showed that Ni-Co bimetallic catalyst had superior performance in terms of activity and stability than other Ni-Me bimetallic catalysts for CO_2 reforming of CH_4. In a 2,000 h stability test over 0.05 g catalyst under the conditions of 750 ^oC, 1 atm, reactant flow rate F = 5.5 L/h (or GHSV =110,000 mL/g_{cat}-h), Ni-Co catalyst showed very stable performance with very low carbon formation. Catalyst characterization was conducted using ICP-MS, BET, XRD, H_2-TPR, CO_2-TPD, CO-chemisorption, TEM, and TG. It was found that the synergy between Ni and Co can significantly improve catalyst performance and reduce carbon formation.

3.1 INTRODUCTION

As introduced in the first chapter, Ni catalysts suffer severe catalyst deactivation due to sintering, metal oxidation (Slagtern et al., 1997), and especially the severe carbon formation (Ashcroft et al., 1991). Tremendous attempts have been made in suppressing carbon formation over Ni-based catalysts when carbon dioxide reforming of methane is studied. Ruchenstein and Hu (Ruchenstein and Hu, 1995; 1996) reported that NiO/MgO has excellent stability and good resistance to carbon formation because of the formation of a solid solution between NiO and MgO, which is believed to suppress CO disproportionation. Tomisshge et al. (2000) investigated the additive effect of Sn, Ge, and

Ga to a NiO-MgO solid solution and found that the addition of Sn can effectively decrease the carbon formation which was mainly resulted from the methane decomposition. The addition of Cr (Wang et al., 2003, Zhang et al., 1998) and Mn (Choi et al., 1998) to supported Ni catalysts was reported to have significant effect on the inhibition of carbide formation which was believed to be the intermediate for carbon formation (Trimm, 1997). Choudhary and Mamman (1998) reported that catalyst performance can be improved when partial NiO is replaced with CoO in the NiO-MgO solid solution. Takanabe et al. (2005) reported that a homogeneous alloy of Co and Ni and the small Ni substitution of Co dramatically improved the catalyst activity and stability. They ascribed the performance enhancement to the improvement of catalyst resistance to metal oxidation. From above literature review, it is clear that bimetallic catalysts exhibit superior performance for carbon dioxide reforming of methane to the corresponding monometallic catalysts (Sinfelt, 1983; Ponec and Bond, 1995). Considerable research has also been conducted on the modification of catalyst supports by using promoters (Dias and Assaf, 2003; Seok et al., 2002; Osaki and Mori, 2001; Quincoces et al., 2001; 2002; Frusteri et al., 1994) in order to overcome the deactivation associated with nickel-based catalysts. It was reported that the addition of K and Ca can significantly inhibit carbon formation due to the favorable adsorption of acidic CO_2 on the basic surface sites (Zhang and Verykios, 1994; Chang et al., 1996). Catalyst surface basicity is believed to help suppress carbon deposition by promoting the activation of CO_2 (Horiuchi et al., 1996; Yamazaki et al., 1992) on the surface of catalysts. However, catalyst deactivation is still a severe problem

for carbon dioxide reforming of methane.

This work applies a new approach of incorporating different properties into the designed Ni-Me/$AlMgO_x$ (Me = Co, Cu, Mn, or Fe) catalyst, aiming at solving the deactivation problem of Ni-based catalyst for CO_2 reforming of CH_4. First, the sintering was supposed to be reduced or eliminated through improving catalyst thermal stability by using high melting point material, MgO. Second, the catalyst activity was supposed to be enhanced by providing high contact area through using high surface area material, Al_2O_3. Third, the synergy of metal-metal was assumed to improve performance by reducing the possibility of metal oxidation. Fourth, a high temperature calcination pre-treatment process was proposed to improve the metal-support interaction to reduce carbon formation. Thus, it was assumed that high metal dispersion, high surface area and SMSI could be incorporated into a Ni-Me/$AlMgO_x$ bimetallic catalyst. Catalyst screening showed that the Ni-Co/$AlMgO_x$ bimetallic catalysts possessed high activity and stability for carbon dioxide reforming of methane. Carbon free operation was achieved in a 250 h stability experiment.

3.2 EXPERIMENTAL

3.2.1 Catalyst preparation

Co-precipitation method as described in section 2.2.3 of Chapter 2 was used to prepared different bimetallic catalysts for screening. The prepared catalysts are represented as Ni-Me (Me = Co, Fe, Cu, or Mn) in this chapter.

3.2.2 Catalyst Characterization

The composition of the catalysts was analysed at the Saskatchewan Research Council Analytical Laboratory using Inductively Coupled Plasma Mass Spectrometry (ICP-MS). Their surface composition was analysed using X-ray photoelectron (XPS) in the Department of Chemical and Materials Engineering at the University of Alberta.

The BET surface area, porous volume and average pore diameter were measured by N_2 adsorption at the temperature of -196 ^{o}C using Micromeritics ASAP 2000. Approximately 0.2 g catalyst was used for each analysis. The degassing temperature was 200 ^{o}C to remove the moisture and other adsorbed gases from the catalyst surface. The metal dispersion and metal surface area were determined by CO-chemisorption. The sample was first reduced using hydrogen at 850-900 ^{o}C for 4 hours. The reduced sample was moved to a sample holder under the protection of the inert gas (He). Three steps were carried out before CO-chemisorption using Mircromeritics ASAP 2000: (1) evacuating the sample for 30 min at 120 ^{o}C; (2) reducing the sample again at 450 ^{o}C for 30 min using H_2; and (3) evacuating the sample for another 30 min at 120 ^{o}C. Finally, CO-chemisorption was conducted at 35 ^{o}C.

X-ray powder diffraction (XRD) analysis was conducted using a Rigaku/Rotaflex Cu rotating anode X-ray diffraction instrument. The catalyst was powdered and mixed with methanol to form a mud which was loaded to the coarse side of a glass plate and placed under the ambient drying condition. The dried sample plate was then loaded in the analysis chamber. Each sample was scanned at a rate of 4 ^{o}/min with 2-Theta varying from

20 to 80^{o}. The reducibility of catalysts was studied in a quartz tube by temperature-programmed reduction (TPR) in CHEMBET-3000. A sample of about 0.1 g was heated from room temperature to 1000 ^{o}C using 3 % H_2/N_2 at a flow rate of 30 mL/min and a ramp rate of 5 ^{o}C/min.

The carbon deposition on spent catalysts was analysed by a Perkin Elmer Pyris Diamond TG/DTA instrument. The spent catalyst was heated in a platinum sample holder in the air from room temperature to 850 ^{o}C at a ramp rate of 5 ^{o}C/min. The transmission electron microscopy (TEM) was employed to investigate the morphology of carbon deposit on the spent catalysts.

3.2.3 Catalyst testing

The evaluation of catalysts was carried out in a bench-top, micro fixed-bed quartz reactor (Autoclave, USA) with an i.d. of 6 mm. In screening of different bimetallic combinations and 2,000 h stability test for Ni-Co catalyst, 0.05 g catalyst was diluted with 0.450 g quartz sand. In order to compare selected catalysts at lower conversions, less amount of catalyst was used so as to maintain the comparison at the same mass transfer regime. In the investigation of effects of Ni-Co content, 0.03 g catalyst was mixed with 0.470 g quartz sand. 0.025 g catalyst mixed with 0.475 g quartz sand was applied in the comparison between bimetallic and monometallic catalysts. The average catalyst particle size is 0.165 mm. All experiments were carried out at 750 ^{o}C and 1 atm, and reactant flow rate F=5.5 L/h. No temperature gradient was observed in catalyst bed. Based on literature (Richardson 1989, Thomas and Thomas 1967) mass transfer was mostly eliminated at

such conditions of high flow rate and small amount of catalyst with small particle size. However, in order to make valid comparison on the same basis, exactly the same reaction conditions were applied in each comparison. Reactant gas consisting of an equimolar mixture of N_2 (99.9 % purity, Praxair Canada Inc.), CH_4 (99.2 % purity, Praxair Canada Inc.) and CO_2 (99.9 % purity, Praxair Canada Inc.) was introduced at the atmospheric pressure. Before testing, the catalyst was reduced by a H_2 (99.9 % purity, Praxair Canada Inc.) and N_2 mixture with a molar ratio of 1:4 at 850-900 ^oC for 4 h. The product gas was analysed by an on-line Agilent 6890N GC, equipped with TCD and a GS-GASPRO capillary column (J&W Scientific) of 60 m in length and 0.32 mm in inner diameter. Helium (Ultra high purity 5.0, PRAXAIR Canada Inc.) was used as the carrier gas.

3.2.3 Data processing

The conversion and selectivity were calculated using the same equations as introduced in section 2.1.3 calculation for conversions and selectivity in Chapter 2. The disappearance rate of reactant was calculated using Eq. 3.1 while the formation rate of product was calculated with Eq. 3.2.

$$-r_i, \text{mol/g}_{cat}\text{-s} = \frac{F_i^o - F_i^f}{m_{cat} \times 60} \tag{3.1}$$

$$r_i, \text{mol/g}_{cat}\text{-s} = \frac{F_i^f}{m_{cat} \times 60} \tag{3.2}$$

where m_{cat} is the weight of test catalyst measured in gram.

The carbon formation was analysed using of thermal gravimetric analysis (TGA) for spent catalysts under the assumption that any weight loss is resulted from the

oxidization of carbon deposition. Therefore, the carbon formation and average formation rate were calculated from Eq. 3.3 and 3.4 respectively.

$$\text{Carbon formation, } g_c/g_{cat} = \frac{m^o - m^f}{m^f} \tag{3.3}$$

$$\text{Average carbon formation rate, } g_c/g_{cat} - h = \frac{m^o - m^f}{m^f \times \text{TOS}} \tag{3.4}$$

where m^o and m^f are the weights of spent catalysts before and after TGA analysis. TOS is the time-on-stream of the corresponding

3.3 RESULTS AND DISCUSSION

3.3.1 Physical properties of the prepared catalysts

Based on the catalyst design, a series of Ni-based bimetallic catalysts with different combinations of Ni-Co, Ni-Mn, Ni-Fe, and Ni-Cu in the frame of $AlMgO_x$ were prepared by coprecipitation method. The determination of the level of metals was first determined based on the relevant literature (Tang et al., 2000). For convenience, the catalysts were denoted as Ni-Co, Ni-Mn, Ni-Fe, and Ni-Cu, respectively. The elemental composition, surface area, porous volume, and average pore diameter are shown in Table 3.1. Ni-Fe, Ni-Cu, and Ni-Mn catalysts had the same level of BET surface area between 14 and 18 m^2/g. Meanwhile, Ni-Co catalyst had a significantly higher surface area of 53 m^2/g. The porous volume followed the order of Ni-Co >> Ni-Cu > Ni-Mn > Ni-Fe, and the average pore diameter followed the order of Ni-Co < Ni-Fe < Ni-Mn < Ni-Cu. The BET analysis indicated the significant difference between Ni-Co combinations and the

others.

Table 3.1 Elemental composition, BET surface area, average pore diameter of catalysts for screening

Catalyst	Elemental Composition (mol %)							BET surface (m^2/g)	Pore volume (ml/g)	Average pore diameter (nm)
	Ni	Fe	Cu	Mn	Co	Al	Mg			
Ni-Fe	6.5	7.9	-	-	-	29.0	56.6	18	0.0565	12.0
Ni-Cu	6.8	-	6.9	-	-	28.6	57.7	15	0.0881	19.6
Ni-Mn	6.0	-	-	9.0	-	27.8	57.1	17	0.0734	16.9
Ni-Co	6.1	-	-	-	9.3	28.2	56.4	54	0.160	10.4

3.3.2 Catalyst screening for CO_2 reforming of CH_4

The activity and stability within a 28 h period was investigated over 0.05 g catalyst at 750 ^oC, 1 atm, F=5.5 L/h, and $CH_4/CO_2/N_2$=1/1/1. The equilibrium conversion of CH_4 is 91.5 % at the reaction conditions. The catalyst activity in terms of CH_4 and CO_2 conversion is shown in Fig. 3.1 and 3.2, respectively. Among the four Ni-Me combinations, Ni-Co catalyst has the highest initial activity (91.4 % CH_4 conversion) and remains at this level throughout the 28 h of time-on-stream (TOS). Ni-Mn and Ni-Fe catalysts also have high initial activities with CH_4 conversions of 85 % and 53 %, respectively. However, they dropped to 63 % and 18 %, respectively, at the end of the 28 h testing. Ni-Cu shows the lowest but relative stable activity, with a CH_4 conversion less than 16 %. The initial activity followed the order of Ni-Co > Ni-Mn > Ni-Fe > Ni-Cu. This order is in good agreement with the order of the BET surface area, porous volume, or average pore diameter (Table 3.1).

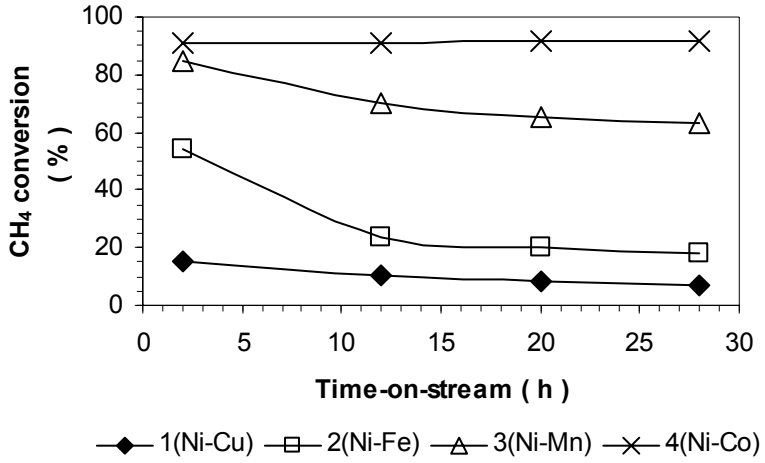

Fig. 3.1 Activity and stability of Ni-Me catalysts in terms of CH_4 conversion at reaction condition: 750 ^oC, 1 atm, 5.5 L/h, and $CH_4/CO_2/N_2$=1/1/1

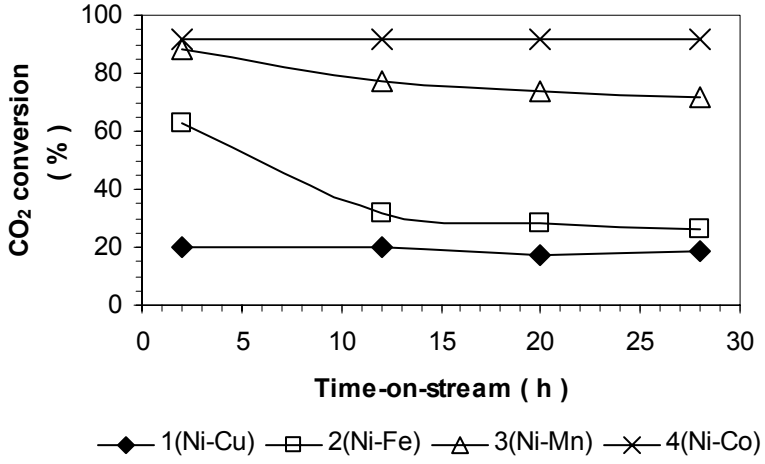

Fig. 3.2 Activity and stability of Ni-Me catalysts in terms of CO_2 conversion at eaction condition: 750 ^oC, 1 atm, 110,000 ml/g_{cat}-h, and $CH_4/CO_2/N_2$=1/1/1

The conversion of CO_2, shown in Fig. 3.2 has the same trend as the CH_4 conversion in Fig. 3.1 for all the Ni-Me catalysts, but the former is slightly larger than the latter. This can be ascribed to the existence of a side reaction of reveres water-gas shift reaction (RWGS), which is resulted from the reaction between the reactant CO_2 and the

reforming product H_2. Consequently, the apparent conversion of CO_2 is higher than CH_4 and also the yield of H_2 is lower than CO. This can be confirmed by the observation of the H_2/CO ratio which is lower than 1 shown in Fig. 3.3. Also, it is clear that the H_2/CO ratio varying between 0.9 and 1.0 for all catalysts is very close. Compared Fig. 3.3 with Fig. 3.1 or 3.2, the H_2/CO ratio can not reflect any difference about activity and stability of different Ni-Me catalysts.

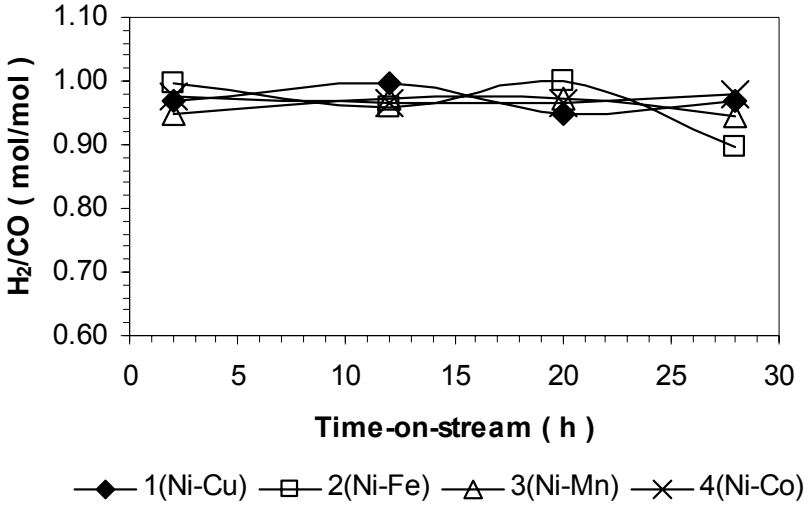

Fig. 3.3 H_2/CO ratio as a function of time-on-stream of Ni-Me catalysts

3.3.3 Carbon deposition and activity of different Ni-Me catalysts

Carbon deposition on spent catalyst and activity decay after 28 h TOS are shown in Table 3.2. The amount of carbon deposition on the spent catalysts was determined using TG/DTA. The carbon formation in terms of g_c/g_{cat} is calculated using the overall weight loss of spent catalyst during TG/DTA analysis up to 850 ^oC in air divided by the finial weight of catalyst. The carbon formation divided by time-on-stream is defined as average carbon formation rate with the unit of g_c/g_{cat}-h. The activity decay is calculated based on

the difference of initial and final CH_4 conversion.

Table 3.2 Carbon formation and activity change of Ni-Me catalyst at 28 h

Catalyst	Carbon formation (mg_c/g_{cat})	Carbon formation rate (mg_c/g_{cat}-h)	CH_4 conversion (%)		Activity decay (%)
			Initial	Final	
Ni-Fe	589.1	21.0	54	18	67
Ni-Mn	152.0	5.4	85	63	26
Ni-Cu	62.1	2.2	16	12.5	22
Ni-Co	57.1	2.0	91	91	0

It can be seen that Ni-Fe catalyst has a high carbon deposition rate of 21.0 mg_c/g_{cat}-h. Correspondingly, it has 67 % activity decay. Ni-Mn catalyst also has a relatively high carbon formation rate of 5.4 mg_c/g_{cat}-h and an activity decay of 26 %. However, Ni-Cu catalyst has a lower carbon formation rate of 2.2 mg_c/g_{cat}-h and a relatively stable performance. Its activity decay is 22 %. Ni-Co catalyst has a low carbon formation rate of 2.04 mg_c/g_{cat}-h. Also, it has a very stable performance in the 28 h period without any activity decay. The activity decay follows the same order as the carbon formation rate: Ni-Fe >> Ni-Mn > Ni-Cu > Ni-Co (Table 3.2). It indicates that the carbon formation is the main reason of catalyst deactivation in carbon dioxide reforming of methane. Ni-Co and Ni-Cu catalysts both have good carbon resistance. However, the latter has a very low activity.

3.3.4 Long-term deactivation test of Ni-Co catalyst

3.3.4.1 Stability and carbon formation

Catalyst screening shows that Ni-Co catalyst does not lose its activity during the 28 h test (Figs 3.1 and 3.2) but carbon formation is observed over spent catalyst (Table

3.2). Therefore, a series of deactivation test experiments are proposed to investigate the activity and carbon formation evolution behavior of the Ni-Co catalyst at different period of time-on-stream. At the conditions of 750 ^{o}C, 1 atm, 110,000 ml/g_{cat}-h, and $CH_4/CO_2/N_2$=1/1/1, Ni-Co catalyst is tested for 20, 200, and 2000 h, respectively. The results of the reaction rate of CH_4 and amount of carbon formation are shown in Fig. 3.4. The use of the common logarithm of time is to show more details for the first 200 h.

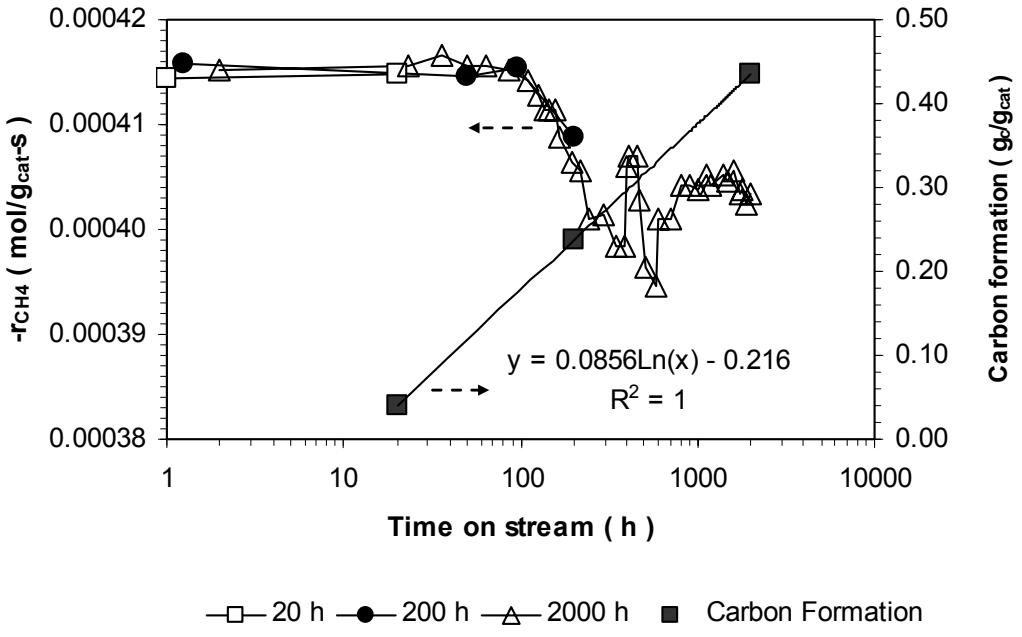

Fig. 3.4 Carbon formation and reaction rate of methane over Ni-Co catalyst at reaction conditions: 750 ^{o}C, 1 atm, 110,000 ml/g_{cat}-h, and $CH_4/CO_2/N_2$ =1/1/1

From Fig 3.4, it can be seen that in the 20 h test the reaction rate of CH_4 remains at around 0.000415 mol/g_{cat}-s but the carbon formation is as high as 0.0408 g_c/g_{cat} over the 20 h period. In the 200 h test, the CH_4 reaction rate remains at 0.000416 mol/g_{cat}-s for 100 h but drops to 0.000409 mol/g_{cat}-s at 200th h. The carbon formation is 0.2374 g_c/g_{cat}

over the 200 h period. In the 2000 h test, the CH_4 reaction rate also starts to drop from the initial 0.000415 to 0.000398 mol/g_{cat}-s at about 300th h, and fluctuates between 0.000395 and 0.000407 mol/g_{cat}-s until 700th h and stay stable at 0.000404 mol/g_{cat}-s for the last 1300 h period. The carbon formation is 0.435 g_c/g_{cat} over the 2000 h period. An empirical equation can be found to describe the relationship between the carbon formation over Ni-Co catalyst and time-on-stream under the reaction conditions (Eq. 3.1). Carbon accumulation becomes significantly slower with the increase of time-on-stream. Regression shows that the relationship between the amount of carbon formed and the time on stream is as follows:

$$\text{Carbon formation amount, } m\text{g}_c/\text{g}_{cat} = 85.6Ln(\text{TOS, h}) - 216 \quad (3.1)$$

The initial carbon formation was high but slowed down when the TOS increased. The average carbon formation rate is 2.0, 1.2, and 0.2 mg_c/g_{cat}-h for the 20, 200, and 2000 h runs, respectively. Further data treatment shows the average carbon formation rate is 2.0 mg_c/g_{cat}-h for the first 20 period of time-on-stream, 1.1 mg_c/g_{cat}-h for the following 180 h period and 0.1 mg_c/g_{cat}-h for the last 1800 h. It is speculated that the rapid carbon formation during the first 100 h leads to the obvious catalytic activity drop in the following 200 h. The slow-down of the carbon formation afterwards results in a stable performance since then. In overall, the catalytic activity drop for the Ni-Co bimetallic catalyst is less than 3 % in the 2000 h period. This catalyst is one of the most stable and most active one that has ever been developed for CO_2 reforming of CH_4. Comparison with

literature data is shown in Table 3.3.

Table 3.3 Performance comparison with literature data

Catalyst (Reference)	T (^{o}C)	GHSV (ml/g_{cat}-h)	Final CH_4 conversion (%)	TOS (h)	Carbon deposition (mg_c/g_{cat})
Ni/MgO (Frusteri et al., 2002)	800	330000	66	12	1330 at 12h
Ni/MgO, K doped (Frusteri et al., 2002)	800	330000	78	12	120 at12h
Ni/ZrO_2-B (Wei et al., 2000)	757	24000	84	600	-
$Ni_{0.03}Mg_{0.97}O$ (Tomishige et al., 1998, Chen et al., 1997)	850	18000	82	2400	-
Ni-Co/$AlMgO_x$ (Zhang et al., 2007)	750	110000	89	2000	440 at2000h
	750	365000	83	250	9 at 250h

Wei et al. (2000) had claimed that Ni/ZrO_2-B was the best catalyst ever with methane conversion of 84 % at 756 ^{o}C and GHSV of 24,000 ml/g_{cat}-h, as shown in Table 3.3. However, it was found that the Ni-Co/AlMgOx possesses higher activity with an initial CH_4 conversion of 89% at a GHSV of 110,000 ml/g_{cat}-h. When the GHSV increased to 400,000 ml/g_{cat}-h, the conversion of CH_4 decreased to 82-83 %, which is still higher than that of the well known $Ni_{0.03}Mg_{0.97}O$ solid solution (Tomishige et al., 1998; Chen et al., 1997) for which the CH_4 conversion was 82 % at 850 ^{o}C with a GHSV=18,000 ml/g_{cat}-h.

To understand further the performances of Ni-Co catalysts, the fresh and spent catalyst were characterized using synchrotron-based x-ray absorption spectroscopy (XAS)

3.3.4.2 Stability and catalyst structure

In the study of heterogeneous catalysis, synchrotron-based XAS has allowed correlation of catalyst performance to its structural and electronic characteristics (Guyot-

Sionnest et al., 1991). The change of catalyst performance is a reflection of the evolution of structural and electronic characteristics of the catalyst in reaction. Fresh, untested Ni-Co catalyst and spent Ni-Co catalysts at different stages of testing are analyzed using PGM and SGM beamlines at the Canadian Light Source (CLS). XAS spectra are recorded in Fluorescence Yield (FLY). The catalyst stability is evaluated in terms of the evolution of catalyst structural and electronic characteristics with time-on-stream. Fig. 3.5 shows the XAS spectra of different reference compounds namely MgO, CoO, NiO, and Al_2O_3 obtained from PGM beamline.

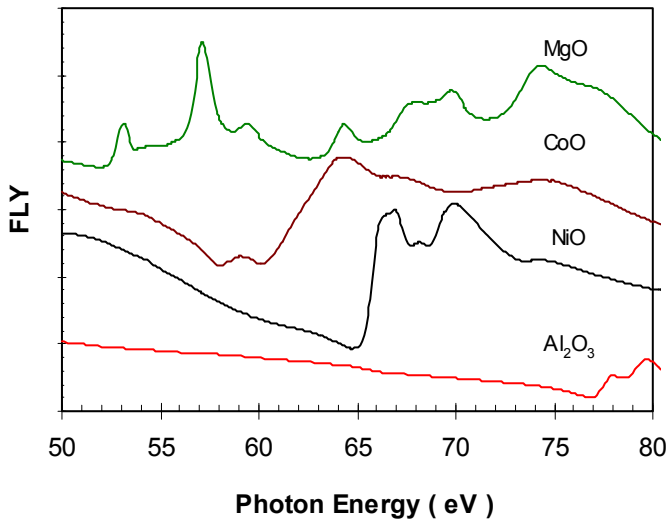

Fig. 3.5 XAS spectra of reference compounds obtained form PGM

Fig. 3.6 shows the XAS spectra of fresh and spent catalysts recorded from PGM beamline. Comparing Fig. 3.5 with Fig. 3.6, it can be seen that the XAS spectra of all fresh and spent catalysts are dominated with MgO XAS spectra. With the increase of time-on-stream, they change slightly. One absorption peak at 62 eV disappeared during the period of 20-200 h. There is no apparent change during the period of 200-2000 h. The

XAS spectra of spent catalysts from the PGM beamline might indicate that MgO is the major contributor to the stability of the support.

The L edge spectra of Ni and Co are obtained from the SGM beamline and shown in Figs 3.7 (Ni 2p) and 3.8 (Co 2p). The L edge spectra are divided in two parts L_{III} and L_{II}. They are dominated by respectively $2p_{3/2}$ and $2p_{1/2}$ character of the core hole. From Figs 3.7 and 3.8, it can be seen that the $L_{III, II}$ absorption edges of both Ni and Co shift to lower photon energy position with the increase of time-on-stream. After 200 h, no obvious changes observed for both Ni 2p and Co 2p XAS spectra. This observation might indicate that the catalyst structure has been stabilized.

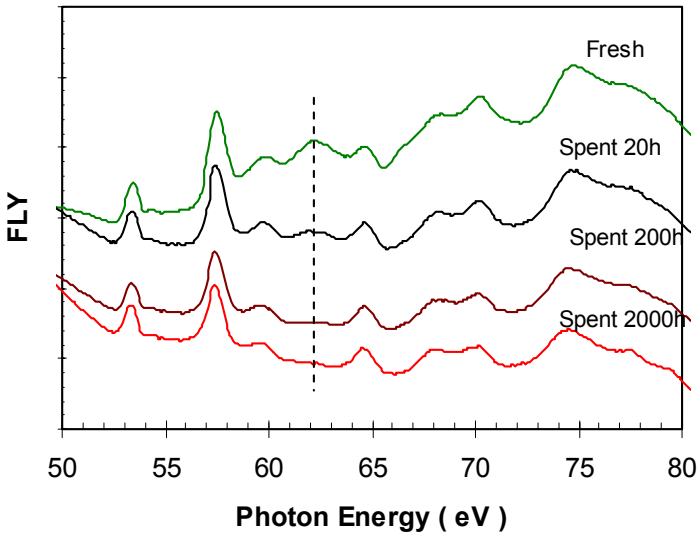

Fig. 3.6 XAS spectra of fresh and spent Ni-Co catalysts obtained from PGM

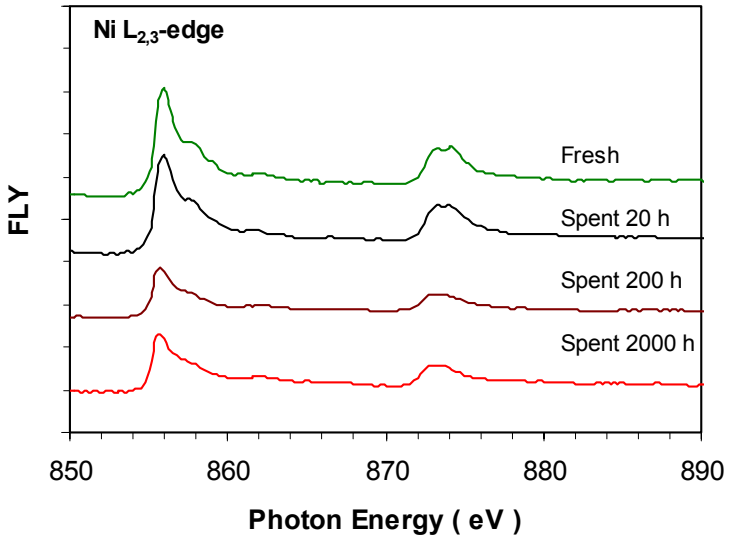

Fig. 3.7 Ni 2p XAS spectra of fresh and spent Ni-Co catalysts obtained from SGM

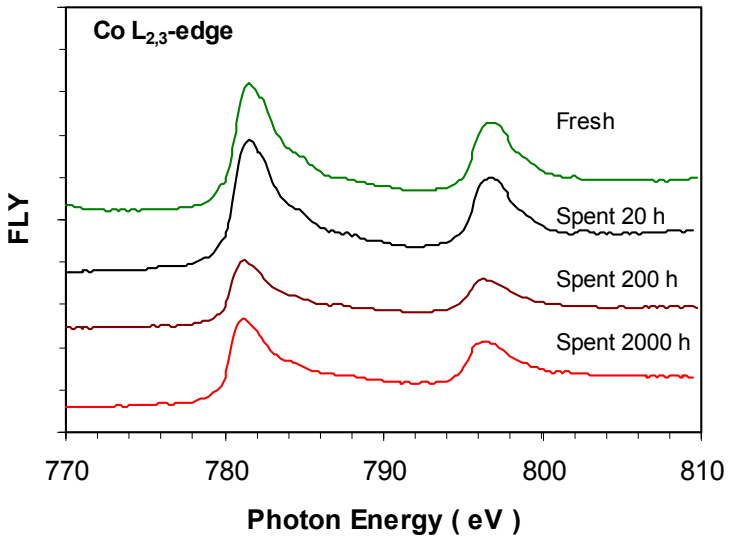

Fig. 3.8 Co 2p XAS spectra of fresh and spent Ni-Co catalysts obtained from SGM

In Figs 3.7 and 3.8 the Ni 2p and Co 2p spectra show that not only Ni and Co become stable after a period of time-on-stream but also take a higher oxidation state of them in the catalysts for CO_2 reforming of CH_4.

3.3.4.3 Stability and product distribution

The ratio of H_2/CO as a function of time-on-stream is shown in Fig. 3.9. RWSR is the major side reaction in the methane dry reforming system (Bradford and Vannice 1999). Its existence will reduce the H_2/CO ratio. The average ratio of H_2 to CO over this catalyst was about 0.965, which may indicate the occurrence but less significant of RWSR. Also, it is interesting to note that the molar ratio of H_2 to CO oscillates between 0.9 and 1.1 during the reaction period. Wei et al. (2000) ascribed this phenomenon to a periodic cycle of carbon deposition and elimination. An efficient periodic cycle of carbon deposition and elimination on the catalyst surface may be one of the contributions that lead to stable catalytic performance (Richardson 1989).

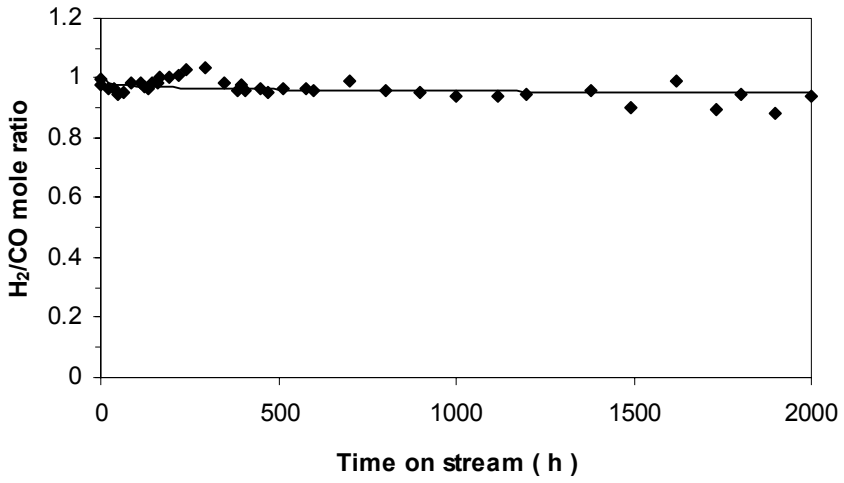

Fig. 3.9 H_2/CO as a function of time-on-stream over Ni-Co catalyst

3.3.5 Comparison Ni and Co monometallic catalysts with Ni-Co catalyst

3.3.5.1 Element composition

To understand the relationship between catalyst properties and performance, comparative investigations have been carried out over Ni and Co monometallic catalysts

and Ni-Co bimetallic catalyst. In the following characterization, lower Ni-Co content bimetallic catalyst was used exclusively unless otherwise specified. Ni or Co content in the monometallic catalysts was made at the same level as the overall Ni and Co content in Ni-Co catalyst. This was done to compare the performance of catalysts with similar total active metal loading. Bulk elemental composition was analyzed using ICP-MS and surface elemental composition was determined by XPS, results shown in Table 3.4.

Table 3.4 Composition of Ni and Co monometallic and Ni-Co bimetallic catalysts

Catalyst	Bulk Composition (mol %)				Surface Composition (mol %)			
	Ni	Co	Al	Mg	Ni	Co	Al	Mg
Ni	6.8	-	27.8	65.4	7.1	-	28.9	64.0
Co	-	9.7	27.6	62.8	-	7.8	31.2	61.0
Ni-Co	3.6	4.9	30.0	61.5	4.3	6.2	29.3	60.2

Comparison between surface composition and bulk composition indicated that $Ni_{surface}/Ni_{bulk}$ was 1.10 in the Ni monometallic catalyst and became 1.19 in the bimetallic catalyst. $Co_{surface}/Co_{bulk}$ was 0.80 and 1.27 in the Co monometallic catalyst and bimetallic catalyst, respectively. The co-existence of Ni-Co in the bimetallic catalyst made Co an apparent surface enrichment but without significant effect on the $Ni_{surface}/Ni_{bulk}$.

3.3.5.2 N_2-physical absorption

N_2-physical absorption was employed to measure the specific surface area and the pore distribution of the catalysts and results are shown in Table 3.5 and Fig. 3.10.

Table 3.5 BET analysis for Ni and Co monometallic and Ni-Co bimetallic catalysts

Catalyst	BET surface (m^2/g)	Average Pore diameter (nm)	Pore Volume (cm^3/g)
Ni	45	9.0	0.1241
Co	24	10.5	0.0630
Ni-Co	56	8.5	0.1561

From Table 3.5, it can be seen that the Ni-Co bimetallic catalyst has higher surface area than Ni or Co monometallic catalyst. Correspondingly, it has smaller average pore diameter. Fig. 3.10A shows Ni-Co has more pores with diameter around 50 Å than the monometallic catalysts. Combined with Fig. 3.10B, it can be seen that the surface area and pore volume follow the same order: Ni-Co catalyst > Ni catalyst > Co catalyst.

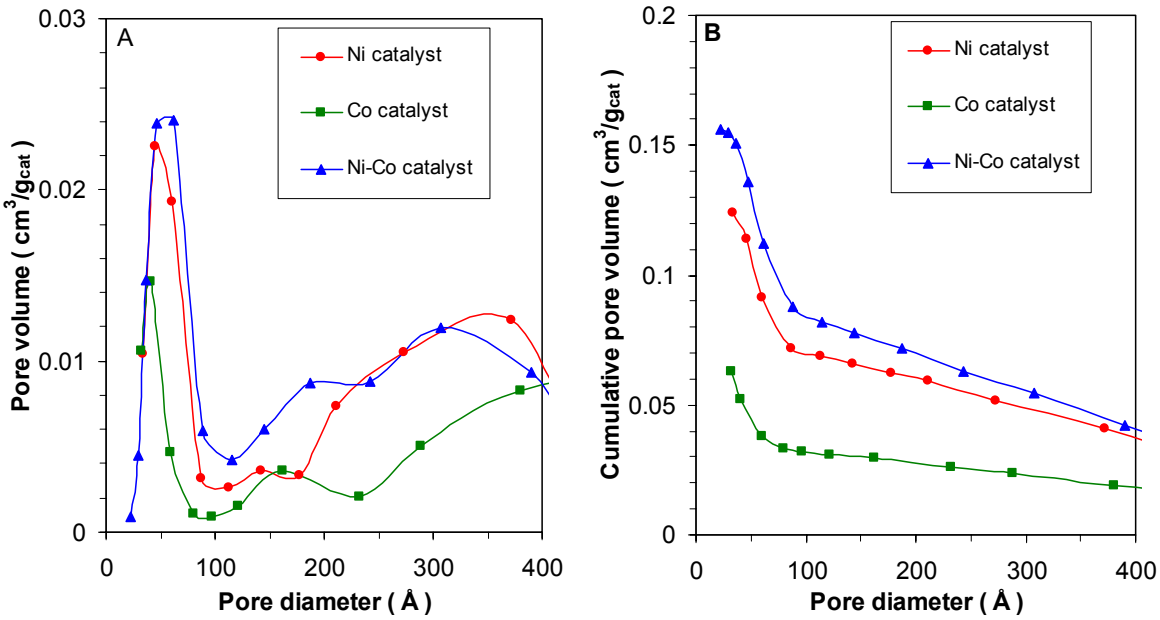

Fig. 3.10 Pore distribution of Ni and Co monometallic and Ni-Co bimetallic catalysts

3.3.5.3 CO-chemisorption

The metallic property of active sites has been confirmed by the experiment during which no conversion of reactants was observed on unreduced catalysts. It indicates that metallic surface is closely related to the catalyst activity and stability. The metallic surface and metal dispersion are measured using CO-chemiosorption. The metallic surface area and metal dispersion of both monometallic and bimetallic catalysts are shown in Table 3.6. With the same level of metal content, the Ni-Co bimetallic has significant higher metallic

surface area (2.9 m^2/g) and metal dispersion (8.8 %) than the monometallic catalysts (1.2 m^2/g and 2.9 % for Ni catalyst and 1.5 m^2/g and 2.1 % for Co catalyst).

Table 3.6 Metallic surface area and metal dispersion of Ni and Co monometallic and Ni-Co bimetallic catalysts

Catalyst	Metallic surface (m^2/g)	Metal dispersion (%)
Ni	1.2	2.9
Co	1.5	2.1
Ni-Co	2.9	8.8

3.3.5.4 Reducibility

Hydrogen temperature-programmed reduction (H_2-TPR) experiment was conducted to investigate the reducibility of the catalysts. The TPR profiles are shown in Fig. 3.11.

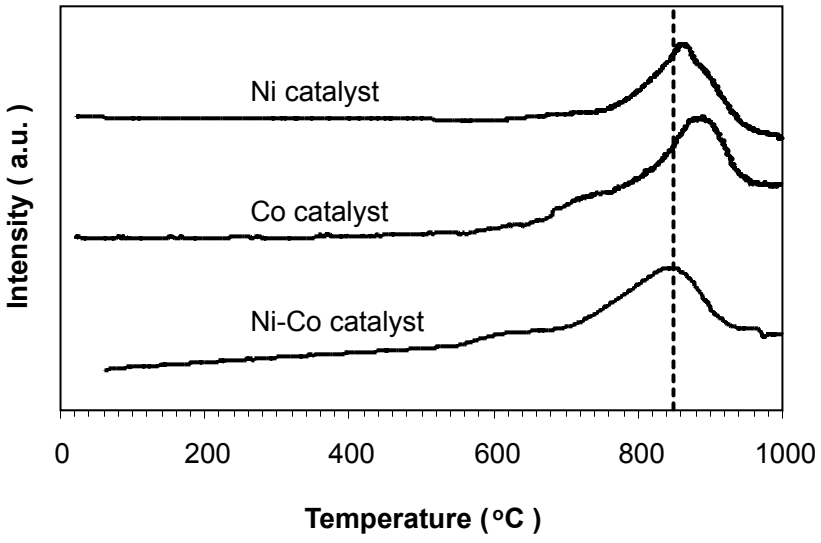

Fig. 3.11 TPR profiles of Ni and Co monometallic and Ni-Co bimetallic catalysts calcined at 900 °C

The reduction peaks in the ranges of 750 -950 ^{o}C and 700-950 ^{o}C for the Ni and Co monometallic catalysts corresponded to the reduction of Ni in a mixed spinel phase $Ni_xMg_{1-x}Al_2O_4$ (Tichit et al., 1997) and Co in a mixed spinel phase $Co_xMg_{1-x}Al_2O_4$ (Ribet et al., 2000), respectively. The reduction peak in Ni-Co bimetallic catalyst between 700 and 940 ^{o}C probably resulted from the reduction of Ni and Co in a very complex quaternary spinel-like phase (Coq et al., 2000). In the high-temperature calcination process, Ni and Co can also form a continuous row of $Ni_xCo_{3-x}O_4$ spinels, $x>0$ (Petrov and Will 1987). The reduction peak maximum of Ni-Co bimetallic catalyst was at a lower temperature (850 ^{o}C) in comparison to those for Ni monometallic catalyst (868 ^{o}C) and Co monometallic catalyst (896 ^{o}C). This could be partially attributed to the surface enrichment of Ni and Co in the Ni-Co catalyst because the Ni or Co on the catalyst surface is easily accessible. Also, the reduction in Ni-Co bimetallic catalyst appeared as a single reduction peak. This might indicate the formation of the Ni-Co alloy during reduction according to Rinkowski et al. (1995). They reported that one-stage reduction of bimetallic catalysts illustrates the alloying of metals in the reduction process.

3.3.5.5 Bulk phases

XRD analysis was used to identify the bulk phase property of the catalysts and the XRD results are shown in Fig. 3.12.

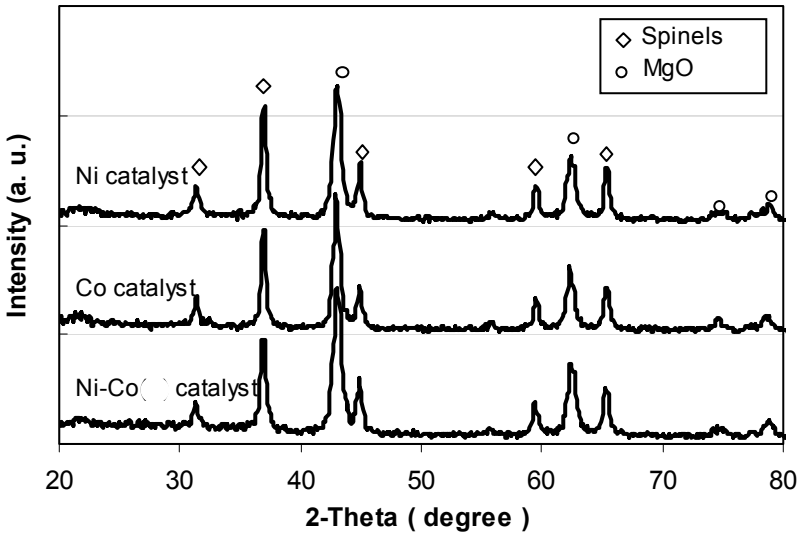

Fig. 3.12 XRD analysis of Ni and Co monometallic and Ni-Co bimetallic catalysts calcined at 900 ^{o}C

As shown in Fig. 3.12, spinel phases and MgO-type phases were observed in all the three samples. No apparent difference was revealed between the XRD patterns of Ni-Co bimetallic catalyst and Ni or Co monometallic catalyst. According to Tichit et al. (1997; 1999; 2000), Ni^{2+}, Co^{2+}, Mg^{2+}, and Al^{3+} belong to the same lattice in the Ni/Co/Al/Mg composite catalysts. A high calcination temperature favours the formation of Ni^{2+}-Al^{3+}, Co^{2+}-Al^{3+}, and Mg^{2+}-Al^{3+} solid solutions of spinel-type and of the stoichiometric $NiAl_2O_4$, $CoAl_2O_4$, and $MgAl_2O_4$ spinel phases (Tichit et al., 1997, Ribet et al., 1999; Coq et al., 2000). The Ni^{2+}-Co^{3+} spinel-type solid solution and $NiCo_2O_4$ spinel can also be formed at high calcination temperatures (Petrov and Will 1987). These spinel-type solid solution phases and spinel phases in the catalysts are quite indistinguishable by XRD (Fig. 3.12) due to their similarity. This result is understandable because the major components of the catalysts are Al and Mg and they could form similar solid structures in

the identical preparation processes.

3.3.5.6 Oxidation states of Ni and Co

XPS was used to analysis the oxidation states of the catalyst, shown in Fig. 3.13.

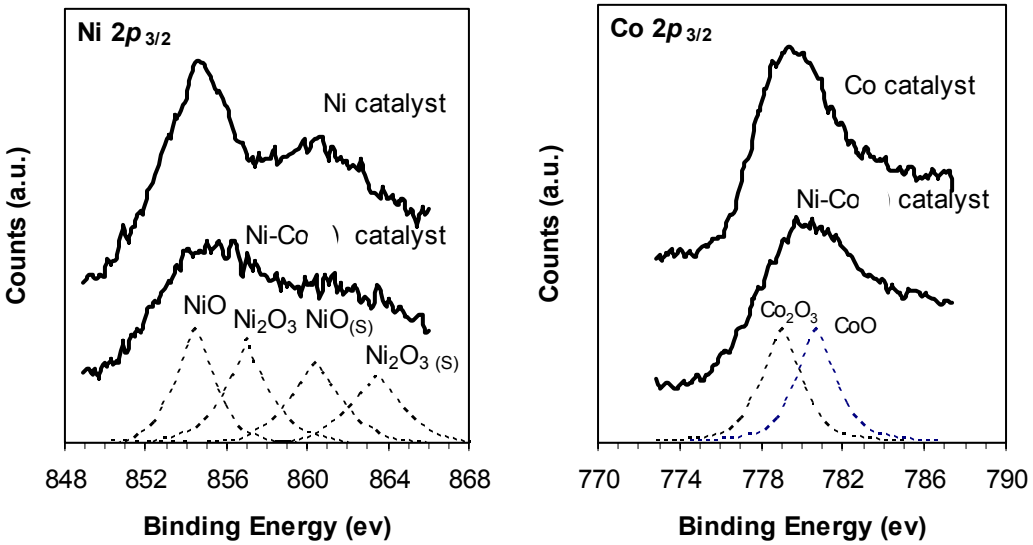

Fig. 3.13 XPS spectra of Ni $2p_{3/2}$ and Co $2p_{3/2}$ in Ni and Co monometallic and Ni-Co bimetallic catalysts calcined at 900 ^{o}C.

Fig. 3.13 shows that Ni^{2+} (854 eV and 860 eV) (Kang and Rhee 2001) was predominant in Ni monometallic catalyst and Co^{3+} (777 eV) (Marco et al., 2001) was in large amount in Co monometallic catalyst. However, other oxidation states for both metals such as Ni^{3+} and Co^{2+} increased in Ni-Co bimetallic catalyst. It is interesting to note that part of Ni shifted from lower oxidation state to higher oxidation state and vice versa in the case of Co. This indicates the occurrence of electron transfer between Ni and Co in the bimetallic catalyst, which is believed to prevent metal from oxidation during the reaction (Frustri et al., 2001). It further confirms the near-distance interaction between the two metal atoms, which may easily form Ni-Co alloy on the catalyst surface during reduction.

3.3.5.7 Comparison of activity and stability of Ni, Co monometallic catalysts with Ni-Co bimetallic catalyst for CO_2 reforming of CH_4

The activity and stability of Ni and Co monometallic catalysts and Ni-Co bimetallic catalyst in a test of 28 h period at 750 ^oC, 1 atm, F=5.5 L/h, $CH_4/CO_2/N_2$=1/1/1, and 0.025 g catalyst are shown in Fig. 3.14. From Fig. 3.14, it is clear that Ni and Co monometallic catalysts have similar performances. Co monometallic catalyst has slightly higher initial activity in terms of CH_4 (0.000601 mol/g_{cat}-s) and CO_2 (0.000684) reaction rates in comparison with Ni monometallic catalyst with reaction rates of CH_4 (0.000559 mol/g_{cat}-s) and CO_2 (0.000652 mol/g_{cat}-s). With the increase in time-on-stream, deactivation takes place. CH_4 reaction rates drop to 0.000517 mol/g_{cat}-s on both monometallic catalysts. CO_2 reaction rates drops to 0.000633 and 0.000618 mol/g_{cat}-s respectively on Co and Ni monometallic catalysts. Compared with monometallic catalysts, Ni-Co shows significant high and stable activity within the 28 h time-on-stream. Initial CH_4 and CO_2 reaction rates of Ni-Co bimetallic catalyst are 0.000745 and 0.000773 mol/g_{cat}-s respectively and remain unchanged at the end of the test.

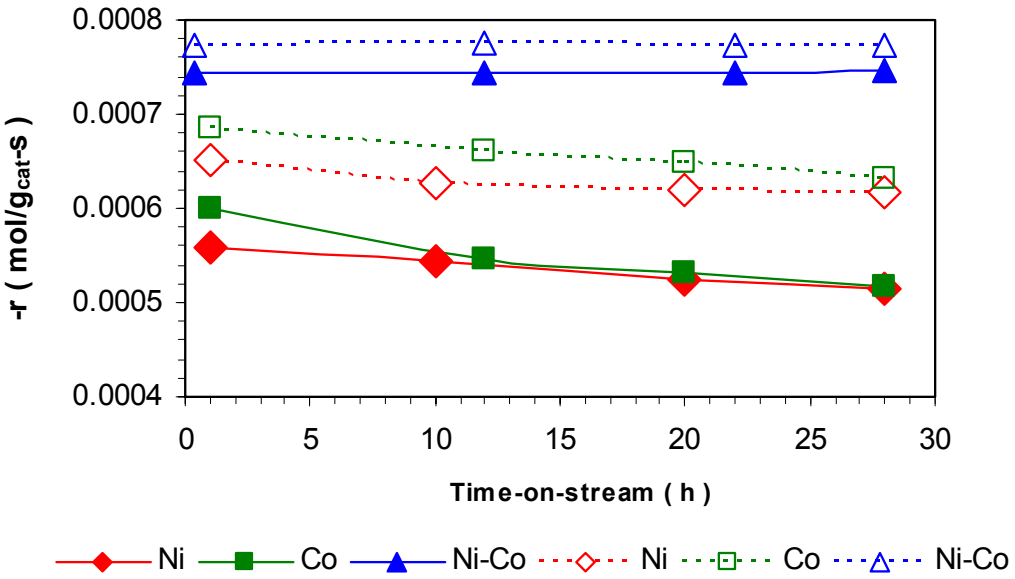

Fig. 3.14 Comparison of stability of Ni-Co bimetallic catalyst and Ni and Co monometallic catalysts (solid line: CH_4 reaction rate; dotted line: CO_2 reaction rate)

Carbon formation analysis for the spent catalysts is shown in Table 3.7. It is found that there is no carbon formed on the Ni-Co bimetallic catalyst during the 28 h time-on-stream while the average carbon formation rates of Ni and Co monometallic catalysts are 0.003186 and 0.003973 g_c/g_{cat}-s respectively. Correspondingly, there is no drop in reactant conversion of Ni-Co bimetallic catalyst but significant decrease in reactant conversions of Ni and Co monometallic catalysts.

Table 3.7 Activity and carbon formation rate of Ni and Co monometallic and Ni-Co bimetallic catalysts

Catalyst	Initial conversion (%)		Final conversion (%)		Average carbon formation rate (g_c/g_{cat}-h)
	CH_4	CO_2	CH_4	CO_2	
Ni	62.9	73.4	58.0	69.5	0.003186
Co	67.6	77.0	58.3	71.2	0.003973
Ni-Co	83.8	87.0	83.9	87.1	0

Carbon formation over Ni, Co monometallic catalysts and Ni-Co bimetallic

catalyst was confirmed through TEM analysis for spent catalysts. It identified that the carbon formed on Ni and Co monometallic catalyst is in the form of filamentous whiskers (Fig. 3.15). It indicates that the filamentous whiskers carbon might be the major cause of catalyst deactivation. Also, from literature it can be found that the carbon formation is closely related to the catalyst properties during CO_2 reforming of CH_4. The relationship between catalyst performance, carbon formation, and catalyst properties is discussed in the following section.

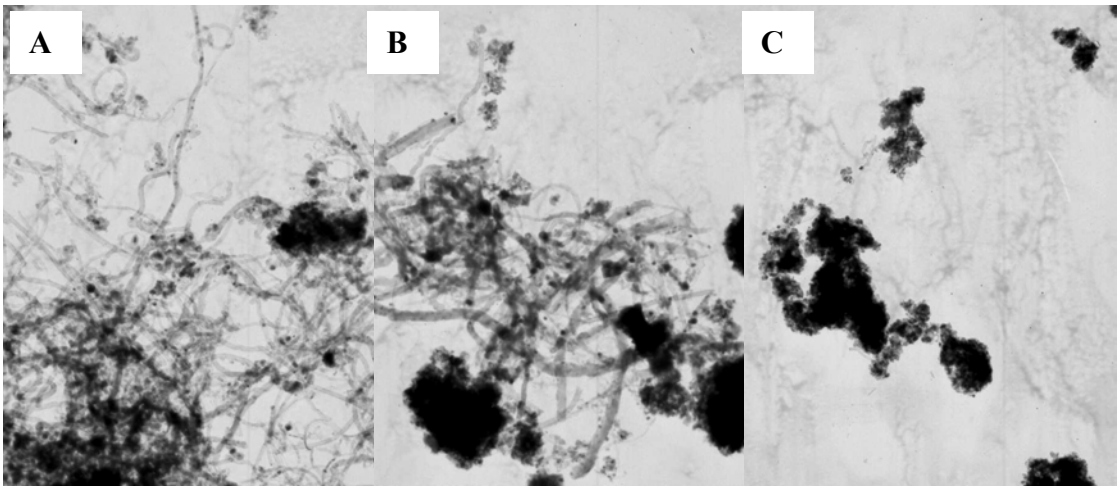

Fig. 3.15 TEM images of spent catalysts. A: Ni catalyst; B: Co catalyst; C: Ni-Co catalyst

3.3.6 Discussion on catalyst activity, stability, and carbon resistance

Catalyst initial activity has direct correlation with active metal content. That is why Ni-Co bimetallic catalyst with higher Ni-Co content had higher initial activity. However, the stability of low Ni-Co content catalyst is better than that of high Ni-Co content catalyst. TG and TEM analysis showed such filamentous whiskers were formed

on the higher Ni-Co content bimetallic catalyst. It demonstrated that the good stability of Ni-Co catalyst with lower Ni-Co content can be ascribed to its higher carbon resistance.

However, when the activity was compared for monometallic and bimetallic catalysts, it was found that the synergy between Ni and Co made significant difference. It shows that Ni and Co monometallic catalysts have similar performances from the test results of Ni and Co monometallic catalysts and Ni-Co bimetallic catalyst at 750 ^{o}C, 1 atm, F=5.5 L/h, $CH_4/CO_2/N_2$=1/1/1, and 0.025 g catalyst shown in Fig. 3.14 and Table 3.7. Fig. 3.14 clearly demonstrates that the activity of Ni and Co monometallic catalysts dropped in the 28 h stability test but the activity of Ni-Co bimetallic catalyst maintained at the same level as its initial value. TG analysis revealed that Ni and Co monometallic catalysts had relatively the same carbon formation rate (0.003186 g_c/g_{cat}-h and 0.003973 g_c/g_{cat}-h, respectively) but Ni-Co bimetallic catalyst did not have detectable carbon formation (Table 3.7). Carbon formation appeared to be the major reason of catalyst deactivation for the monometallic catalysts. Bradford and Vannice (1999) reported that inactive carbon in the form of filamentous whiskers was primarily responsible for the catalyst deactivation.

Different authors attributed carbon resistance to different properties. Ruchenstein and Hu (1995; 1996) attributed the stability and carbon resistance of NiO/MgO to the formation of a solid solution between NiO and MgO. Zhang et al. (1996) and Chang et al. (1996) believed that the promotion of the basicity of catalysts by adding K and Ca enhanced the adsorption of CO_2 and thus suppressed the carbon formation. Other papers (Chen et al., 1999; Ji et al., 2001; Wang and Lu, 1998) have indicated that high carbon

resistance was due to the strong metal-support interaction (SMSI). However, in this case, it is believed that there was formation of solid solutions not only in bimetallic catalyst but also in the monometallic catalysts (Fig. 3.13). The TPR profiles indicate that the bimetallic catalyst had SMSI which confirms the work of previous researchers (Ahn et al., 2006). In case of monometallic and bimetallic catalysts, in this reasearch there was no basicity when they were measured using CO_2-TPD (TPD results are not shown because all CO_2-TPD profiles were smooth flat lines without any CO_2-desorption peaks). Compared the carbon resistance between Ni-Co bimetallic catalyst and Ni and Co monometallic catalysts, it is believeed that the excellent carbon resistance of Ni-Co is resulted from the synergy of Ni and Co, and better metal dispersion. In addition, the formation of various spinel-type solid solutions, the SMSI, and the good sintering resistance of MgO phasees also played their roles in the high catalytic activity and excellent carbon resistance.

3.4 CONCLUSIONS

Ni-Co bimetallic catalysts made by coprecipitating Ni-, Co-, Al-, and Mg-containing precursor solutions demonstrate superior performance for carbon dioxide reforming of methane. The synergy of Ni and Co in the bimetallic catalysts not only provides high activity but also excellent carbon resistance and thus makes the catalysts with outstanding stability. Comparative studies conducted with Ni and Co monometallic catalysts and Ni-Co bimetallic catalyst show that the superior performance of Ni-Co catalysts comes from high BET surface area, small pore diameter, relative easy

reducibility, good metal dispersion, high metallic surface, formation of different types of solid solutions, and SMSI.

4 EFFECTS OF Ni AND Co CONTENTS ON THE Ni-Co/AlMgOx BIMETALLIC CATALYSTS

This chapter, except section 4.3.1-Effects of Ni/Co ratio, was copyrighted and published in **Applied Catalysis A: General:** Zhang, J., Wang, H., Dalai, A.K., "Effects of metal content on activity and stability of Ni-Co bimetallic catalysts for CO_2 reforming of CH_4", *Appl. Catal.* A 339 (2) 121-129 (**2008**).

CONTRIBUTION OF Ph.D. CANADIDATE

Experiments were planned and performed by Jianguo Zhang. Hui Wang and Ajay K. Dalai provided guidance in planning the experiment. The submitted manuscript was written by Jianguo Zhang, while Hui Wang and Ajay K. Dalai provided comments and suggestions for revision.

CONTRIBUTION OF THIS CHAPTER TO THE OVERALL STUDY

Focusing on the Ni-Co/$AlMgO_x$ bimetallic catalysts designed and developed in Chapter 2 and Chapter 3, this paper investigated the effects of Ni/Co ratio and Ni-Co overall content. The work involves the catalyst preparation, catalyst testing, and catalyst characterization. This work revealed that carbon-free operation for CO_2 reforming of CH_4 can be achieved over Ni-Co bimetallic catalysts through adjusting Ni-Co content.

ABSTRACT

Ni-Co bimetallic catalysts with a general formula of Ni-Co/$AlMgO_x$ prepared using coprecipitation has shown excellent stability and high activity for CO_2 reforming of CH_4 as discussed in Chapter 3. This chapter focuses on the effects of Ni/Co ratio and Ni-Co content of the catalyst, attempting to eliminate carbon formation on the catalyst. Catalyst samples with Ni and Co loadings ranging between 2.54 and 18.9 wt% and 3.87 and 16.8 wt%, respectively, were prepared and the activity and stability for CO_2 reforming of CH_4 was tested at 750 ^oC and 1 atm using a high GHSV of 180,000 mL/g_{cat}-h. The results show that catalysts with lower Ni-Co content (2.57-4.99 wt% for Ni and 3.87-6.27 wt% for Co) had high and stable activity with no deactivation and no detectable carbon formation and that those of higher Ni-Co content (7.22-18.8 wt% for Ni and 10.9-16.8 wt% for Co) experienced deactivation with significant carbon formation in a 250 h period. The catalysts were characterized using XRD, H_2-TPR, TG/DTG-TPO, N_2-physisorption, and CO-chemisorption. It was found that catalyst with lower Ni-Co content has larger surface area and better metal dispersion and therefore gives rise to smaller metal particles (<10 nm) which is essential to the complete suppression of the carbon formation on catalysts.

4.1 INTRODUCTION

In the development of Ni-based catalysts for CO_2 reforming of methane, the focus is always directed on the effective suppression of carbon formation, or carbon deposition, on catalyst surface during reaction (Hu and Ruchenstein, 2002; 2004; Bradford and Vannice, 1999). Although tremendous attempts have been made and a number of papers have been published, carbon formation is still a great challenge for Ni-based catalyst, which prevents CO_2 reforming of CH_4 from being a widely commercialized technology. In fact, there is great potential in the application of CO_2 reforming of CH_4 technology in areas such as conversion of biomass and landfill gases into "Green Power" (Vasileiadis and Ziaka-Vasileiadou, 2004). Also, the synthesis gas with a lower H_2/CO ratio produced through CO_2 reforming of CH_4 is the desired feedstock for Fischer-Tropsch synthesis (Ginsburg et al., 2005).

A very stable and highly active Ni-Co bimetallic catalyst with a general formula Ni-Co/AlMgO_x has been presented in Chapter 3, which was prepared by coprecipitation method and has undergone through 2,000 h stability test for CO_2 reforming of CH_4 where no significant deactivation was observed (Zhang et al., 2006; 2007). Compared with other reported catalysts used for CO_2 reforming of CH_4, this Ni-Co bimetallic catalyst is able to remarkably suppress carbon deposition during the reaction. With a very small amount of carbon formed during the initial period of reaction, the catalyst still maintains a high activity for a long time. The excellent performance of this catalyst results from the

synergic combination of the following contributing factors. The co-precipitation preparation method and high-temperature calcinations make the catalyst with a stable $Ni_xMg_{1-x}Al_2O_4$ and $Co_xMg_{1-x}Al_2O_4$ spinel-like framework structure and strong metal-support interaction (SMSI). This method also facilitates small metal particle size after the precipitate is reduced. The combining use of Al and Mg oxides provides the catalyst with not only relative high surface area but thermal stability. The formation of Ni-Co alloy during the catalyst reduction effectively suppresses the carbon formation which is more difficult to overcome by Ni active sites themselves. Previous research has also shown that the variation in Ni-Co content in catalyst would affect the severity of carbon deposition, suspecting the change of Ni-Co content may alternate the size of active sites to which carbon formation is sensitive. Many authors have observed the sensitiveness of carbon deposition to metal particle size on catalyst surface. Work by Rostrup-Nielsen indicates (Rostrup-Nielsen, 1984) that large nickel clusters are susceptible to carbon formation. When using promoters K and Ca to suppress carbon deposition, Osaki et al. (2001) believed that K divided the Ni surface into small particles and thus inhibited carbon formation. Various authors have observed the critical Ni particle size below which carbon formation could be significantly reduced or eliminated. Tang et al. (2000) reported that a 10 nm metallic nickel particle was critical to inhibiting carbon formation. Kim et al. (2000) suggested a critical particle size of suppressing carbon formation was 7 nm.

This chapter focuses on the effects of Ni-Co content on catalyst properties and catalyst performance with an attempt to eliminate carbon formation for CO_2 reforming of

CH_4 over Ni-Co bimetallic catalysts. A series of catalysts with different Ni/Co ratio and Ni-Co contents are comparatively investigated. The relationship between catalyst performance and catalyst properties is discussed. The major cause of carbon formation on Ni-Co bimetallic catalyst is identified. And finally, carbon free operation for CO_2 reforming of CH_4 over a Ni-Co bimetallic catalyst is achieved.

4.2 EXPERIMENTAL

4.2.1 Catalyst preparation

Ni-Co/$AlMgO_x$ catalysts with different Ni/Co ratio and Ni-Co contents were prepared using the same method described in previous chapters. The catalyst made was denoted as 0.16Ni0.18Co, 0.06Ni0.09Co, 0.04Ni0.05Co, and 0.02Ni0.03Co, respectively, with the number indicating the mole fraction on the metal basis in the catalysts.

4.2.2 Catalyst Characterization

The catalysts were characterized using N_2 adsorption for specific surface area and pore distribution, TPR for reducibility, CO-chemisorption for metallic surface area and metal disperation, XRD for crystal structures, TG/DTG for carbon formation, and TEM for particle size. They were described in detail in the experimental section of Chapter 3.

4.2.3 Catalyst testing

In this work, the amount of catalyst used in each test was 30 mg. Reactant feed was introduced into the reactor at a GHSV of 180,000 mL/g_{cat}-h. Detailed catalyst testing procedure was described in chapter 2 and chapter 3.

4.3 RESULTS AND DISCUSSION

4.3.1 Effects of Ni/Co ratio

4.3.1.1 Elemental composition

A series of Ni-Co bimetallic catalysts with various Ni/Co ratios were made to investigate the effects of Ni/Co ratio. The effect of Ni content is investigated by increasing it from zero to 24 mol% while Co content is maintained constant. The effect of Co content is studied by varying it from zero to 24 mol% when Ni content is unchanged. The designed elemental composition of Ni-Co bimetallic catalysts with various Ni/Co ratios are listed in Table 4.1. It may be noticed that the content of Al and Mg is also changing with the change of Ni/Co ratio. It happens due to the characteristic of co-precipitation preparation of catalysts when total metal element content is normalized to unit. In this work, the Al/Mg ratio is maintained at 0.4-0.8.

Table 4.1 Ni/Co ratio and elemental composition

Ni/Co ratio	Designed Elemental composition (mol%)			
	Ni	Co	Al	Mg
0/1	0	6	31	63
1/1	6	6	30	58
2/1	12	6	30	52
4/1	24	6	29	38
1/0	6	0	32	62
1/2	6	12	26	56
1/4	6	24	20	50

4.3.1.2 Effects of Ni/Co ratio on BET surface area

By keeping either Ni or Co constant and changing another, the effects of Ni/Co ratio on the BET surface area are shown in Fig. 4.1 A and B.

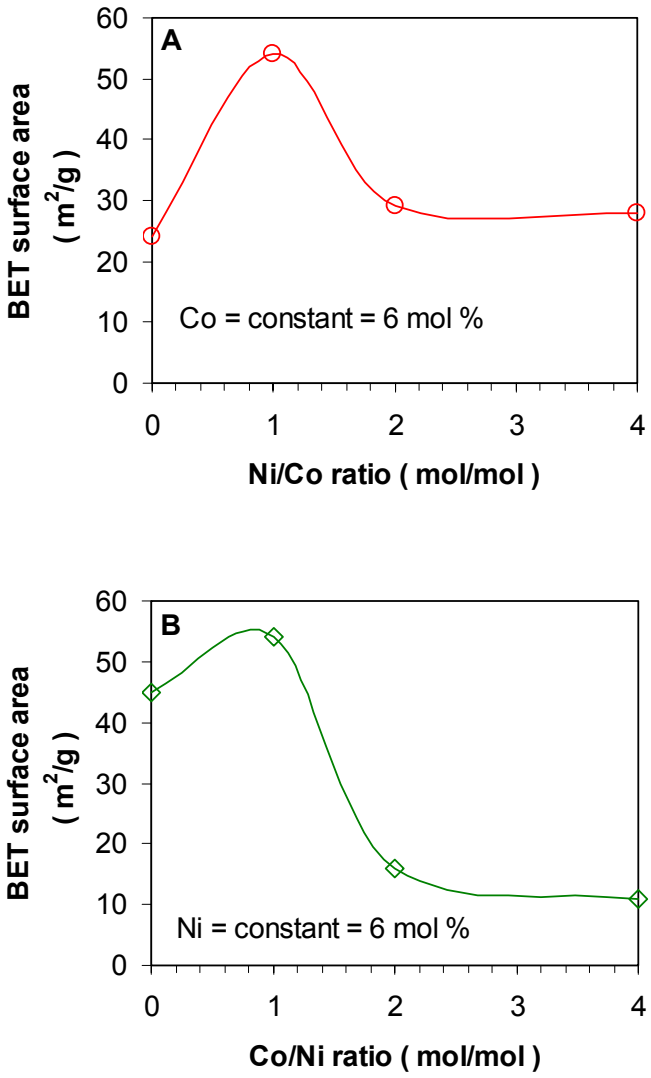

Fig. 4.1 Effects of Ni/Co ratio on the BET surface area of the samples

When Co content is constant, the designed Ni/Co ratio of 1 gives the highest surface area of 54 m^2/g. In comparison with Ni/Co=1, other ratios show no significant difference with a surface area between 24 and 29 m^2/g when the Ni/Co ratios are 0, 2, and 4 (Fig. 4.1A). From Fig. 4.1B, it can be seen that the increase in Co/Ni ratio with the exception of Co/Ni=1 makes the surface area decreased significantly from 45 m^2/g at Co/Ni=0 to 16 and 11 m^2/g at Co/Ni=2 and 4. Therefore, from the prospective of large

surface area, a Ni/Co ratio between 0.6 and 1.5 is preferred.

4.3.1.3 Effects of Ni/Co ratio on pore distribution

Fig. 4.2A shows the pore volume as a function of pore diameter and Fig. 4.2B shows the cumulative volume as a function of pore diameter.

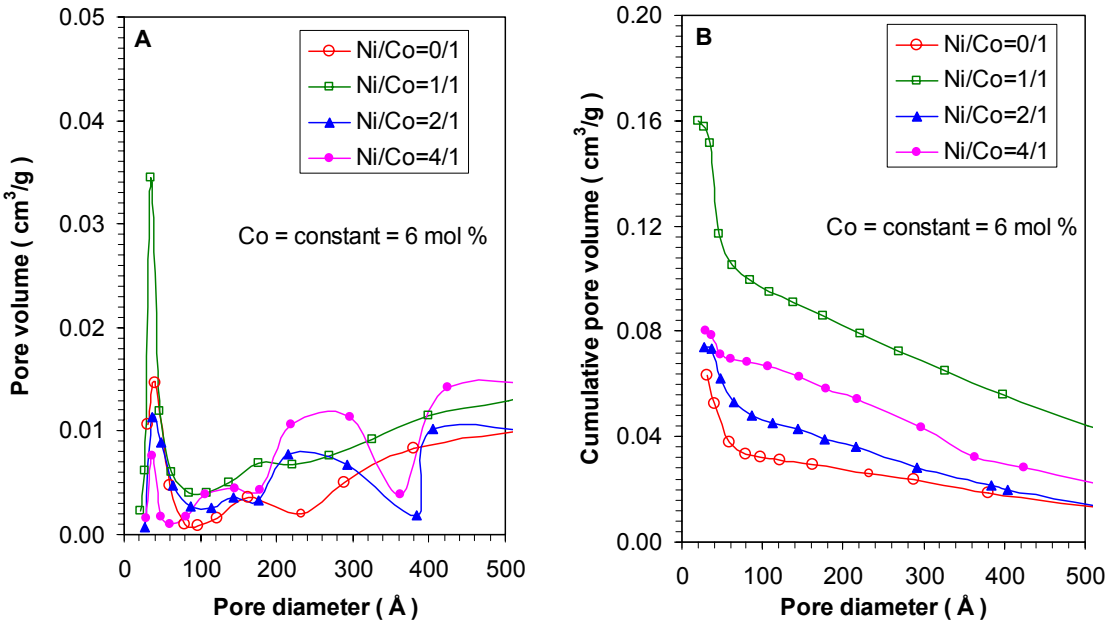

Fig. 4.2 Pore volume distribution as a function of Ni/Co when Co content is constant

Clearly the samples with a Ni/Co ratio close to 1 have higher pore volume. All peak maxima of the samples are at around 35 Å. Correspondingly, the catalyst with Ni/Co=1 has the highest accumulative pore volume. With the increase in Ni/Co ratio, the pore volume and accumulative pore volume of the samples is dropping. In the case of maintaining Ni content constant, the pore volume distribution is shown Fig. 4.3.

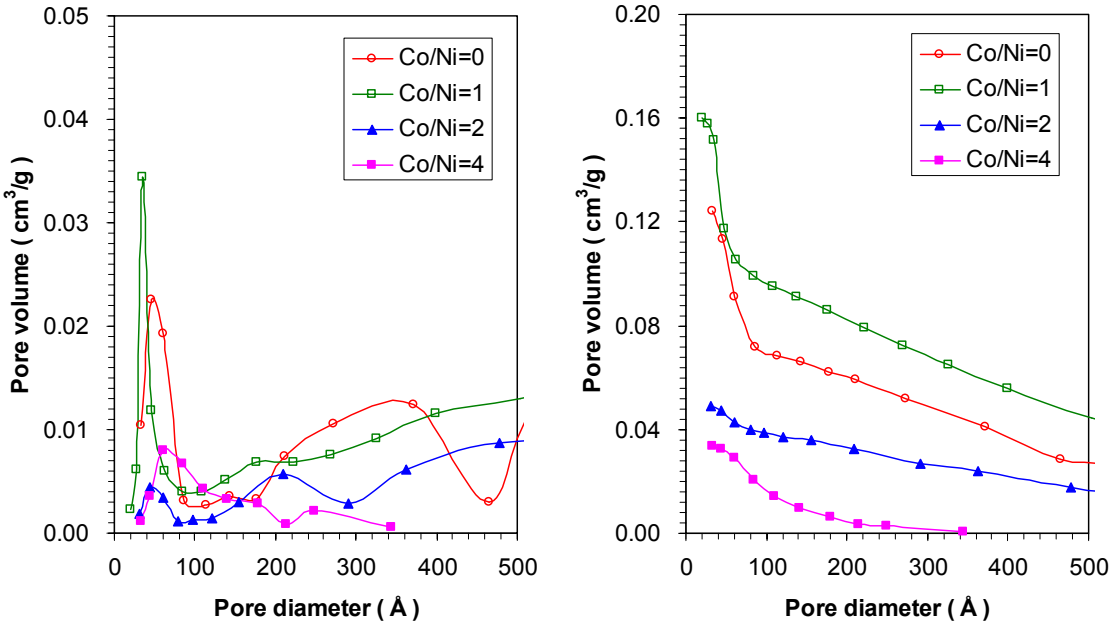

Fig. 4.3 Pore volume distribution as a function of Co/Ni when Ni content is constant

From Fig. 4.3, it can be seen that similar pattern are shown, i.e. the sample with Co/Ni=1 has the highest volume. However, the peak maximums of the samples are moving toward to bigger pores with the increase in Co/Ni ratio (Fig. 4.3 A). For different samples, the pore diameter where the pore volume peak maximum is follows the order: Ni/Co=1 (35 Å) < Ni/Co=0 (43 Å) < Ni/Co=2 (45 Å) < Ni/Co=4 (60 Å). The accumulative pore volumes are following the same order: Ni/Co=1 (0.160 cm^3) < Ni/Co=0 (0.124 cm^3) < Ni/Co=2 (0.049 cm^3) < Ni/Co=4 (0.033 cm^3). From the pore distribution it can be seen that a Ni/Co ratio of unity gives the highest pore volume with smallest average pore diameter.

4.3.1.4 Effects of Ni/Co ratio on phase structure

The XRD spectra for the samples with various Ni/Co or Co/Ni ratios are shown in Fig. 4.4. Spinel phases and MgO-type phases were observed in all the three samples. No clear difference was revealed among the samples except the intensity is slightly different with different Ni/Co or Co/Ni ratios.

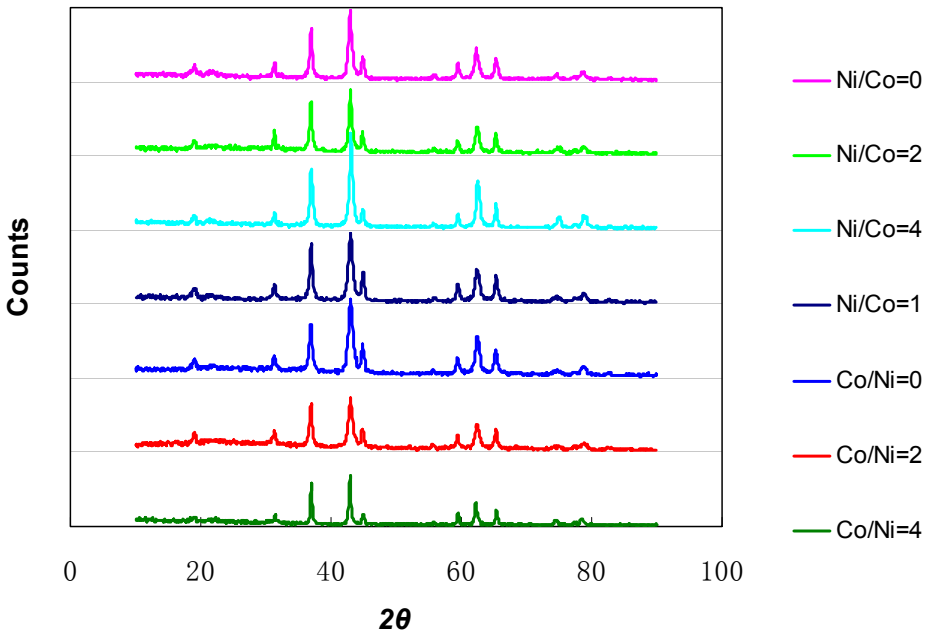

Fig. 4.4 XRD analysis for the Ni-Co/AlMgO$_x$ catalysts with various Ni/Co or Co/Ni ratios calcinated at 900 ^{o}C

Ni^{2+}, Co^{2+}, Mg^{2+}, and Al^{3+} are in the same lattice in the Ni/Co/Al/Mg composite catalysts (Tichit et al., 1997; Ribet et al., 1999; Coq et al., 2000). A high calcination temperature favours the formation of Ni^{2+}-Al^{3+}, Co^{2+}-Al^{3+}, and Mg^{2+}-Al^{3+} solid solutions of spinel-type and of the stoichiometric $NiAl_2O_4$, $CoAl_2O_4$, and $MgAl_2O_4$ spinel phases (Tichit et al., 1997; Ribet et al., 1999; Coq et al., 2000). The Ni^{2+}-Co^{3+} spinel-type solid solution and $NiCo_2O_4$ spinel can also be formed at high calcination temperatures (Petrov

and Will 1987). These spinel-type solid solution phases and spinel phases in the catalysts are quite indistinguishable by XRD (Fig. 4.4) due to their similarity. From the XRD analysis, it shows that XRD analysis does not provide enough information for the investigation of Ni/Co or Co/Ni ratios in the samples.

4.3.1.5 Effects of Ni/Co ratio on catalyst activity for CO_2 reforming of CH_4

The activity of the samples was tested using 0.03g catalyst at various GHSV for CO_2 reforming of CH_4 at 750 ^oC, 1 atm, and $CH_4/CO_2/N_2$=1/1/1. Fig. 4.5 shows the activity of catalysts with various Ni/Co ratios in terms of reactant conversion.

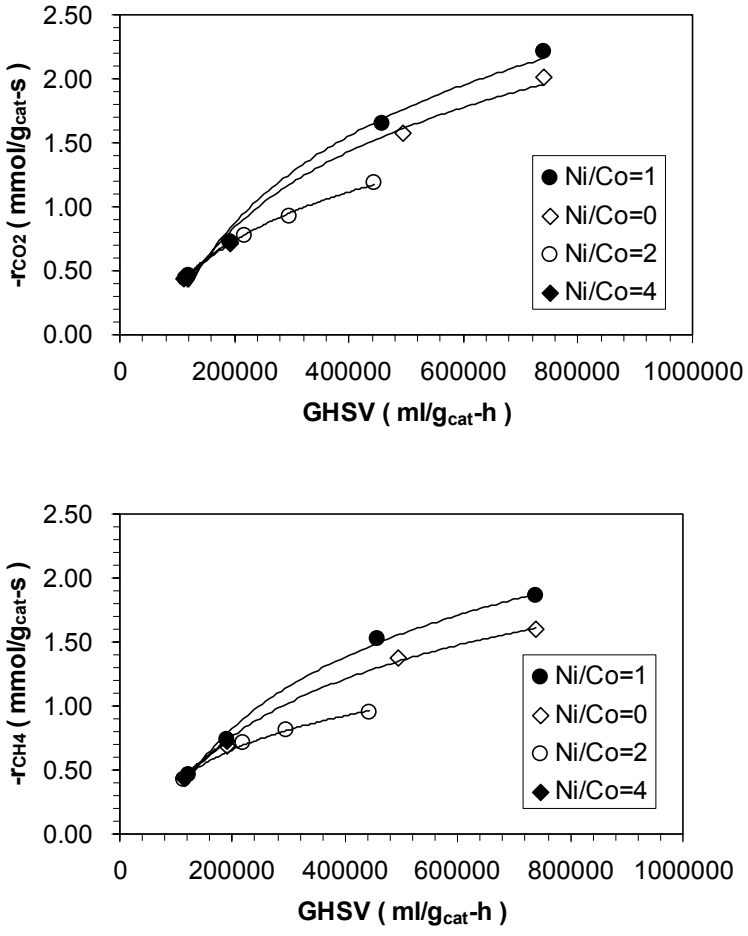

Fig. 4.5 Activity of catalyst with various Ni/Co ratios for CO_2 reforming of CH_4

From Fig. 4.5, it is clearly that at lower GHSVs all sample showed close activity. However, with the increase in GHSV, it is clear that the catalyst with Ni/Co=1 had the highest activity. The activity of the samples followed the order: Ni/Co=1 > Ni/Co=0 >Ni/Co=2 >Ni/Co=4. Also, it can be noticed that there was no results for Ni/Co=4 when GHSVs were higher than 200,000 mL/gcat-h and no results for Ni/Co=2 when GHSVs higher than 450,000 mL/g_{cat}-h. That was because the experiments were terminated due to pressure build up in the reactor, which caused by the carbon formation on these two catalysts. The activity of samples with various Co/Ni ratios is shown in Fig. 4.6.

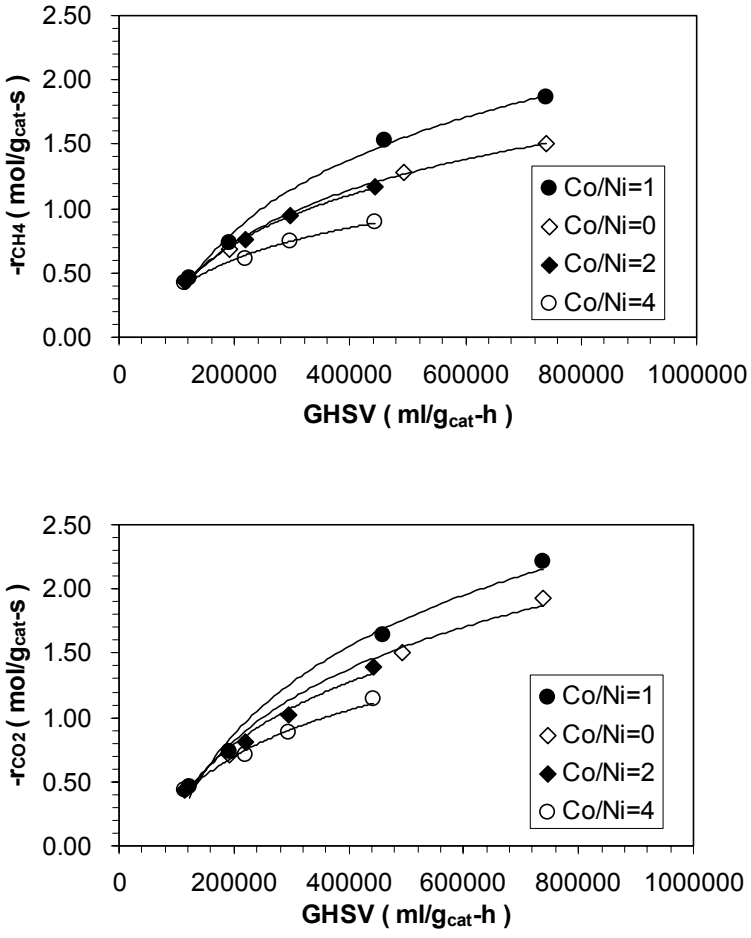

Fig. 4.6 Activity of catalyst with various Co/Ni ratios for CO_2 reforming of CH_4

Fig. 4.6 shows the similar results as Fig. 4.5, i.e. the sample with Co/Ni=1 had the highest activity. Activity followed the order of: Co/Ni=1 > Co/Ni=0 >Co/Ni=2 >Co/Ni=4.

The effects of Ni/Co ratios and Co/Ni ratios on the properties and performances of the samples clearly indicated that the catalyst with Ni/Co=1 had the highest BET surface area and the highest activity for CO_2 reforming of CH_4. It is recommended that a Ni/Co ratio between 0.6 and 1.5 should be applied. In the following section, the effects of Ni-Co content on catalyst properties and performance is discussed.

4.3.2 Effects of Ni-Co content on catalyst properties and performance for CO_2 reforming of CH_4

4.3.2.1 Bulk properties of the samples

The phase structure of the unreduced catalysts (calcined precipitates) was analyzed using X-ray diffraction (XRD). The XRD patterns of the calcined precipitates are shown in Fig. 4.7. A phase assigned to spinel-like structures with the characteristic diffraction peaks at 2θ of 30.7°, 36.8°, 44.4°, 59.8°, and 65.2° (Tsyganok et al., 2003) was observed in all samples with different Ni-Co content. The spinel-like phases could be $Ni_xMg_{1-x}Al_2O_4$, $Co_xMg_{1-x}Al_2O_4$, or their composites, which are indistinguishable by XRD due to their similar morphology (Tichit et al., 1997; Coq et al., 2000). As the Ni-Co content increases, obvious increase in peak intensity was observed for the peaks at 2θ = 41.5° and 61.2°, indicating the increase in the amount of Ni-Mg-O solid solution and Co-Mg-O solid solution (Ruckenstein and Yu, 1997; Chen et al., 1997). The XRD analysis shows that all the samples under calcination at 900 °C have been well-crystallized. It can also be seen

from the XRD patterns that the bulk phases of the samples were not alternated significantly with the change of Ni-Co content.

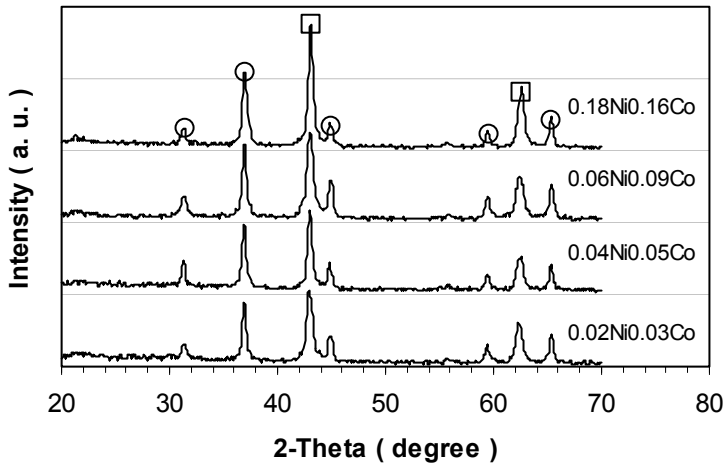

Fig. 4.7 XRD patterns for samples with different Ni-Co content calcined at 900 ^{o}C ○Spinel-like structures □ Solid solutions

The reducibility of the catalyst samples was measured using hydrogen temperature-programmed reduction (TPR). From the TPR profiles, shown in Fig. 4.8, following observations can be made: (1) For the bimetallic catalysts with different Ni-Co content, only one domain exists for the H_2 consumption which is featured by a single broad peak instead of two separate peaks for Ni and Co reduction, respectively. This may indicate the formation of Ni-Co alloy to some extent. Rinkowski et al. (1995) also reported the one-stage reduction of bimetallic Ni-Pt catalysts which they believe to illustrate the alloying of metals in the reduction process. (2) The H_2 consumption domain appears at broader temperature range of 650-900 ^{o}C for 0.18Ni0.16Co but at higher temperatures (700-950 ^{o}C) for other samples with lower Ni-Co content. The reduction of the bimetallic catalysts

between 650 ^{o}C and 950 ^{o}C is probably resulted from the reduction of Ni and Co in a very complex quaternary spinel-like phase (Coq et al., 2000). The shift of peak maximum to higher temperatures with the decrease of Ni-Co can be ascribed to the increase of metal-support interaction (Ann et al., 2006).

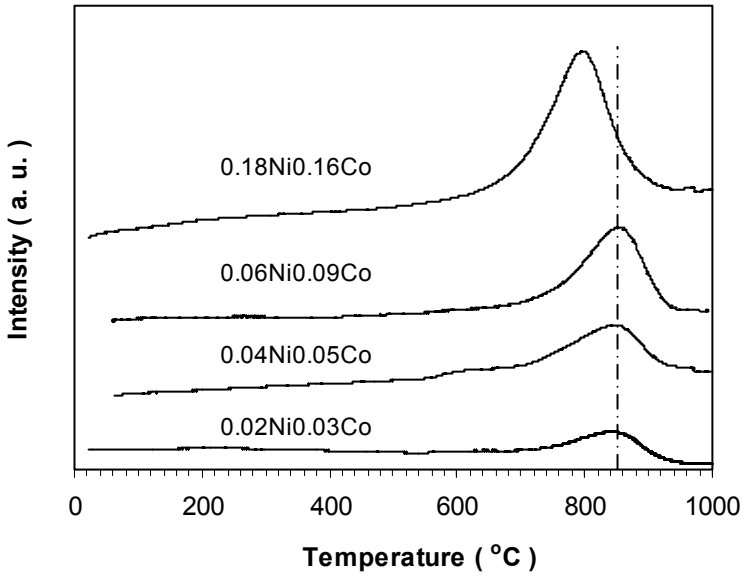

Fig. 4.8 Temperature-programmed reduction of the samples with different Ni-Co content calcinated at 900 ^{o}C

4.3.2.2 Surface area and pore size distribution of the catalysts

N_2-physisorption was employed to measure the surface area and pore size distribution. The BET specific surface area of the precipitates after calcination at 900 ^{o}C, ranging between 27 and 70 m^2/g, is given in Table 4.2. The surface area follows the order of 0.02Ni0.03Co > 0.04Ni0.05Cu > 0.06Ni0.09Co > 0.18Ni0.16Co, with a decrease at a higher (Ni+Co)/(Al+Mg) ratio (Fig. 4.9). On the other hand, the decrease of surface area with the decrease of Al-Mg content provides evidence for the stabilizing role of Al and Mg in the catalysts (Ribet et al., 1999).

Table 4.2 Composition and specific surface area of Ni-Co bimetallic catalysts calcined at 900 °C

Sample	Ni:Co:Al:Mg* (atomic ratio)	Ni (wt%)	Co (wt%)	BET surface area (m^2/g)
0.02Ni0.03Co	2:3:32:63	2.57	3.87	70
0.04Ni0.05Co	4:5:30:61	4.99	6.27	56
0.06Ni0.09Co	6:9:28:56	7.22	10.9	45
0.18Ni0.16Co	18:16:26:40	18.8	16.8	27

*Oxygen content was calculated stoichiometrically based on the oxidizing valence of metals: Ni^{2+}, Co^{3+}, Al^{3+} and Mg^{2+}.

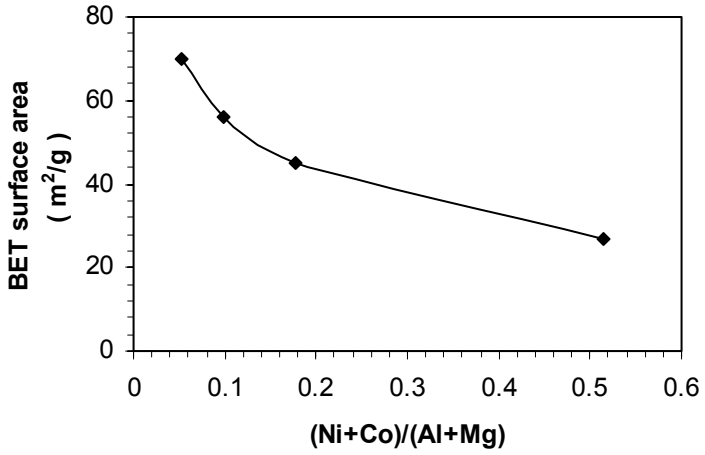

Fig. 4.9 Variation of BET surface area with various (Ni+Co)/(Al+Mg) ratios

The pore size distribution is shown in Fig. 4.10 which was obtained from the adsorption branch of the N_2 isotherm by the Barret-Joyner-Halenda (BJH) method (Rostrup-Neilsen and Hansen, 1993; Barret et al., 1951). It indicates that the pores culminate at around 30 Å (Fig. 10A). With the increase of Ni-Co content, the small pores, typically less than 100 Å, drops significantly from around 0.045 cm^3/g_{cat} of 0.02Ni0.03Co to 0.0075 cm^3/g_{cat} of 0.18Ni0.16Co (Fig. 10B). The N_2-physisorption reveals that the Ni-

Co content has significant effects on the specific surface areas and pore size distribution of the catalysts.

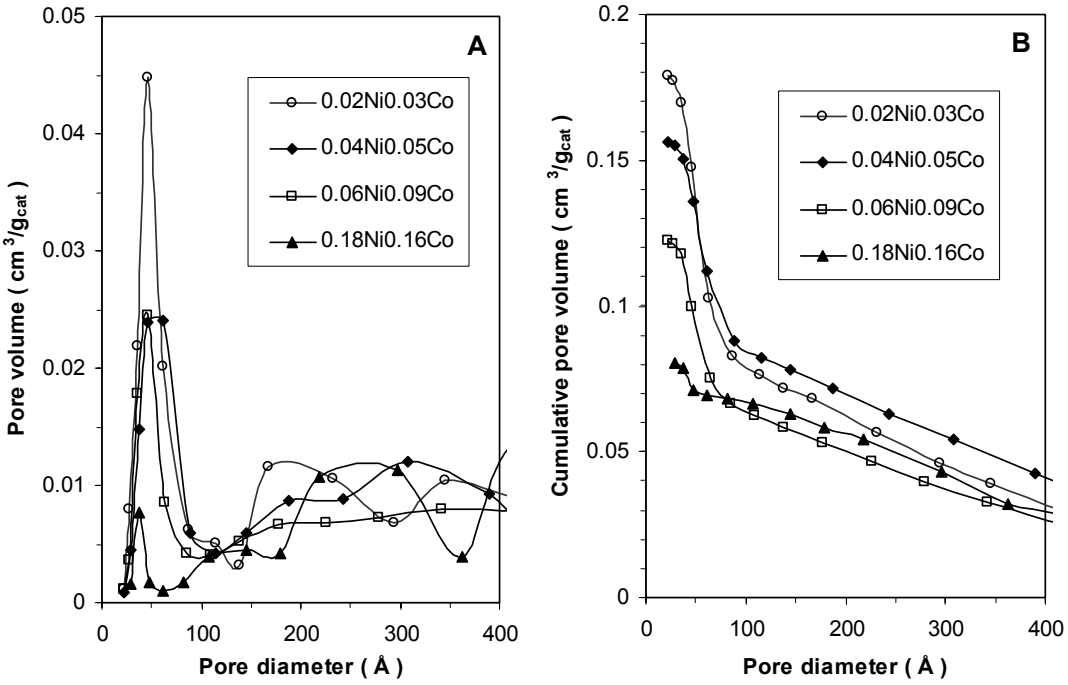

Fig. 4.10 Pore size distribution of the catalysts with different Ni-Co content

4.3.2.3 Metal dispersion and particle size

The metallic surface area and metal dispersion of the samples obtained through CO-chemisorption are tabulated in Table 4.3. The metal dispersion was calculated based on total Ni-Co content in the catalysts. Table 4.3 clearly shows that the metal dispersion increases with the decrease of Ni-Co content following the order: 0.03Ni0.02Co > 0.04Ni0.05Co > 0.06Ni0.09Co > 0.18Ni0.16Co. The metallic surface area increases with Ni-Co content, but it abruptly drops for 0.18Ni0.16Co.

Table 4.3 Metallic surface area and metal dispersion of Ni-Co bimetallic catalysts with different Ni-Co content

Sample	Metallic Area (m^2/g)	Metal Dispersion (%)
0.02Ni0.03Co	1.7	9.5
0.04Ni0.05Co	2.9	8.8
0.06Ni0.09Co	4.1	7.5
0.18Ni0.16Co	1.7	1.3

The metal particle morphology and size distribution are investigated using TEM and are shown in Fig. 4.11. The TEM pictures show that 0.18Ni0.16Co has the most contrasted metal particles with around 20 % particles larger than 10 nm (Fig. 4.11A). As the metal content was reduced, the amount of the large metal particles decreased significantly. When the Ni-Co content was reduced further to 0.04Ni0.05Co and 0.02Ni0.03Co, all particle sizes were smaller than 10 nm. Also, the portion of the smaller particle was increased with the decrease in the Ni-Co content. From 0.18Ni0.16Co to 0.02Ni0.03Co, the portion of particle between 1 and 5 nm was increased from 52 % to 76 %. Another observation was that the boundary between metals and support in cases of 0.04Ni0.05Co and 0.02Ni0.03Co became indistinct in comparison with the higher Ni-Co content catalysts as one can see from Fig. 4.11

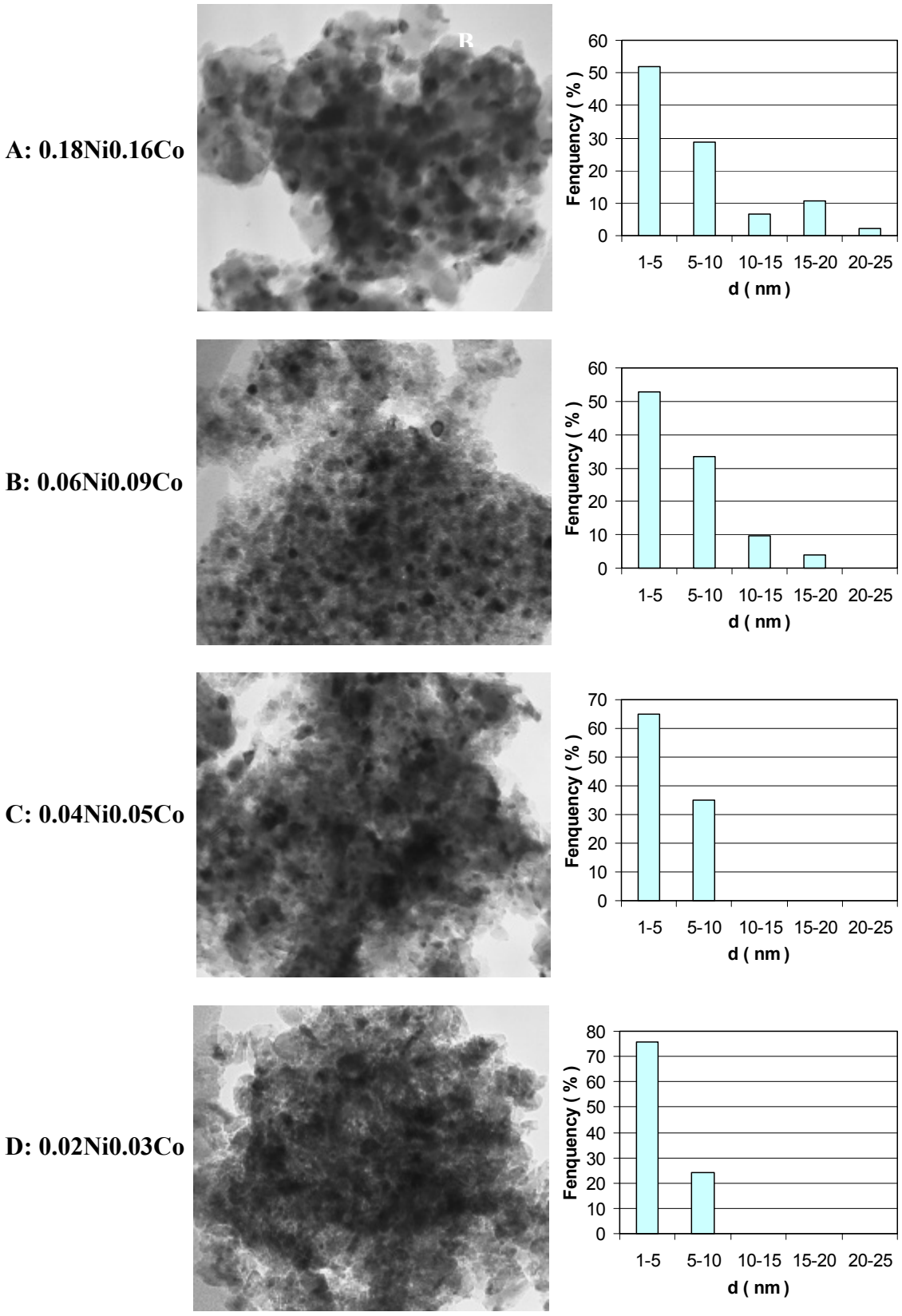

Fig. 4.11 TEM image of Ni-Co catalysts with different metal content and particle size

4.3.2.4 CO_2 reforming of CH_4 and carbon formation

The catalysts were tested at 750 ^oC, 1 atm, and 180,000 mL/g_{cat}-h. Fig. 12A shows the CH_4 disappearance rate versus time-on-stream over the bimetallic catalysts with different Ni-Co content. Fig. 12B presents the same results in terms of CH_4 conversion. At the reaction conditions, the equilibrium CH_4 conversion is 94.5 %. Both the activity and stability followed the order: 0.02Ni0.03Co > 0.04Ni0.05Co > 0.06Ni0.09Co > 0.18Ni0.16Co. The apparent deactivation was not observed for 0.02Ni0.03Co during the period of 250 h. The catalyst maintained a stable CH_4 reaction rate at 0.666 mmol/g_{cat}-s. For catalyst 0.04Ni0.05Co, the activity increased gradually with time in the first 50 h and then remained with a stable CH_4 reaction rate which was 0.621 mmol/g_{cat}-s. The higher reaction rate at the initial period was reported and was ascribed to the formation of new active sites when the catalyst was exposed to the reaction mixture (Ruckenstein and Hu 1996, Zhang et al., 1996; Tsopiroaro and Verykios, 2001). However, apparent deactivation was observed over catalysts 0.06Ni0.09Co and 0.18Ni0.16Co. During the 250 h time-on-stream, the reaction rates of CH_4 over 0.06Ni0.09Co and 0.18Ni0.16Co has dropped from 0.629 mmol/g_{cat}-s to 0.481 mmol/g_{cat}-s and from 0.516 mmol/g_{cat}-s to 0.376 mmol/g_{cat}-s, respectively.

Table 4.4 gives the amount of carbon deposit on the spent catalysts which have undergone 250 h time-on-stream. The results were obtained using thermal gravimetric analysis (TG/TGA). Combined with Fig. 4.12, it is clear that 0.02Ni0.03Co and 0.04Ni0.05Co, which showed higher activity and stability, had no detectable carbon

formation and no deactivation. However, 0.06Ni0.09Co and 0.18Ni0.16Co which showed relatively low activity and significant deactivation had carbon formation up to 0.30 and 0.46 g_c/g_{cat}, respectively.

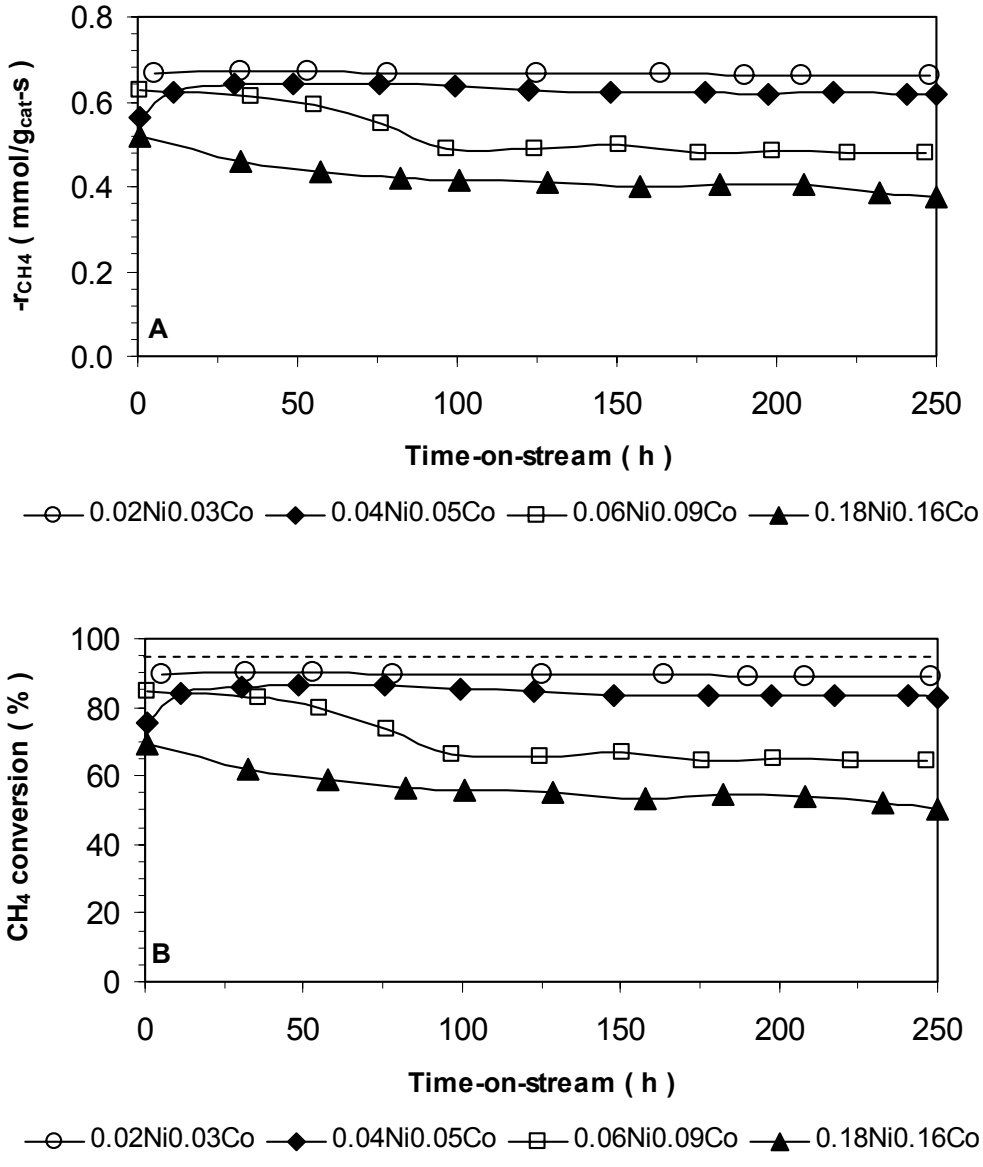

Fig. 4.12 Activity as a function of TOS of catalysts with different Ni-Co content

Table 4.4 Carbon formation of the bimetallic catalysts with different Ni-Co contents

Sample	Carbon deposit at 250 h (g_c/g_{cat})
0.02Ni0.03Co	0
0.04Ni0.05Co	0
0.06Ni0.09Co	0.300
0.18Ni0.16Co	0.446

The thermo-gravimetric (TG) and differential thermo-gravimetric (DTG) profiles of the temperature programmed oxidation (TPO) in air of the spent catalysts are shown in Fig. 4.13 The slight weight loss over 0.02Ni0.03Co and 0.04Ni0.05Co occurring at around 100 ^{o}C (Fig. 4.13A) was probably resulted from the evaporation of moisture. However, the carbon deposits over 0.06Ni0.09Co and 0.18Ni0.16Co were oxidized at around 420-650 ^{o}C (Fig. 4.13A and 4.13B). Further TEM analysis revealed no detectable carbon deposits over 0.02Ni0.03Co and 0.04Ni0.05Co (Fig. 4.14C and 4.14D), but clear filamentous carbon in the form of carbon nanotubes was found over spent 0.06Ni0.09Co and 0.18Ni0.16Co catalysts (Fig. 4.14A and 4.14B). The catalyst testing and carbon analysis indicated that catalyst with high Ni-Co content is more susceptible to carbon formation and deactivation.

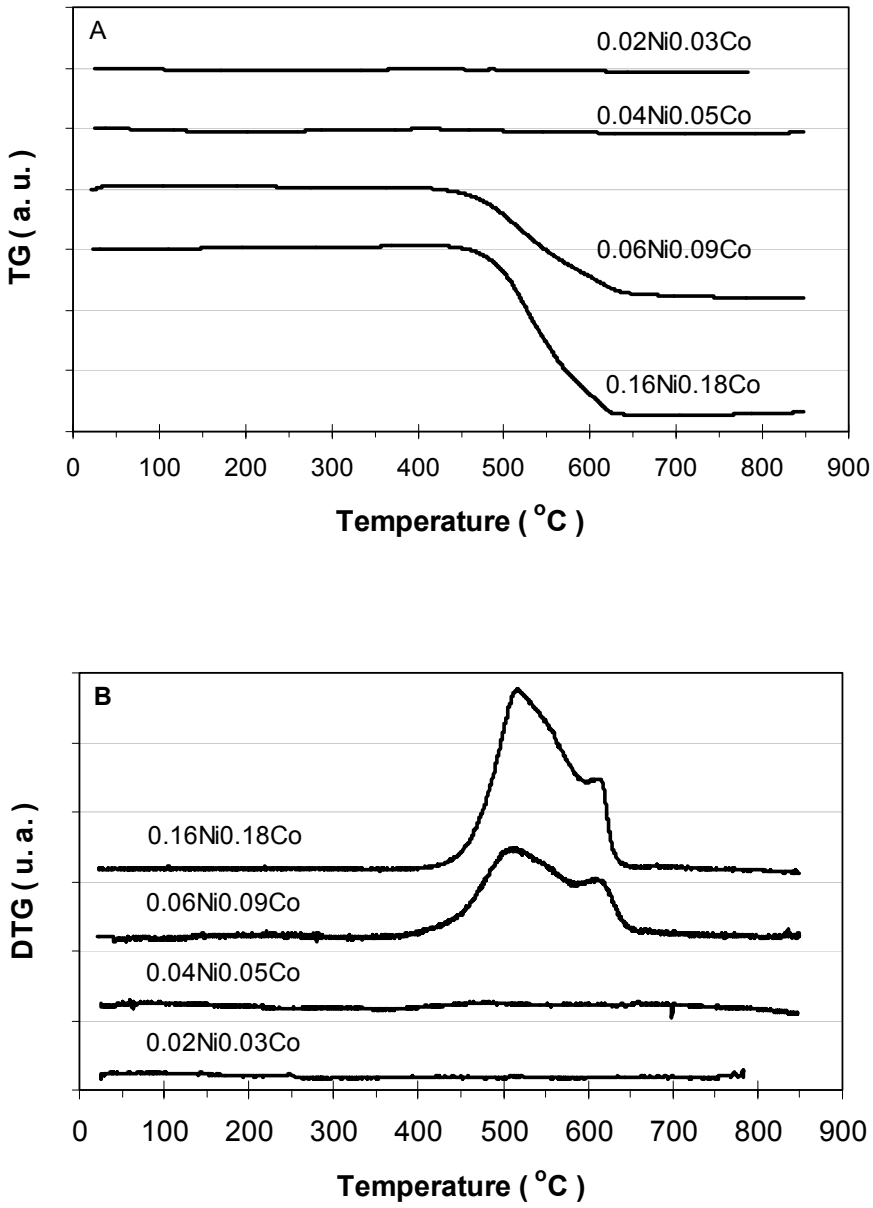

Fig. 4.13 TG (A) and DTG (B) profiles of TPO in air for the catalysts after 250 h reaction at 750 °C, 1 atm, GHSV=180,000 mL/g_{cat}-h, and $CH_4/CO_2/N_2$=1/1/1

A: 0.18Ni0.16Co

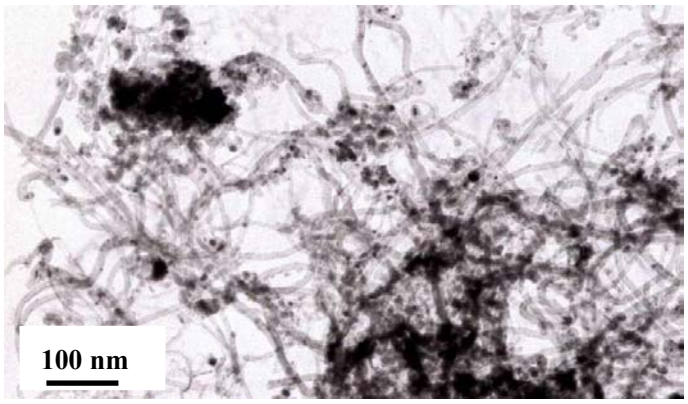

B: 0.06Ni0.09Co

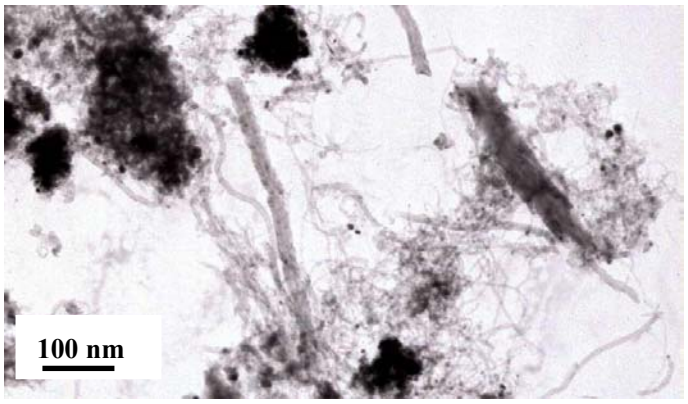

C: 0.04Ni0.05Co

D: 0.02Ni0.03Co

Fig. 4.14 TEM images of different Ni-Co content catalysts after 250 h TOS

4.3.2.5 Effects of Ni-Co content on properties and activity of Ni-Co bimetallic catalysts for CO_2 reforming of CH_4

N_2-physisorption has revealed that 0.18Ni0.16Co has lower surface area and fewer small pores than other catalysts with lower Ni-Co content (Table 4.2 and Fig. 4.9). This probably can be attributed to the relative less Al element in the sample, which is supposed to facilitate high surface area. On the other hand, less Mg ratio in this catalyst can also result in a lower surface area due to the weakening in its stabilizing role in the high-temperature calcination process. Contrarily, 0.02Ni0.03Co with higher Al-Mg content has a higher surface area and more small pores (Table 4.2 and Fig.4.9). The activity of the catalysts in terms of CH_4 reaction rate follows the same order as their surface area and the amount of small pores: 0.02Ni0.03Co > 0.04Ni0.05Co > 0.06Ni0.09Co > 0.18Ni0.16Co. It is indicated that the catalysts with high BET surface area can provide large contact area for the reactants, thus resulting in high reaction activity. However, the active site on the catalysts must be metals not metal oxides, which has been proved by the observation that the precipitates won't have any activity until they are reduced in H_2-contaning gas. Therefore, catalyst activity may depend even more on the metallic surface area rather than the BET surface. Nonetheless, comparing data in Table 4.3 and Fig. 4.12, the initial activity of the catalysts doesn't seem to have clear connections with metallic area. It appears that the number of active sites which determines the catalyst activity is not proportional to the metallic surface area.

0.18Ni0.16Co, the highest Ni-Co content catalyst, has the lowest initial activity.

The lower-temperature peak in the TPR profiles (Fig. 4.8) indicates that this sample possessed weaker support metal interaction (Wang et al., 2003). The estimation of H_2 consumption from the peak area for this catalyst (Fig. 4.8) suggests that the extent of reduction of Ni and Co was high. But 0.18Ni0.16Co had the lowest metallic surface area. Sintering most likely happened to this high metal content, weak metal-support interaction sample during the high-temperature reduction process (Bond 2004). The sintering led to the loss of both surface area and metallic area, and hence the number of active sites became less. Wang et al. (2003) attributed the low metal dispersion to the formation of the free bulk-like metal oxide phase in the high metal content catalyst. The mobility of such a phase during reduction facilitates sintering (Xu et al., 2001). On the other hand, according to Norval et al. (1980), the number of active centres is usually less than the total number of surface metallic atoms. A good metal dispersion will help generate more active sites on the catalyst surface, even though sometimes the metal loading and metallic surface is lower. Table 4.3 clearly shows that the metal dispersion was better when the Ni-Co content was lower and correspondingly, Fig. 4.12 shows the catalyst activity followed the same trend. With lower metal content, the spinel-like phases and solid solutions can produce a highly dispersed active phase and a large active surface area when the catalyst is prepared at high calcined temperature (Wang et al., 2003). Also, the particle size distribution indicates that the portion of smaller particle increases with decrease in Ni-Co content. It has been reported that sulfur blockage can dramatically reduce the concentration of large ensembles resulting in carbon-free steam reforming of methane

without sacrifice catalyst activity (Rostrup-Nielsen, 1984; Andersen et al., 1987; Bengaard et al., 2002). This provide another evidence that small particle size facilitates reforming reaction but suppressing carbon formation. One can see that the surface area, metal dispersion, the percentage of smaller-than-5 nm particles, and the activity of the catalysts follow the same order: 0.02Ni0.03Co > 0.04Ni0.05Co > 0.06Ni0.09Co > 0.18Ni0.16Co. Therefore, the high activity of Ni-Co bimetallic catalysts can be attributed to their high surface area, high metal dispersion, and small particle size, which might result from low Ni-Co content and the high-temperature calcination process.

4.3.2.6 Carbon formation and stability of the Ni-Co bimetallic catalysts for CO_2 reforming of CH_4

The 250 h time-on-stream evaluation also clearly showed that the catalysts with lower Ni-Co content had better stability (Fig. 4.12). 0.18Ni0.16Co and 0.06Ni0.09Co suffered obvious activity loss of 27 % and 24 % respectively (calculation was based on the difference between initial and final reaction rate of methane during the 250 h period). However, 0.04Ni0.05Ni and 0.02Ni0.03Co did not experience deactivation (the decrease in CH_4 reaction rate was less than 1 % within 250 h). TG/DTG analysis for spent catalysts indicated that the occurrence of carbon formation was only observed for 0.18Ni0.16Co and 0.06Ni0.09Co catalysts. This suggests that carbon formation is most likely the major reason for catalyst deactivation. Theoretically, carbon deposition may result from the following reactions:

$$CH_4 \leftrightarrow C + 2H_2 \qquad \Delta H = 74.87 \text{ kJ} \qquad (4.1)$$

$$2CO \leftrightarrow CO_2 + C \qquad \Delta H = -172.46 \text{ kJ} \qquad (4.2)$$

$$CO + H_2 \leftrightarrow C + H_2O \qquad \Delta H = -131.30 \text{ kJ} \qquad (4.3)$$

At high reaction temperatures, reaction (4.1) is thermodynamically favored, but reaction (4.2) and (4.3) are not. In contrast, the reversibility of reactions (4.2) and (4.3) may facilitate carbon removal processes through gasification of coke at high temperatures. Two kinds of carbons are most often observed in CO_2 reforming of CH_4 (Goula et al., 1996; Quincoces et al., 2001; Ito et al., 1999; Montoya et al., 2000; Frusteri et al., 2002): filamentous (whisker-like) carbon produced by adsorbed carbon atoms derived mainly from methane decomposition; and encapsulating hydrocarbon films (shell-like) formed by polymerization. TEM (Fig. 4.14) analysis showed that filamentous carbon was formed on 0.18Ni0.16Co and 0.06Ni0.09Co, but no encapsulating carbon was observed, indicating that the CH_4 decomposition might provide the major carbon species for carbon formation on 0.18Ni0.16Co and 0.06Ni0.09Co catalysts. It is believed that the CH_4 decomposition is the initial step of reforming reaction, resulting from the dissociative adsorption of CH_4 on the surface of metal (Eq. 4.4) (Hickman and Schmidt, 1993).

$$CH_4 + M \rightarrow M\text{-}C + 2H_2 \qquad (4.4)$$

where M represents the metal particle of catalysts. The carbon species is present as M-C or carbide-like species which contains no C-H bond (Chang et al., 2000; Verykios, 2003). Carbon formation occurs when the formation rate of carbon species is higher than its removal rate by reacting with oxygen species. The efficiency of removal of carbon species may depend on the activation of CO_2 (Bitter et al., 1999; Nagaoka et al., 2001). Based on

Tsipouriari and Verykios et al. (2001), the activation of CO_2 occurs on the support (Eq. 4.5) and a primary step of carbon species removal can be expressed by Eq. 4.6.

$$CO_2 + S \rightarrow S\text{-}CO_2 \quad (4.5)$$

$$S\text{-}CO_2 + M\text{-}C \rightarrow 2CO + M + S \quad (4.6)$$

where S represents the surface of the support.

Higher CH_4 conversion on 0.04Ni0.05Co and 0.02Ni0.03Co catalysts than on 0.18Ni0.16Co and 0.06Ni0.09Co should suggest higher CH_4 dissociation rate and thus higher carbon formation rate on the catalyst of lower Ni-Co contents. However, TG/DTG and TEM analysis did not detect carbon formation on 0.04Ni0.05Co and 0.02Ni0.03Co catalysts. This implies that the removal rate of carbon species by reaction (4.6) is efficient enough on 0.04Ni0.05Co and 0.02Ni0.03Co. Segner et al. (1984) reported that the activation of CO_2 is structure sensitive, small particle size prompting its activation. Also, Rostrup-Nielsen (1991) reported that large Ni particle favors carbon formation. Catalyst testing (Fig. 4.12) and particle size distribution (Fig. 4.11) showed that the catalysts with large portion of particles greater than 10 nm lost significant activity but no deactivation and carbon formation occurred over catalysts without particles larger than 10 nm. It indicates that an particle size of 10 nm is critical to inhibiting carbon formation over Ni-Co bimetallic catalysts for CO_2 reforming of CH_4. Therefore, the efficient removal of carbon species or carbon resistance of 0.04Ni0.05Co and 0.02Ni0.03Co might be ascribed to its higher metal dispersion and smaller particle size (Figs. 4.11C and 4.11D).

A conceptual model, shown in Fig. 4.15, is used to explain why the catalyst with

lower Ni-Co content has better resistance to carbon formation during the CO_2 reforming of CH_4 reaction.

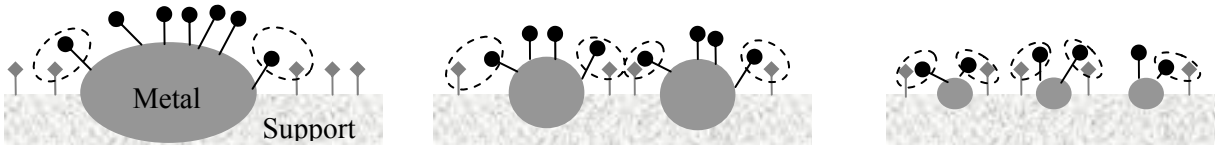

A B C

Fig. 4.15 Concept model of carbon removal and carbon formation over the Ni-Co bimetallic catalyst for CO_2 reforming of CH_4
A: Catalyst with metal particles larger than 20 nm; B: Catalyst with metal particles between 10 and 20 nm; C: Catalyst with metal particles smaller than 10 nm

- Carbon species derived from the dissociative adsorption of CH_4 on the surface of metal particle (M)
- Activated CO_2 on the surface of support (S)

- Removal reaction of carbon species: $S\text{-}CO_2 + M\text{-}C \rightarrow 2CO + S + M$

On a large metal particle, for example > 20 nm, the carbon species formed near the periphery of the metal particle is easy to react with activated CO_2 to form CO (Fig. 4.16A). The carbon species far away from the periphery of the metal particle tend to form carbon since they cannot reach the activated CO_2. With the increase in time-on-stream, carbon deposition will accumulate on the large particles which results in activity loss. However, catalyst activity will tend to be stable and carbon formation rate will significantly decrease when the larger particles have been covered with carbon. The activity and carbon formation evolution behavior as a function of time-on-stream during the 2000 h testing using 0.06Ni0.09Co catalyst supports this explanation (Zhang et al., 2007). With the

decrease in metal particle size by lowering the Ni-Co content, the portion of carbon species closer to particle periphery (edge active sites) increases, resulting in carbon being reacted and forming CO, and hence less carbon deposition on the catalysts surface (Fig. 4.15B). When the metal particle is smaller than the critical size of 10 nm, which is obtained from the particle size distribution (Figs. 4.11B and 4.11C) and carbon analysis of spent catalysts (Table 4.4, Fig.4.13, and Fig. 4.14), almost all the carbon species are formed in the vicinity of the activated CO_2; the former is easily reacted with the latter, allowing all the carbon to form CO. Therefore, the carbon formation on the catalyst surface is eliminated (Fig. 4.15C).

4.4 CONCLUSIONS

Ni/Co and Co/Ni ratios investigation showed that high surface area and high activity for CO_2 reforming of CH_4 are those Ni-Co/AlMgOx catalysts with a Ni/Co or Co/Ni ratio between 0.6 and 1.5. Adjusting the Ni-Co content of the bimetallic catalysts, whose Ni/Co or Co/Ni ratio is between 0.6 and 1.5, is able to change the metal dispersion and metal particle size. The better metal dispersion and smaller metal particle are obtained at lower Ni-Co content. Small metal particles are crucial to the suppression of carbon deposition. Therefore, the Ni-Co bimetallic catalyst with close unity Ni/Co ratio and lower total metal content shows higher activity and greater stability. The metal particle size on 0.04Ni0.05Co and 0.02Ni0.03Co are all smaller than 10 nm, and thus the carbon formation over the two is undectable for the reaction of CO_2 reforming of CH_4.

5 EFFECTS OF THE CATALYST CALCINATION TEMPERATURES ON Ni-Co/AlMgO$_x$

A paper based on this chapter was prepared for submission to **Applied Catalysis A: General:** Zhang, J., Wang, H., Dalai, A.K., "Effects of calcinations temperature on the properties and performances of Ni-Co bimetallic catalysts for CO_2 reforming of CH_4", submitted to *Appl. Catal. A*.

CONTRIBUTION OF Ph.D. CANADIDATE

Experiments were planned and performed by Jianguo Zhang. Hui Wang and Ajay K. Dalai provided guidance in planning the experiment. The submitted manuscript was written by Jianguo Zhang, while Hui Wang and Ajay K. Dalai provided comments and suggestions for revision.

CONTRIBUTION OF THIS CHAPTER TO THE OVERALL STUDY

This paper investigated the effects of calcination temperatures on the Ni-Co/AlMgO$_x$ bimetallic catalyt for CO_2 reforming of CH_4. The work involves the catalyst preparation, catalyst testing, and catalyst characterization. It was found that the calcination temperatures can significantly affect catalyst phase sturtures and surface properties, thus can have significant effects on catalyst activity, stability, and carbon formation for CO_2 reforming of CH_4.

ABSTRACT

In the previous study, it has been found that Ni/Co ratio and Ni-Co content have significant effects on catalyst properties and performance. Carbon free operation was achieved for CO_2 reforming of CH_4 using Ni-Co/$AlMgO_x$ catalyst through optimizing Ni and Co loading. This Chapter focuses on the effects of calcination temperatures on the 0.06Ni0.09Co catalysts as one critical procedure to optimize the catalyst preparation. The specific surface area, pore distribution, particle size, phase structure, metal-support interaction, and reducibility of the 0.06Ni0.09Co catalyst were characterized using BET, TEM, XRD, and TPR equipment. Calcination effects on the performance of catalysts were tested for CO_2 reforming of CH_4 at 750 ^oC, 1 atm, and $CH_4/CO_2/N_2$=1/1/1. Carbon deposition over the spent catalyst was analyzed using TG/DTG and TEM. It was found that with the increase in calcination temperature from 400 ^oC to 1100 ^oC, the interaction between metals and catalyst support became stronger which resulted in the difficulty of reduction and growth of particle size. At lower temperatures such as 400 ^oC, the metal component was dominated by mixed Ni and Co oxides like NiO, CoO, and Co_3O_4, etc., which possess weak metal-support interaction. At high temperatures such as 900 ^oC, the active component existed in the form of solid solution and spinels, which are difficult to reduce and have strong metal-support interaction (SMSI). At a calcination temperature of 1100^oC, the catalyst lost its surface area and pores but particle size increased significantly. Larger particle favored carbon formation and compromised it stability for CO_2 reforming

CH_4. Further testing was conducted on 0.04Ni0.05Co at 750 ^oC, 1 atm, $CH_4/CO_2/N_2$ =1/1/0, and GHSV 750,000 mL/g_{cat}-h. A calcination temperature between 700-900 ^oC was recommended for the Ni-Co/$AlMgO_x$ bimetallic catalysts.

5.1 INTRODUCTION

The thermal treatment of calcination has major effects on the nature of active sites. For example, high-temperature calcination enhances the metal-support interaction (Chen and Ren, 1994, Bhattacharyya and Chang, 1994) but it also favors the growth of particle size (Praserthdam et al., 2004) and makes the reduction of catalyst difficult (Bradford and Vannice, 1999). Wang et al. (1998) observed that the phase transformation of Ni catalysts supported on γ-Al_2O_3 and the formation of spinel nickel aluminate ($NiAl_2O_4$) during calcination, which makes the reduction of catalyst difficult. Wang et al. (1998) also reported that the low activity of Ni/MgO for CO_2 reforming of CH_4 can be ascribed to its low reducibility due to the formation of solid solution during the calcination process. Thus, when a catalyst is being developed, proper selection of calcination parameters – especially calcination temperature – is crucial to the achievement of desired catalyst properties and performance. This work investigates the effects of calcination conditions on catalyst properties and catalytic performance of Ni-Co/$AlMgO_x$ bimetallic catalysts for CO_2 reforming of CH_4.

5.2 EXPERIMENTAL

5.2.1 Catalyst preparation

As described in Chapter 4, 0.06Ni0.09Co and 0.04Ni0.05Co catalysts were prepared. They were calcinated at various temperatures in this chapter and the resulting catalyst subtypes were designated 0.06Ni0.09Co-400, 0.06N0.09iCo-600, 0.06Ni0.09Co-900, 0.06Ni0.09Co-1100, and 0.04Ni0.05Co-500, 0.04Ni0.05Co-600, 0.04Ni0.05Co-700, 0.04Ni0.05Co-800, 0.04Ni0.05Co-900, and 0.04Ni0.05Co-1000, in accordance with Ni-Co content and calcination temperatures.

5.2.2 Catalyst Characterization and testing

BET, CO-Chemisportion, TPR, TG/DTA, TEM, XRD technologies were used to characterizated the catalysts. And the bench-top quartz reactor was used to test the catalysts. Detailed description for catalyst testing and characterization can be found in previous chapters.

5.3 EFFECTS OF CALCINATION ON 0.06Ni0.09Co CATALYST

5.3.1 Catalyst characterization

5.3.1.1 N_2-physisorption

N_2-physisorption was employed to characterize the surface area, pore volume, and average pore diameter of catalysts calcined at various temperatures. The results are presented in Table 5.1. The increase in calcination temperature from 400 to 1100 ^oC clearly indicated a dramatic decrease of BET surface area from 198 to 9 m^2/g. The pore volume decreased from 0.278 to 0.029 cm^3/g and the average pore size increased from 5.5 nm to 13.5 nm. Fig.5.1 depicts the pore area and pore volume distribution of the catalysts calcined at various temperatures. As temperature increased, the surface area and pore volume corresponding to the pores with diameter between 2 nm and 4 nm decreased. It indicated that a significant portion of pores with the diameter of 2-4 nm collapsed at higher temperatures. In the case of 0.06Ni0.09Co-1100, the pore area and pore volume from pores with diameter of 2-4 nm were hardly measurable.

Table 5.1 Surface area, pore volume, and average pore diameter of 0.06Ni0.09Co catalysts calcined at various temperatures

Catalysts	Calcination Temperature (^oC)	BET surface area (m^2/g)	Pore Volume (cm^3/g)	Average pore diameter (nm)
0.06Ni0.09Co-400	400	198	0.278	5.5
0.06Ni0.09Co-600	600	174	0.309	6.5
0.06Ni0.09Co-900	900	54	0.158	10.5
0.06Ni0.09Co-1100	1100	9	0.029	13.5

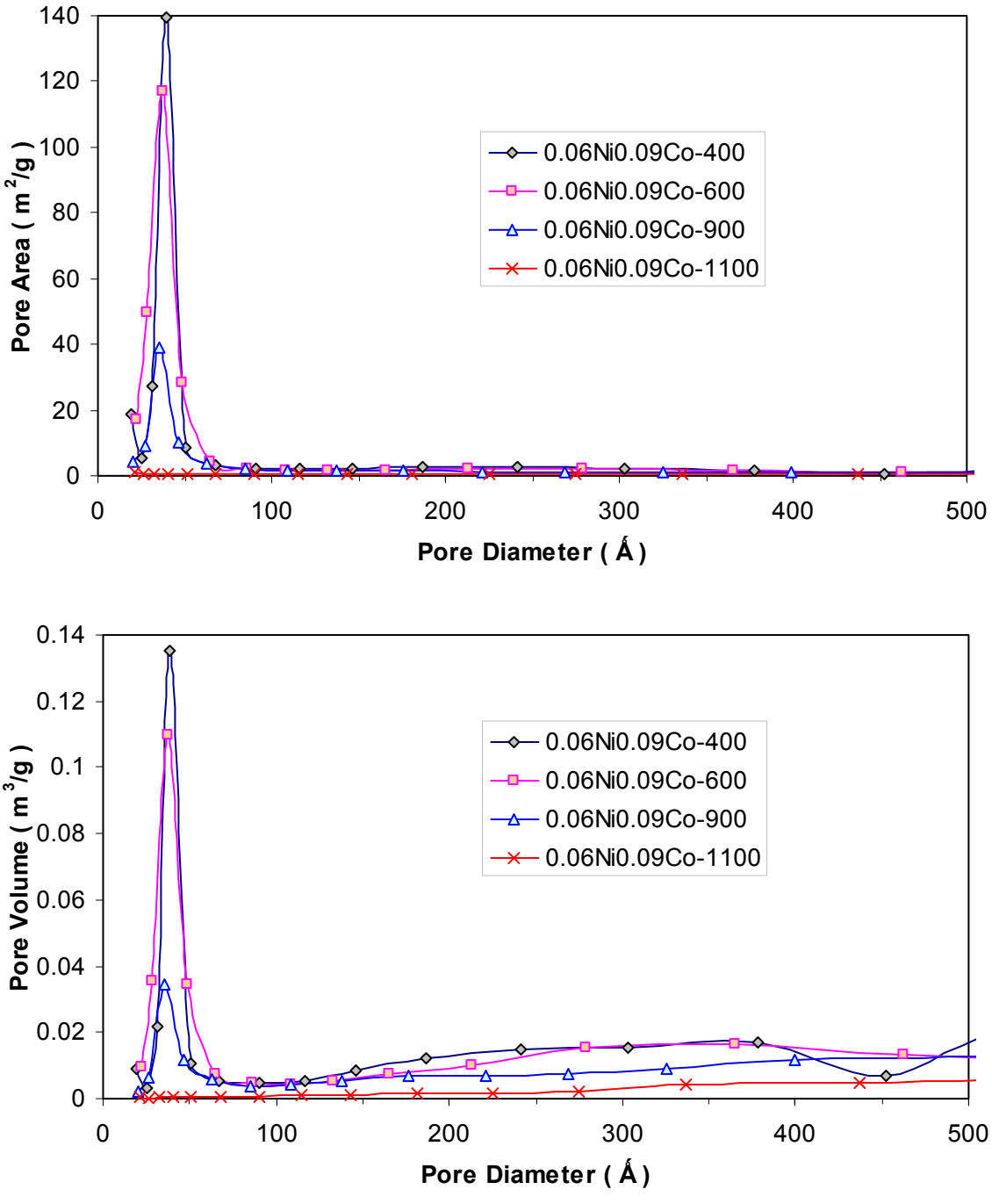

Fig. 5.1 Pore area and pore volume distribution of 0.06Ni0.09Co bimetallic catalysts calcined at various temperatures

5.3.1.2 X-ray diffraction (XRD)

Fig. 5.2 shows XRD diffractogram of 0.06Ni0.09Co catalysts calcinated at various temperatures.

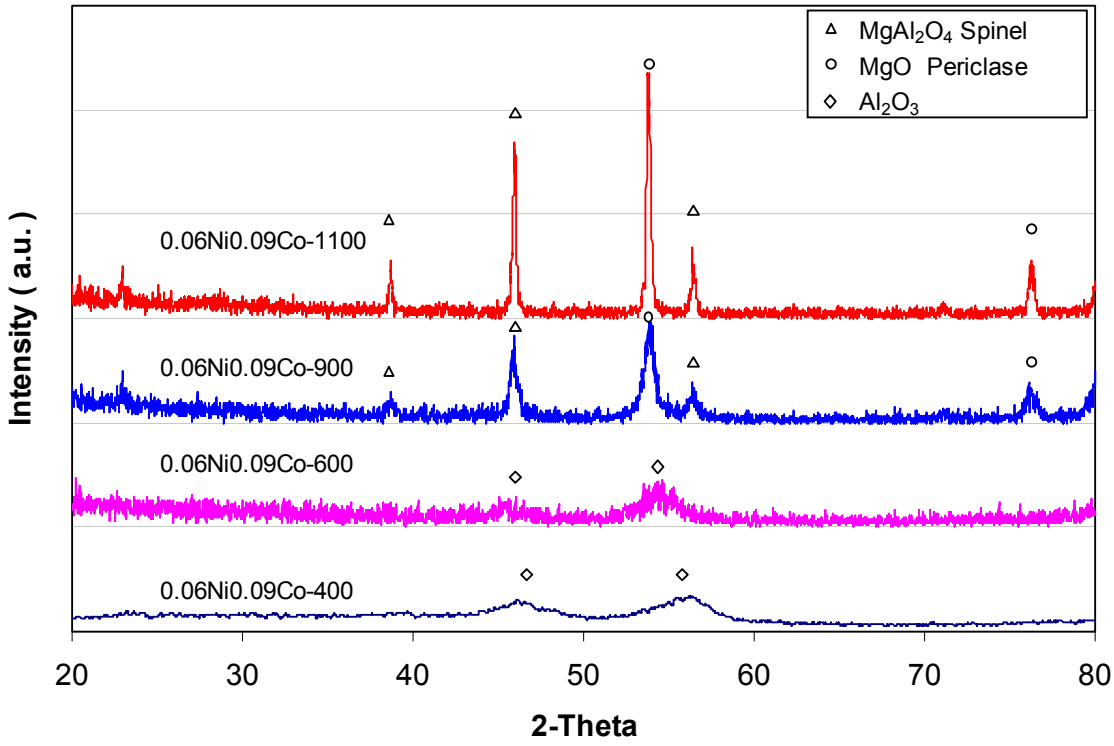

Fig. 5.2 XRD diffractogram of 0.06Ni0.09Co catalysts calcinated at variou temperatures

When calcination temperature was below 600 ^{o}C, small diffraction peaks of γ-Al_2O_3 were observed. With the increase in calcinations temperature, γ-Al_2O_3 disappeared as shown by the catalyst 0.06Ni0.09Co-900 and 0.06Ni0.09Co-1100, while diffraction peaks of $MgAl_2O_4$ spinel and MgO periclase appeared. The appearance of $MgAl_2O_4$ spinel indicated that the phase transformation took place at high-temperatures through solid-state reaction between MgO and Al_2O_3. The presence of MgO periclase can be attributed to the

transformation from the remaining extra MgO in the catalysts at higher temperature. The increase in calcination temperature from 900 to 1100 ^{o}C also resulted in larger crystals as shown by the changes of peak sharpness. However, it is of interest to note that there was no Ni or Co diffraction peak observed. One possibility is that the relative low amount of metals were well dispersed throughout the catalyst, which may be below the detection limit of the technique. Another possibility is that Ni^{2+}, Co^{2+}, Mg^{2+}, and Al^{3+} belong to the same lattice according to Tichit et al. (1997; 1999; 2000). The formation of Ni^{2+}-Al^{3+}, Co^{2+}-Al^{3+}, and Mg^{2+}-Al^{3+} solid solutions of spinel-type and of the stoichiometric $NiAl_2O_4$, $CoAl_2O_4$, and $MgAl_2O_4$ spinel phases (Tichit et al., 1997; 1999; 2000) at high calcinations temperatures. The Ni^{2+}-Co^{3+} spinel-type solid solution and $NiCo_2O_4$ spinel can also be formed at high calcination temperatures (Petrov and Will 1987). These spinel-type solid solution phases and spinel phases in the catalysts are indistinguishable by XRD (Fig. 5.2) due to their similarity.

5.3.1.3 Temperature-programmed reduction (TPR)

The XRD analysis revealed the formation of $MgAl_2O_4$ spinel and MgO periclase, but did not provide information on active components such as Ni and Co. The active components (Ni and Co) were analysed by TPR for catalysts calcined at various temperatures, as shown in Fig. 5.3. From the TPR profile of 0.06Ni0.09Co-400, it can be seen that there were two broad reduction peaks ranging from 280-400 ^{o}C and 650-900 ^{o}C, respectively. The broad unresolved peaks with shoulders indicated the existence of several different species. The low temperature reduction peak can be ascribed to the mixed

reducible Ni and Co oxides, which may contain NiO, CoO, and Co_3O_4 (Perez-Lopez et al., 2006; Ribet et al., 1999). The high temperature reduction peak showed the evidence of Ni- and Co-containing spinel phases such as $NiAl_2O_4$ and $CoAl_2O_4$ in the catalysts (Perez-Lopez et al., 2006; Ribet et al., 1999), which were formed through the solid-state reaction between active metal species and support phases. The Ni and Co species in different reduction temperature ranges clearly demonstrated their different degree of interaction with the support (Lemonidou and Vasalos 2002). The shifting of reduction toward higher temperatures, as shown by the TPR profile of 0.06Ni0.09Co-600, -900, and -1100, was due to the increase in metal support interactions (Richardson et al., 1996). Also interestingly, with the increase in calcination temperature, the low-temperature reduction phases disappeared (see the profile of 0.06Ni0.09Co-900 and 0.06Ni0.09Co-1100 in Fig. 5.3). It can be attributed to the phase transformation of mixed Ni and Co oxides to Ni and Co-containing solid solutions of spinel type and stoichometric $NiAl_2O_4$ and $CoAl_2O_4$ spinels (Ribet et al 1999, Perez-Lopez et al 2006).

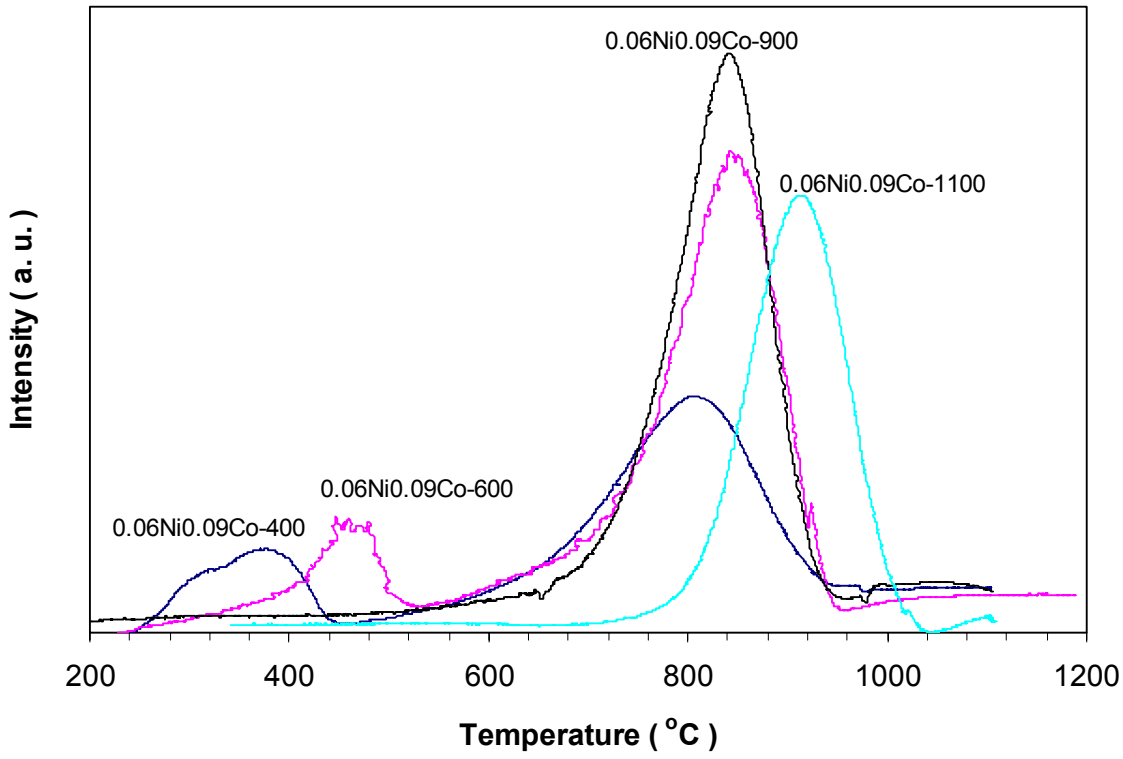

Fig. 5.3 TPR profile of 0.06Ni0.09Co catalysts calcined at various temperatures

5.3.1.4 Transmission electron microscopy (TEM)

The morphology of catalysts was analyzed using TEM technique. As shown in Fig. 5.4, it is clear that the particle size was growing with the increase in calcination temperatures. The support phase and metals were dispersed evenly in the sample when calcinated at 400 ^{o}C (Fig.5.4 A). From the TEM images of catalyst 0.06Ni0.09Co-600 and 0.06Ni0.09Co-900, it can be seen that the metal particles aggregated to larger ones in comparison with those in 0.06Ni0.09Co-400. Also, the support showed to melt together decorated with the aggregated metals, which is very clear in the TEM image of 0.06Ni0.09Co-1100 (Fig. 5.4D). This may be attributed to the solid-state reaction between different species at higher temperatures.

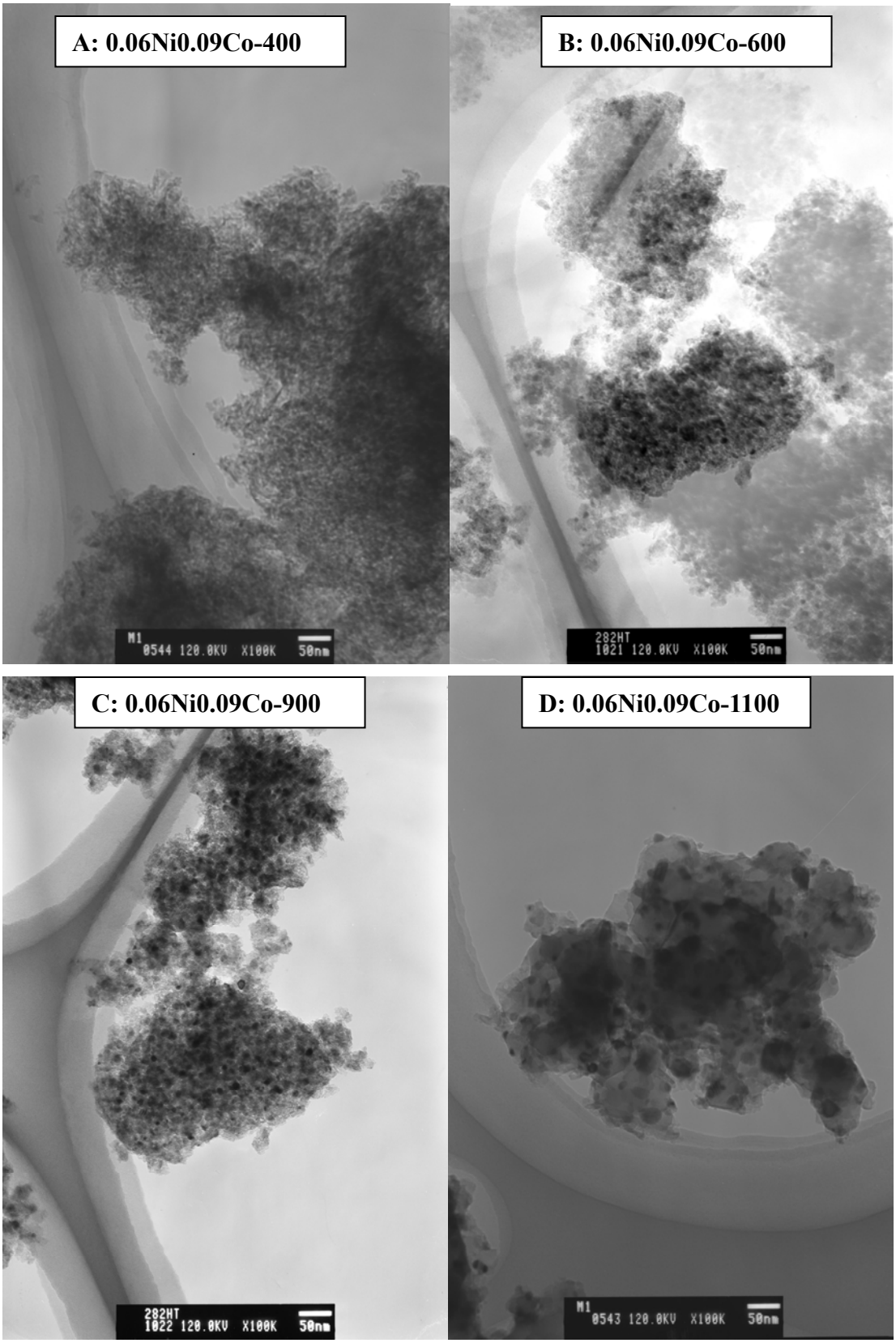

Fig. 5.4 TEM image of 0.06Ni0.09Co catalyst calcinated at various temperatures

5.3.2 Catalyst testing

5.3.2.1 Activity for CO_2 reforming of CH_4 of 0.06Ni0.09Co

The catalytic activity of 0.06Ni0.09Co samples was tested at 750 ^oC, 1 atm, and various gas hourly space velocity (GHSV) in terms of CH_4 reaction rate. Fig. 5.5 depicts the CH_4 reaction rate as a function of GHSV over the four catalysts calcined at four different temperatures.

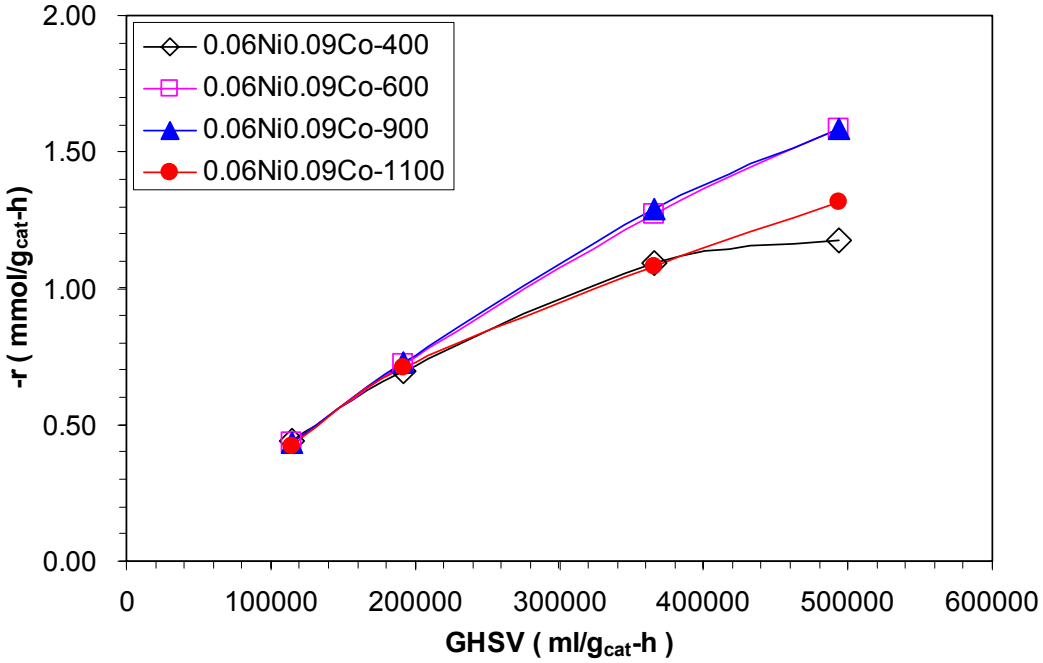

Fig. 5.5 GHSV effects on the reaction rate of CH_4 over 0.06Ni0.09Co catalysts calcined at various temperatures for CO_2 reforming of CH_4 at 750^oC, 1atm, and $N_2/CH_4/CO_2$=1/1/1

At a GHSV less than 200,000 mL/g_{cat}-h, no clear differences were observed in the CH_4 reaction rate among the four catalysts. As the GHSV increased to the range between 200,000 and 360,000 mL/g_{cat}-h, the CH_4 reaction rate over 0.06Ni0.09Co-600 and 0.06Ni0.09Co-900 increased rapidly. The CH_4 reaction rate over different catalysts in this

GHSV range followed the order: 0.06Ni0.09Co-900~0.06Ni0.09Co-600>0.06Ni0.09Co-1100~0.06Ni0.09Co-400. With the further increase in GHSV, the CH_4 reaction rates were increasing. From the test shown in Fig. 5.5, it can be seen that the activity of the catalysts followed the order: 0.06Ni0.09Co-900~0.06Ni0.09Co-600>0.06Ni0.09Co-1100> 0.06Ni0.09Co-400. The 0.06Ni0.09Co-900 and 0.06Ni0.09Co-600 showed comparable activity for CO_2 reforming of CH_4. The 0.06Ni0.09Co-400 had the lowest activity for CO_2 reforming of CH_4 in comparison with 0.06Ni0.09Co-600, -900, and -1100.

5.3.2.2 Stability of 0.06Ni0.09Co calcined at different temperatures

The effect of calcination temperature on catalyst stability for CO_2 reforming of CH_4 was investigated through testing the catalytic activity as a function of time-on-stream. The results are shown in Fig. 5.6.

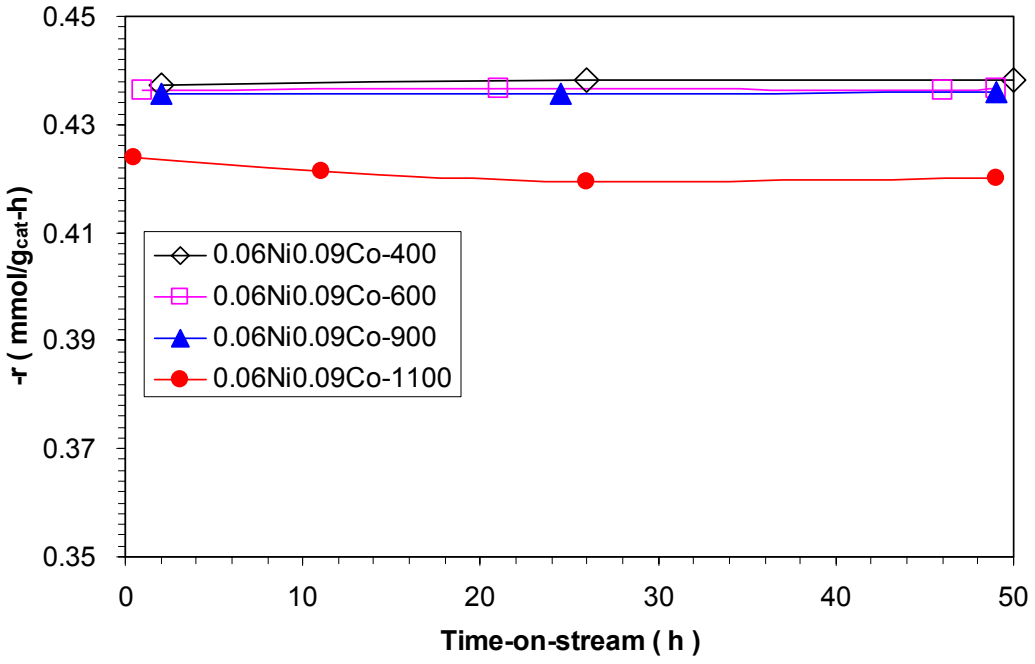

Fig. 5.6 The stability of 0.06Ni0.09Co catalysts calcined at different temperatures for CO_2 reforming of CH_4 at 750 ^oC, 1 atm, 110,000 mL/g_{cat}-h, and $CH_4/CO_2/N_2$=1/1/1

From Fig. 5.6, it can be seen that at the GHSV of 110,000 ml/g_{cat}-h, 0.06Ni0.09Co-400, -600, and -900 exhibited very similar activity and stability for the 50 h when the reforming reactions were conducted at 750 ^{o}C and 1 atm, while 0.06Ni0.09Co-1100 showed slightly lower activity but still good stability with a activity decay less than 1% (calculation is based on the difference between initial and final reaction rate of CH_4). The results in Fig. 5.6 indicate that the stability differences of the catalysts for CO_2 reforming of CH_4 reforming can not be evaluated clearly at the reaction conditions. The stability was further tested at the GHSV of 365,000 mL/g_{cat}-h at 750 ^{o}C and 1 atm in order to get a clear picture about the calcination temperature effects on catalyst stability. Also, the time-on-stream was extended to 100 h as shown in Fig. 5.7.

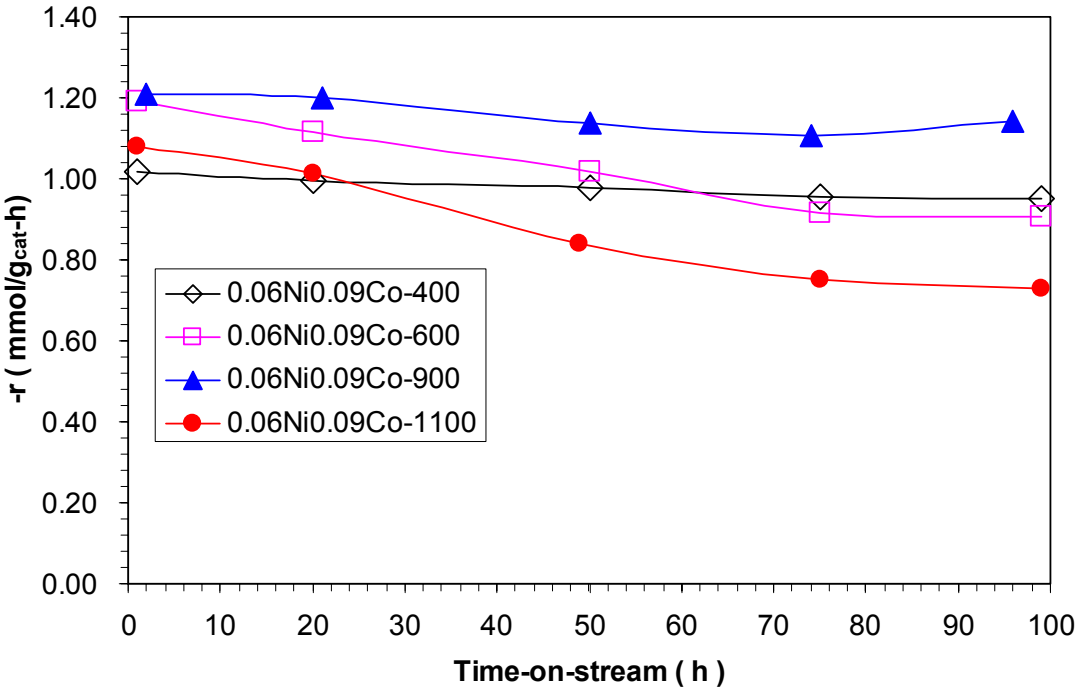

Fig. 5.7 The stability of Ni-Co catalysts calcined at different temperatures for CO_2 reforming of CH_4 at 750^{o}C, 1 atm, 365,000 mL/g_{cat}-h, and $CH_4/CO_2/N_2$=1/1/1

From the figure it is clear that 0.06Ni0.09Co-900 showed the highest activity and stability in the 100 h time-on-stream, with no significant drop in CH_4 reaction rate (5 % activity decay). 0.06Ni0.09Co-600 had the same initial activity as did 0.06Ni0.09Co-900, but at the end of 100 h, the reaction rate of CH_4 dropped from 1.193 mmol/g_{cat}-s to 0.903 mmol/g_{cat}-s (24 % activity deacay). The reaction rate of CH_4 over catalyst 0.06Ni0.09Co-1100 decreased from1.081 mmol/g_{cat}-s to 0.728 mmol/g_{cat}-s (33 % activity decay). Interestingly, 0.06Ni0.09Co-400 showed a relatively low but stable activity during the 100 h time-on-stream with the initial and final CH_4 rate of 1.020 and 0.950 mmol/g_{cat}-s (7 % activity decay).

5.3.2.3 Carbon deposition over 0.06Ni0.09Co calcined at different temperatures

TG/DTG was used to measure the average carbon deposition rate and to identify the carbon species for the catalysts after the reaction. The average carbon deposition rate was calculated by the amount of carbon measured using TG divided by the weight of catalyst and the reaction time, while the different carbon species was identified through DTG profiles. The results are listed in Table 5.2.

Table 5.2 The carbon deposition over 0.06Ni0.09Co catalysts

Catalyst	Calcination Temperature (^oC)	Reaction Temperature (^oC)	GHSV (ml/g_{cat}-h)	TOS (h)	Average Carbon Deposition Rate (mg_{carbon}/g_{cat}-h)
0.06Ni0.09Co-400	400	750	110,000	50	2.460
			365,000	100	9.616
0.06Ni0.09Co-600	600	750	110,000	50	6.335
			365,000	100	9.929
0.06Ni0.09Co-900	900	750	110,000	50	1.649
			365,000	100	2.305
0.06Ni0.09Co-1100	1,100	750	110,000	50	9.238
			365,000	100	12.908

From the table, it is clear that the average carbon deposition rate follows the order: 0.06Ni0.09Co-1100>0.06Ni0.09Co-600>0.06Ni0.09Co-400>0.06Ni0.09Co-900 at identical GHSV and time-on-stream conditions. It is noteworthy that when calination temperature increased from 600 to 900 ^{o}C, the average carbon deposition rate decreased dramatically from 6.335 mg_{carbon}/g_{cat}-h to 1.649 g_{carbon}/g_{cat}-h at 110,000 mL/g_{cat}-h, and from 9.929 mg_{carbon}/g_{cat}-h to 2.305 mg_{carbon}/g_{cat}-h at a 365,000 mL/g_{cat}-h. However, when calcination increased continuously from 900 ^{o}C to 1100 ^{o}C, the average carbon deposition rate increased nearly 5 times more rapidly, to 9.238 mg_{carbon}/g_{cat}-h and 12.908 mg_{carbon}/g_{cat}-h respectively. It was found that the average carbon deposition rate followed the same order as the extent of catalytic activity decay (described in previous section).

The DTG profiles of temperature programmed oxidation in air for the spent catalysts were used to identify different carbon deposits as shown in Fig.5.8. For all samples two domains exist for the oxidation of carbon deposits, in the low-temperature (<550 ^{o}C, LT) and high temperature (>550 ^{o}C, HT) ranges. Also, they are featured by broad peaks, which provide evidence of the oxidation of various carbon species in each domain. It can be seen that most of carbon deposits were in LT range and only small portion was in the HT range.

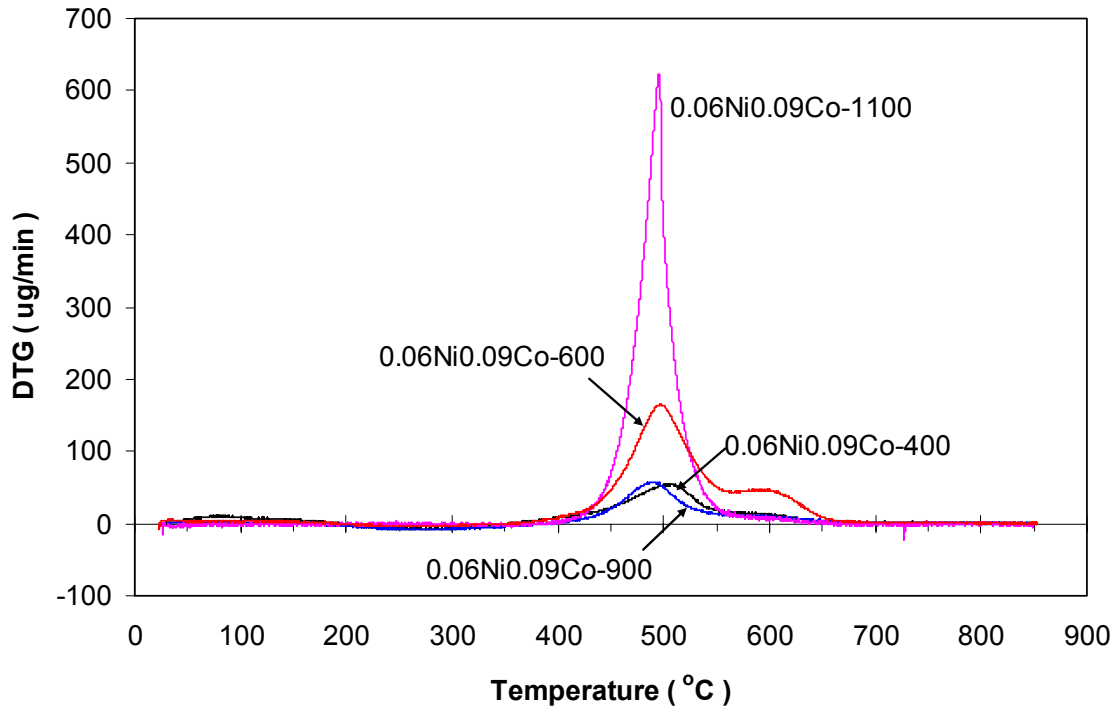

Fig. 5.8 Carbon deposition analysis by TG/DTG after 50 h time-on-stream at 110,000 mL/g_{cat}-h, 750 °C, and $CH_4/CO_2/N_2$=1/1/1

The TEM micrographs of the spent catalysts were also used to characterize the features of the carbon deposits as shown in Fig. 5.9. Filamentous whisher-like carbon were identified over all the catalysts. Clear nanotubes with diameters larger than 25 nm were found over catalysts 0.06Ni0.09Co-400, 0.06Ni0.09Co-600 and 0.06Ni0.09Co-1100. Very fine wisher-like carbon was found over the 0.06Ni0.09Co-900 catalyst. It was reported that the size of nanotubes are dependent on the size of metallic particles over the catalysts (Ji et al., 2001) according to its growth mechanism. However, in this work it appears that the size of nanotubes was independent of size of metal particles, considering Fig. 5.4.

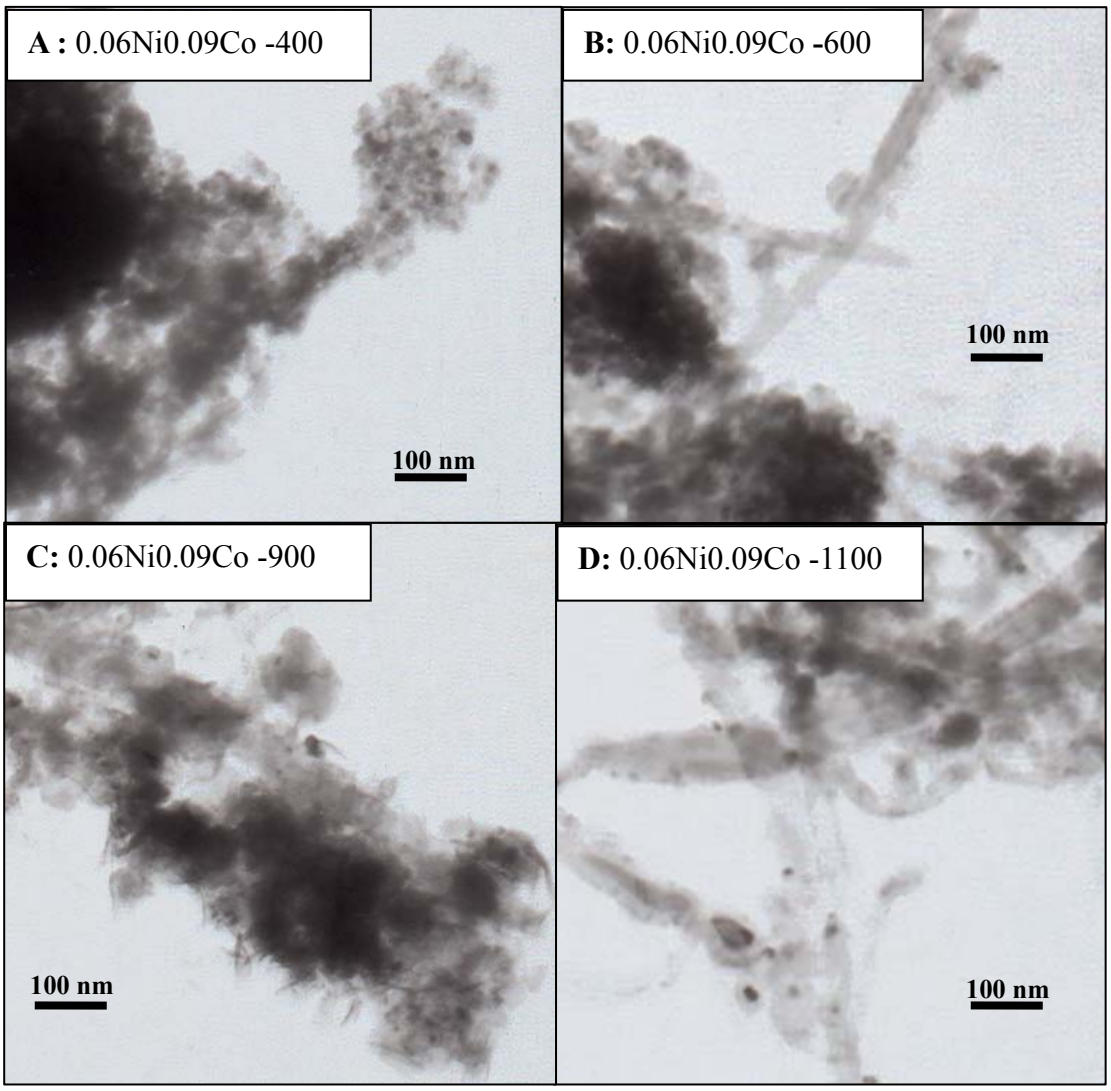

Fig. 5.9TEM images of carbon deposit on different 0.06Ni0.09Co catalysts calcined at different temperatures after 50 h time-on-stream at 110,000 mL/g_{cat}-h, 750^{o}C, and $CH_4/CO_2/N_2$=1/1/1

5.4 DISCUSSION BASED ON THE EFFECTS OF CALCINATION TEMPERATURES ON 0.06Ni0.09Co CATALYSTS

5.4.1 Catalyst activity and active sites

The results of the CO_2 reforming of CH_4 experiments revealed the significant effects of catcination temperatures on the catalyst performance. This occurs because the

catalyst performance is dependent on active sites of the catalyst, which are strongly affected by catalyst calcination pre-treatment and are finally formed during the catalyst activation process. It has been proved the metallic property of active sites (Zhang et al., 2007). 0.06Ni0.09Co-600 and 0.06Ni0.09Co-900 displayed the highest initial activity. It can be deduced that 0.06Ni0.09Co-600 and 0.06Ni0.09Co-900 had the highest number of active sites for CO_2 reforming of CH_4 under the assumption of activity proportional to number of active sites. Close activity in terms of CH_4 reaction rate (Fig. 5.5) showed that the number of active sites for CO_2 reforming of CH_4 in 0.06Ni0.09Co-600 and 0.06Ni0.09Co-900 were close. Lower initial activity of 0.06Ni0.09Co-400 and 0.06Ni0.09Co-1100 showed the lower number of active sites for CO_2 reforming of CH_4. Therefore, the initial number of active sites for CO_2 reforming of CH_4 on the different catalysts followed the same order as the initial activity of the catalysts: 0.06Ni0.09Co-900~0.06Ni0.09Co-600>0.06Ni0.09Co-400~0.06Ni0.09Co-1100. However, also from Fig. 5.5, the finial activity of catalysts at the end of 50 h showed that the final number of active sites for CO_2 reforming of CH_4 at the same reaction conditions were changed and followed the order: 0.06Ni0.09Co-900>0.06Ni0.09Co-400>0.06Ni0.09Co-600> 0.06Ni0.09Co-1100. The difference between the initial and final activity after same period of reaction at the same conditions might indicate the existence of different active sites over the catalysts. At this point of time, it can be said that the different reduction domains of the TPR profiles of catalysts (Fig. 5.3) might be attributed to the formation of different active sites during activation (reduction) considering the metallic property of active sites.

For the convenience of discussion, it is assumed that there are two types of active sites on the catalysts: low temperature (LT) activated active sites and high temperature (HT) activated active sites, which are corresponding to the LT reduction domain and HT reduction domain, respectively. The LT activated active sites could be reduced from the mixed reducible metal oxides such as NiO, CoO, and Co_3O_4, which are featured with weak metal-support interaction. The HT activated active sites are formed through the reduction of Ni and Co containing solid solutions and spinels such as $NiAl_2O_4$ and $CoAl_2O_4$ with strong metal-support interaction.

The initial activity results of catalyst testing showed that both types of active sites were active for CO_2 reforming of CH_4. However, the activity decay of different samples (Fig. 5.7) showed that deactivation can not occur on both types of active sites. In the following section, the activity decay (deactivation) is discussed considering carbon deposition and active sites.

5.4.2 Carbon deposition and active sites

From Fig.5.7, it can be seen that 0.06Ni0.09Co-600 had the same initial activity as 0.06Ni0.09Co-900 but had higher degree activity decay. Considering Table 5.2 and Figs. 5.8 and 5.9, the higher degree of activity decay of 0.06Ni0.09Co-600 can be ascribed to its higher carbon deposition. Carbon deposition on catalysts has been well discussed in literature as the major cause of catalyst deactivation for CO_2 reforming of CH_4. If the same initial activity indicated the same number of active sites, the higher carbon on 0.06Ni0.09Co-600 than on 0.06Ni0.09Co-900 provided evidence of more carbon-

deposition prone active sites on 0.06Ni0.09Co-600 than on 0.06Ni0.09Co-900. Two factors which have significant effects on carbon deposition and well discussed in literature are particle size and metal-support interaction. Generally, it is believed that particle sizes necessary for carbon deposition are larger than those for CO_2 reforming of CH_4, and CO_2 reforming of CH_4 is not structure sensitive, i.e. it can occur on both small and large particles (Rostrup-Nielsen, 1991; Tang et al., 2000; Osaki et al., 2001). Also, strong metal-support interaction can enhance the resistance to carbon deposition but may reduce the activity due to its effect on catalyst reduction (Bhattacharyya et al., 1994; Wang et al., 1998; Tomishige et al., 1998; Xu et al., 2001). From the TEM micrograms (Fig. 5.4B and C), similar particle size can be observed on both 0.06Ni0.09Co-600 and 0.06Ni0.09Co-900. However, 0.06Ni0.09Co-600 had significant portion of LT activated active sites, which had weak support-metal interaction. At this point of moment, the higher carbon deposition of 0.06Ni0.09Co-600 might be attributed to the LT activated active sites with weak support-metal interaction. Questions with 0.06Ni0.09Co-400 might come up considering its LT activated active sites (Fig. 5.3) and its relatively low carbon deposition (Table 5.2) and stable performance (Fig. 5.7). But when referring to the TEM microgram, one can find that the 0.06Ni0.09Co-400 had much smaller particle sizes than 0.06Ni0.09Co-600 (Fig. 5.4A and B). Therefore, it can be deduced that the LT activated active sites had better carbon resistance when its particle sizes were smaller, although it did have strong metal-support interaction. Thus, the low carbon deposition rate and stable performance of 0.06Ni0.09Co-400 can be attributed to its small particle sizes.

0.06Ni0.09Co-1100 had very strong metal-support interaction (Fig. 5.3) but much larger particle size (Fig. 5.4D). The low initial activity of 0.06Ni0.09Co-1100 can be attributed to the strong metal-support interaction, which reduced its degree of reduction and thus activity (Wang et al., 1998). The high carbon deposition on 0.06Ni0.09Co-1100 can explain its high degree of deactivation, which can be ascribed to its large particle size (Rostrup-Nielsen, 1991). From the discussion it can be seen that the carbon deposition is a complicated process that can be affected by different factors such as particle size and metal-support interaction, etc.

5.4.3 Origin of carbon deposition

Theoretically, carbon deposition is resulted from the following reactions:

$$CH_4 \leftrightarrow C + 2H_2 \qquad \Delta H = 74.87 \text{ kJ} \qquad (5.1)$$

$$2CO \leftrightarrow CO_2 + C \qquad \Delta H = -172.46 \text{ kJ} \qquad (5.2)$$

As revealed by the TG/DTG and TEM analyses, the temperature of calcination affects not only the activity and carbon deposition rate, but also the form of carbon deposition. Filamentous whisker-like carbon and encapsulating shell-like carbon are the two most commonly observed carbons in CO_2 reforming of CH_4 (Kroll et al., 1996; Ito et al., 1999; Quincoces et al., 2001). Frusteri et al. (2002) reported that the lower amount of carbon deposits with a shell-like morphology generated by the Bouduard reaction or carbon monoxide disproportionation (Eq. 5.2) was observed over Ni-based catalyst during CO_2 reforming of CH_4 at 800 ^oC, while a large amount of filamentous whisker-like carbon originated from CH_4 decomposition (Eq. 5.1) was formed at 650 ^oC. Considering the

quantity of carbon deposition, the result revealed by TG/DTG over 0.06Ni0.09Co catalysts was in agreement with Frusteri's observation. Most of the carbon deposited over 0.06Ni0.09Co catalysts was filamentous and whisker-like in form. Also, this can be confirmed by the analysis of thermodynamics. From the thermodynamics perspective, CH_4 decomposition is favored at high reaction temperature of 750 ^oC but the Bouduard reaction is suppressed at elevated temperatures (Kroll et al., 1996). The TG/DTG analysis (Fig. 5.8) showed a large amount of filamentous whisker-like carbon on the spent 0.06Ni0.09Co-1100 catalyst, which can be ascribed to its large particle sizes (Fig.5.4D). Also, the TG/DTG analysis (Fig. 5.8) showed that there was more shell-like carbon formed on 0.06Ni0.09Co-600 catalyst than on other catalysts. Bradford and Vannice suggested that shell-like carbon formed by the Bouduard reaction is initiated by the adsorption of CO, which induces the migration of carbon to the subsurface of the Ni layer, thereby resulting in the formation of inactive carbon on the back of metal crystallites (Bradford and Vannice, 1999). However, it is known that CH_4 mainly cracks on metallic Ni at high temperature to form H_2 and surface carbon species (Kalenik and Wolfe, 1991; Cambell et al., 1993), which is removed by the oxygen species to offer an active and stable performance (Verykios, 2003). The metal-support interaction then plays an important role in inhibiting the migration of carbon into the subsurface of the catalyst to form inactive carbon. The formation of more inactive carbon over 0.06Ni0.09Co-600 catalyst might be the reason why 0.06Ni0.09Co-600 had the largest activity decay among the four catalysts. The shell-like inactive carbon was more likely to form over

0.06Ni0.09Co-600, which has the LT activated active sites with weak metal-support interaction (Fig. 5.3) and in the form of relative large particles (Fig. 5.4 B). However, it was not likely to occur on 0.06Ni0.09Co-400 due to its small particle sizes (Fig. 5.4A). As for 0.06Ni0.09Co-900, it can be seen that it had strong metal-support interaction (Fig. 5.3) but also relatively good particle size distribution (Fig. 5.4C), which might be the reason why it showed relatively high and stable performance (Fig. 5.7) with very low carbon deposition (Table 5.2, Fig. 5.8 and 5.9).

5.5 EFFECTS OF CALCINATION ON 0.04Ni0.05Co CATALYSTS

The effects of calcinations temperatures on catalyst with different Ni-Co content were also investigated. The activity and stability of 0.04Ni0.05Co catalysts calcinated at various temperatures are reported in Fig. 5.10, at 750 ^{o}C, 1 atm, 720,000 mL/g_{cat}-h, and $CH_4/CO_2/N_2$=1/1/0. It is clear that at such a high gas hourly space velocity (GHSV), the conversion of CH_4 over all the catalysts dropped. Catalyst 0.04Ni0.05Co-800 showed the best stability with the initial and final CH_4 conversion of 69 % and 61 %, respectively. Catalyst 0.04Ni0.05Co-500, 600, 700, and 900 illustrated very similar performance with a slightly lower CH_4 conversion over the catalyst calcinated at 500 ^{o}C (Fig. 5.10). However, catalyst 0.04Ni0.05Co-1000 had significantly lower activity and stability in comparison with other catalysts (Fig. 5.10). The testing for catalysts with different Ni-Co content calcinated at various temperatures demonstrated that a calcination temperature range of 700-900 ^{o}C could be recommended for the Ni-Co/AlMgOx bimetallic catalysts for CO_2

reforming of CH_4.

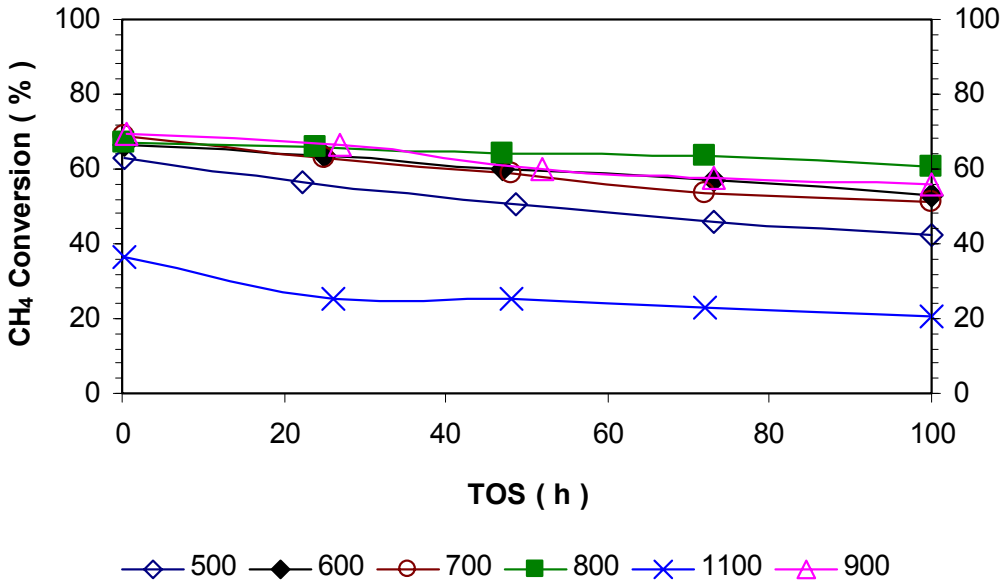

Fig. 5.10 The activity and stability of 0.04Ni0.05Co catalysts calcined at different temperatures for CO_2 reforming of CH_4 at 750°C, 1 atm, 720,000 mL/g_{cat}-h, and $CH_4/CO_2/N_2$=1/1/0

5.5 CONCLUSIONS

Experiments have shown that the calcinations temperature has a significant effect on the catalyst properties and catalytic performance of Ni-Co/AlMgOx catalysts for CO_2 reforming of CH_4. Calcination temperature can affect both catalyst particle sizes and metal-support interaction which are two most important factors for carbon resistance. At a low calcination temperature of 400 °C, small particle sizes (5.5 nm) can be formed on 0.06Ni0.09Co catalyst with no strong metal support interaction. When calcinated at 600 °C, larger particle sizes can be developed but the metal-support interaction can not change significantly, which results in higher carbon deposition rate and activity decay. A calcination temperature of 900 °C has been shown to be suitable for the development of

strong metal-support interaction without resulting in oversizing of particles, thus good activity and stability can be achieved on 0.06Ni0.09Co/AlMgOx bimetallic catalysts for CO_2 reforming of CH_4. When the calcination temperature reachs 1100 ^oC, strong metal-support interaction is developed but also oversize particles are produced. The too strong metal-support interaction of 0.06Ni0.09Co-1100 compromised its initial activity due to the difficulty of reduction and the oversize particles enhanced the carbon deposition rate, thus high carbon deposition and high degree activity decay. Combined with the testing on 0.04Ni0.05Co catalysts, a calcination temperature range of 700-900 ^oC is recommended for the Ni-Co/AlMgOx bimetallic catalysts for CO_2 reforming of CH_4.

6 EXPERIMENTAL AND KINETIC STUDIES

A similar version of this paper has been copyrighted and publised in Industrial and Engineering Chemistry Research: Zhang, J., Wang, H., Dalai, A.K., "Kinetic studies of CO_2 reforming of CH_4 over Ni-Co/AlMgOx bimetallic Catalyst", *Ind. Eng. Chem. Res.,* 48 (2), 677-684 (2009).

CONTRIBUTION OF Ph.D. CANADIDATE

Experiments were planned and performed by Jianguo Zhang. Hui Wang and Ajay K. Dalai provided guidance in planning the experiment. The submitted manuscript was written by Jianguo Zhang, while Hui Wang and Ajay K. Dalai provided comments and suggestions for revision.

CONTRIBUTION OF THIS PAPER TO THE OVERALL STUDY

This paper investigated the effects of experimental conditions at a constant overall pressure on the Ni-Co/AlMgOx bimetallic catalyt for CO_2 reforming of CH_4. The work involves the catalyst preparation, catalyst pre-treament, catalyst testing, and kinetic model development. Power Law model was used to fit the data. Also, a Langmuir-Hinshelwood model was developed assuming that the dissociation of CH_4 and the reaction between C species and activated CO_2 are the rate-determining steps over the Ni-Co/AlMgOx catalyst.

ABSTRACT

The kinetics of CO_2 reforming with CH_4 over a Ni-Co/$AlMgO_x$ bimetallic catalyst was investigated as a function of temperature and partial pressures of CO_2 and CH_4. In the temperature range of 650-750 ^oC, the apparent activation energies were estimated to be 69.4 and 25.9 kJ/mol for CH_4 and CO_2 consumption and 85.1 and 61.8 kJ/mol for H_2 and CO formation, respectively. It was found that the reforming rate in terms of CH_4 consumption was less sensitive to CO_2 partial pressures than to CH_4 partial pressures. At a constant CH_4 partial pressure, the increase in CO_2 partial pressure did not cause significant change in the reforming rate, whereas at a constant CO_2 partial pressure the reforming rate increased with the increase in CH_4 partial pressure. The increase in extra CO_2 at a constant CH_4 pressure led to decreases in hydrogen (H_2) formation but increase in carbon monoxide (CO) formation due to the simultaneous occurrence of the reverse water-gas shift reaction (RWGS). The Power-Law (P-L) model was used to fit the data and also a Langmuir-Hinshelwood (L-H) type of kinetic model was developed assuming that the dissociation of CH_4 and the reaction between C species and activated CO_2 are the rate-determining steps over the Ni-Co/$AlMgO_x$ bimetallic catalyst. The experimental data have a good fit with both the P-L model and the L-H model.

6.1 INTRODUCTION

Experimental and kinetic studies have been performed over different Ni-based catalysts. As early as 1960s, Bodrov and Apel'baum (1967) have reported that the rate of CO_2 reforming of CH_4 over nickel surface in the temperature range of 800-900 ^oC can be described by the same kinetic equation as that for steam (H_2O) reforming of CH_4. Bodrov's model is based on the assumption that CH_4 does not react with CO_2 but with steam; the H_2 formed reacts rapidly with CO_2 by the reverse water-gas shift reaction and the steam is thus regained. Assuming that CH_4 dissociation is the rate determining step, Zhang and Verykios (1994) developed a Langmuir-Hinshelwood model for CO_2 reforming of CH_4 over Ni/CaO-Al_2O_3. Also isotopic effects of CH_4/CD_4 in CO_2 reforming of CH_4 over Ni/SiO_2 catalyst indicated the dissociation of CH_4 to be the rate-determining step (Wang and Au, 1996). However, Slagtern et al. (1997) reported that the surface reaction between C species from CH_4 cracking and oxygen-adsorbed species derived from CO_2 dissociation is rate-determining step. Hu and Ruckenstein (1997) also concluded that the surface reaction between C and O species is the rate-determining step over Ni catalysts through transient response analysis. The above review for literature suggests that the CH_4 cracking and the surface reaction between C species and O species are generally accepted by different research groups as rate-determining steps over various Ni based catalysts. Bradfrod and Vannice (1996) investigated kinetics of CO_2 reforming of CH_4 over various Ni catalysts and developed a kinetic model based on CH_4 dissociative adsorption to form

CH_x species and CH_xO decomposition as rate-determining steps. Also, Tsipouriari and Verykios (2001) reported another kinetic model by assuming that the CH_4 cracking and surface reaction between C and oxycarbonate species are rate-determining steps over Ni/La_2O_3 catalyst. Even though different rate-determining steps are suggested in mechanism studies, Langmuir-Hinshelwood type of model has been commonly used in the kinetic studies of CO_2 reforming of CH_4 (Bradford and Vannice, 1996; 1999; Zhang and Verykios, 1994; Tsipouriari and Verykios, 2001; Olsbye et al., 1997; Wang and Lu, 1999; Nandini et al., 2006). However, the L-H type of model has different formula depending on catalyst systems. Therefore, it is necessary to develop a new kinetic model for the $Ni\text{-}Co/AlMgO_x$ catalyst as there is no general kinetic model available for CO_2 reforming of CH_4.

In previous work, a series of bimetallic catalysts for CO_2 reforming of CH_4 (Zhang et al., 2007) have been developed. It was found that the $Ni\text{-}Co/AlMgO_x$ bimetallic catalysts have excellent activity and stability for CO_2 reforming of CH_4. Adjusting Ni-Co content leads to low carbon or carbon-free operation of CO_2 reforming of CH_4 (Zhang et al., 2008). At the conditions of 750 ^oC, 1 atm, 180,000 mL/g_{cat}-h, and $CH_4/CO_2/N_2=1/1/1$, 250 h carbon free operation for CO_2 reforming of CH_4 have been achieved over $Ni\text{-}Co/AlMgO_x$ bimetallic catalysts with lower Ni-Co content (Zhang et al., 2008). In this work, experimental and kinetic studies of CO_2 reforming of CH_4 have been performed over the Ni-Co/AlMgOx bimetallic catalyst with 4 mol% Ni and 5 mol% Co. The effects of partial pressures of reactants have been investigated in the temperature range 650-750

^{o}C at 310 kPa. Apparent activation energies for reactant consumption and product formation were estimated. Both power-law model and L-H model were developed to fit the kinetic data for CO_2 reforming of CH_4 using Ni-Co/$AlMgO_x$ catalyst.

6.2 EXPERIMENTAL

6.2.1 Catalyst preparation and activation

Ni-Co/$AlMgO_x$ bimetallic catalyst was prepared by coprecipitation method as described in previous chapters. The Ni-Co/$AlMgO_x$ bimetallic catalyst was activated by heating at 800 ^{o}C for 4 h in the flow of 30 mL/min H_2-N_2 mixture with 20 % H_2. The activated catalyst was then stabilized for 24 h at 750 ^{o}C, 1 atm, $CH_4/CO_2/N_2$=1/1/1, and a low GHSV of 180,000 mL/g_{cat}-h.

6.2.2 Experiment procedure

The experimental design and reactant conversions are shown in Table 6.1. Experiments were performed in the temperature range of 650-750 ^{o}C, with a feed of $CH_4/CO_2/N_2$ in total flow rate of 300 mL/min and total pressure of 310 kPa (Table 6.1). Due to the high activity of the Ni-Co/$AlMgO_x$ bimetallic catalyst, the amount of catalyst used for this study was as low as 0.01 g, to maintain low conversions. The catalyst had an average particle size of 0.165 mm diluted with quartz sands. N_2 was the balance inert gas to maintain the overall pressure constant when CH_4 or CO_2 partial pressure varied. The N_2 was also functioned as an internal reference for GC analysis.

Table 6.1 Kinetic experiment design and reactant conversion of the CO_2 reforming of CH_4 over Ni-Co/$AlMgO_x$ catalyst at 95% confidence interval

Run	Temperature (^oC)	Inlet partial pressure (kPa)			Conversion (%)	
		CH_4	CO_2	N_2	CH_4	CO_2
1-1	750	62	31	217	18.2±2.6	47.2±3.2
1-2	750	62	62	186	26.2±2.4	41.2±1.9
1-3	750	62	124	124	32.2±1.2	27.2±1.9
1-4	750	62	186	62	32.8±1.7	22.3±3.3
1-5	750	31	62	217	35.4±2.0	29.7±2.3
1-6	750	124	62	124	17.2±1.1	35.1±2.4
1-7	750	186	62	62	16.8±1.8	48.8±2.5
1-8	750	62	62	186	24.6±1.2	39.8±2.0
2-1	700	62	31	217	15.8±1.4	33.7±4.1
2-2	700	62	62	186	19.4±1.3	36.6±2.1
2-3	700	62	124	124	23.0±1.4	20.9±2.0
2-4	700	62	186	62	23.8±2.0	16.6±3.6
2-5	700	31	62	217	30.3±2.1	25.6±2.4
2-6	700	124	62	124	13.7±1.1	28.2±2.6
2-7	700	186	62	62	11.6±1.9	28.6±3.3
2-8	700	62	62	186	19.0±1.3	37.1±2.1
3-1	650	62	31	217	8.2±1.5	20.6±4.9
3-2	650	62	62	186	10.9±1.5	29.7±2.3
3-3	650	62	124	124	13.2±1.6	14.2±2.2
3-4	650	62	186	62	14.1±2.2	11.5±3.8
3-5	650	31	62	217	19.8±2.5	18.3±2.6
3-6	650	124	62	124	8.6±1.2	19.2±3.0
3-7	650	186	62	62	6.8±2.0	18.7±4.1
3-8	650	62	62	186	11.3±1.5	29.5±2.3

6.3 RESULTS AND DISCUSSION

6.3.1 Catalyst deactivation

Although previous study (see chapter 3-5) showed that carbon deposition on the catalyst used for the kinetic measurement was not detectable, repeated runs (run 1-8, 2-8, and 3-8 in Table 1) were conducted after the kinetic data were collected at every temperature level, to ensure that the catalyst deactivation could be ruled out. From Table 6.1, it is clear that the catalyst was very stable during the kinetic measurement as shown by the reactant conversions of the repeated runs.

6.3.2 Effects of mass transfer and heat transfer

The effects of internal and external mass transfer were evaluated experimentally with a feed mixture composed of $CH_4/CO_2/N_2$=1/1/3 at 750 ^oC and 310 kPa. In a fixed bed reactor, the limitation of external mass transfer is typically tested through the variation of feed flow rate (Tsipouriari and Verykios, 2001; Nandini et al., 2006). At a fixed residence time obtained through maintaining a constant W/F ratio, higher flow rate leads to higher mass transfer rate. When the reforming rate does not change with the change of flow rate, limitation of external mass transfer is negligible. In this work, the reforming rate of CO_2 reforming of CH_4 was expressed in terms of CH_4 consumption rate. Fig. 6.1 shows the reforming rate as a function of feed flow rate at a constant W/F of 0.002 g_{cat}-s/mL. It is clear that the reforming rate increased with the increase in feed flow. However, the reforming rate barely changed when the feed flow rate was increased from 200 to 400 mL/min. It indicated that the external mass transfer effect can be neglected

when the feed flow rate was higher than 200 mL/min. In this work, the kinetic studies were conducted at a feed flow rate of 300 mL/min.

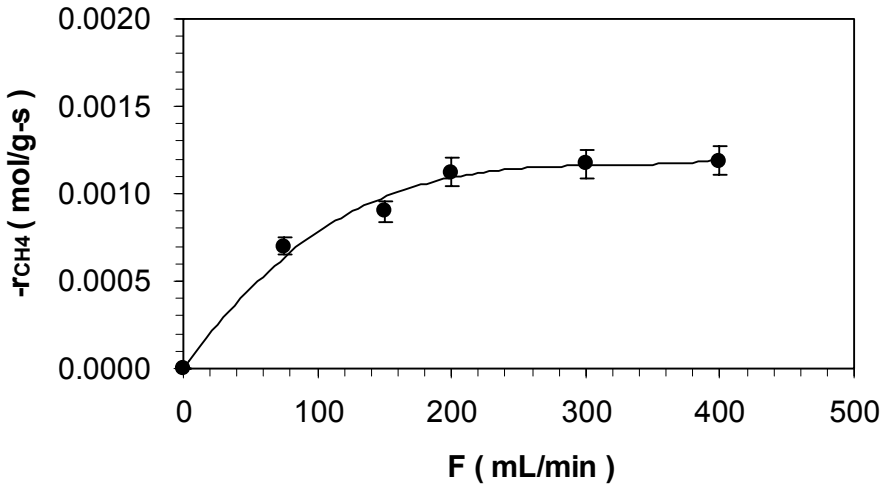

Fig. 6.1 Effect of flow rate on reaction rate of Ni-Co/AlMgO$_x$ catalyst at 750 ^oC, 310 kPa, and W/F = 0.002 g_{cat}-s/mL. Error shows the 95 % confidence interval.

In heterogeneous catalysis, the variation of catalyst particle size is usually used to check the limitation of internal mass transfer (Tsipouriari and Verykios, 2001; Nandini et al., 2006). Internal mass transfer is dependent on particle radius but kinetics is independent on radius (Forni, 1999). A clear change in reaction rate with the change in particle size under certain reaction conditions indicates the internal mass transfer controlling regime. As shown in Fig. 6.2, the effect of internal mass transfer was tested using four different catalyst particle sizes to carry out CO_2 reforming of CH_4 at 750 ^oC, 310 kPa, and W/F of 0.002 g_{cat}-s/mL. It can be seen that the reforming rate was increased when the catalyst particle size was reduced from 0.300 to 0.200 mm. However, only slight change in reforming rate was observed when the particle size was further reduced from 0.200 to 0.085 mm. The results shown in Fig. 6.3 suggest that the internal mass transfer

can be neglected when catalyst particle size was less than 0.200 mm. Therefore, a catalyst particle size of 0.165 mm was selected for the kinetics study in this work.

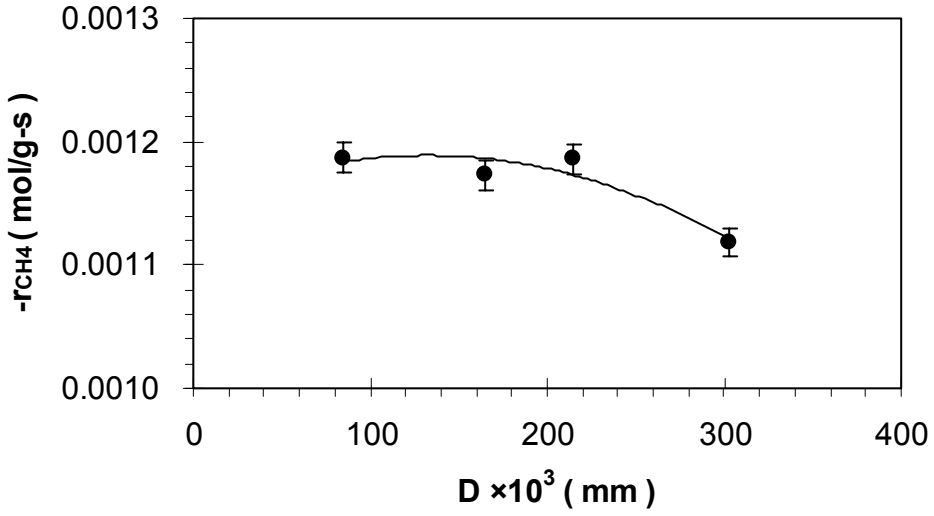

Fig. 6.2 Effect of catalyst particle size on reforming rate over Ni-Co/AlMgO$_x$ catalyst at 750 ^{o}C, 310 kPa, and W/F = 0.002 g$_{cat}$-s/mL. Error bas shows the 95 % confidence interval of reaction rate.

The effects of heat transfer limitations were also ruled out using Anderson criterion which is shown by Eq. 6.2.

$$\frac{\left|(-\Delta H_r)\right|\langle R\rangle d_p^2}{4\lambda_p T_s} < 0.75\frac{T_S R}{E_a} \tag{6.2}$$

where, ΔH_r is reaction enthalpy (275.6 kJ/mol at 750 ^{o}C), $\langle R\rangle$ average reaction rate per unit catalyst particle volume (0.6 mol/m^3-s), d_p the average catalyst particle diameter (0.000165 m), λ_p the thermal conductivity of catalyst particle (7.45 W/m/K at 750 ^{o}C, which was estimated using the thermal conductivity of Al_2O_3 and MgO considering that they are the main compositions of the catalyst), T_s surface temperature of catalyst particle (1023 K), R gas constant (8.314 Pa-m^3/mol-K), and E_a apparent activation energy (69.4

kJ/mol). When substituting the numbers into Eq. (2), the value of the left-hand side is 1.5 $\times 10^{-7}$, which is far less than the value of the right-hand side, 9.2×10^{-2}. It was clearly estimated that the catalyst particle was at isothermal condition under the reaction conditions using Anderson criterion.

6.3.3 Effect of partial pressure on reforming rate

The influence of partial pressures of CH_4 and CO_2 on the rate of CO_2 reforming of CH_4 reaction rate was carried out over the Ni-Co/$AlMgO_x$ bimetallic catalyst at 310 kPa and W/F 0.002 g_{cat}-s/mL, and 650-750 ^oC. The effect of CO_2 partial pressure at different temperatures were investigated by applying a constant CH_4 partial pressure of 62 kPa while the CO_2 partial pressure was varied between 31 kPa and 186 kPa as shown in Fig. 6.4. It can be seen that the reforming rate was increased with the increase in CO_2 partial pressure in the range 31-124 kPa. However, the increase of reforming rate became slower at higher CO_2 partial pressures in the range 124-186 kPa. The relatively constant reaction rate in the range 124-186 kPa can be ascribed to the restriction of thermodynamic equilibrium at limited availability of CH_4 (62 kPa). Also, it can be seen that at a lower temperature, the effect of CO_2 partial pressure was less significant in comparison with those at higher temperatures.

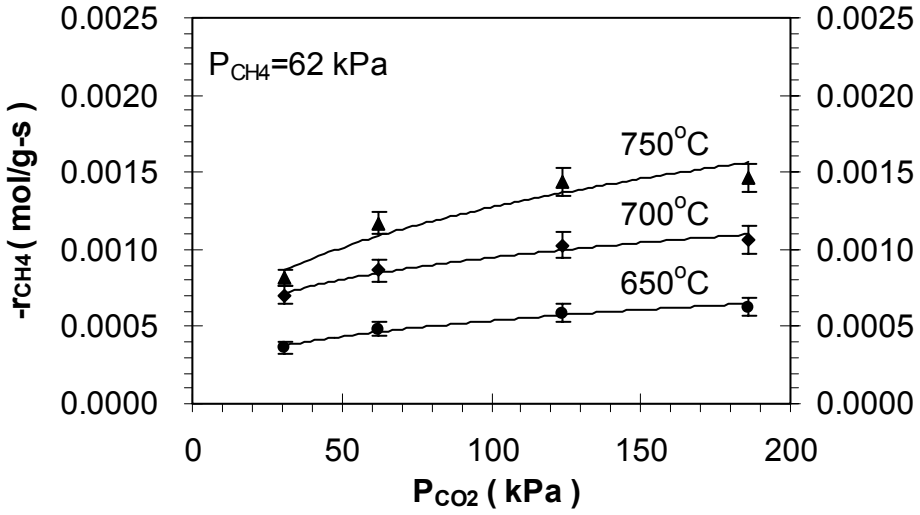

Fig. 6.3 Effect of CO_2 partial pressure on the reforming rates of CO_2 reforming of CH_4 over Ni-Co/AlMgO_x catalyst at 310 kPa and W/F = 0.002 g_{cat}-s/mL. Error bar shows the 95 % confidence interval of reaction rate.

The effects of CH_4 partial pressures on the reaction rate of CH_4 were studied at a constant CO_2 partial pressure of 62 kPa. Results at different temperatures are shown in Fig. 6.5. It is clear that the reforming rate was affected by the partial pressure of CH_4 in the whole experimental range 31-186 kPa. The acceleration of reforming rate slowly decreased with the increase in CH_4 partial pressure at a constant CO_2 partial pressure. Comparison of data in between Fig. 6.4 and Fig. 6.5 indicates that the reforming rate was more sensitive to CH_4 partial pressure than to CO_2 partial pressure. It probably can be attributed to that the adsorption of CH_4 to the surface of catalyst was stronger than that of CO_2 at higher partial pressures.

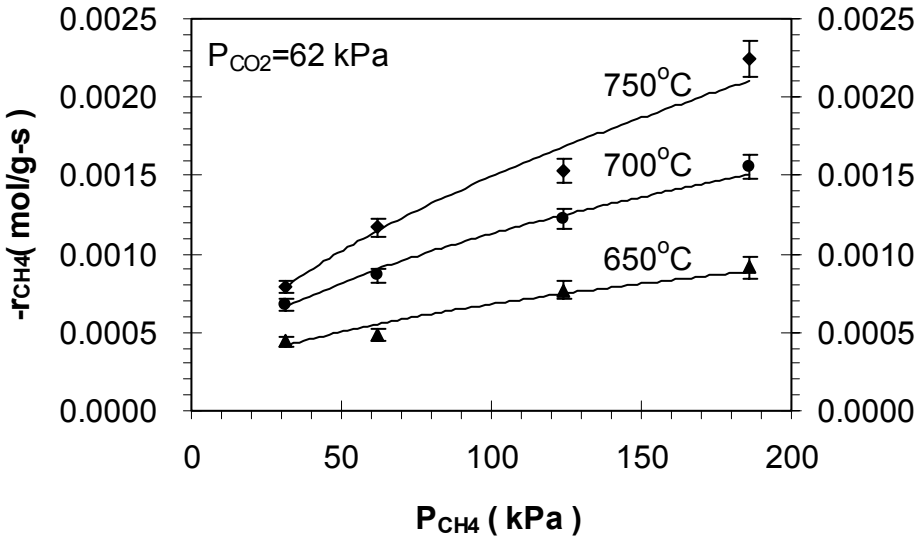

Fig. 6.4 Effect of CH_4 partial pressure on the reforming rates of CO_2 reforming of CH_4 over Ni-Co/$AlMgO_x$ catalyst at 310 kPa and W/F=0.002 g_{cat}-s/mL. Error bar shows the 95 % confidence interval of reaction rate.

6.3.4 Effect of reactant partial pressure on formation rate of products

Fig. 6.6 shows the effect of reactant partial pressures on the formation rate of CO at 750, 700, and 650 ^oC, respectively. From Fig. 6.6A, it can be seen that the formation rate of CO increased with the increase in CO_2 partial pressure while it did not change significantly with the increase in CH_4 partial pressure (Fig. 6.6B). This observation can be ascribed to the influence of reverse water gas shift reaction (RWGS).

$$CO_2 + H_2 \rightarrow CO + H_2O \qquad (6.3)$$

At constant CH_4 partial pressure, the reaction rate of CO_2 reforming of CH_4 was restricted due to limited availability of CH_4. However, the formation of CO still can be enhanced significantly through the RWGS reaction between H_2 and excess CO_2 when CO_2 partial pressure was increased continuously as shown in Fig. 6.6A. At constant CO_2 partial

pressure, the formation rate of CO only increased slightly with the increase in CH_4 partial pressure (Fig. 6.6B).

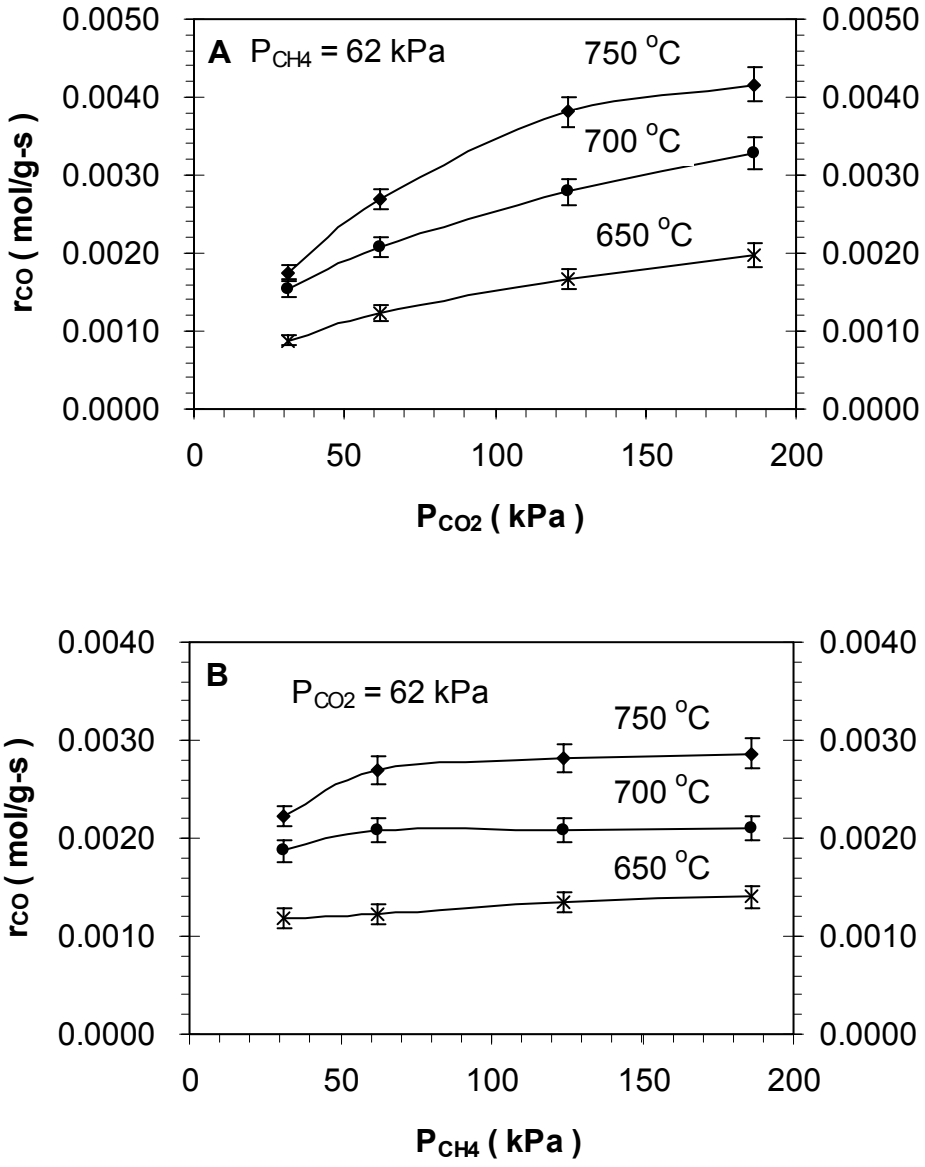

Fig. 6.5 Effect of reactant partial pressures on the formation rates of CO over Ni-Co/AlMgOx catalyst at 310 kPa and 0.002 g_{cat}-s/mL. Error bar shows the 95 % confidence interval of reaction rate.

The effects of reactant partial pressures on the formation rate of H_2 at 750, 700, and 650 °C are shown in Fig. 6.7. It is clear that at constant CH_4 partial pressure the H_2

formation rate increased in the low CO_2 partial pressure range 31-62 kPa (Fig.6.7A). The increase in H_2 formation was due to the increase in reaction rate of CO_2 reforming of CH_4 when more CO_2 was available. The formation rate of H_2 was relatively stable in the CO_2 partial pressure range 62-124 kPa (Fig.6.7A). In this CO_2 partial pressure range, the reaction rate of CO_2 reforming of CH_4 should be increasing slightly but limited by the availability of CH_4. At the same time, the RWGS reaction could be also increasing with the availability of excess CO_2. When the increase of CO_2 reforming of CH_4 is equivalent to the increase of RWGS, the formation of H_2 will remain constant. However, the formation rate of CO will continue to increase. This can be confirmed by the increasing formation rate of CO in the CO_2 partial pressure range of 62-124 kPa (Fig. 6.6A). With the further increase in CO_2 partial pressure from 124 kPa to 186 kPa, the formation rate of H_2 dropped (Fig. 6.7A). It was because the increase of the H_2 formation rate from CO_2 reforming of CH_4 reaction was less than the consumption rate of H_2 from RWGS reaction when CH_4 was limited but CO_2 was in excess. At constant CO_2 partial pressure, the formation rate of H_2 first slightly increased and then was kept constant with the increase of CH_4 partial pressure (Fig. 6.7B). It indicated that both CO_2 reforming of CH_4 reaction and RWGS were restricted when limited CO_2 was available.

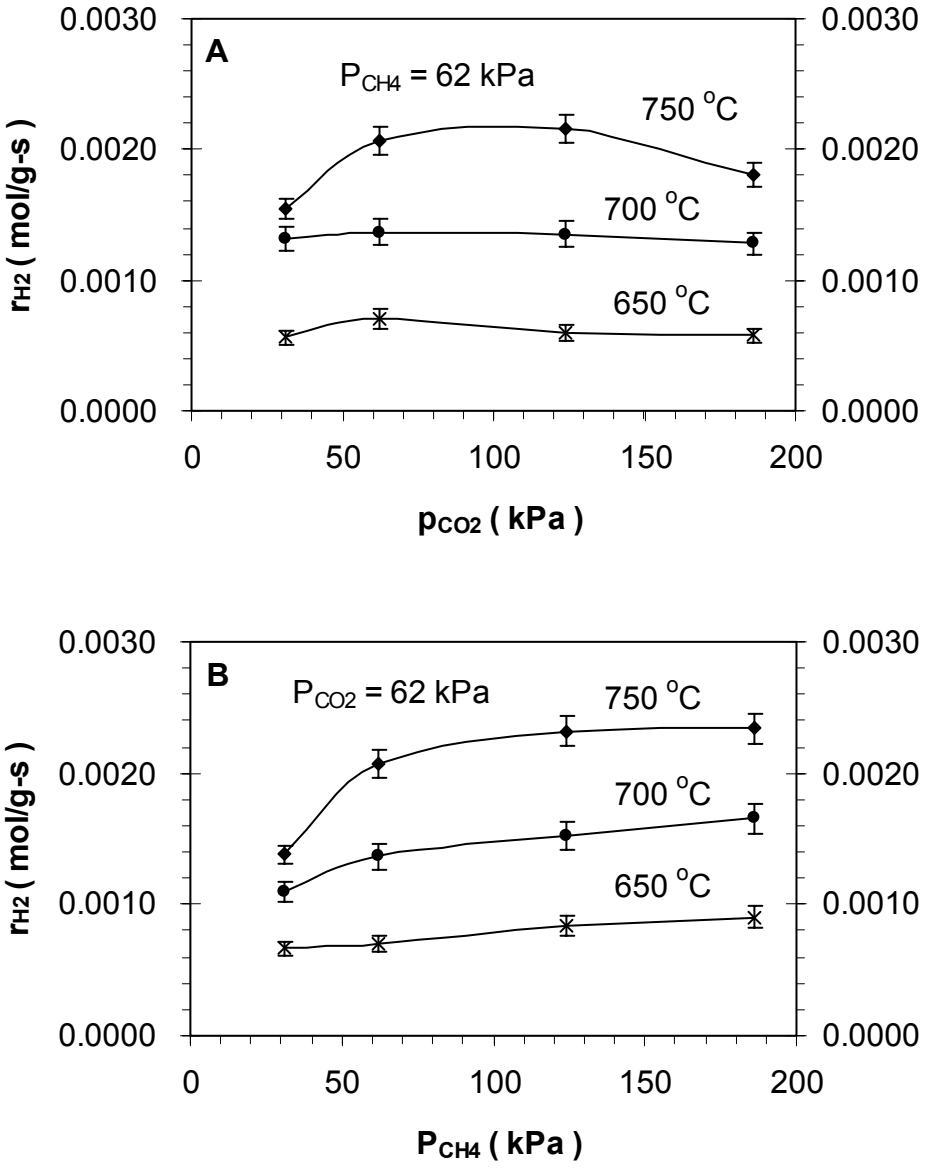

Fig. 6.6 Effect of reactant partial pressures on the formation rates of H_2 over Ni-Co/AlMgO_x catalyst at 310 kPa and W/F=0.002 g_{cat}-s/mL. Error bar shows the 95 % confidence interval of reaction rate.

6.3.5 Side reverse water gas shift (RWGS) reaction

As discussed in above section, the effects of RWGS were clearly indicated by the difference between CO and H_2 formation rate. Referring to Eq. 6.1 and Eq. 6.3, it is clear that the production of every one CO molecule through RWGS reaction results in the

consumption of one H_2 molecule, i.e. every one RWGS reaction produces one CO but consumes one H_2. The same formation rates of CO and H_2 should have been expected if CO_2 reforming with CH_4 were the only reaction (Eq. 6.1). However, the occurrence of RWGS reaction (Eq. 6.3), actually, increased the CO formation rate and reduced the H_2 formation rate. RWGS reaction rate can be calculated using the 0.5 times difference between CO and H_2 formation rates if assuming RWGS is the only side reaction in CO_2 reforming with CH_4 reaction system. It has been reported that carbon formation on the Ni-Co/$AlMgO_x$ bimetallic catalysts is very low (Zhang et al., 2007; 2008) so that it is negligible in comparison with the formation of CO and H_2. Therefore, it is reasonable to assume the RWGS is the only side reaction when the product formation is considered. In this work, the reaction rate of RWGS was estimated based on above assumption in order to have quantitative understanding about its effects on the CO_2 reforming with CH_4 reaction system. Fig. 6.8 A shows the RWGS reaction rate as a function of CO_2 partial pressure. At constant CH_4 partial pressure, the RWGS reaction rate increased almost linearly with the increase in CO_2 partial pressure. At higher temperatures, the reaction rate increased faster as more H_2 was available at higher conversion of CH_4 at higher temperature. However, as shown in Fig. 6.8B, at constant CO_2 partial pressure the reaction rate of RWGS was suppressed as the CH_4 concentration increased. It indicated that CH_4 reforming reaction was competing for CO_2 with RWGS reaction. The suppression of RWGS reaction at availability of additional CH_4 can be expected since the equilibrium constant K of CO_2 reforming with CH_4 is much higher than that of RWGS

reaction at the reaction temperatures studied.

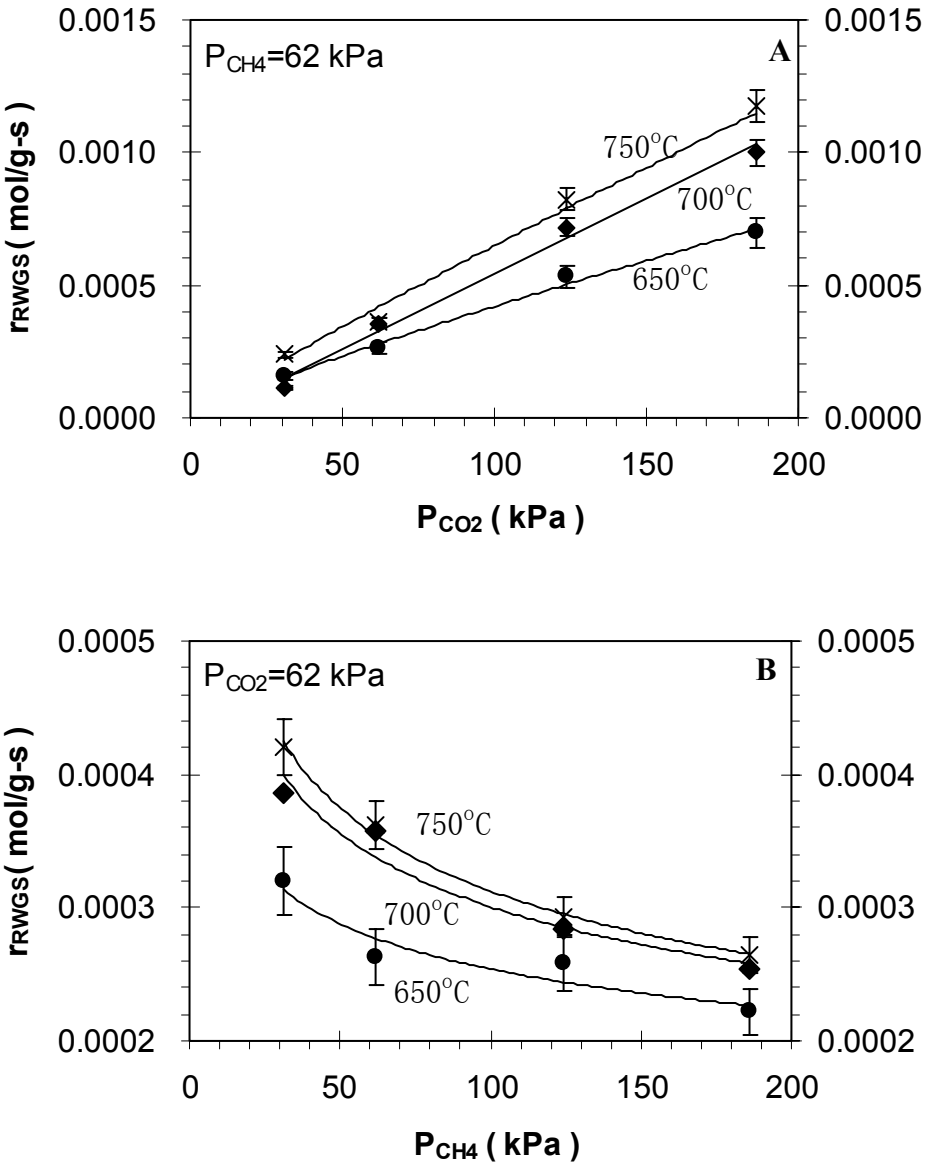

Fig. 6.7 Reaction rate of RWGS reaction as a function of CO_2 partial pressures. Error bar shows the 95 % confidence interval.

6.3.6 Effect of temperatures and apparent activation energy

The effect of temperatures on the reaction rate of CO_2 reforming of CH_4 over Ni-Co/$AlMgO_x$ bimetallic catalyst was investigated in temperature range 650-750 ^oC at 310

kPa, $CH_4/CO_2/N_2$=1/1/3, and W/F=0.002 g_{cat}-s/mL. Results in the form of Arrhenius plots are shown in Fig. 6.9. The apparent activation energies were then estimated for CH_4, CO_2 consumption, H_2, and CO formation. Comparison of apparent activation energies of Ni-Co/$AlMgO_x$ bimetallic catalyst with reported Ni-based catalysts are listed in Table 6.2 (Bradford and Vannice 1996, Wang and Lu 1999, Lemonidon and Vasalos 2002). From Table 6.2, it is clear that the apparent energy is very different over different catalysts. The disagreement in apparent activation energy is probably due to the difference of catalyst systems applied in the relevant studies. Tsipouriari and Verykios (2002) reported that the catalyst supports of Ni may influence significantly the activation energy by altering the rate-controlling step in the reaction sequence. The proximity of apparent activation energy values for CH_4, CO_2, and CO suggests that the rate-controlling step for CO formation is the same as that for CH_4 and CO_2 consumption (Lemonidon and Vasalos 2002). In a review by Bradford and Vannice (1999), it was reported that the activation energies of CO_2 reforming of CH_4 are typically between 33 and 100 kJ/mol while high values up to 160 kJ/mol are obtained for some catalysts. However, for the case of Ni-Co/$AlMgO_x$ bimetallic catalyst in this work, the apparent activation energy of CO_2 consumption was much lower than that of CH_4 consumption (Table 6.2). Also, it was lower than the reported activation energies for CO_2 consumption (Table 6.2). Possibly this difference was due to the presence of strong Lewis base of MgO (Li et al., 1994) in the support of Ni-Co/$AlMgO_x$ bimetallic catalyst, which can facilitate the activation of CO_2. Also, the existence of RWGS reaction might be an important factor influencing the activation of

CO_2. Concerning the activation energies for CO and H_2, the apparent energy of H_2 formation is always higher than that for CO formation (Table 6.2). It has been ascribed to be the result of the RWGS influence on the reaction mechanism (Bradford 1996).

Table 6.2 Apparent activation energy (*Ea*, kJ/mol) over Ni based catalysts

Catalyst	*Ea*(CH_4)	*Ea*(CO_2)	*Ea*(H_2)	*Ea*(CO)	Reference
Ni-Co/AlMgOx (650-750 ^oC)	69.4	25.9	85.1	61.8	This work
Ni/Al_2O_3 (500-700 ^oC)	50.9	56.1	-	80.5	Wang and Lu 1999
Ni/TiO_2 (400-550 ^oC)	108.9	87.9	146.5	87.9	Bradford and Vannice 1996
Ni/CaO-Al_2O_3 (620-690 ^oC)	106.8	98.8	147.4	103	Lemonidou and Vasalos 2002

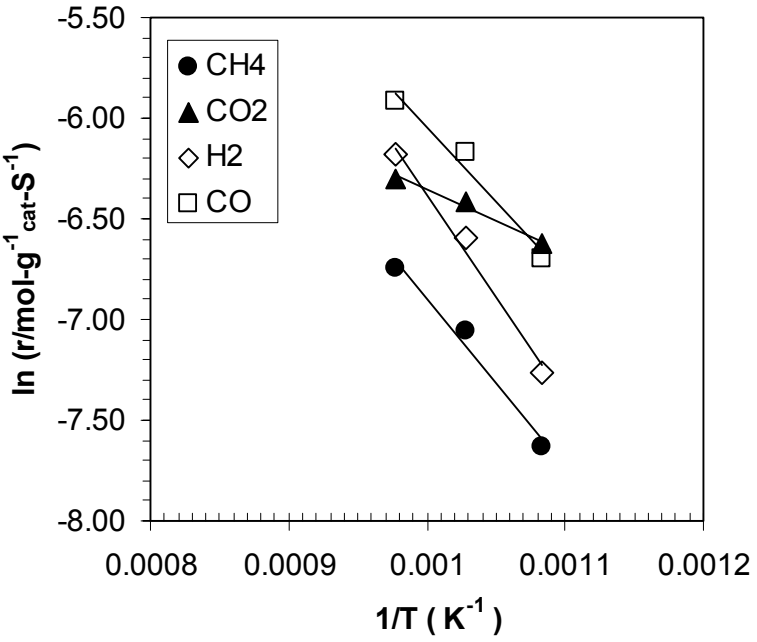

Fig. 6.8 Effect of temperatures on the reaction rates of CO_2 reforming of CH_4 at 310 kPa, $CH_4/CO_2/N_2$=1/1/3, and W/F=0.002 g_{cat}-s/mL

6.3.7 Kinetic models

6.3.7.1 Power law model

A general power law model can be expressed by Eq. 6.4.

$$-r_{CH_4} = kP_{CH_4}^{m} P_{CO_2}^{n} \quad (6.4)$$

The values of the power law rate coefficient *k* and the indices *m* and *n* are different for different catalysts. The values of the parameters of Ni based catalysts are summarized in Table 6.3

Table 6.3 Parameters of power law equation

Catalyst	m	n	Reference
Ni/SiO_2	-0.3-0.8	0-0.6	Takanabe et al., 2005; Osaki et al., 1997
Ni/Al_2O_3	0.6-1.0	0-0.3	Takanabe et al., 2005
Ni/MgO	1.0	0	Rostrup-Nielsen and Hanse, 1993

The power low model (Eq.6.4) was used to describe the reforming rate of CO_2 reforming of CH_4 over Ni-Co/$AlMgO_x$ bimetallic catalyst. Also, The reaction rate constant, *k*, was further expressed in an Arrhenius equation (Eq. 6.5). The values of the parameters and the R squared value for the power-law model are estimated and listed in Table 6.4.

$$k = k_0 e^{-E/RT} \quad (6.5)$$

Table 6.4 Estimated parameters of the power law model of Ni-Co bimetallic catalyst at 95 % confidence interval

k_0 (mol/g_{cat}-s-$kPa^{(m+n)}$)	E (kJ/mol)	m	N	R^2
0.089 ± 0.027	63.8 ± 0.4	0.483 ± 0.037	0.291 ± 0.040	0.951

As shown in Table 6.1, the conversions are in a range of 4.8-51.3 %. Some of which may be too high for the differential reaction rate analysis. Therefore, the P-L rate

equation was used for the intergral equation (Eq. 6.6) to assess the validity of the rate law.

$$\frac{W}{F^{i}_{CH_4}} = \int_0^X \frac{dX}{-r_{CH_4}} \tag{6.6}$$

where W is the catalyst mass, $F^{i}_{CH_4}$ is the initial inlet CH_4 mole flow rate, and X is CH_4 conversion.

Using Eq. 6.6, the CH_4 conversion X can be calculated at each reaction condition. The comparison of experimental CH_4 conversion and calculated CH_4 conversion using integral equation and P-L rate equation is shown in Fig. 6.10, where solid points are calculated CH4 conversions using integral method and P-L rate law and solid line is made through experimental CH_4 conversions. Dotted lines in Fig. 6.10 defined the 95 % confidence interval of the experimental CH_4 conversion. It can be seen that most of the calculated CH_4 conversions using integral method fall into the 95 % confidence interval of experimental CH_4 conversions. Also, it is evident that most of the calculated conversions are distributed around the lower 95 % confidence level of experimental CH_4 conversion. The comprison showed that the P-L model and differential method can describe the can the reaction with satisfactory results. Simplicity is the major advantage of power law model. However, power law model might be not very accurate. Therefore, other type models may be preferred to the power law form because it is more likely to be amenable to extrapolation. In the following section, a Langmuir-Hinshelwood (LH) mechanism model was developed.

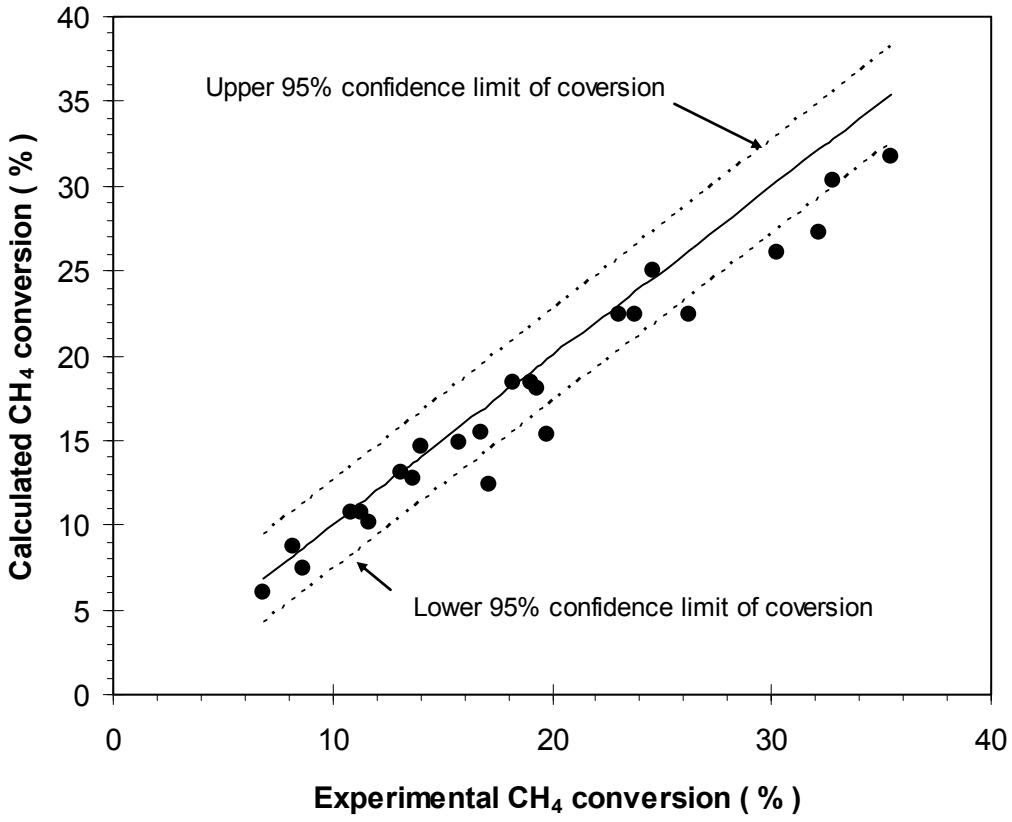

Fig.6.9 Comparison of experimental CH_4 conversion with calculated CH_4 conversion using integral method (Eq. 6.6) and P-L rate law (Eq.6.4)

6.3.7.2 Consideration of reaction mechanism – Langmuir-Hinshelwood mechanism

Steps plausible to describe the reaction mechanism of CO_2 reforming of CH_4 over the Ni-Co/$AlMgO_x$ bimetallic catalyst was proposed in this work based experimental observation and literature.

1) The reversible adsorption and dissociation of CH_4 can be assumed as the initial steps for the reforming reaction (Hickman and Schmidt 1993). Due to the metallic

properties of active sites on Ni-Co/AlMgO$_x$ bimetallic catalysts Zhang et al. (2007), the methane was supposed to adsorb and dissociate on metal particles (Eq. 6.7 and 6.8), leading to the formation of H_2 and C species.

. $$CH_4 + M \xleftrightarrow{K_1} M - CH_4, \quad \text{Equilibrium} \qquad (6.7)$$

. $$M - CH_4 \xrightarrow{k_2} M - C + 2H_2, \ \text{Slow} \qquad (6.8)$$

where M represents the metal particle of the reduced Ni-Co/AlMgO$_x$ catalyst. It was supposed that the CH_4 adsorption was at equilibrium while the dissociation of CH_4 was a slow step. The carbon species was present as M-C or carbide-like species which contains no C-H bond (Chang et al., 2000).

2) In CO_2 reforming of CH_4, the activation of CO_2 can be assumed to be another important step. CO_2 is a linear triatomic molecule and has two sets of π molecular orbital which is orthogonal. The carbon is a Lewis acid centre and the oxygen is weak Lewis base. The formation of an active site-CO_2 complex via direct coordination is one of the most powerful and universal ways to activate the inert CO_2 molecule to undergo chemical reactions (Gibson, 1996). The support of Ni-Co/AlMgO$_x$ bimetallic catalyst is mainly composed of MgO which is a strong Lewis base (Li et al., 1994). Therefore, the activation of CO_2 was supposed to occur on the Lewis base centre of the support (S) and was at equilibrium.

$$CO_2 + S \xleftrightarrow{K_3} S - CO_2, \quad \text{Equilibrium} \qquad (6.9)$$

3) The CO_2 reforming of CH_4 reaction was assumed to terminate through the reaction between carbon species (M-C) derived from CH_4 decomposition and activated CO_2 (S-CO_2) and it also considered to be a slow step (Tsipouriari and Verykios, 2001).

$$S\text{-}CO_2 + M\text{-}C \xrightarrow{k_4} 2CO + M + S, \quad \text{Slow} \qquad (6.10)$$

4) RWGS is the most common side reaction in CO_2 reforming of CH_4. It is important to take its occurrence into account. Besides step (6.10), activated CO_2 can also react with surface hydrogen species which originated from the decomposition of CH_4 and was assumed at equilibrium with the gaseous H_2 (Bradfrod and Vannice, 1996). The occurrence of RWGS results in the consumption of H_2 and the formation of CO which can be confirmed by the observation of CO/H_2 is higher than unity (Zhang et al., 2007).

$$H_2 + M \leftrightarrow 2M\text{-}H, \quad \text{Equilibrium} \qquad (6.11)$$

$$S\text{-}CO_2 + M\text{-}H \rightarrow CO + M\text{-}OH + S, \quad \text{Slow} \qquad (6.12)$$

$$M\text{-}OH + M\text{-}H \leftrightarrow H_2O + 2M, \quad \text{Fast} \qquad (6.13)$$

6.3.7.3 L-H type of model

Literature survey shows that L-H type of kinetic model is widely used to describe CO_2 reforming of CH_4 system (Bradford and Vannice, 1999; Wang and Au, 1996). A summary of rate expressions derived for Ni-based catalysts is tabulated in Table 6.5.

Table 6.5 Reported L-H models for CO_2 reforming of CH_4 over Ni-based catalysts

Model	Catalyst	Reference
$-r_{CH_4} = \dfrac{kP_{CH_4}}{1 + a\dfrac{P_{H_2O}}{P_{H_2}} + bP_{CO}}$	Ni foil	Bodrov and Apel'baum, 1967
$-r_{CH_4} = \dfrac{aP_{CH_4}P_{CO_2}^2}{(a + bP_{CO_2}^2 + cP_{CH_4})^2}$	Ni/Al_2O_3, $Ni/CaO\text{-}Al_2O_3$	Zhang and Verykios, 1994
$-r_{CH_4} = \dfrac{\hat{k}_1 P_{CH_4}P_{CO_2}}{\dfrac{\hat{k}_{-1}\overline{K}}{\hat{k}_7}P_{CO}P_{H_2}^{(4-x)/2} + \left(1 + \dfrac{\hat{k}_1}{\hat{k}_7}P_{CH_4}\right)P_{CO_2}}$	Ni/TiO_2 Ni/C Ni/SiO_2 Ni/MgO	Bradford and Vannice, 1996
$-r_{CH_4} = \dfrac{kP_{CH_4}P_{CO_2}}{(a + K_1P_{CH_4} + K_2P_{CO})(1 + K_3P_{CO_2})}$	$Ni/La/Al_2O_3$	Olsbye et al., 1997
$-r_{CH_4} = \dfrac{k_3K_1K_2P_{CH_4}P_{CO_2}P_{CO}P_{H_2}}{(P_{CO}P_{H_2}^2 + K_1P_{CH_4}P_{CO} + K_2P_{CO_2}P_{H_2}^2)^2}$	Ni/SiO_2	Kroll et al., 1998
$-r_{CH_4} = \dfrac{k_3P_{CH_4}P_{CO_2}}{(1 + K_1P_{CH_4})(1 + K_2P_{CO_2})}$	Ni/Al_2O_3 $Ni/CeO_2\text{-}Al_2O_3$	Wang and Lu, 2000
$-r_{CH_4} = \dfrac{K_1k_2K_2k_4P_{CH_4}P_{CO_2}}{(K_1k_2K_3P_{CH_4}P_{CO_2} + K_1k_2P_{CH_4} + K_3k_4P_C$	Ni/La_2O_3	Tsipouriari and Verykios, 2001
$-r_{CH_4} = \dfrac{k_{1L}P_{CH_4}}{\dfrac{k_{1L}P_{CH_4}P_{CO}}{k_{7L}K_aP_{CO_2}} + \dfrac{K_bP_{CO_2}P_{H_2}^{1/2}}{Pco} + \dfrac{k_{1L}P_{CH_4}}{k_{7L}} +$	Ni-K/CeO_2-Al_2O_3	Nandini et al., 2006

From above proposed mechanism, a L-H model (Eq. 6.14) for CO_2 reforming of CH_4 over the Ni-Co/$AlMgO_x$ bimetallic catalyst was developed based on the following assumptions: 1) step (6.10) is rate-limiting step; 2) the concentration of total metallic active sites for reforming reaction is constant C_{MT}; 3) the coverage of metallic active sites for reforming reaction by species of H and OH is negligible; 3) the coverage of active sites for CO_2 activation is negligible in comparison with its total concentration $C_{ST,}$ which is also supposed to be constant.

$$-r_{CH_4} = \frac{aP_{CH_4}P_{CO_2}}{bP_{CH_4} + cP_{CO_2} + dP_{CH_4}P_{CO_2}} \tag{6.14}$$

$$a = C_{MT}C_{ST}K_1k_2K_3k_4 \tag{6.15}$$

$$b = K_1k_2 \tag{6.16}$$

$$c = C_{ST}K_3k_4 \tag{6.17}$$

$$d = C_{ST}K_1K_3k_4 \tag{6.18}$$

Preliminary estimation for the parameters of the L-H model (Eq. 6.14) was performed using least-squares analysis and the Marquardt-Levenberg algorithm. Estimation of the parameters was based on the minimization of the sum of residual squares of the observed and the predicated reforming rates. It showed that $d(\sim 10^{-13}) << b(\sim 10^{-8})$ and $d(\sim 10^{-13}) << c(\sim 10^{-8})$. Therefore, the L-H model (Eq. 6.14) was simplified to Eq. 6.19.

$$-r_{CH_4} = \frac{aP_{CH_4}P_{CO_2}}{bP_{CH_4} + cP_{CO_2}} \tag{6.19}$$

After the values of all of the parameters were estimated at 750, 700, and 650 ^oC,

the parameters of the simplified L-H model (Eq. 6.19) were further expressed in the form of Arrhenius equations (Eq. 6.20-6.22).

$$a = a_0 e^{-E_a / RT} \tag{6.20}$$

$$b = b_0 e^{-E_b / RT} \tag{6.21}$$

$$c = c_0 e^{-E_c / RT} \tag{6.22}$$

where a_0, b_0, and c_0 are preexponential factors for rate constant a, b, and c. E_a, E_b, and E_c are activation energies and reaction enthalpies. The estimated values of these parameters are shown in Table 6.6. The CH_4 conversions were calculated using the simplified L-H model (Eq. 6.20) and intergral equation (Eq. 6.6) to assess the validity of the model. The comparison of experimental CH_4 converison with the calculated CH_4 conversion is shown in Fig. 6.11. It is clear that most of the calculated CH_4 conversions fall into the 95 % confidence interval of experimental CH_4 conversion. Also, the calculated CH_4 conersions are more evenly distributed throughout the 95 % confidence interval.

Table 6.6 Parameter estimates of the L-H model

Parameter	Estimate	Unit
a_0	1.35×10^{-8}	$(mol/g\text{-}s)^2 \bullet (kPa)^{-2}$
E_a	25.9	kJ/mol
b_0	9.25×10^{-8}	$(mol/g\text{-}s) \bullet (kPa)^{-1}$
E_b	-40.6	kJ/mol
c_0	2.46×10^{-7}	$(mol/g\text{-}s) \bullet (kPa)^{-1}$
E_c	-38.3	kJ/mol

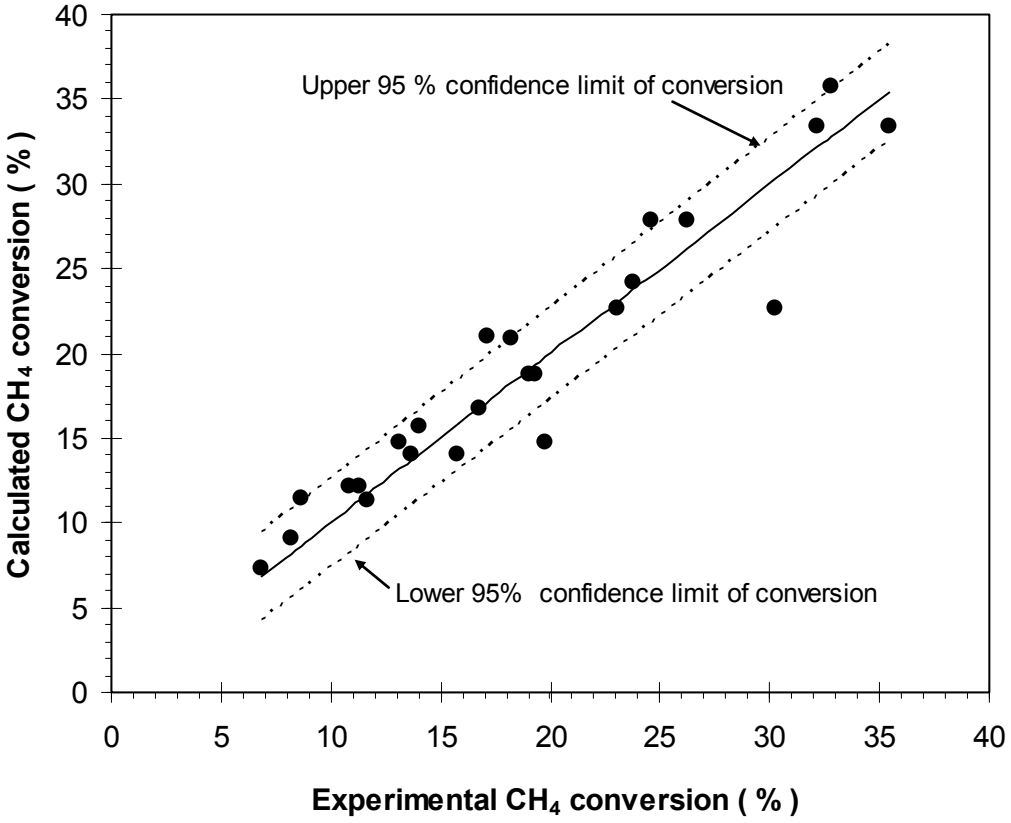

Fig. 6.10 Comparison of experimental CH_4 conversion with the calculated CH_4 convervison using intergral method (Eq. 6.6) and L-H model (Eq. 6.19)

6.4 CONCLUSIONS

The kinetics of the reaction of CO_2 reforming of CH_4 was investigated over Ni-Co/$AlMgO_x$ bimetallic catalyst in the temperature range 650-750 ^oC through variation of CO_2 and CH_4 partial pressures, respectively. The reaction mechanism was proposed based on literature and experimental observation. The dissociation of CH_4 and the reaction between C species and activated CO_2 were suggested as rate-determining steps. Both the P-L model and the L-H kinetic model were used to fit the kinetic measurement data with satisfactory results.

NOMENCLATURE

a, a_0, b, b_0, c, c_0	Constant
C_{MT}	Concentration of total metallic active sites, mol/m^3
C_{ST}	Concentration of total active sites for CO_2 activation, mol/m^3
d_p, D	Average catalyst particle diameter, m
E_a, E_b, E_c	Apparent activation energy, kJ/mol
ΔH_r	Reaction enthalpy, kJ
k, k_0, k_1, k_2,k_3, k_4,k_{1L},k_{7L}, $\hat{k}_1$ $\hat{k}_{-1}$, $\hat{k}_7$, $\hat{k}_{-7}$	Specific rate of reaction
K_a, K_b, K_1, K_2, K_3, K_4, $\overline{K}$	Chemical equilibrium constant
m, n	Reaction order
P	Pressure, kPa
$-r$, r	Reaction rate per unit catalyst weight, mol/g-s
$\langle R \rangle$	Average reaction rate per unit catalyst particle volume, mol/m^3-s
R	Ideal gas constant
R^2	Square of correlation coefficient
T_s	Surface temperature of catalyst particle, K
T	Temperature, K
λ_p	Thermal conductivity of catalyst particle, W/m/K

7 CONCLUSIONS AND RECOMMENDATIONS

7.1 CONCLUSIONS

In the development of CO_2 reforming of CH_4 process, long-term stable operation with high reactant conversion and product yield at low temperature and pressure is desirable. Higher reactant conversion and high product yield can be achieved at higher reaction temperatures. Also, high reaction temperature can alleviate the carbon formation problem, which is believed to be the major cause of catalyst deactivation in CO_2 reforming of CH_4. However, special material is needed to make the reactor being operated at high reaction temperature. Extremely high temperature will result in dramatic increase of capital investment and reduction of the life of reactor tubes. Therefore, the operation conditions are proposed based above stoichometric and thermodynamic discussion: 1) a temperature range between 1000-1300 K; 2) a pressure range between 1-3 atm; and 3) a CO_2/CH_4 ratio range between 1-1.3. However, under above conditions carbon formation is thermodynamically feasible. Therefore, developing a catalyst over which carbon formation can be kinetically suppressed is the only possible way to achieve carbon-free operation of CO_2 reforming of CH_4 at the proposed reaction conditions (Wang et al., 1996). The catalyst with desired catalytic properties for CO_2 reforming of CH_4 is designed following Dowden's strategy. A catalyst composition with a general formula Ni-

Me/AlMgOx (Me = Co, Fe, Mn, or Cu) is proposed based on stoichiometric analysis, thermodynamic analysis, and proposed surface mechanism considering literature and experience.

Catalyst screening showed that Ni-Co bimetallic catalysts made by coprecipitating Ni-, Co-, Al-, and Mg-containing precursor solutions demonstrate superior performance for carbon dioxide reforming of methane in comparison with Ni-Me (Me = Fe, Cu, or Mn) combinations. The synergy of Ni and Co in the bimetallic catalysts not only provides high activity but also excellent carbon resistance and thus makes the catalysts with outstanding stability. Comparative studies conducted with Ni and Co monometallic catalysts and Ni-Co bimetallic catalyst show that the superior performance of Ni-Co catalysts comes from high BET surface area, small pore diameter, relatively easy reducibility, good metal dispersion, high metallic surface, formation of different types of solid solutions, and SMSI.

Optimization for Ni and Co loading showed that high surface area and high activity for CO_2 reforming of CH_4 are those Ni-Co/AlMgOx catalysts with a Ni/Co or Co/Ni ratio between 0.6 and 1.5. Adjusting the Ni-Co content of the bimetallic catalysts, whose Ni/Co or Co/Ni ratio is between 0.6 and 1.5, is able to change the metal dispersion and metal particle size. The better metal dispersion and smaller metal particle are obtained at lower Ni-Co content. Small metal particles are crucial to the suppression of carbon deposition. Therefore, the Ni-Co bimetallic catalyst with the Ni/Co ratio close to unity and lower total metal content shows higher activity and greater stability. The metal particle size on 0.04Ni0.05Co and 0.02Ni0.03Co is smaller than 10 nm, and thus no detectable

carbon deposition on the two catalysts for CO_2 reforming of CH_4.

Optimization for the catalyst pre-treatment indicated that calcination temperatures have significant effects on the catalyst properties and catalytic performance of Ni-Co/AlMgOx catalysts for CO_2 reforming of CH_4. Calcination temperature can affect both catalyst particle sizes and metal-support interaction which are two most important factors of carbon resistance. At a low calcination temperature of 400 ^oC, small particle sizes can be formed with no strong metal support interaction. When calcinated at 600 ^oC, larger particle sizes can be developed but the metal-support interaction can not change significantly, which results in higher carbon deposition rate and activity decay. A calcination temperature 900 ^oC has shown to be good for the development of strong metal-support interaction without resulting in oversizing of metal particles, thus good activity and stability can be achieved on Ni-Co/AlMgOx bimetallic catalysts for CO_2 reforming of CH_4. When the calcination temperature reachs 1100 ^oC, strong metal-support interaction is developed but also oversize particles are produced. The too strong metal-support interaction of NiCo-1100 compromised its initial activity due to the difficulty of reduction and the oversize particles which enhanced the carbon deposition rate, resulting in high carbon deposition and high degree activity decay. Therefore, a calcination temperature range between 700 and 900 ^oC is recommended for the Ni-Co/AlMgOx bimetallic catalysts for CO_2 reforming of CH_4.

The experimental and kinetic investigation was conducted over Ni-Co/AlMgOx bimetallic catalyst in the temperature range 650-750 ^oC through variation of CO_2 and CH_4

partial pressures, respectively. The reaction mechanism was proposed based on literature and experimental observation. The dissociation of CH_4 and the reaction between C species and activated CO_2 were suggested as rate-determining steps. The L-H kinetic model which was derived from the proposed mechanism was used to fit the kinetic measurement. It was found that the L-H type model was better than power-law model in fitting the kinetic data with more satisfactory results.

7.2 RECOMMENDATIONS

The Ni-Co/AlMgOx bimetallic catalyst has been newly developed for CO_2 reforming of CH_4 in the Applied Catalysis Lab at the University of Saskatchewan since 2004. As a new catalyst system with complicated composition, sufficient characterization for the catalyst is necessary for an accurate understanding of the relationship between its property and performance. More accurate characterization is desirable for its phase structure, surface structure, and electrical structure, as well as their relationship with catalyst activity, deactivation, and carbon formation. Also, the specific role of each component in the Ni-Co/AlMgOx bimetallic catalyst needs to be clarified. The reaction mechanism and carbon formation mechanism on the Ni-Co/AlMgOx bimetallic catalysts should be investigated in the future work. In summary, the following aspects of work are of interest in the future works.

1) Catalyst preparation conditions:

The major variables which may have potential significant effects during the Ni-

Co/AlMgOx preparation using co-precipitation method include pH control and temperature control. The final titration pH can significantly affects catalyst composition and catalyst structure. The particle size might be affected by the preparation temperature since the crystal growth is temperature sensitive. Also, other factors such as concentration of metal salt and precipitation speed may worth further study.

2) Catalyst pre-treatment process

In previous research, it has been shown that the calcinations temperatures have significant effects on the catalyst properties and performances. Another two important variables during the pre-treatment which are not investigated due to time limit include calcination time at final calcination temperatures and temperature ramp rates.

3) Catalyst activation process

In previous research, the catalyst activation program was set based on experience without specific investigation. But it is sure that catalyst activation process has significant effects on the catalyst performances. Four parameters, including reduction temperature, reduction time, reduction temperaurte ramp rate, and reduction atmosphere or reduction gas composition during the activation process, are important.

4) Precise catalyst characterization

The previous study focused on catalyst development. Basic characterization and testing were performed. However, the previous catalyst characterization is far from enough to gain a good understanding for the catalyst properties which include the phase structure, surface property, metal particles or particles, and local chemistry environment.

Therefore, comprehsive precise characterization plan in the further should be made and budgeted to gain a clear understanding of the Ni-Co/AlMgOx catalysts for CO_2 reforming of CH_4.

5) Kinetics and Mechanism

Due to the instrument limit, there was no experiment performed to investigate the reaction mechanism. However, the reaction mechanism is critical to understanding the surface properties and performances of the catalysts. Kinetic study for the Ni-Co/AlMgOx catalyst was conducted at an overall pressure of 310 kPa, which was relatively narrow due to the limit of quartz reactor. A wider pressure range is desired to peformed experimental and kinetic studies. It is recommended to conduct further kinetic study at a higher overall pressure using stainless steel reactor in the future.

REFERENCES:

1. Ahn, I.Y., Kim, W.J., and Moon, S.H., "Performance of La_2O_3- or Nb_2O_5-added Pd/SiO_2 catalysts in acetylene hydrogenation," Appl. Catal. A 308, 75-84 (2006).
2. Alyea, E.C., He, D., and Wang, J., "Alcohol synthesis from syngas. I: Performance of alkali-promoted Ni-Mo (MOVS) catalysts", Appl. Catal. A 104, 77-85 (1993).
3. Anderson, J.B., "A criterion for isothermal behavior of a catalyst pellet," Chem. Eng. Sci. 18,147 (1963).
4. Aparicio, L.M., "Transient Isotopic Studies and Microkinetic Modeling of Methane Reforming over Nickel Catalysts," J. Catal. 165, 262-274 (1997).
5. Ashcroft, A.T., Cheetham, A.K., Green, M.L.H., and Vernon, P.D.F., "Partial oxidation of methane to synthesis gas using carbon dioxide." Nature 352, 225-226 (1991).
6. B.K. Cho, "Chemical modification of catalyst support for enhancement of transient catalytic activity: nitric oxide reduction by carbon monoxide over rhodium," J. Catal. 131 74-87 (1991).
7. Basini, L., and Sanfilippo, D., "Molecular aspects in syn-gas production: the CO_2-reforming reaction case," J. Catal. 157, 162-178 (1995).
8. Becerra, A., Iriarte, M.E., Dimitrijewit, M., and Castro-Luna, A., "Promoting effects of rhodium on supported nickel catalysts in the dry reforming of methane," Bol. Soc. Chil. Quím. 47, 385-91 (2002).
9. Bhat, R.N., and Sachtler, W.M.H., "Potential of zeolite supported rhodium catalysts for the CO_2 reforming of CH_4," Appl. Catal. A 150, 279-296 (1997).
10. Bhattacharyya, A., and Chang, V.W., "Rapid catalytic reforming of methane with CO_2 and its application to other reactions," Stud. Surf. Sci. Catal. 88, 207-213 (1994).
11. Bitter, J., Seshan, K., and Lercher, A., "Mono and bifunctional pathways of CO_2/CH_4 reforming over Pt and Rh based catalysts," J. Catal. 176, 93-101 (1998).
12. Bitter, J., Seshan, K., and Lercher, A., "The state of zirconia supported platinum catalysts for CO_2/CH_4 reforming," J. Catal. 171, 279-286 (1997).
13. Blom, R., Dahl, I.M., Slagtern, A., Sortland, B., Spjelkavik, A., and Tangstad, E., "Carbon dioxide reforming of methane over lanthanum-modified catalysts in a fluidized-bed reactor," Catal. Today 21, 535-543 (1994).
14. Bodrov, I.M., and Apel'baum, L.O., "Reaction kinetics of methane and carbon dioxide on a nickel surface", Kinet. Catal. 8, 326 (1967).
15. Bradford, and M.C.J., Vannice, M.A., "CO_2 reforming of CH_4," Catal. Rev. Sci. Eng. 41, 1 (1999).
16. Bradford, M.C.J., and Vannice, M.A., "Catalytic reforming of methane with carbon dioxide over nickel catalysts II. Reaction kinetics," Appl. Catal. A 142, 97-122 (1996).
17. Bradford, M.C.J., and Vannice, M.A., "CO_2 reforming of CH_4 over supported Pt catalysts," J. Catal. 173, 151-157 (1997).
18. Bradford, M.C.J., and Vannice, M.A., "Metal-support interactions during the CO_2 reforming of CH_4 over model TiOx/Pt catalysts," Catal. Lett. 48, 31-38 (1997).
19. Burch, R. and Petch, M.I., "Investigation of the synthesis of oxygenates from carbon monoxide/hydrogen mixtures on supported rhodium catalysts," Appl. Catal. A 88, 39-60 (1992).
20. Chang, J., Park, S., Yoo, J., and Park, J.-M., "Catalytic behaviour of supported KNiCa catalyst and mechanistic consideration for carbon dioxide reforming of methane", J. Catal. 195, 1 (2000).

21. Chang, J.-S., Park, S.-E., and Chon, H., "Catalytic activity and coke resistance in the carbon dioxide reforming of methane to synthesis gas over zeolite-supported Ni catalysts," Appl. Catal. A.145, 111-124 (1996).
22. Chang, Z., Wu, Q., Li, J., and Zhu, Q., "Effects of promoters and preparation procedures on reforming of methane with carbon dioxide over Ni/Al_2O_3 catalyst," 30, 147-155 (1996).
23. Chen, Y.G., and Ren, J., "Conversion of methane and carbon dioxide into synthesis gas over alumina-supported nickel catalysts-effect of $Ni-Al_2O_3$ interactions," Catal. Lett., 29, 39-48 (1994).
24. Chen, Y.G., Tomishige, K., Yokoyama, K., and Fujimoto, K., "Catalytic performance and catalyst structure of nickel–magnesia catalysts for CO_2 reforming of methane," J. Catal. 184, 479-490 (1999).
25. Choi, J.-S., Moon, K.-I., Kim, Y.G., Lee, J.S., Kim, C.-H., and Trimm, D.L., "Stable carbon dioxide reforming of methane over modified Ni/Al_2O_3 catalysts," Catal. Lett. 52, 43-47 (1998).
26. Choudhary, V.R., and Mamman, A.S., "Simultaneous oxidative conversion and CO_2 or steam reforming of methane to syngas over CoO-NiO-MgO catalyst," J. Chem. Technol. Biotechnol. 73, 345-350 (1998).
27. Choudhary, V.R., Updade, B.S., and Mamman, A.S., "Large enhancement in methane-to-syngas conversion activity of supported Ni catalysts due to precoating of catalyst supports with MgO, CaO or rare-earth oxide" Catal. Lett. 32, 387-390 (1995).
28. Chubb, T.A., "Characteristics of CO_2-CH_4 reforming-methanation cycle relevant to the solchem thermochemical power system," Solar Energy 24, 341-345 (1980).
29. Claridge, J.B., Green, M.L.H., and Tsang, S.C., "Methane conversion to synthesis gas by partial oxidation and dry reforming over rhenium catalysts," Catal. Today 21, 455-460 (1994).
30. Clark, E.L., Kallenberger, R.H., Browne, R.Y., and Phillips, J.R., "Synthesis gas production reaction of light hydrocarbons, steam, and carbon dioxide in commercial equipment", Chem. Eng. Progr. 45, 651-654 (1949).
31. Coq, B., Tichit, D., and Rihet, S., "Co/Ni/Mg/Al layered double hydroxides as precursors of catalysts for the hydrogenation of nitriles: hydrogenation of acetonitrile," J. Catal. 189,117-128 (2000).
32. Cornils, B., Herrmann, W.A., Schlogl, R., and Wong, C.H., "Catalysis from A to Z, second, completely revised and enlarged edition," WILEY-VCH Verlag GmbH & Co. KGaA, Weinheim (2003).
33. Delmon, B., Grange, P., Jacobs, A., and Poucelet, G., "Preparation of catalysts II," Studies in Surface and Catalysis, Volume II, Elsevier, Amsterdam (1979).
34. Delmon, B., Jacobs, A., and Poucelet, G., "Preparation of catalysts I," Studies in Surface and Catalysis, Volume I, Elsevier, Amsterdam (1976).
35. DIAS, J.A.C., and Assaf, J.M., "Influence of calcium content in $Ni/CaO/\gamma-Al_2O_3$ catalysts for CO_2-reforming of methane," Catal. Today 85, 59-68 (2003).
36. DOE, "Carbon dioxide emissions from the electric power in the United States", Washington, DC, (2000).
37. Dowden, D.A., Schnell, C.R., and Walker, G.T., "The design of complex catalysts," Fourth International Congress on Catalysis, Rice University, Houston, p. 1120-1131 (1968).
38. Efstathiou, A.M., Kladi, A., Tsipouriari, V.A., and Verykios, X.E., "Reforming of methane with carbon dioxide to synthesis gas over supported rhodium catalysts: II. A steady-state tracing analysis: mechanistic aspects of the carbon and oxygen reaction pathways to form CO," J. Catal.

158, 64-75 (1996).
39. Environment Canada, "Canada's GHG Inventory", Quebec (2004).
40. EPA, "Global Warming – Methane", http://www.epa.gov/methane/sources.html, (2006).
41. Erdohelyi, A., Cserenyi, J., and Solymosi, F., "Activation of CH_4 and Its Reaction with CO_2 over Supported Rh Catalysts," J. Catal. 141, 287-299 (1993).
42. Erdohelyi, A., Cserenyi, J., Papp, E., and Solymosi, F., "Catalytic reaction of methane with carbon dioxide over supported palladium," Appl. Catal. A 108, 205-219 (1994).
43. Erdohelyi, A., Fodor K., and Solymosi, F., "Decomposition of methane and its reaction with CO_2 over Rh/ZSM-5 catalyst," Stud. Surf. Sci. Catal. 107, 525-536 (1997).
44. Fei, J. Hou, Z., Zheng, X., and Yashima, T., "Doped Ni catalysts for methane reforming with CO_2," Catal. Lett. 98, 241-246 (2004).
45. Ferreira-Aparicio, P., Fernandez-Garcia, M., Guerrero-Ruiz, A., and Rodríguez-Ramos, I., "Evaluation of the role of the metal–support interfacial centers in the dry reforming of methane on alumina-supported rhodium catalysts," 190, 296-308 (2000).
46. Fischer, V.F., and Tropsch, H., "Die umwandlung von methan in wasserstoff und kohlenoxyd," Brennst.-Chem. 25, 39-46 (1928).
47. Fogler, H. Scott., "Elements of chemical reaction engineering," PRENTICE-HALL, Englewood Cliffs, New Jersey, p452-491 (1986).
48. Forni, L., "Mass transfer and heat transfer in catalytic reactions", Catal. Today 52, 147 (1999).
49. Fraenkel, D., Levitan, R., and Levy, M., "A solar thermochemical pipe based on the CO_2-CH_4 (1:1) system," Int. J. Hydrogen Energy 11, 267-277 (1986).
50. Gadalla, A.M. and Bower, B., "The role of catalyst support on the activity of nickel for reforming methane with CO_2," Chem. Eng. Sci. 43, 3049-3062 (1988).
51. Gadalla, A.M., and Sommer, M.E., "Synthesis and characterization of catalysts in the system Al_2O_3-MgO-NiO-Ni for methane reforming with CO_2," J. Am. Ceram. Soc. 72, 683-687 (1989).
52. Gaigneaux, E., De Vos, D.E., Grange P., Jacobs, P.A., Martens, J.A., Ruiz, P., and Poncelet, G., "Scientific bases for the preparation of heterogeneous catalysts," Processing of the 8th International Symposium, Louvain-la-Neuve, Belgium, September 9-12 (2002).
53. Gibson, D.H., "η2-coordination of CO_2 was found both experimentally and theoretically," Chem. Rev. 96, 2063 (1996).
54. Ginsburg, Jason M., Pina, J., El Solh, T., Lasa, Hugo, I. de, "Coke formation over nickel catalyst under methane dry reforming conditions: thermodynamic and kinetic models," Ind. Eng. Chem. Res., 44, 4846-4854 (2005).
55. Gronchi, P., Fumagalli, D., Rosso, R.D., Centola, P., "Carbon deposition in methane reforming with carbon dioxide," J. Thermal Anal. Cal. 47, 227-234 (1996).
56. Gustafso, B.L., and Walden, J.V., "Conversion of carbon dioxide to carbon monoxide," US Patent 5068057 (1991).
57. Guyot-Sionnest, N.S., Villain, F., Bazin, D., Dexpert, H., Le Peltier, F., Lynch, J., and Bournonville, J.P., "In situ high temperature and high pressure exafs studie of Pt/Al_2O_3 catalysts. Part I: Reduction and deactivation," Catalysis Letters 8, 283-295 (1991).
58. Hei, M., Chen, H., Yi, J., Lin, Y., Wei, G., and Liao, D., "CO_2-reforming of methane on transition metal surfaces," Surface Science 417, 82-96 (1998).
59. Hickman, D.A., and Schmidt, L.D., "Production of syngas by direct catalytic oxidation of methane," Science 259, 343-345 (1993).

60. Horiuchi, T., Sakuma, K., Fukui, T., Kubo, Y., Osaki, T., and Mori T., "Suppression of carbon deposition in the CO_2-reforming of CH_4 by adding basic metal oxides to a Ni/Al_2O_3 catalyst," Appl. Catal. A 144, 111-120 (1996).
61. Hou, Z., Yokota, O., Tanaka, T., and Yashima, T., "Investigation of CH_4 reforming with CO_2 on meso-porous Al_2O_3-supported Ni catalyst," Catal. Lett. 89, 121-127 (2003).
62. Hougen, K., Watson, R.A. Ragatz, Chemical Process Principles, Part 1, John Wiley&Sons, New York, 1954
63. Hu, Y. H., and Ruckenstein, E., "Catalytic conversion of methane to synthesis gas by partial oxidation and CO_2 reforming," Adv. Catal. 48, 297-345 (2004).
64. Hu, Y., and Ruckenstein, E., "Binary MgO-based solid solution catalysts for methane conversion t syngas", Catal. Rev. 44, 423 (2002).
65. Hu, Y.H., and Ruckenstein, E., "Transient response analysis via a broadened pulse combined with a step change or an isotopic pulse: application to CO_2 reforming of methane over NiO/SiO_2", J. Phys. Chem. B 101, 7563 (1997).
66. Hu. Y.H., and Ruckenstein E., "An optimum NiO content in the CO_2 reforming of CH_4 with NiO/MgO solid solution catalysts," Catal. Lett., 36, 145-149 (1996).
67. Hu. Y.H., and Ruckenstein E., "CH_4 TPR-MS of NiO/MgO solid solution catalysts," 13, 2055-58 (1997).
68. Hu. Y.H., and Ruckenstein E., "Temperature-programmed desorption of CO adsorbed on NiO/MgO," J. Catal. 163, 306-311 (1996).
69. Hu. Y.H., and Ruckenstein E., "The characterization of a highly effective NiO/MgO solid solution catalyst in the CO_2 reforming of CH_4," 43, 71-77 (1997).
70. Huang, T.J., Li, H.J, and Yu, T.C., "A comparison of oxygen-vacancy effect on activity behaviors of carbon dioxide and steam reforming of methane over supported nickel catalysts," Catal. Lett. 105, 239-247 (2005).
71. I.S. Metclfe, S. Sundaresan, AIChE J. 34, 195 (1988).
72. IUPAC Compendium of Chemical Terminology, 2nd Edition (1997).
73. Ji, L., Tang, S., Zeng, H.C., Lin, J., and Tan, K.L., "CO_2 reforming of methane to synthesis gas over sol–gel-made Co/γ-Al_2O_3 catalysts from organometallic precursors," Appl. Catal. A 207, 247-255 (2001).
74. Jolivet, J.-P., Henry, M. and Livage, Jacques, "Metal oxide chemistry and synthesis," JOHN WILEY & SONS, LTD, Toronto (1994) p.3-52.
75. Kang, J.K., and Rhee, S., "Chemical vapor deposition of nickel oxide films from $Ni(C_5H_5)_2/O_2$," Thin Solid Films 391, 57-61 (2001).
76. Kim, D.K., Stöwe, K., Müller F., and Maier, W.F., "Mechanistic study of the unusual catalytic properties of a new Ni-Ce mixed oxide for the CO_2 reforming of methane," J. Catal. 247, 101-111 (2007).
77. Kim, G.J., Cho, D.S., Kim, K.H., and Kim, J.H., "The reaction of CO_2 with CH_4 to synthesize H_2 and CO over nickel-loaded Y-zeolites," Catal. Lett., 28, 41-52 (1994).
78. Kroll, V.C.H., Swaan, H.M., and Mirodatos, C., "Methane reforming reaction with carbon dioxide over Ni/SiO_2 catalyst: II. A nechanistic study," J. Catal. 164, 387-398 (1996).
79. Kroll, V.C.H., Swaan, H.M., and Mirodatos, C., "Methane reforming reaction with carbon dioxide over Ni/SiO_2 catalyst: I. deactivation studies," J. Catal. 161, 409-422 (1996).
80. Kroll, V.C.H., Tjatjopoulos, G.J., Mirodatos, C., "Kinetics of methane reforming over Ni/SiO_2

catalysts based on a stepwise mechanistic model", Stud. Surf. Sci. Catal. 119, 753 (1998).

81. Kyle, B.G., "Chemical and process thermodynamics, third edition", Prentice Hall PTR, New Jersey, 1999, p433-511.
82. Lemonidou, A.A., and Vasalos, I., "Carbon dioxide reforming of methane over 5 wt.% Ni/CaO-Al_2O_3 catalyst", Appl. Catal. A 228, 227 (2002).
83. Levy, M., Levitan, R., Meirovitvh, E., Segal, A., Rosin, H., and Rubin, R., "Chemical reactions in a solar furnace 2: Direct heating of a vertical reactor in an insulated receiver. Experiments and computer simulations," Sol. Energy 48, 395-402 (1992).
84. Lewis, W.K., Gilliland, E.R., and Reed, W.A., "Reaction of methane with copper oxide in a fluidized bed," Ind. Eng. Chem., 41, 1227-37 (1949).
85. Li, C., Fu, S., Zhang, H., and Xin, Q., "An infrared spectroscopic study on the lewis base properties of metal oxides by using a novel probe molecule: boric acid trimethyl ester", J. Chem. Soc. Chem. Commun. 17, 18 (1994).
86. Liu, B.S., and Au, C.T., "Carbon deposition and catalyst stability over La_2NiO_4/γ-Al_2O_3 during CO_2 reforming of methane to syngas," Appl. Catal. A. 244, 181-195 (2003).
87. Marco, J.F., Gancedo, J.Ramon, Gracia, M., and Gantier, J.L., "Cation distribution and magnetic structure of the ferromagnetic spinel $NiCo_2O_4$," J. Mater. Chem. 11 3087-3093 (2001)
88. Mark, M.F., and Maier W.F., "Active surface carbon – a reactive intermediate in the production of synthesis gas from methane and carbon dioxide," Angew. Chem. Inst. Ed. Engl. 33, 1657-1660 (1994).
89. Mark, M.F., and Maier W.F., "CO_2-reforming of methane on supported Rh and Ir catalysts," J. Catal. 164, 122-130 (1996).
90. Masai, M., Kado, H., Miyake, A., Nishiyama, S., and Tsuruya, S., "Methane conversion" Elsevier, Amsterdam (1988) p.76.
91. McCrary, J.H., and McCrary, G.E., "An experimental study of the CO_2-CH_4 reforming-methanation cycle as a mechanism for converting and transporting solar energy," Solar Energy 29, 141-151 (1982).
92. Menad, S., Ferreira-Aparicio, P., Cherifi, O., Guerrero-Ruiz, A., and Rodríguez-Ramos, I., "Designing new high oxygen mobility supports to improve the stability of Ru catalysts under dry reforming of methane," Catal. Lett. 89, 63-67 (2003).
93. Metclfe, I.S., Sundaresan, S., "***AIChE J***. 34 (1988) 195
94. Nagaoka, K., Seshan, K., Lercher, J., and Aika, K., "Activation mechanism of methane-derived coke (CHx) by CO_2 during dry reforming of methane – comparison for Pt/Al_2O_3 and Pt/ZrO_2," Catal. Lett. 70,109-116 (2000).
95. Nakamura, J., Aikawa, K., Sato, K., and Uchijima, T., "Role of support in reforming of CH_4 with CO_2 over Rh catalysts," Catal. Lett. 25, 265-270 (1994).
96. Nandini, A., Pant, K.K., and Dhingra, S.C., "Kinetic study of the catalytic carbon dioxide reforming of methane to synthesis gas over Ni-K/CeO_2-Al_2O_3", Appl. Catal. A 308, 119 (2006).
97. Noronha, F.B., Shamsi, A., Taylor, C., Fendley, E.C., Stagg-Williams, S., and Resasco, D.E., "Catalytic performance of Pt/ZrO_2 and Pt/Ce-ZrO_2 catalysts on CO_2 reforming of CH4 coupled with steam reforming or under high pressure," Catal. Lett. 90, 13-21 (2003).
98. Olsbye, U., Wurzel, T., and Mleczko, L., "Kinetic and reaction engineering studies of dry reforming of methane over a Ni/La/Al_2O_3 catalyst", Ind. Eng. Chem. Res. 36, 5180 (1997).
99. Osaki T., and Mori, T., "Role of potassium in carbon-free CO_2 reforming of methane on K-

promoted Ni/Al_2O_3 catalysts," J. Catal. 204, 89-97 (2001).

100. Osaki, T., "Effect of reduction temperature on the CO_2-reforming of methane over TiO_2-supported Ni catalyst," 93, 643-647 (1997).
101. Osaki, T., Horiuchi, T., Suzuki, K., and Mori T., "Kinetics, intermediates and mechanism for the CO2-reforming of methane on supported nickel catalysts," J. Chem. Soc., Faraday Trans. 92, 1627-31 (1996).
102. Osaki, T., Horiuchi, T., Suzuki, K., and Mori, T., "Catalyst performance of MoS_2 and WS_2 for the CO_2-reforming of CH_4 -suppression of carbon deposition," Appl. Catal. 155, 229 (1997).
103. Osaki, T., Masuda, H., and Mori, T., "Intermediate hydrocarbon species for the CO_2-CH_4 reaction on supported Ni catalysts," Catal. Lett. 29, 33-37 (1994).
104. Osaki, T., Masuda, H., Horiuchi, T., and Mori, T., "Highly hydrogen-deficient hydrocarbon species for the CO_2-reforming of CH4 on Co/Al_2O_3 catalyst," Catal. Lett. 34, 59-63 (1995).
105. Ostrupnielsen, J.R., and Hansen, J.H.B., "CO_2-Reforming of Methane over Transition Metals," J. Catal. 144, 38-49 (1993).
106. Pena, M.A., Gomez, J.P., and Fierro, J.L.G., "New catalytic routes for syngas and hydrogen production", Appl. Catal. A 144, 7-57 (1996).
107. Perry, R.H., and Green, R.W., "Physical and chemical data," Perry's Chemical Engineers' Handbook, 7th edition, Section 2 (1997).
108. Petrov, K., and Will, G., "A new cobalt-nickel oxide spinel prepared under high pressure in an oxygen atmosphere," J. Materials Sci. Lett. 6, 1153-1155 (1987).
109. Ponec,V., and Bond, G.C., "Catalysis by metals and alloys," Elsevier, Amsterdam, 1995.
110. Portugal, U. L., Santos, A., Damyanova, S., Marques,C., and Bueno, J., "CO_2 reforming of CH_4 over Rh-containing catalysts, " J. Mol. Catal. 184, 311 (2002).
111. Potdar, P.S., Roh, H.S., Jun, K.W., Ji, M., and Liu, Z.W., "Carbon dioxide reforming of methane over Co-precipitated Ni-Ce-ZrO_2 catalysts," Catal. Lett. 84, 95-100 (2002).
112. Qin, D., and Lapszewicz, J., "Study of mixed steam and CO_2 reforming of CH_4 to syngas on MgO-supported metals," Catal. Today 21, 551-560 (1994).
113. Qin, D., Lapszewicz, J., and Jiang, X., "Comparison of partial oxidation and steam-CO_2 mixed reforming of CH_4 to syngas on MgO-supported metals," J. Catal. 159, 140-149 (1996).
114. Quincoces, C.E., Dicundo, S., Alvarez, A.M., and Gonzalez, M.G., "Effect of addition of CaO on Ni/Al_2O_3 catalysts over CO_2 reforming of methane," Mater. Lett. 50, 21-27 (2001).
115. Quincoces, C.E., Vargas, S.P.D., Grange, P., and Gonzales, M.G., "Role of Mo in CO_2 reforming of CH_4 over Mo promoted Ni/Al_2O_3 catalysts," Mater. Lett. 56 698-704 (2002).
116. Rasko, J., and Solymosi, F., "Reactions of adsorbed CH_3 species with CO_2 on Rh/SiO_2 catalyst," Catal. Lett. 46, 153-7 (1997).
117. Reitmeier, R., Atwood, K., Bennet, H., and Baugh, H., "Production of synthesis gas by reacting light hydrocarbons with steam and carbon dioxide," Ind. And Eng. Chem.40, 620-626 (1948).
118. Ribet, S., Tichit, D., Coq, B., Ducourant, B., and Morato, F., "Synthesis and activation of Co–Mg–Al layered double hydroxides," J. Solid. State Chem. 142, 382-392 (1999).
119. Richardson, B., Turk, B., and Twigg, M.V., Appl. Catal. A 148, 97 (1996).Aparicio, L.M., "Transient Isotopic Studies and Microkinetic Modeling of Methane Reforming over Nickel Catalysts," J. Catal. 165, 262-274 (1997).
120. Richardson, J.T. and Paripatyadar, S.A., "CO_2 reforming of CH_4 with supported Rh", Appl. Catal. 61, 293-309 (1990).

121. Richardson, J.T., "Principles of catalyst development," Plenum Press, New York (1989) p.28-31
122. Richardson, J.T., "Principles of catalyst development." Plenum Press, New York and London (1982) p. 135-183.
123. Richardson, J.T., Garrait, M., and Hung, J. –K., "Carbon dioxide reforming with Rh and Pt–Re catalysts dispersed on ceramic foam supports," Appl. Catal. A 255, 69-82 (2003).
124. Rihkowski, J.M., Paryjczak, T., Lenik, M., Farbotko, M., and Goralski, J., **"**Temperature-programmed reduction of alumina-supported Ni–Pt systems," J. Chem. Soc., Faraday Trans. 91, 3481-3484 (1995).
125. Roh, H.S., Jun, K.W., Baek, S.C., and Park, S.E., "A highly active and stable catalyst for carbon dioxide reforming of methane: Ni/Ce–ZrO2/θ-Al2O3," Catal. Lett. 81, 147-151 (2002).
126. Roh, H.S., Koo, K.Y., Jeong, J.H., Seo, Y.T., Seo, D.J., Seo, Y.S., Yoon, W.L., and Park, S.B., "Combined reforming of methane over supported Ni catalysts," Catal. Lett. April (2007).
127. Rostrup-Nielsen, J.R. "Industrial relevance of coking,"Catal. Today 37, 225 (1997).
128. Rostrup-Nielsen, J.R., and Hansen, J.H., "CO_2-reforming of methane over transition metals," J. Catal. 144, 38-49 (1993).
129. Ruckenstein E., and Hu. Y.H., "Carbon dioxide reforming of methane over nickel/alkaline earth metal oxide catalysts," Appl. Catal. 133, 149-161 (1995).
130. Ruckenstein E., and Hu. Y.H., "Role of Support in CO2 reforming of CH_4 to syngas over Ni catalysts," J. Catal. 162, 230-238 (1996).
131. Ruckenstein E., and Hu. Y.H., "The effect of precursor and preparation conditions of MgO on the CO_2 reforming of CH_4 over NiO/MgO catalysts," 154, 185-205 (1997).
132. Rudnitskii, L.A., Solboleva, T.N., and Alekseev, A.M., "Hysteresis of thermogravimetric curves of nickel catalysts for methane conversion in CH_4+CO_2 mixture," React. Kinet. Catal. Lett. 26, 149-151 (1984).
133. Sakai, Y., Saito, H., Sodesawa, T., and Nozaki, F, "Catalytic reactions of hydrocarbon with carbon dioxide over metallic catalysts," React. Kinet. Catal. Lett. 24, 253-257 (1984).
134. Schuurman, Y., Marquez-Alvarez. C., Kroll, V.C.H., and Mirodatos, C., "Unraveling mechanistic features for the methane reforming by carbon dioxide over different metals and supports by TAP experiments," Catal. Today 46, 185-192 (1998).
135. Schuurman, Y., Mirodatos, C., Ferreira-Aparicio, P., Rodríguez-Ramos, I., and Guerrero-Ruiz, A., "Bifunctional pathways in the carbon dioxide reforming of methane over MgO-promoted Ru/C catalysts," Catal. Lett. 66, 33-37 (2000).
136. Seok, S., Han, S., and Lee, J., "The role of MnO in Ni/MnO-Al_2O_3 catalysts for carbon dioxide reforming of methane," Appl. Catal. A 215, 31-38 (2001).
137. Seok, S.H., Choi, S.H., Park, E.D., Han, S.H., and Lee, J.S., "Mn-Promoted Ni/Al_2O_3 Catalysts for Stable Carbon Dioxide Reforming of Methane," J. Catal. 209, 6-15 (2002).
138. Seok, S.H., Choi, S.H., Park, E.D., Han, S.H., and Lee, J.S., "Mn-promoted Ni/Al_2O_3 catalysts for stable carbon dioxide reforming of methane," J. Catal. 209, 6-15 (2002).
139. Seshan, K., Barge, H.W., Hally, W., Keulen, A.N.J., Ross, J.R.H., "Natural gas conversion" Elsevier, Amsterdam (1994) p.285
140. Sinfelt, J.H. "Bimetallic catalysts: discovery, concepts and applications," Wily, New York, 1983.
141. Slagtern, A., Olsbye, U., Blom, R., and Dahl, I.M., "Characterization of Ni on La modified Al_2O_3 catalysts during CO_2 reforming of methane," Appl. Catal. 165, 379-390 (1997).
142. Slagtern, A., Olsbye, U., Blom, R., and Dahl, I.M., Stud. Surf. Sci. Catal. 107, 497 (1997).

143. Solymosi, F., "The bonding, structure and reactions of CO_2 adsorbed on clean and promoted metal surfaces," J. Mol. Catl., 65, 337-358 (1991).
144. Solymosi, F., Kustan, G., and Erdohelyi, A., "Catalytic reaction of CH_4 with CO_2 over alumina-supported Pt metals," Catal. Lett. 11, 149-156 (1991).
145. Somorjai, G.A., "Introduction to surface chemistry and catalysis," Wiley-Interscience, New York (1994).
146. Souza, M.M.V.M., Aranda, D.A.G., and Schmal, M., "Reforming of methane with carbon dioxide over $Pt/ZrO_2/Al_2O_3$ catalysts," J. Catal. 204, 498-511 (2001).
147. Swaan, H.M., Kroll, V.C.H., Martin, G.A., and Mirodatos, C., "Deactivation of supported nickel catalysts during the reforming of methane by carbon dioxide," Catal. Today 21, 571-578 (1994).
148. Takanabe, K., Nagaoka, K., Nariai, K., and Aika, K.I, "Titania-supported cobalt and nickel bimetallic catalysts for carbon dioxide reforming of methane," J. Catal. 232, 268-275 (2005).
149. Takano, A., Tagawa, T., and Goto, S., "Carbon dioxide reforming of methane on supported nickel catalysts," J. Chem. Eng. Japan 27, 727-731 (1994).
150. Takayasu, O., Hirose, E., Matsuda, N., and Matsuua, I., Chemistry Express 6, 447-450 (1991).
151. Takayasu, O., Hongo, N., and Masuura, "Noble metal promoted $Ni_{0.03}Mg_{0.97}O$ solid solution catalysts for the reforming of CH_4 with CO_2," Stud. Surf. Sci. Catal. 77, 305-309 (1993).
152. Tang, S., Ji, L., Lin, J., Zeng, H.C., Tan, K.L., and Li, K., "CO_2 reforming of methane to synthesis gas over sol–gel-made $Ni/\gamma\text{-}Al_2O_3$ catalysts from organometallic precursors," J. Catal. 194, 424-430 (2000).
153. Tang, S.B., Qiu, F.L., and Lu, S.J., "Effect of supports on the carbon deposition of nickel catalysts for methane reforming with CO_2," Catal. Today 24, 253-255 (1995).
154. Teuner, S.C.; Neumann, P.; Linde, F.V., "The CALCOR standard and CALCOR economy processes", Oil Gas European Magazine 3, 44 (2001).
155. Thomas, J.M., and Thomas, W.J., "Introduction to the principles of heterogeneous catalysis," Academic Press, London and New York (1967) p.14-66.
156. Tichit, D., Medina, F., Coq, B., and Dutartre, R., "Activation under oxidizing and reducing atmospheres of Ni-containing layered double hydroxides," Appl. Catal. A 159, 241-258 (1997).
157. Tokunaga, O., and Ogasawara, S., "Reduction of carbon dioxide with methane over Ni-catalyst" React. Kinet. Catal. Lett. 39, 69-74 (1989).
158. Tokunaga, O.; Osada, Y.; Ogasawara, S., "Reaction of CO_2/CH_4 as a high-level heat transport system", Fuel 68, 990-994 (1989).
159. Tomishige, K., Himeno,Y., Matsuo, Y., Yoshinaga, Y., and Fujimoto, K., "Catalytic performance and carbon deposition behavior of a NiO-MgO solid solution in methane reforming with carbon dioxide under pressurized conditions," Ind. Eng. Chem. Res. 39,1891-1897 (2000).
160. Tomishige, K., Kanazawa, S., Sato, M., Ikushima, K., and Kunimori, K., "Catalyst design of Pt-Modified Ni/Al_2O_3 catalyst with flat temperature profile in methane reforming with CO_2 and O_2," Catal. Lett. 84, 69-74 (2002).
161. Trimm, D., "Design of industrial catalysts," Elsevier, New York, 1980
162. Trimm, D.L., "Coke formation and minimisation during steam reforming reactions," Catal. Today 37, 233-238 (1997).
163. Tsipopuriari, V.A., Efstathiou, A.M., Zhang, Z., and Verykios, X.E., "Reforming of methane with carbon dioxide to synthesis gas over supported Rh catalysts," Catal. Today 21, 579-587 (1994).

164. Tsipouriari, V.A., and Verykios, X.E., "Carbon and oxygen reaction pathways of CO_2 reforming of methane over Ni/La_2O_3 and Ni/Al_2O_3 catalysts studied by isotopic tracing techniques," J. Catal. 187, 85-94 (1999).
165. Tsipouriari, V.A., and Verykios, X.E., "Kinetic study of the catalytic reforming of methane with carbon dioxide to synthesis gas over Ni/La_2O_3 catalyst," Catal. Today 64, 83-90 (2001).
166. Tsipouriari, V.A., and Verykios, X.E., "Kinetic study of the catalytic reforming of methane with carbon dioxide to synthesis gas over Ni/La_2O_3 catalyst," Catal. Today 64, 83-90 (2001).
167. Tsyganok, A., Suzuki, K., Hamakawa, S., Takehira, K., and Hayakawa, T., "Mg–Al layered double hydroxide intercalated with [Ni(edta)]2− chelate as a precursor for an efficient catalyst of methane reforming with carbon dioxide," Catal. Lett. 77, 75-86 (2001).
168. Tsyganok, A.I., Tsunoda, T., Hamakawa, S., Suzuki, K., Takehira, K., and Hayakawa, T., "Dry reforming of methane over catalysts derived from nickel-containing Mg–Al layered double hydroxides," J. Catal. 213, 191-203 (2003).
169. Twigg, M.V., "Catalyst handbook, second edition," Wolfe Publishing Ltd, London (1989), p34-48.
170. Udengaard, N.R.; Hansen, J.-H. B.; Hanson, D. C.; Stal, J. A., "Sulfur passivated reforming process lowers syngas H_2/CO ratio", Oil & Gas Journal, 90, 62 (1992).
171. Vernon, P.D.F., Green, M.L.H., Cheetham, A.K., and Ashcroft A.T., "Partial oxidation of methane to synthesis gas, and carbon dioxide as an oxidising agent for methane conversion," Catal. Today 13, 417-426 (1992).
172. Wachtman, John B., and Kalman, Zwi H., "Characterization of materials," Butterworth-Heinemann, Manning (1992) p.145-461.
173. Walter, K., Buyevskaya, O., Wolf, D., and Baerns, M., "Rhodium-catalyzed partial oxidation of methane to CO and H_2. In situ DRIFTS studies on surface intermediates," Catal. Lett. 29, 261-270 (1994).
174. Wang, H.Y., and Au, C.T., "CH_4/CD_4 isotope effects in the carbon dioxide reforming of methane to syngas over SiO_2 spported nickel catalysts", Catal. Lett. 38, 77 (1996).
175. Wang, J.B., Kuo, L.-E., and Huang, T.-J., "Study of carbon dioxide reforming of methane over bimetallic Ni-Cr/yttria-doped ceria catalysts," Appl. Catal. A 249, 93-105 (2003).
176. Wang, S., and Lu, G.Q., "A comprehensive study on carbon dioxide reforming of methane over $Ni/\gamma\text{-}Al_2O_3$", Ind. Eng. Chem. Res. 38, 2615 (1999).
177. Wang, S., and Lu, G.Q., "Reaction kinetics and deactivation of Ni-based catalysts in CO_2 reforming of methane", React. Eng. Pollut. Prev 75 (2000).
178. Wang, S., and Lu, G.Q., Carbon dioxide reforming of methane to produce synthesis gas over metal-supported catalysts: state of the art," Energy & Fuel, 10, 896-904 (1996).
179. Wang, S., and Lu, G.Q.M., "CO_2 reforming of methane on Ni catalysts: Effects of the support phase and preparation technique," Appl. Catal. B 16, 269-277 (1998).
180. Webb. Paul A., Orr, C., Camp, Ronnie, W., Olivier James P., and Yunes, Y. Simon, "Analytical methods in fine particles technology," Micromeritics Instrument Corporation, Norcross, GA, USA (1997) p.219-268.
181. Wei, J.-M., Xu, B.-Q., Li, J.-L., Cheng, Z.-X., and Zhu, Q.-M., "Ultra stable Ni/ZrO_2 catalyst for carbon dioxide reforming of methane," Appl. Catal. A 196 L167-169 (2000).
182. Wijngaarden R.J., Kronberg, A., and Westerterp, K.R., "Industrial catalysis – optimizing catalysts and processes," WILEY-VCH Verlag GmbH, D-69496 Weinheim, (1998), p.25-59.
183. Worley, J., and Kvech, S., "ICP-MS," Web Source:

http://www.cee.vt.edu/ewr/environmental/teach/smprimer/icpms/icpms.htm

184. Worner, A., and Tamme, R., "CO_2 reforming of methane in a solar driven volumetric receiver–reactor", Catal. Today 46, 165 (1998).

185. Yamazaki, O., Nozaki, T., Omata, K., and Fujimoto, K., "Reduction of carbon dioxide by methane with Ni-on-MgO-CaO containing catalysts," 21, 1953-1954 (1992).

186. Yan, Q.G., Weng, W.Z., Wan, H.L., Toghiani, H., Toghiani, R.K., and Pittman, C.U., "Activation of methane to syngas over a Ni/TiO_2 catalyst," Appl. Catal. A 239, 43-58 (2003).

187. Zachariasen, William H., "Theory of X-ray diffraction in crystals," Chapman & Hall, New York; J. Wiley; London (1945) p. 1-69.

188. Zhang , X., Lee, C., D. Mingos, M.P., and Hayward, D.O., "Carbon dioxide reforming of methane with Pt catalysts using microwave dielectric heating," Catal. Lett. 88, 129-139 (2003).

189. Zhang, H. B., Chen, P., Lin, G.-D., and Tsai,K.-R., "Development of coking-resistant Ni-based catalyst for partial oxidation and CO_2-reforming of methane to syngas," Appl. Catal. A 166, 343-350 (1998).

190. Zhang, J., Wang, H., and Dalai, A.K., "Effects of metal content on activity and stability of Ni-Co bimetallic catalysts for CO_2 reforming of CH_4", Appl. Catal. A. in press (2008).

191. Zhang, J., Wang, H., and Dalai, A.K., "The development of Ni-Co bimetallic catalyst for CO_2 reforming of CH_4", J. Catal. 249, 300 (2007).

192. Zhang, Z.; and Verkios, X.E., "Mechanistic aspects of carbon dioxide reforming of methane to synthesis gas over Ni catalysts", Catal. Today 21, 589 (1994).

193. Zhang, Z.L., and Verykios, X.E., "A stable and active nickel-based catalyst for carbon dioxide reforming of methane to synthesis gas," J. Chem. Soc. Chem. Commun. 71-72 (1994).

194. Zhang, Z.L., and Verykios, X.E., "Comparative study of carbon dioxide reforming of methane to synthesis gas over Ni/La_2O_3 and conventional nickel-based catalysts," J. Phys. Chem. 100, 744-754 (1996).

APPENDIX A: CALIBRATION OF MASS FLOW CONTROLLERS

A: N_2 mass flow controller (setpoint vs measurement at STP)

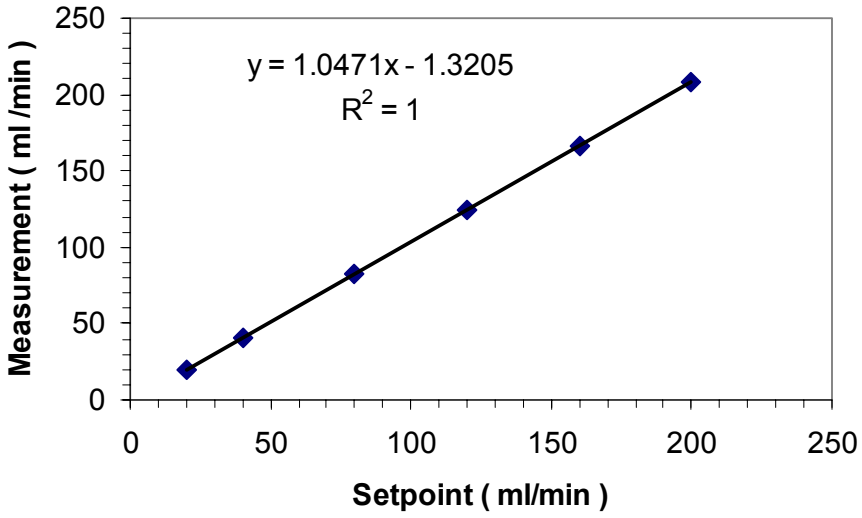

B: CH_4 mass flow controller (setpoint vs measurement at STP)

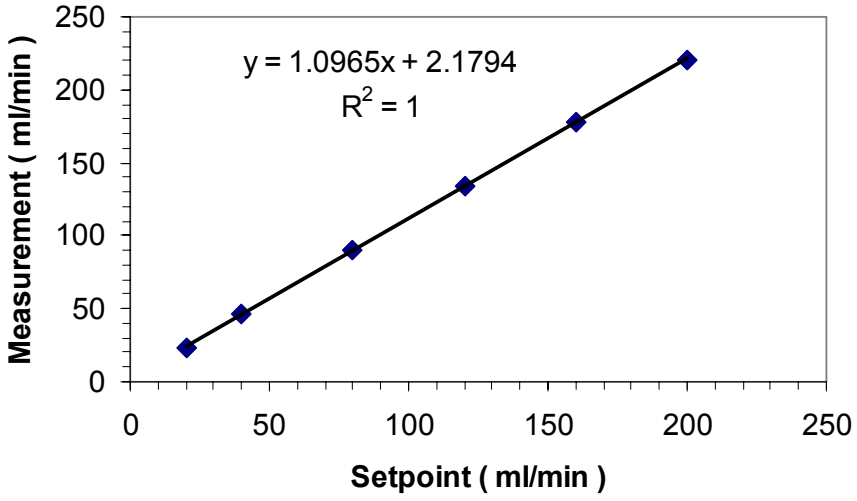

C: CO_2 mass flow controller (setpoint vs measurement at STP)

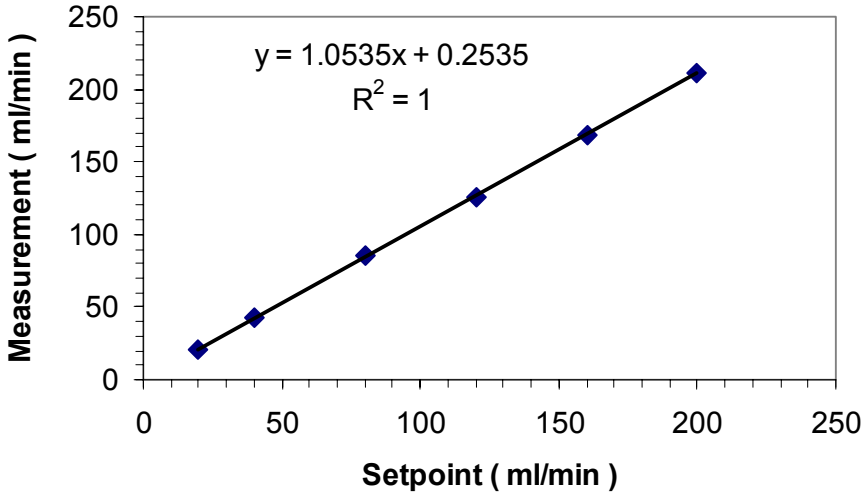

APPENDIX B: CALIBRATION OF GAS CHROMATOGRAPHY

```
======================================================================
                          Calibration Table
======================================================================


Calib. Data Modified  :      Saturday, June 14, 2008 8:18:44 PM

Calculate             :      Normalized Percent
Based on              :      Peak Area

Rel. Reference Window :      5.000 %
Abs. Reference Window :      0.000 min
Rel. Non-ref. Window  :      5.000 %
Abs. Non-ref. Window  :      0.000 min
Use Multiplier & Dilution Factor with ISTDs
Uncalibrated Peaks    :      not reported
Partial Calibration   :      No recalibration if peaks missing

Curve Type            :      Linear
Origin                :      Forced
Weight                :      Linear (Amnt)

Recalibration Settings:
Average Response      :      Average all calibrations
Average Retention Time:      Floating Average New 75%

Calibration Report Options :
    Printout of recalibrations within a sequence:
        Calibration Table after Recalibration
        Normal Report after Recalibration
    If the sequence is done with bracketing:
        Results of first cycle (ending previous bracket)

Signal 1: TCD1 A,

RetTime   Lvl   Amount      Area     Amt/Area  Ref Grp Name
 [min] Sig      [mol%]
-------|--|--|----------|----------|----------|---|--|---------------
  2.421  1 14   22.95000   13.35100    1.71897        H2
           13   25.02000   14.72100    1.69961
           12   26.95000   15.92800    1.69199
           11   28.61000   17.75700    1.61120
           10   30.27000   18.00800    1.68092
            9   31.95000   20.03600    1.59463
            7   34.32000   21.74400    1.57837
            6   34.99000   21.87700    1.59940
            5   36.21000   22.84300    1.58517
            4   37.55000   23.82700    1.57594
            3   38.61000   24.65400    1.56607
  2.790  1  3   20.35000  782.98300 2.59903e-2        N2
            4   20.83000  818.63400 2.54448e-2
            5   21.20000  830.47600 2.55275e-2
            6   21.92000  830.19200 2.64035e-2
            7   22.42000  872.38000 2.56998e-2
            9   22.73000  866.56400 2.62300e-2
           10   23.23000  873.20300 2.66032e-2
           11   23.49000  896.55200 2.62004e-2
           12   24.20000  924.27000 2.61828e-2
           13   25.06000  924.76300 2.70988e-2
           14   25.73000  946.17300 2.71938e-2
  3.188  1 14   23.43000  913.99000 2.56349e-2        CO
           13   25.32000  992.75000 2.55049e-2
           12   27.17000 1096.20000 2.47856e-2
           11   28.94000 1191.07000 2.42975e-2
           10   30.43000 1210.92200 2.51296e-2
```

RetTime [min]	Sig	Lvl	Amount [mol%]	Area	Amt/Area	Ref	Grp	Name
		9	32.04000	1295.40000	2.47337e-2			
		7	33.92000	1398.35000	2.42572e-2			
		6	34.99000	1402.00000	2.49572e-2			
		5	36.37000	1498.20000	2.42758e-2			
		4	37.78000	1516.96000	2.49051e-2			
		3	38.65000	1555.62300	2.48454e-2			
3.998	1	3	1.26000	35.47800	3.55150e-2			CH4
		4	1.99000	52.98900	3.75550e-2			
		5	3.22000	89.76300	3.58722e-2			
		6	3.89000	108.00600	3.60165e-2			
		7	4.45000	131.64900	3.38020e-2			
		9	6.71000	193.35900	3.47023e-2			
		10	8.11000	229.16100	3.53900e-2			
		11	9.47000	276.92700	3.41967e-2			
		12	10.80400	314.01000	3.44065e-2			
		13	12.26000	350.13000	3.50156e-2			
		14	13.43000	408.24000	3.28973e-2			
9.952	1	3	1.14000	54.84300	2.07866e-2			CO2
		4	1.84000	81.42600	2.25972e-2			
		5	3.00000	137.34000	2.18436e-2			
		6	4.21000	191.43600	2.19917e-2			
		7	4.89000	230.01900	2.12591e-2			
		9	6.57000	305.28000	2.15212e-2			
		10	7.95000	359.58000	2.21091e-2			
		11	9.49000	445.62000	2.12962e-2			
		12	10.88000	503.04000	2.16285e-2			
		13	12.34000	560.79000	2.20047e-2			
		14	13.45000	614.73000	2.18795e-2			

Peak Sum Table

No Entries in table

Calibration Curves

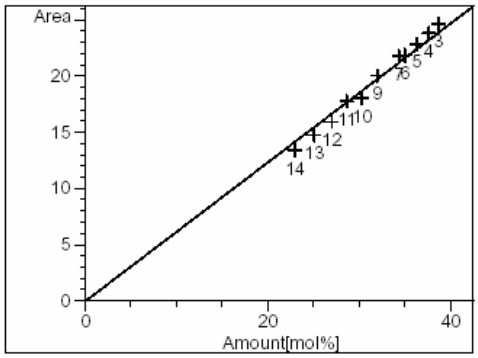

H2 at exp. RT: 2.421
TCD1 A,
Correlation: 0.99950
Residual Std. Dev.: 0.62642
Formula: y = mx
m: 6.18099e-1
x: Amount[mol%]
y: Area
Calibration Level Weights:
Level 14 : 1
Level 13 : 0.917266
Level 12 : 0.851577
Level 11 : 0.802167
Level 10 : 0.758176
Level 9 : 0.71831
Level 7 : 0.668706
Level 6 : 0.655902
Level 5 : 0.633803
Level 4 : 0.611185
Level 3 : 0.594406

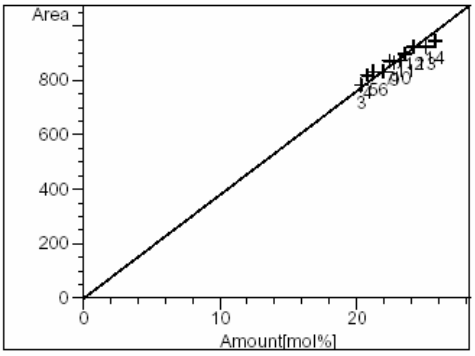

N2 at exp. RT: 2.790
TCD1 A,
Correlation: 0.99978
Residual Std. Dev.: 19.40349
Formula: y = mx
m: 38.08803
x: Amount[mol%]
y: Area
Calibration Level Weights:
Level 3 : 1
Level 4 : 0.976956
Level 5 : 0.959906
Level 6 : 0.928376
Level 7 : 0.907672
Level 9 : 0.895293
Level 10 : 0.876022
Level 11 : 0.866326
Level 12 : 0.840909
Level 13 : 0.812051
Level 14 : 0.790906

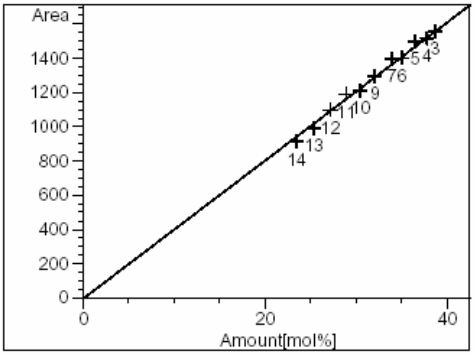

CO at exp. RT: 3.188
TCD1 A,
Correlation: 0.99986
Residual Std. Dev.: 21.61546
Formula: y = mx
m: 40.31476
x: Amount[mol%]
y: Area
Calibration Level Weights:
Level 14 : 1
Level 13 : 0.925355
Level 12 : 0.862348
Level 11 : 0.809606
Level 10 : 0.769964
Level 9 : 0.731273
Level 7 : 0.690743
Level 6 : 0.66962
Level 5 : 0.644212
Level 4 : 0.620169
Level 3 : 0.60621

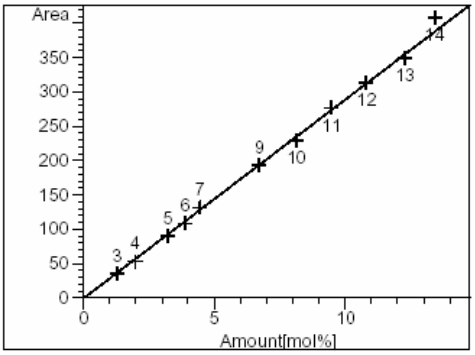

CH4 at exp. RT: 3.998
TCD1 A,
Correlation: 0.99955
Residual Std. Dev.: 7.07704
Formula: y = mx
m: 28.96674
x: Amount[mol%]
y: Area
Calibration Level Weights:
Level 3 : 1
Level 4 : 0.633166
Level 5 : 0.391304
Level 6 : 0.323907
Level 7 : 0.283146
Level 9 : 0.187779
Level 10 : 0.155364
Level 11 : 0.133052
Level 12 : 0.116623
Level 13 : 0.102773
Level 14 : 0.09382

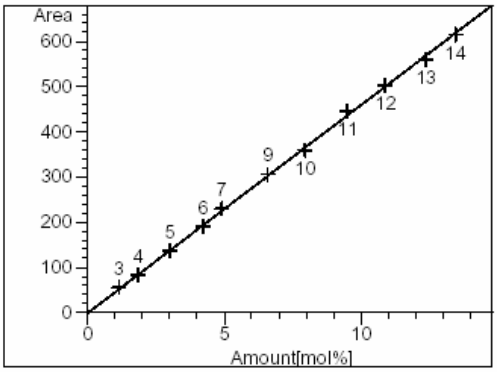


```
CO2 at exp. RT: 9.952
TCD1 A,
Correlation:                0.99988
Residual Std. Dev.:         4.94895
Formula: y = mx
      m:      45.98870
      x: Amount[mol%]
      y: Area
Calibration Level Weights:
    Level 3     : 1
    Level 4     : 0.619565
    Level 5     : 0.38
    Level 6     : 0.270784
    Level 7     : 0.233129
    Level 9     : 0.173516
    Level 10    : 0.143396
    Level 11    : 0.120126
    Level 12    : 0.104779
    Level 13    : 0.092382
    Level 14    : 0.084758
```

==========

APPENDIX C: TEMPERATURE PROFILE OF REACTOR

1) Reactor temperature measurement

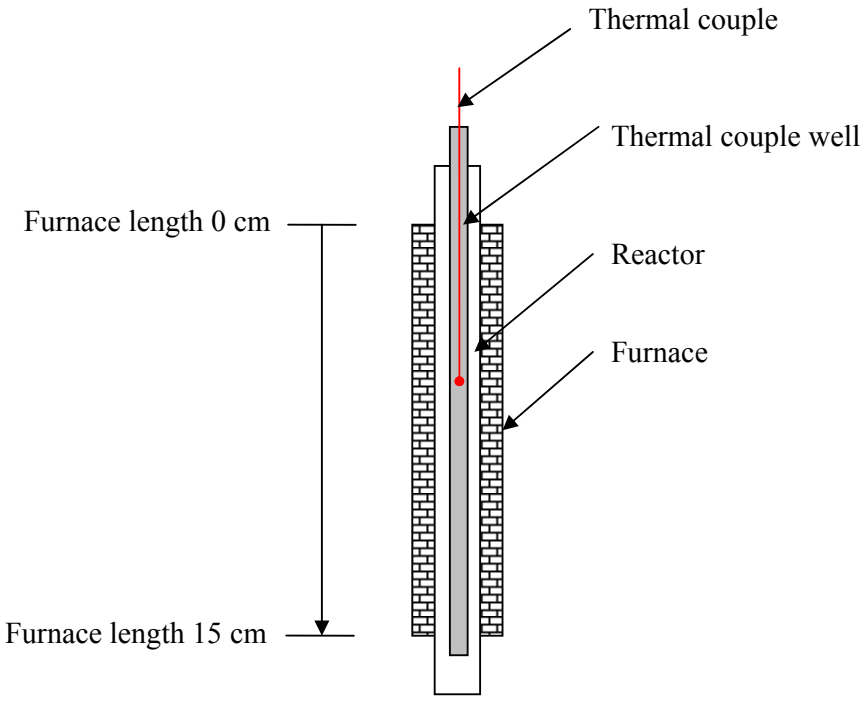

2) Reactor temperature profile with furnace length

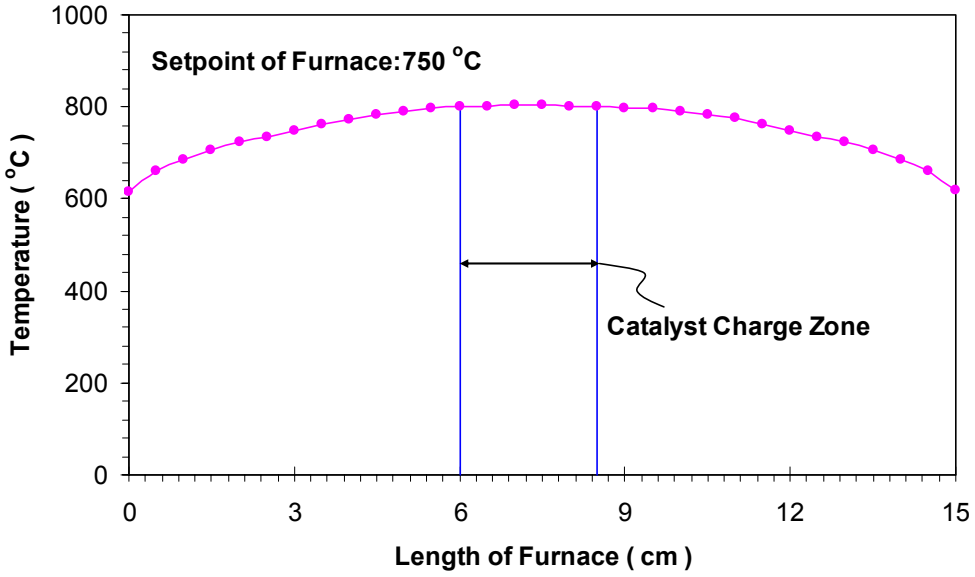

APPENDIX D: CALCULATION OF GIBBS FREE ENERGY CHANGE OF REACTION USING THIRD LAW METHOD

The Gibbs free energy change of a reaction (ΔG^o) is a function only of temperature and can be calculated by third law method (Kyle, 1999):

$$\Delta G^o = \Delta H^o - T\Delta S^o$$

where ΔH^o is standard enthalpy change and ΔS^o is standard entropy change of the reaction. The standard enthalpy change ΔH^o of a reaction at temperature T can be calculated according to the following equation:

$$\Delta H^o = \Delta H^o_{298K} + \int_{298\,K}^{T} \sum (v_i c^o_{p,i}) dT$$

where $c_p{}^o$ is the mole constant-pressure heat capacity of species i and $\sum$ signifies the sum over all species. The standard entropy change ΔS^o at temperature T can be calculated as follows:

$$\Delta S^o = \Delta S^o_{298.K} + \int_{298\,K}^{T} \frac{\sum (v_i c^o_{p,i})}{T} dT$$

The thermal property data used for the calculation are listed as follows:

Table D-1 Enthalpy of formation, Gibbs function of formation, and absolute entroy at 25 ^{o}C, 1 atm (Çengel and Boles, 2006; *Perry and Green, 1997)

Substance	h^o_f (kJ/kmol)	g^o_f (kJ/kmol)	s^o (kJ/kmol·K)
Carbon (solid)	0	0	5.74
Hydrogen	0	0	130.68
Carbon monoxide	-110,530	-137,150	197.65
Carbon dioxide	-393,520	-394,360	213.80
Water vapor	-241,820	-228,590	188.83
Methane	-74,850	-50,790	186.16
Acetylene	226,730	209,170	200.85
Ethylene	52,280	68,120	219.83
Ethane	-84,680	-32,890	229.49
Methanol	-200,670	-162,000	239.70
Formaldehyde*	-108,600	-102,600	218.66

Data are from Çengel's textbook unless otherwise specified by the sign of star of "*".

Table D-1 Ideal gas specific heats of various common gases (Çengel and Boles, 2006)

$c_P = a + bT + cT^2 + dT^3$ (T in K, c_P in kJ/kmol·K)							
Substance	a	$b\times10^2$	$c\times10^5$	$d\times10^9$	Temp. range, K	% error	
						Max.	Avg.
Hydrogen	29.11	-0.1916	0.4003	-0.8704	273-1800	1.01	0.26
Carbon monoxide	28.16	0.1675	0.5372	-2.222	273-1800	0.89	0.37
Carbon dioxide	22.26	5.891	-3.501	7.469	273-1800	0.67	0.22
Water vapor	32.24	0.1923	1.055	-3.595	273-1800	0.53	0.24
Methane	19.89	5.024	1.269	-11.01	273-1500	1.33	0.57
Acetylene	21.80	9.2143	-6.527	18.21	273-1500	1.46	0.59
Ethylene	3.95	15.64	-8.344	17.67	273-1500	0.51	0.13
Ethane	6.90	17.27	-6.406	7.285	273-1500	0.83	0.28
Methanol	19.0	9.152	-1.22	-8.039	273-1500	0.18	0.08
Formaldehyde	22.81	4.078	0.713	-8.701	273-1500	1.41	0.62

in the thesis are taken from the fifth edition of Thermodynamics edited by Çengel and Boles (2006) and the seventh edition of Perry's Chemical Engineers' Handbook edited by Perry and Green (1997). They are listed from the following tables:

The physical and chemical data used for the calculation in the thesis are taken from the fifth edition of Thermodynamics edited by Çengel and Boles (2006) and the seventh edition of Perry's Chemical Engineers' Handbook edited by Perry and Green (1997).

References:

Çengel, Yunus A., and Boles, Michael A., "Thermodynamics-An Engineering Approach," McGraw Hill Higher Education, 5th edition, Appendix 1, p883-993 (2006).

Kyle, B.G., "Chemical and process thermodynamics, third edition", Prentice Hall PTR, New Jersey, p433-511 (1999)

Perry, R.H., and Green, R.W., "Physical and chemical data," Perry's Chemical Engineers' Handbook, 7th edition, Section 2 (1997).

APPENDIX E: CALCULATION OF CONVERSION AND SELECTIVITY

When experiments are carried out with N_2 as the internal reference, the calculations are performed assuming that N_2 is an inert. The molar flow rate of N_2 is the same before and after reaction, i.e., $F_{N_2}^{i} = F_{N_2}^{f} = F_{N_2}$ (mol/min), where superscripts i and f are used to indicate initial and final flow rate, respectively. Hence, the flow rate of every species in product stream can be calculated using the following equation based on the results of the gas chromatography (GC) analysis.

$$F_j^f, \text{ mol/min} = \frac{f_j^f}{f_{N_2}^f} \times F_{N2}$$

where f_j^f is the fraction of species j in the product obtained from the GC analysis. The conversion (X_j) and selectivity (S_j) can be calculated as follows:

$$X_j = \frac{F_j^i - F_j^f}{F_j^i} \times 100\,\%$$

$$S_{H_2} = \frac{F_{H_2}^f}{2 \times (F_{CH_4}^i - F_{CH_4}^f)} \times 100\,\%$$

$$S_{CO} = \frac{F_{CO}^f}{(F_{CH_4}^i - F_{CH_4}^f) + (F_{CO_2}^i - F_{CO_2}^f)} \times 100\,\%$$